NASA CONTRACTOR REPORT 177436

Hover Performance Tests of Baseline Metal and Advanced Technology Blade (ATB) Rotor Systems for the XV-15 Tilt Rotor Aircraft

K. Bartie, H. Alexander, M. McVeigh, S. La Mon, and H. Bishop

Prepared by
BOEING VERTOL COMPANY
Philadelphia, PA
for
Ames Research Center

under contract
NAS2-11250

NASA
National Aeronautics and
Space Administration

Ames Research Center
Moffett Field, California 94035

FOREWORD

The research and development activity reported in this document was performed by the Boeing Vertol Company for the National Aeronautics and Space Administration, Ames Research Center, under Contract NAS2-11250. Mr. M.D. Maisel (Aeroflightdynamics, AVSCOM, Ames Research Center) was the NASA program manager, and Mr. D.J. Giulianetti (NASA) was deputy program manager. Other Ames Research Center personnel who made a significant contribution to this phase of the program included Messrs. M.K. Betzina, F.F. Felker III, L.A. Young, and D.B. Signor. Mr. H.R. Alexander was the Boeing Vertol Company program manager.

The following Boeing Vertol personnel made significant contributions to this test program:

D. Ekquist K. Farrance W. Grauer I. Walton	Wind Tunnel Test Engineering
F. Devlin N. Ross	Instrumentation and Control System Design
K. Bartie R. Benson C. Coleman M. McVeigh	Aerodynamics
H. Bishop M. Cawthorne S. La Mon H. Silcox	Stress
S. Botwinik D. Reed R. Smith R. Ricks	Dynamics
J. Mayer W. McLean D. Podgurski	Wind Tunnel Design and Project Management

Mr. Hank Silcox and Mr. Joseph Mayer merit special mention for their design of the balance system used to measure rotor performance. This was a major advance in balance technology and the accuracy and reliability of the measured performance data was an important component in the success of the program.

H.R. Alexander

ABSTRACT

Rotor hover performance data were obtained for the full scale Advanced Technology Blade (ATB) designed for the XV-15. The ATB rotor thrust-weighted solidity is 0.10. The test was conducted as part of contract NAS2-11250 at the NASA-Ames Outdoor Aeronautical Research Facility (OARF). The XV-15 basic rotor (solidity = .089) was also tested. Variations of the ATB tip planform and cuff planform were also tested. A peak figure of merit of 0.806 was demonstrated for the ATB and a value of 0.791 for the XV-15 steel blades. Measurements of the downwash in the wake at 0.4R below the disc are also presented.

KEY WORDS

Rotor
Hover Performance
Tilt Rotor
XV-15
Rotor Blade
Rotor Loads
Static Performance Test

TABLE OF CONTENTS

TABLE OF CONTENTS (Continued)

LIST OF FIGURES

LIST OF FIGURES (Continued)

LIST OF FIGURES (Continued)

LIST OF FIGURES (Continued)

LIST OF FIGURES (Continued)

LIST OF FIGURES (Continued)

LIST OF TABLES

LIST OF SYMBOLS

Symbol	Definition	Units
a	airfoil section lift-curve slope	rad^{-1}
A_1	lateral cyclic	degrees
B	number of rotor blades	-
B_1	longitudinal cyclic	degrees
c	blade chord	ft.
c_T	blade thrust-weighted chord, $\frac{\int_0^1 cx^2dx}{\int_0^1 x^2dx}$	ft.
C_d	section drag coefficient	-
C_ℓ	section lift coefficient	-
C_{NF}	rotor normal force coefficient, $NF/\rho\pi R^2 V_T^2$	-
C_P	rotor power coefficient, $HPx550/\rho\pi R^2 V_T^3$	-
$C_{P_{pro}}$	rotor profile power coefficient, profile power/$\rho\pi R^2 V_T^3$	-

LIST OF SYMBOLS (Continued)

Symbol	Definition	Units
C_{P_i}	rotor induced power coefficient, induced power/$\rho\pi R^2 V_T^3$	-
C_T	rotor thrust coefficient, $T/\rho\pi R^2 V_T^2$	-
DL	wing download	lb.
EI_C	blade chordwise stiffness	lb.in.^{2}
EI_F	blade flapwise stiffness	lb.in.^{2}
FM	rotor figure of merit, $C_T{}^{3/2}/\sqrt{2C_P}$	-
g	acceleration due to gravity	ft./sec.^{2}
GJ	rotor torsional stiffness	lb.in.^{2}
I_p	blade pitch inertia	lb.in.^{2}
k	rotor induced efficiency factor	-
M_T, M_{TIP}	blade tip Mach Number	-
NF	rotor normal force	lb.
PM	rotor pitching moment	in. lb.
P_{si}	static pressure at the i^{th} tube in the downwash rake	lb./ft.^{2}
P_{ti}	total pressure at the i^{th} tube in the downwash rake	lb./ft.^{2}
r	radial station on blade	ft.

LIST OF SYMBOLS (Continued)

Symbol	Definition	Units
R	blade radius	ft.
R_e	airfoil Reynolds Number	-
RM	rotor rolling moment	in. lb.
SF	rotor side force	lb.
T	rotor thrust	lb.
T_∞	rotor thrust out of ground effect	lb.
v_i	induced velocity	ft./sec.
V_T, V_{TIP}	rotor tip speed	ft./sec.
V, V_W	wind velocity	ft./sec.
V_{WIND}	wind velocity	knots
x	nondimensional blade position, r/R	-
YM	rotor yawing moment	in. lb.
α	shaft angle of attack	degrees
β	hub gimbal angle	degrees
Ω	rotor rotational speed	radians/sec. or RPM
ψ_W	ambient wind azimuth	degrees

LIST OF SYMBOLS (Continued)

Symbol	Definition	Units
ρ	air density	slugs/ft.^{3}
σ	local rotor solidity, $Bc/\pi R$	-
σ_T	thrust weighted rotor solidity, $Bc_T/\pi R$	-
θ_0	blade root collective pitch angle	degrees
$\theta_{.75}$	blade collective pitch angle at r/R = 0.75	degrees
μ	rotor advance ratio, V/V_{TIP}	-

Subscript	Definition	Units
H	conditions when wind velocity is zero	-

1.0 SUMMARY

This document presents isolated rotor test results conducted in two phases at Ames Research Center in March and July/August 1984. In March a benchmark test of the XV-15 steel blades was performed and in July/August the Advanced Technology Blade, including a number of variations, was tested. Between these two test periods, the facility was occupied by a scaled version of the V-22 rotor. All rotors tested were 25 ft. in diameter. The V-22 test is reported in Reference 1.

Figure 1.1 shows the XV-15 aircraft in several modes of operation. Figure 1.2 shows the baseline version of the ATB mounted on the test stand at NASA-Ames. Figure 1.3 shows the untwisted blade planform and distribution of airfoil sections for the baseline configuration.

The performance indices of both the XV-15 rotor and the ATB rotors turned out to be significantly better than expected. Predicted and test values of figure of merit as a function of C_T for both rotors are shown in Figure 1.4. These results, along with those from configuration variations, are discussed in detail in Section 7.0. Possible reasons for the poor quality of the predictions are identified, and suggestions are made for improvements in predictions capability.

The test facility used for this program was the Outdoor Aeronautical Research Facility at Ames Research Center. Major improvements to the power transmission and performance measuring components of the NASA test rig were funded under the program. These included provision of a 4:1 reduction gear box which permitted testing beyond the power levels available in the XV-15 aircraft. A major improvement in the test hardware was the development of a six-component balance with minimal load interaction, absence of thermal drift, and direct measurement of rotor thrust and torque. These features of the program are discussed further in Section 3.0 and in more detail in Reference 2.

The tests provided definitive thrust and torque data for the XV-15 steel blade and the Advanced Technology Blades. Hover performance for both rotors (and for the V-22 rotor tested using the same equipment) was significantly better than that predicted using contemporary theory. The measured peak figures of merit were all in the region .79 - .81, whereas predicted values did not exceed .79. In addition, peak performance occurs at a higher value of C_T than predicted, and does not drop off as fast as predicted at the higher values of C_T.

The airflow velocity distribution was measured at a distance approximately 0.4R downstream from the rotor plane. Vapor trails of the tip vortices were generated at high C_T's in some atmospheric conditions and photographs of these have been used to estimate the rate of wake contraction and velocity variation as a function of distance from the rotor planes. These additional data have been used to initiate improvements in prediction methodology.

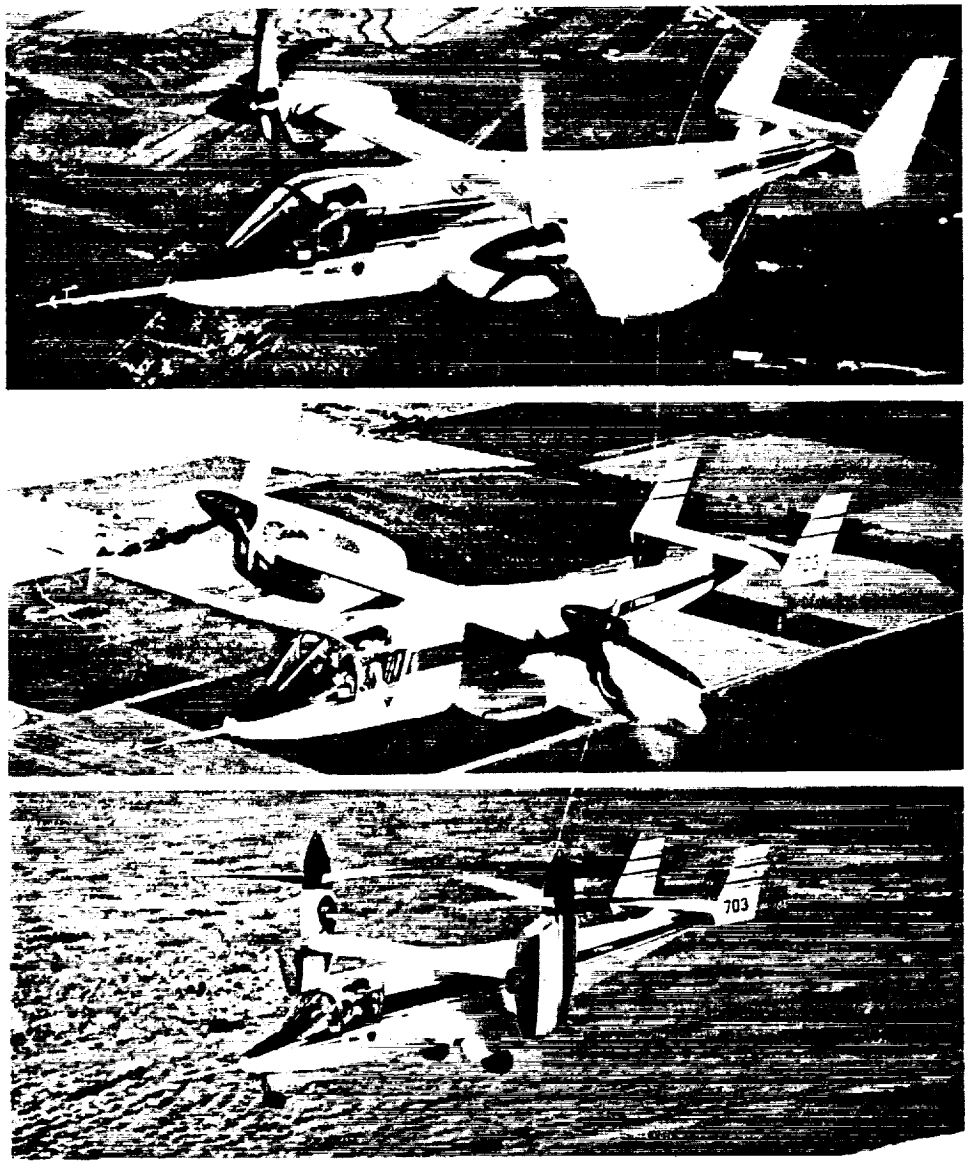

Figure 1.1 XV-15 Tilt Rotor Research Aircraft in Cruise, Transition, and Hover

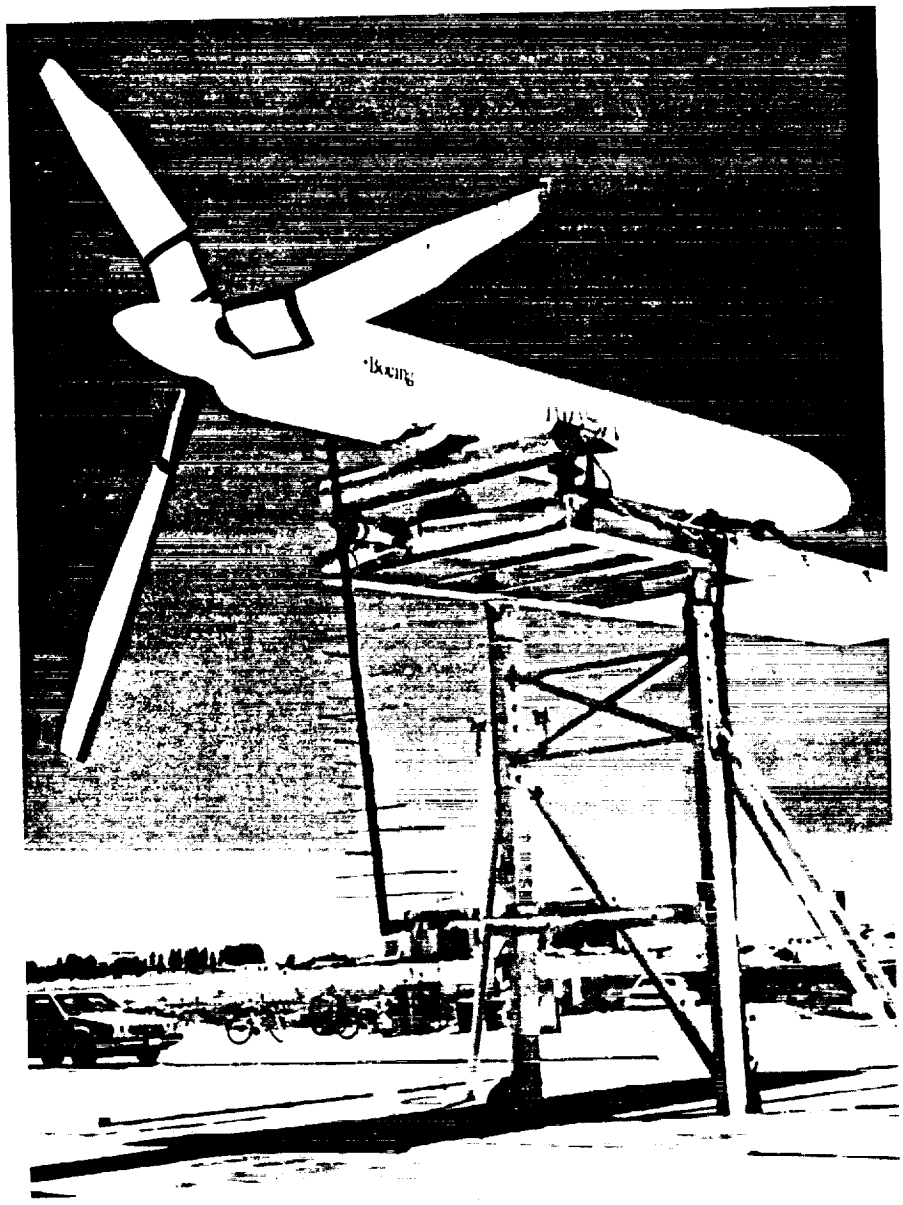

Figure 1.2 Baseline ATB Mounted on NASA-Ames OARF (Outdoor Aerodynamic Research Facility)

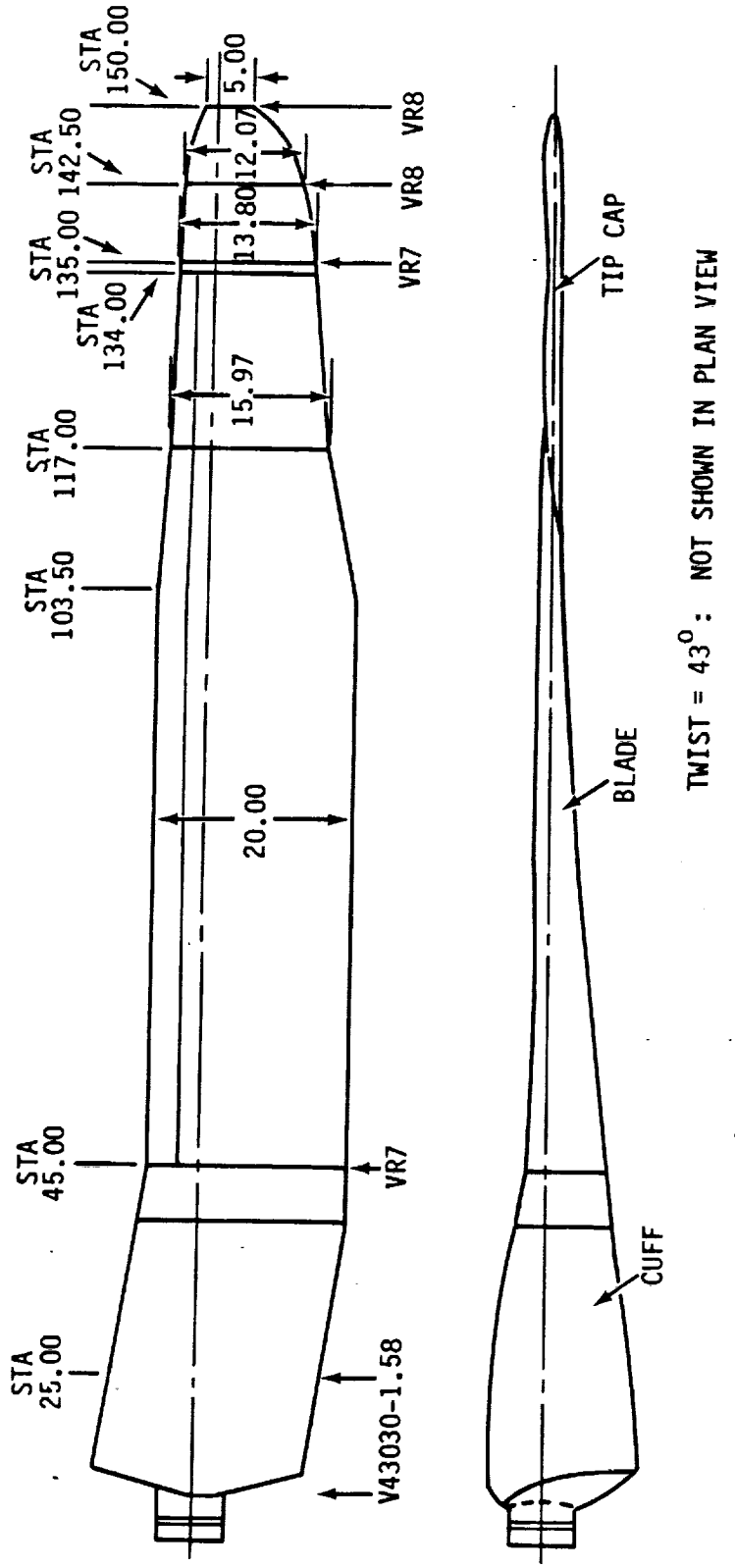

Figure 1.3 Advanced Technology Blade

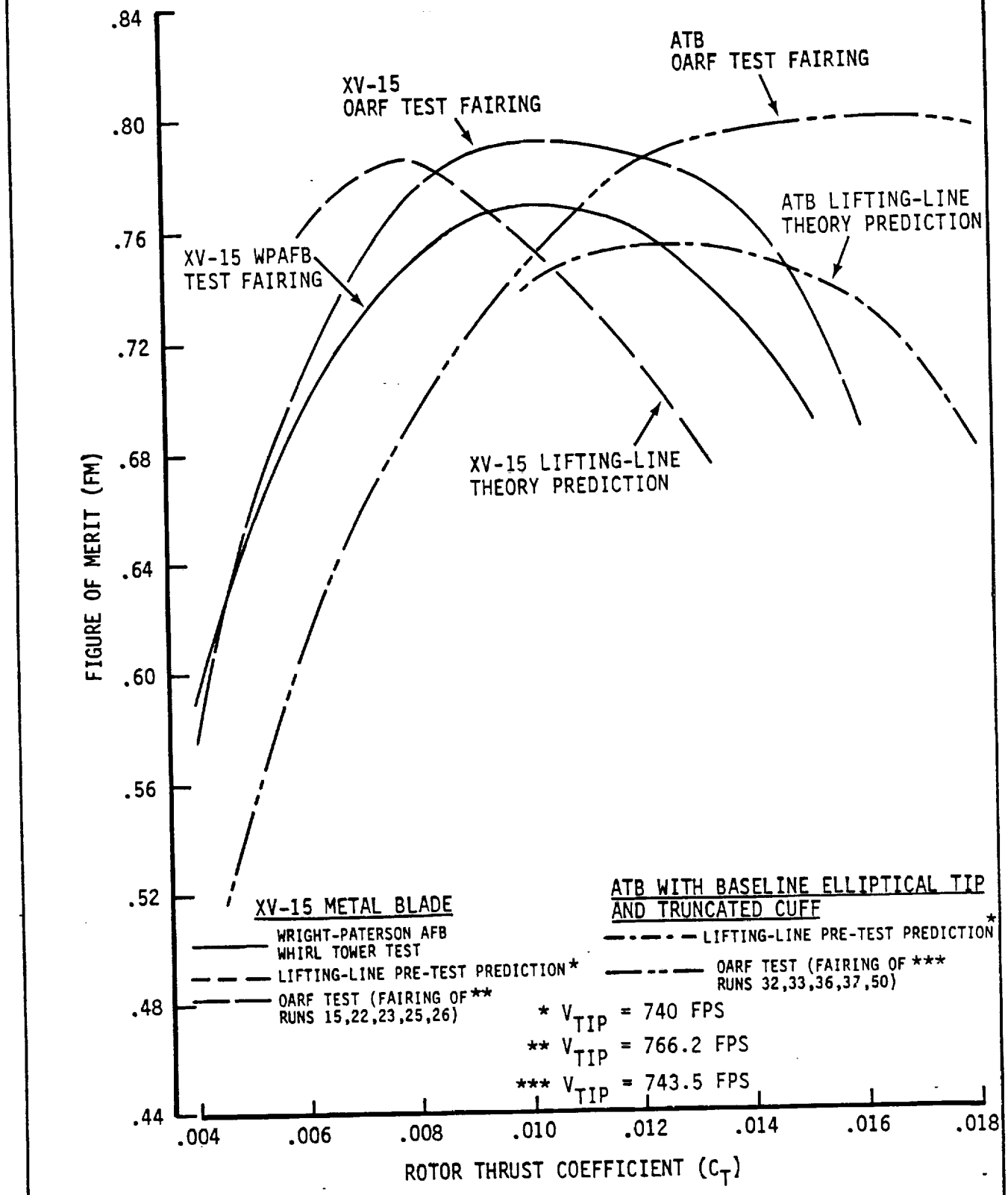

Figure 1.4 Pretest Predictions and OARF Test Results for XV-15 Metal Blade and Baseline ATB Rotor

Blade bending moments were recorded at a number of stations and critical stations were monitored for safety. This included data near the tip which has been used to improve the mathematical modelling in this region. The test included eight hours of endurance and structural validation testing during which control inputs were cycled and blade frequency data was accumulated.

Over the test period Ames Research Center engineers monitored the near and far-field noise levels generated by rotor operation. The Advanced Technology Blades were found to generate significantly less noise than the XV-15 metal blades.

A summary of the rotor performance results along with conclusions and recommendations are given in Section 10.0.

2.0 INTRODUCTION

The XV-15 tilt rotor demonstrator aircraft has been flying successfully since 1977 using rotor blades of the original design. These blades have a rectangular planform and the material is steel. The blade design was optimized for a 9000 lbs. gross weight aircraft and there was no change to the rotor design when the gross weight became 13,000 lbs.

This, along with a number of other factors including fatigue strength limitations of the metal blades, led NASA to initiate a program to develop composite blades optimized to different performance criteria and exploiting the range of design options made feasible by composite materials. Other objectives of the Advanced Technology Blade program were to demonstrate fabrication techniques appropriate to highly twisted composite blades suitable for tilt rotor applications.

This report documents the XV-15 Advanced Technology Blade Rotor Test conducted at the Outdoor Aeronautical Research Facility (OARF) at NASA-Ames during April 1984 and July 1984. The report includes a description of the test apparatus and instrumentation, a presentation of the results, and a discussion of the implications of the results. The detailed, fully-corrected test data may be obtained from NASA-Ames 40' x 80' wind tunnel staff in the form of computer tabulations.

3.0 DESCRIPTION OF TEST INSTALLATION

3.1 Test Stand

The Outside Aerodynamic Research Facility at NASA-Ames consists of a large concrete pad (Fig. 3.1) with a steel platform at the center of which is mounted a test stand carrying the propeller test rig. Details of the layout of the stand are given in Fig. 3.2. The supporting test stand consists of a horizontal frame carrying the motor and drive system. This frame is supported in front by two braced vertical steel beams and in the rear by a single, smaller beam. The rotor centerline lies 22 feet above the metal

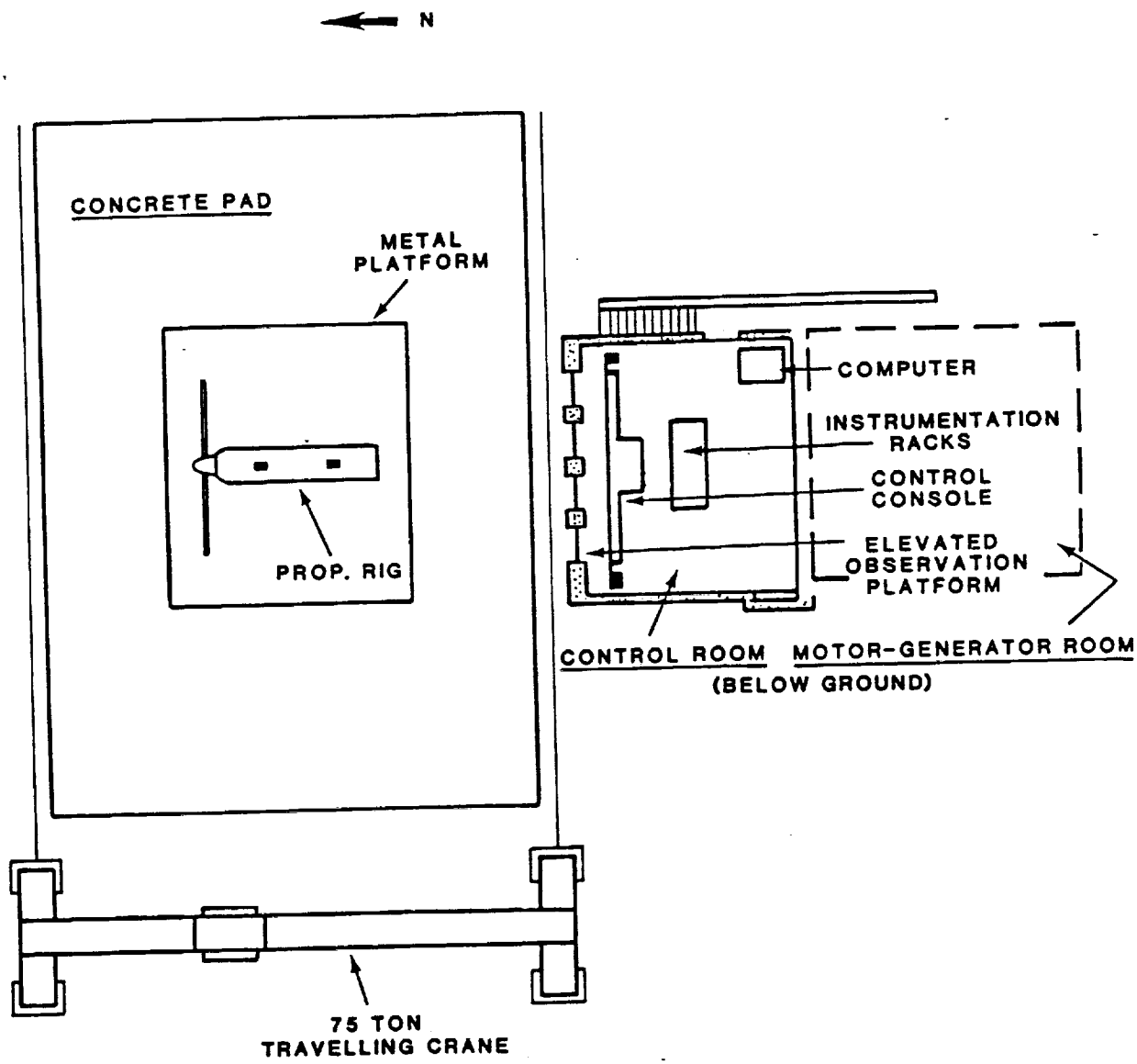

Figure 3.1 Plan View of NASA-Ames OARF

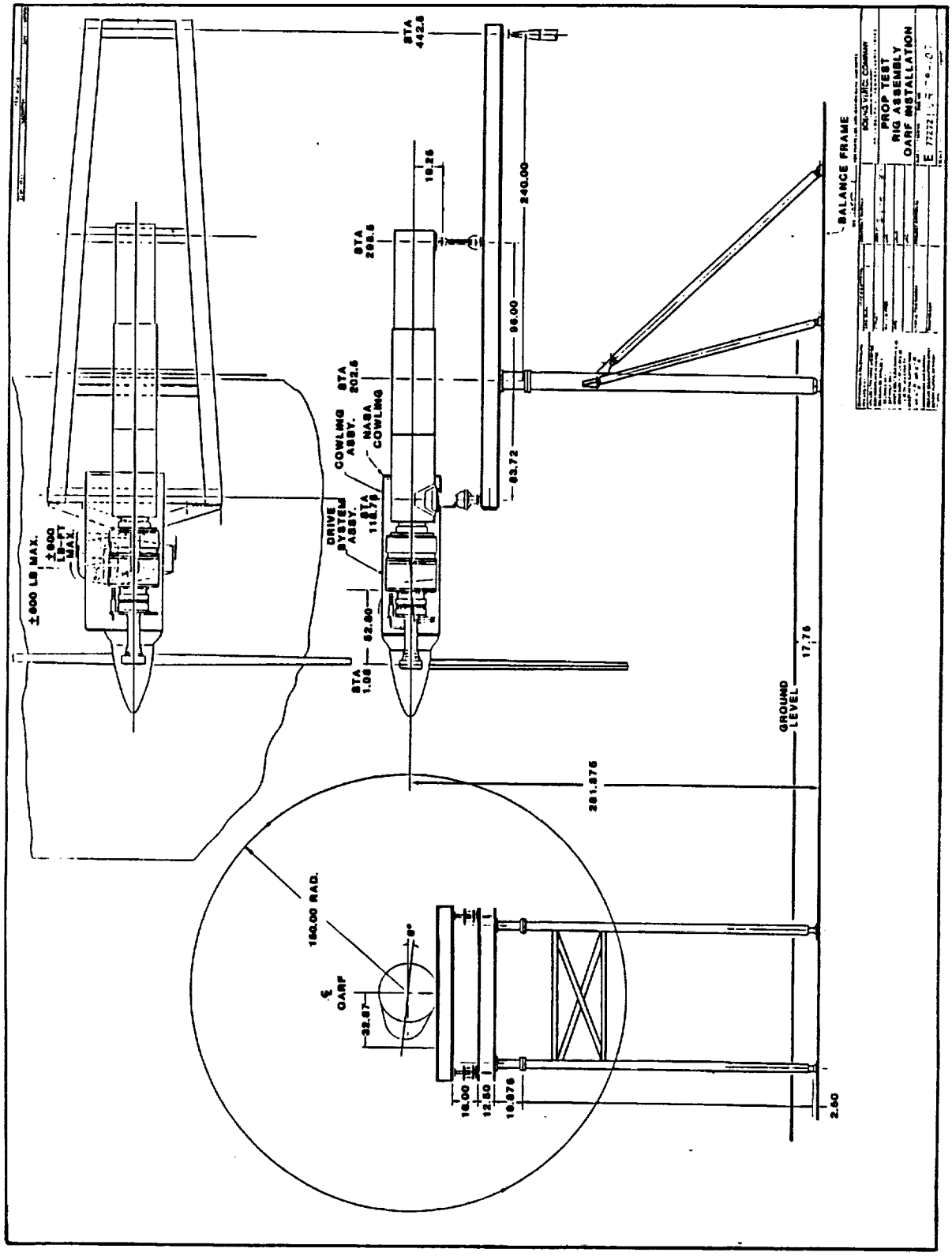

Figure 3.2 Three-View of Test Stand

platform providing 9.5 feet of clearance between the blade tips and the ground. The rotor hub, controls, six-component balance, gearbox and electric motor with services are mounted in-line within a 28-inch diameter cylindrical cowling. The motor housing is mounted on three load cells to provide rotor force and moment data that is independent of, and supplemental to, data from the main balance. The propeller test stand is described in more detail in Reference 2. Additional details and strength and safety analyses are provided in Reference 3.

3.2 Motor and Drive System

The test stand is powered by an electric motor driving through a new 4:1 reduction gearbox. The gearbox is oil cooled; the motor is water cooled. Gearbox output shaft torque limit is 252,000 in.lb. corresponding to the electric motor limit of 3,000 HP at 3000 RPM. This was sufficient to test well beyond the current (design maximum 163,000 in.lb.) operating torque limit of the XV-15. The gearbox is a Cincinnati Gear Co. epicyclic gear unit with a modified aft case to interface with the NASA motor package. The gearbox unit mounts directly to the face of the motor unit and supports the rotor balance through the balance mounting ring. The system consists of a sun gear around which are arranged a number of planets rolling within an annulus providing a coaxial design with power transmission at more than one point. Fig. 3.3 presents the gearbox operating envelope and shows that the hover RPM of the ATB and XV-15 rotors (565 RPM) is within the available operating range. Maximum RPM was limited to 625 RPM by the blade retention strap. Operating time below 370 RPM is also limited because of gear tooth and bearing lubrication considerations. However, this RPM is below the present range of interest. The motors and gearbox may rotate in either direction, however all the rotors tested were designed to rotate in the clockwise direction (viewed from the rear).

3.3 Balance

The test stand is furnished with a six-component balance. As shown in Figures 3.4 and 3.5, the rotor balance system is mounted between the hub/stack assembly baseplate and the transmission (through the balance mounting ring). The balance has two sections. The front section is a multi-flexured, torque-sensing element which measures the frictional torque of the bearings. The rear thrust-measuring section of the balance system consists of two flexure plates mounted on either end of cylindrical spacer units. These flexure elements measure thrust and also normal force, side force, pitching moment and yawing moment. The primary torque measurement is made by strain gages mounted on the drive shaft forward flexible coupling. Additional strain gages on the flexible couplings measure the axial load in the drive shaft. This is a function of the axial motion of the main thrust measuring flexures and amounts to approximately 3% of the total load.

Balance strain gages are of the foil type and are temperature compensated. The primary sensitivities are in the thrust and torque directions with a maximum error of 50 lb. of thrust and 25 in.lb. of torque. The balance is designed to withstand the loss of one rotor blade without yielding and has

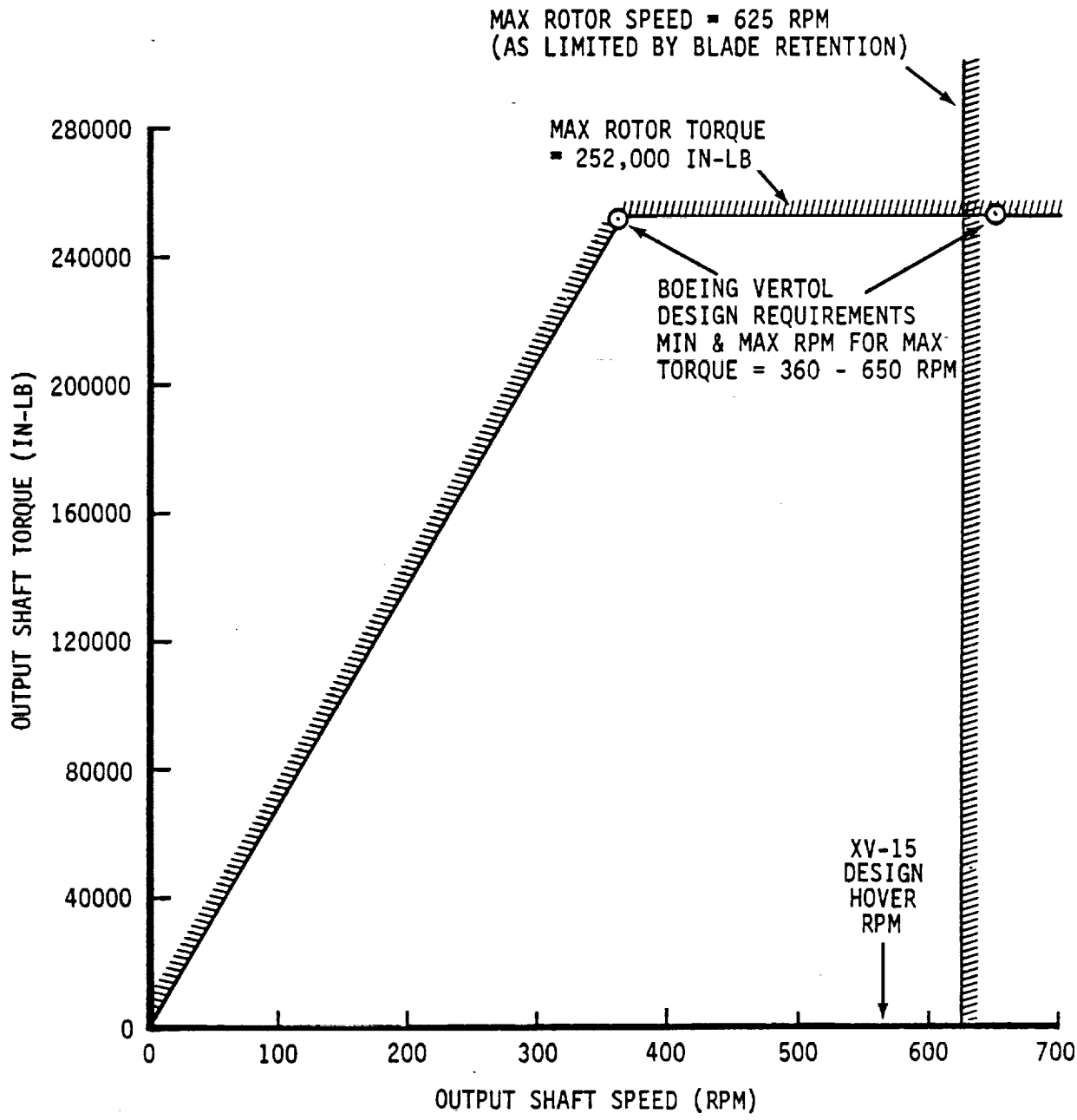

Figure 3.3 Gearbox Operating Envelope

ORIGINAL PAGE IS
OF POOR QUALITY

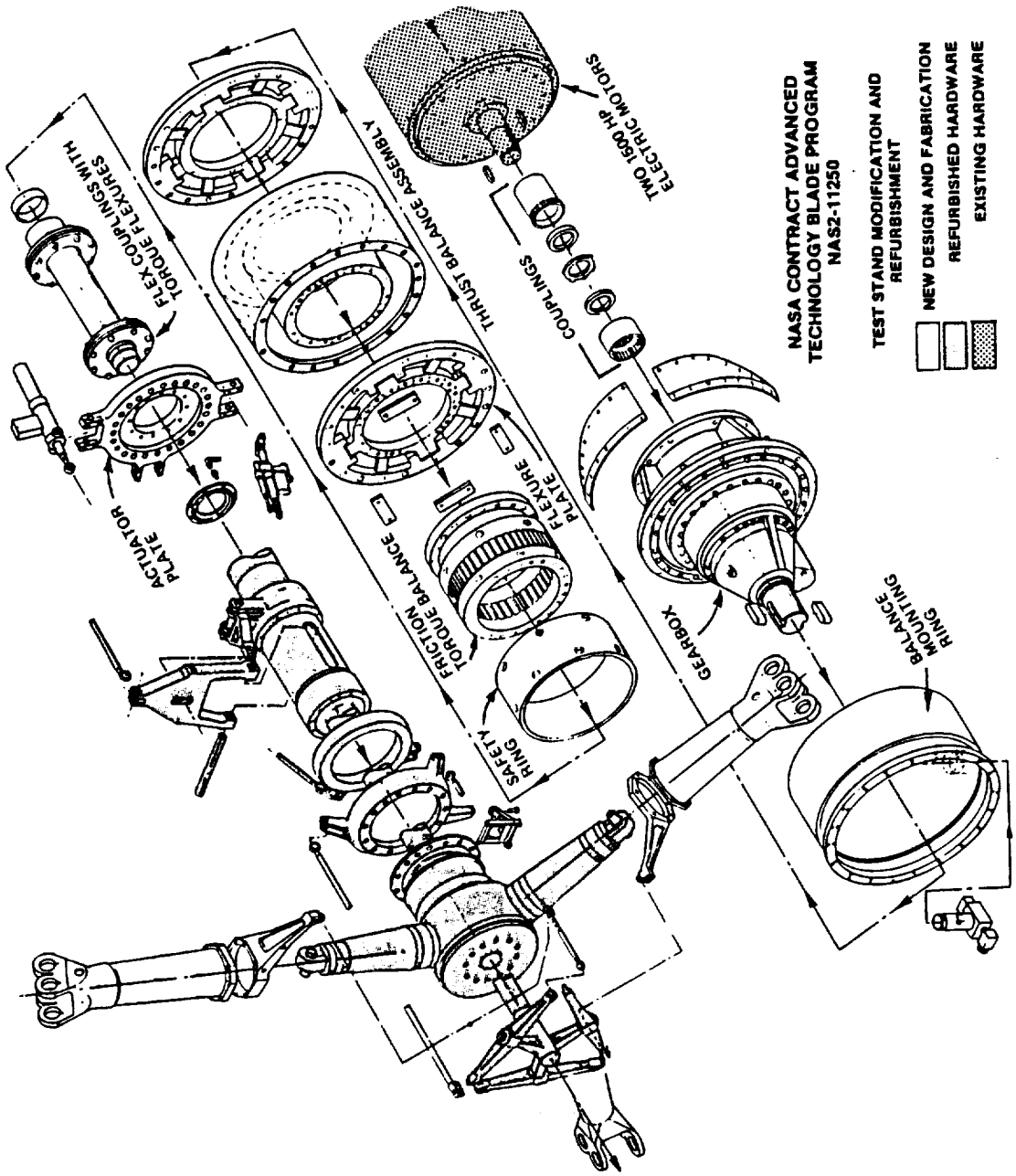

Figure 3.4 Six-Component Rotor Balance System

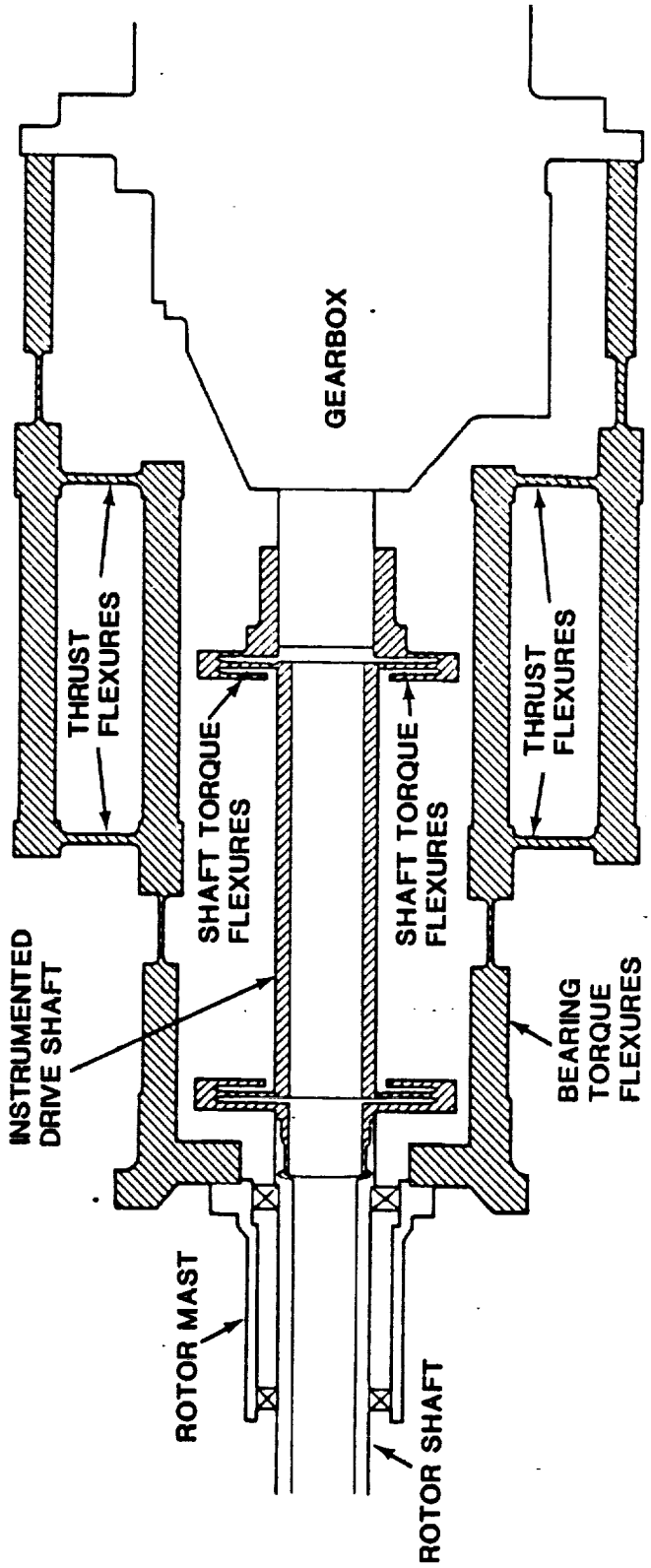

Figure 3.5 Schematic of Balance System

infinite life over the normal operating load range. Axial load range is -400 to 16,000 lb. and the torque range is 0 to 252,000 in.lb. Table 3.1 summarizes the design load ranges and accuracies for the rotor balance. The flexible couplings are designed to measure a maximum torque of 252,000 in.lb. with an accuracy of ± 120 in.lb.

3.5 Hub and Controls

The 3-bladed gimballed rotor hub and upper controls are XV-15 rotor components defined by BHT Drawing No. 300-018-012. The ATB pitch housing was designed to be compatible with this hub. The upper controls provided control by collective, longitudinal and lateral pitch. Collective pitch motion was transmitted through the center of the shaft and was controlled by a hydraulic actuator. Longitudinal and lateral cyclic motion was provided through the rotating swashplate. The motions of the nonrotating swashplate were controlled by electric linear actuators. Both collective and cyclic pitch actuator control systems were open loop with the electric cyclic pitch actuators rate-limited to 0.5 deg/sec. Collective pitch motion was limited to a range of -4 to 25 degrees; cyclic pitch was electrically limited to ± 3.0 degrees and a mechanical stop was provided at ± 4.0 degrees.

The complete hub/stack assembly was mounted on a base plate (actuator plate) which was also the mounting point for the control actuators and the connecting element to the balance system. A slipring assembly with 48 rings was incorporated within the stack to provide transmission of data from the rotating components to the data acquisition system.

A cowling covered the upper controls and balance and was attached to the motor casing. The cowling provided weather protection.

3.6 Rotors

3.6.1 Advanced Technology Blade Rotor

The ATB rotor is a three-bladed, 25 ft. diameter rotor with a thrust-weighted solidity (σ_T) of 0.10, which is 12.3% more than the solidity of the XV-15 steel blades (.089). The blades are of composite construction. Theoretical blade chord, twist, and thickness/chord distributions for the baseline ATB are given in Figures 3.6, 3.7, and 3.8 respectively. Sectional properties are given in Figures 3.9 through 3.13. Estimated blade frequencies in the cyclic and collective modes are shown in Figure 3.14 along with test measurements. The blades were inspected for fidelity to the design values of twist, chord, airfoil contour and surface condition, and were found to be acceptable.

The rotor blades were instrumented to record flap, lag, and torsional moments at selected spanwise positions. Details of the instrumentation are given in Section 4.0, Table 4.1.

Figure 3.15 is an exploded view of the advanced technology blade with callouts of the various materials. Figure 3.16 presents the baseline ATB configuration with the alternate tip and cuff sections that were tested.

Table 3.1 Rotor Balance Load Range and Accuracy

COMPONENT	LOAD RANGE	ACCURACY	% OF MAX. LOAD
AXIAL FORCE (THRUST)	-400/16,000 LB	± 50 LB	0.3
NORMAL FORCE	± 600 LB	± 12 LB	2.0
SIDEFORCE	± 600 LB	± 12 LB	2.0
PITCHING MOMENT	± 20,000 IN-LB	± 400 IN-LB	2.0
YAWING MOMENT	± 20,000 IN-LB	± 400 IN-LB	2.0
ROLLING MOMENT (FRICTION TORQUE)	± 15,000 IN-LB	± 25 IN-LB	0.16

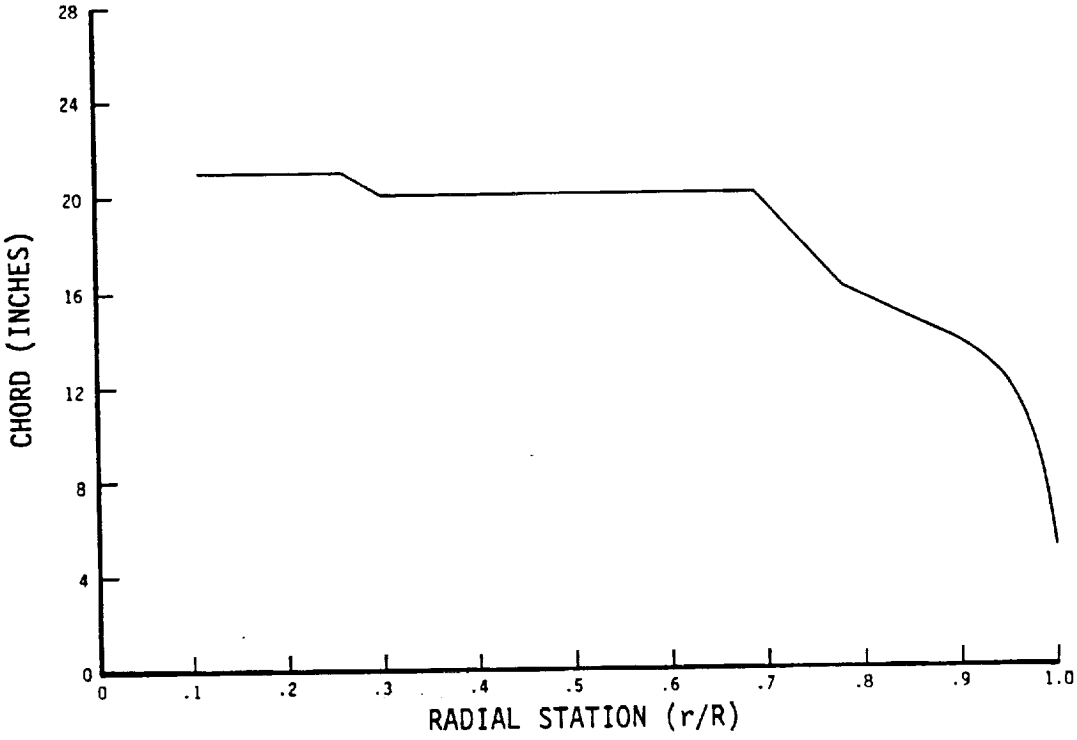

Figure 3.6 Baseline ATB Chord Distribution

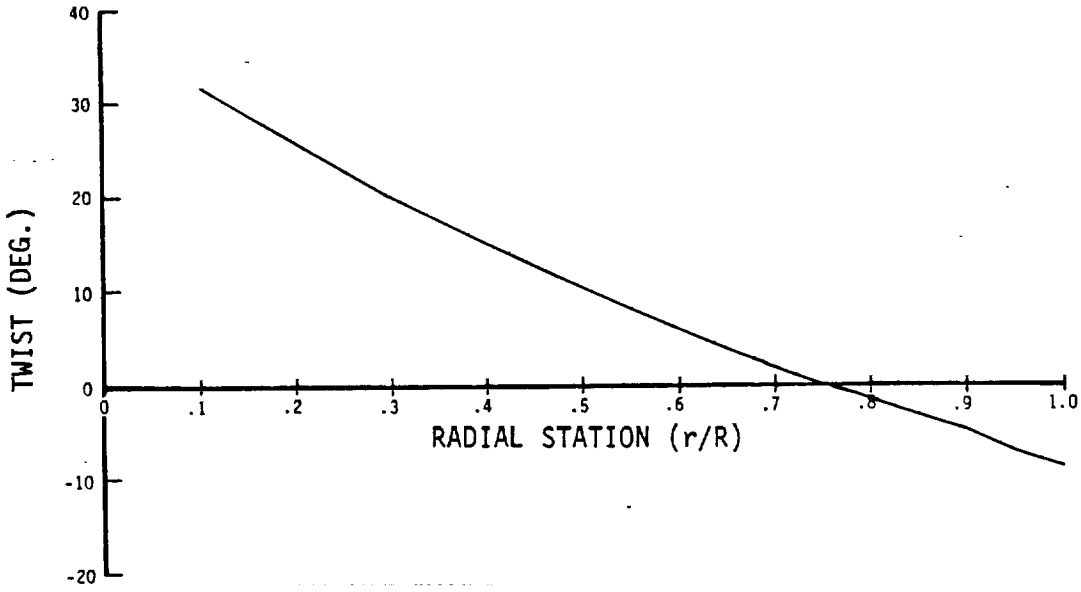

Figure 3.7 Baseline ATB Twist Distribution

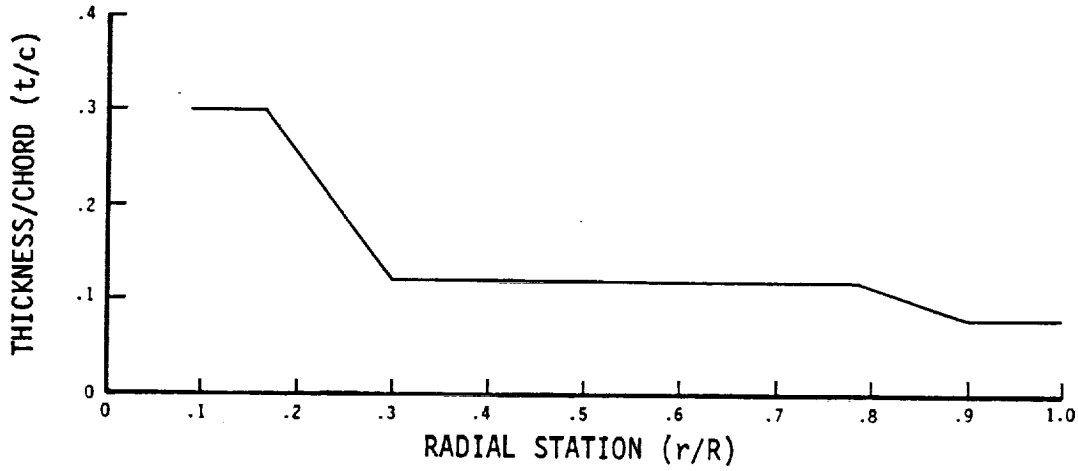

Figure 3.8 Baseline ATB Thickness/Chord Distribution

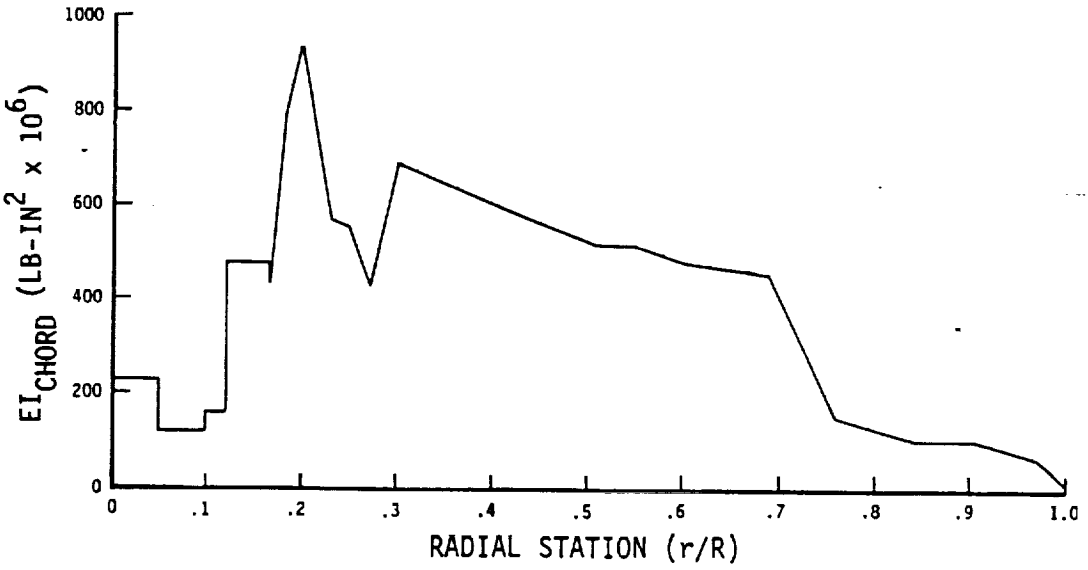

Figure 3.9 Baseline ATB Chordwise Stiffness Distribution

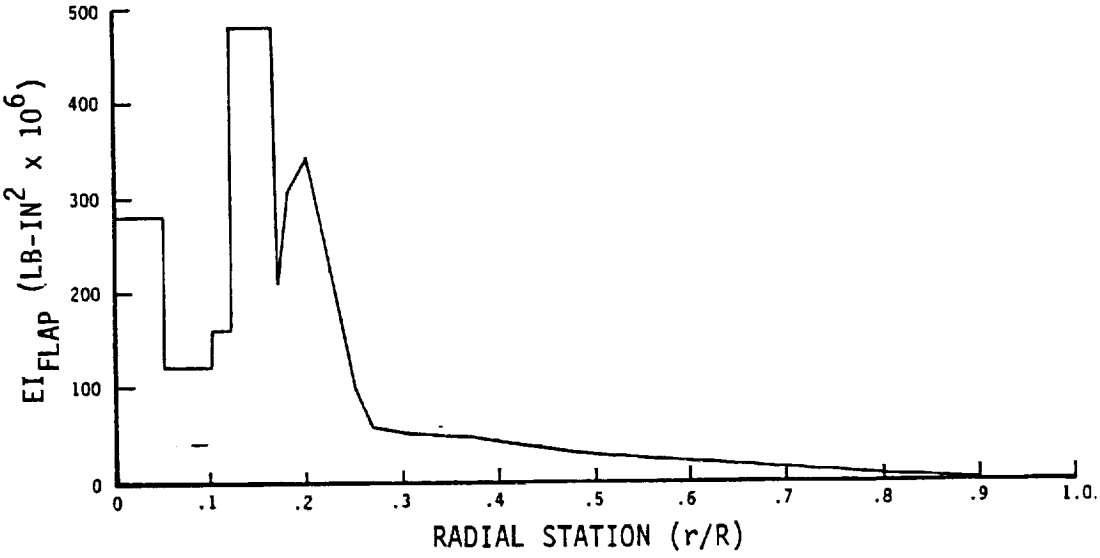

Figure 3.10 Baseline ATB Flapwise Stiffness Distribution

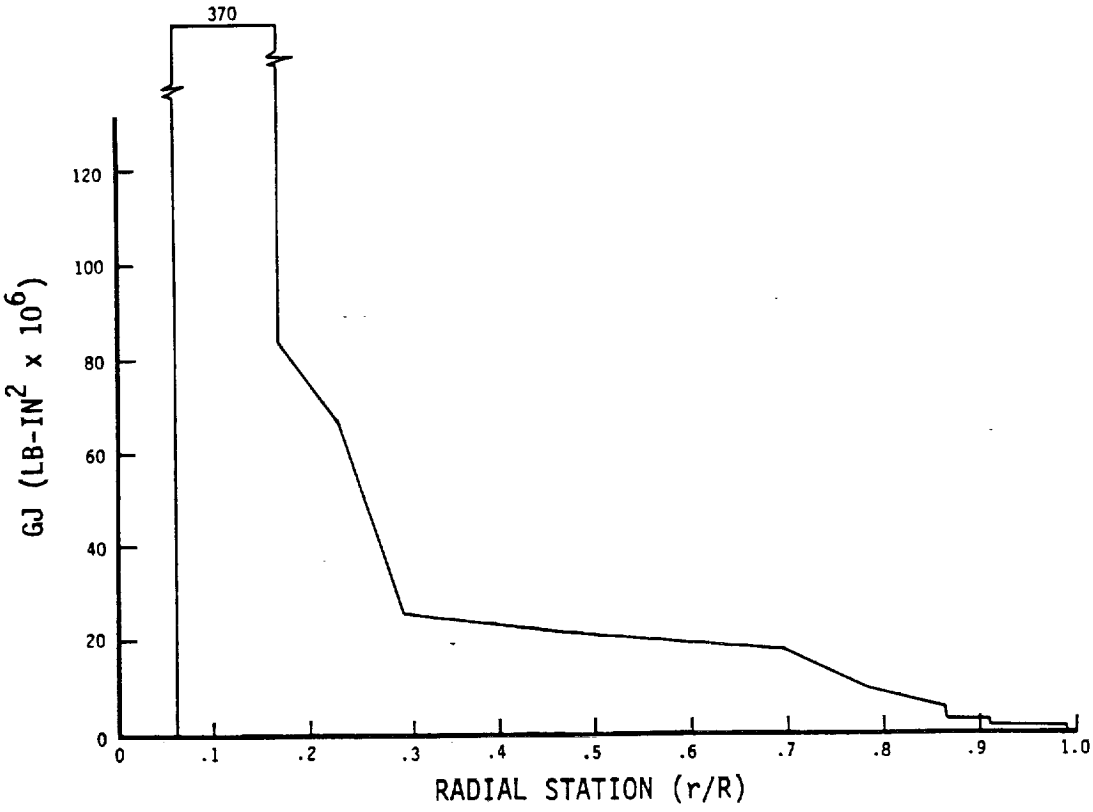

Figure 3.11 Baseline ATB Torsional Stiffness Distribution

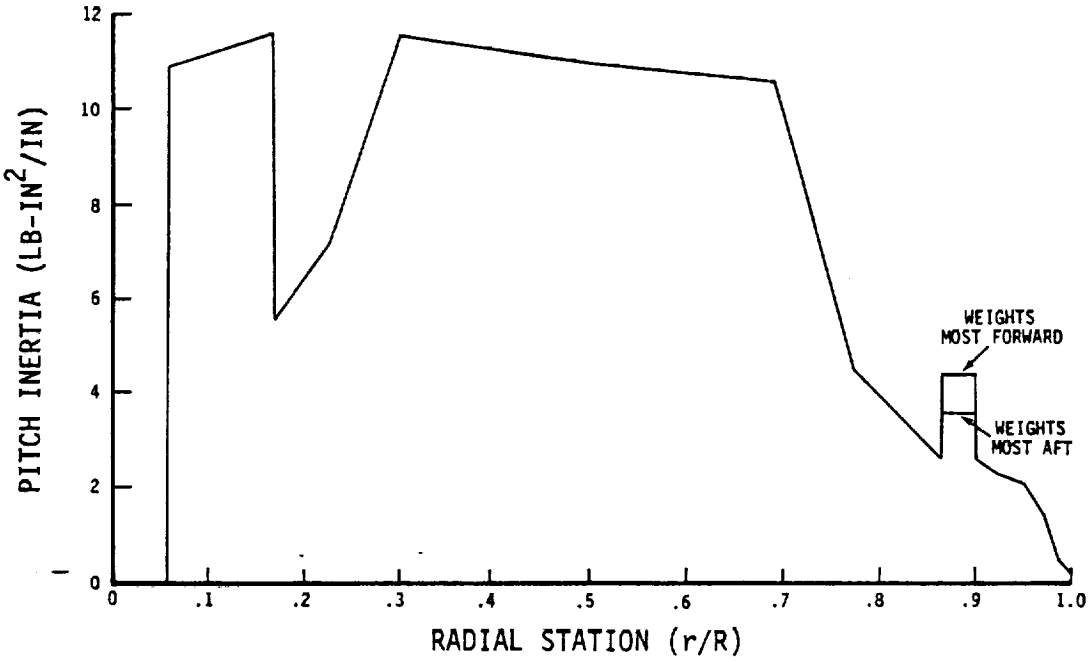

Figure 3.12 Baseline ATB Pitch Inertia Distribution

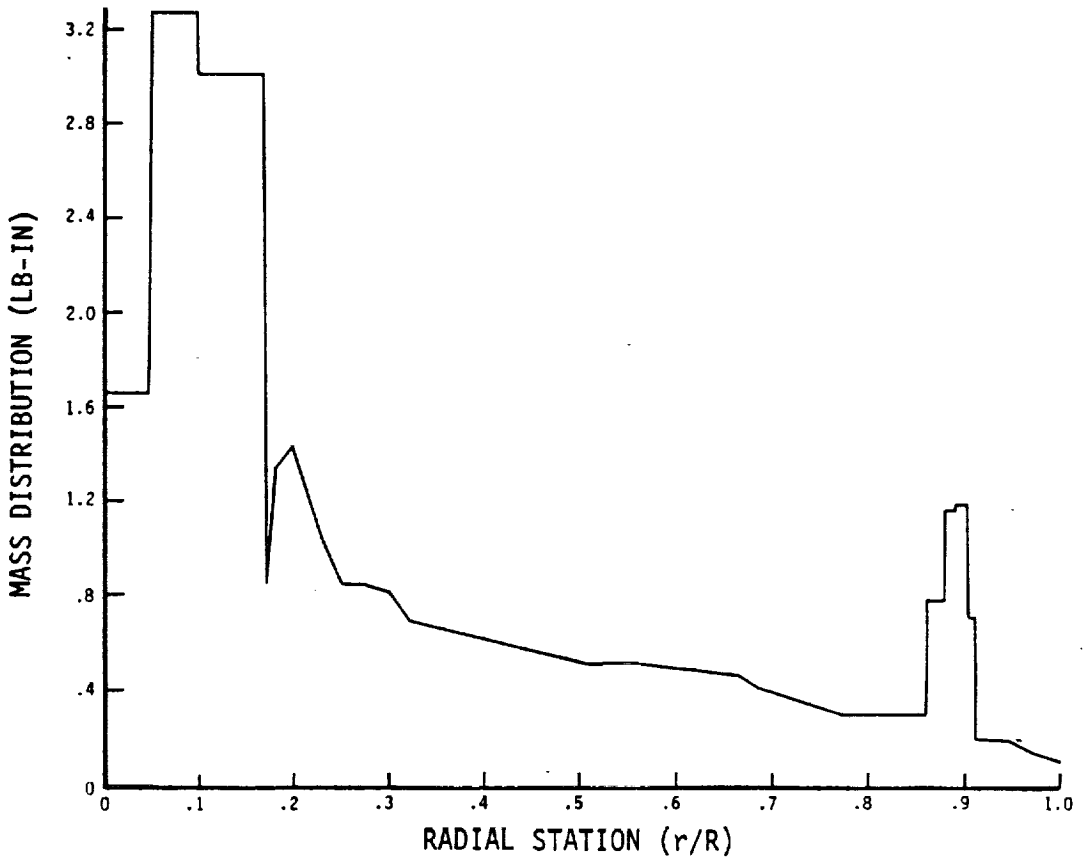

Figure 3.13 Baseline ATB Mass Distribution

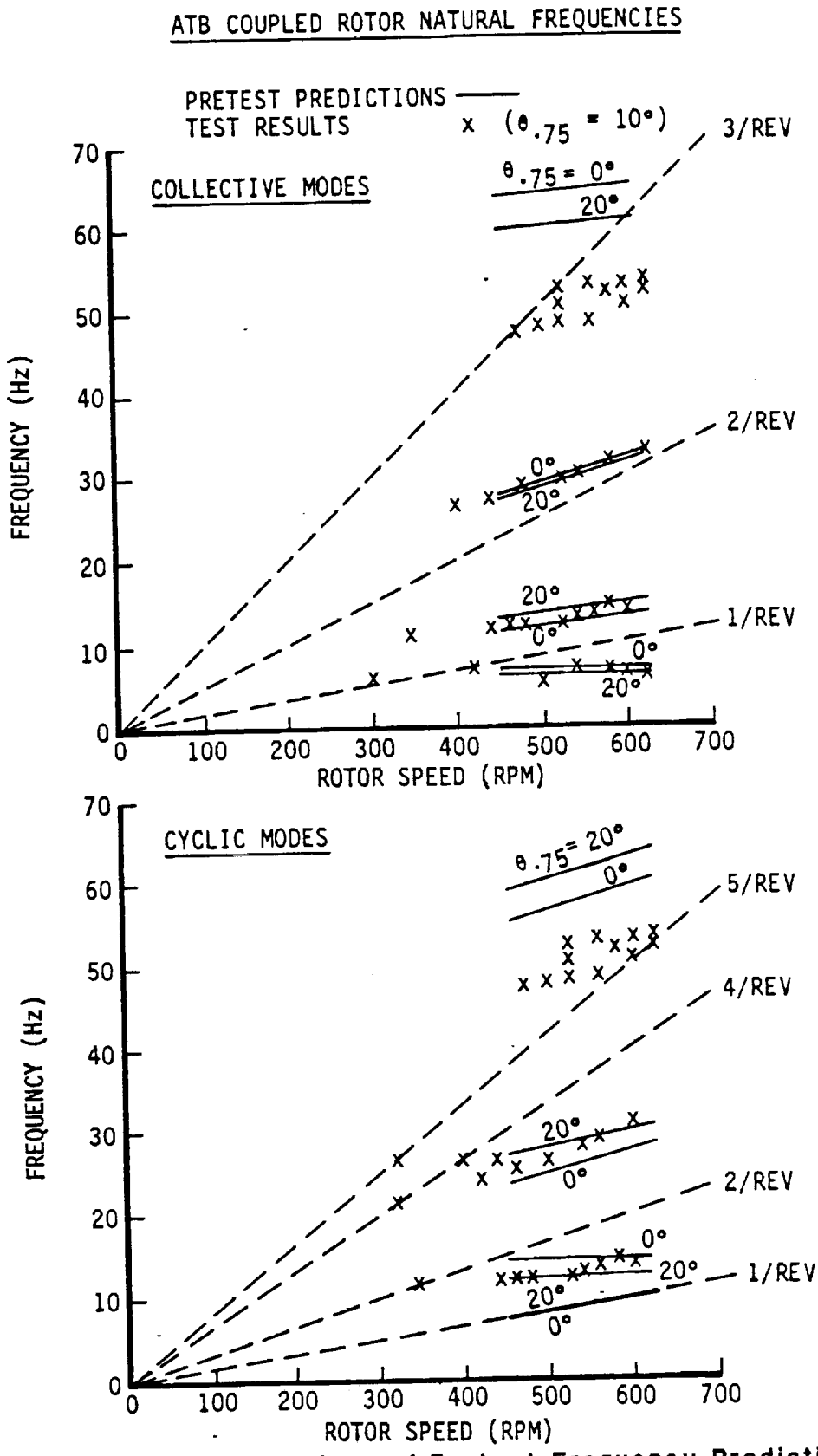

Figure 3.14 Comparison of Pretest Frequency Predictions with Per Rev Crossings and Spectral Analysis Peaks for Collective and Cyclic Modes

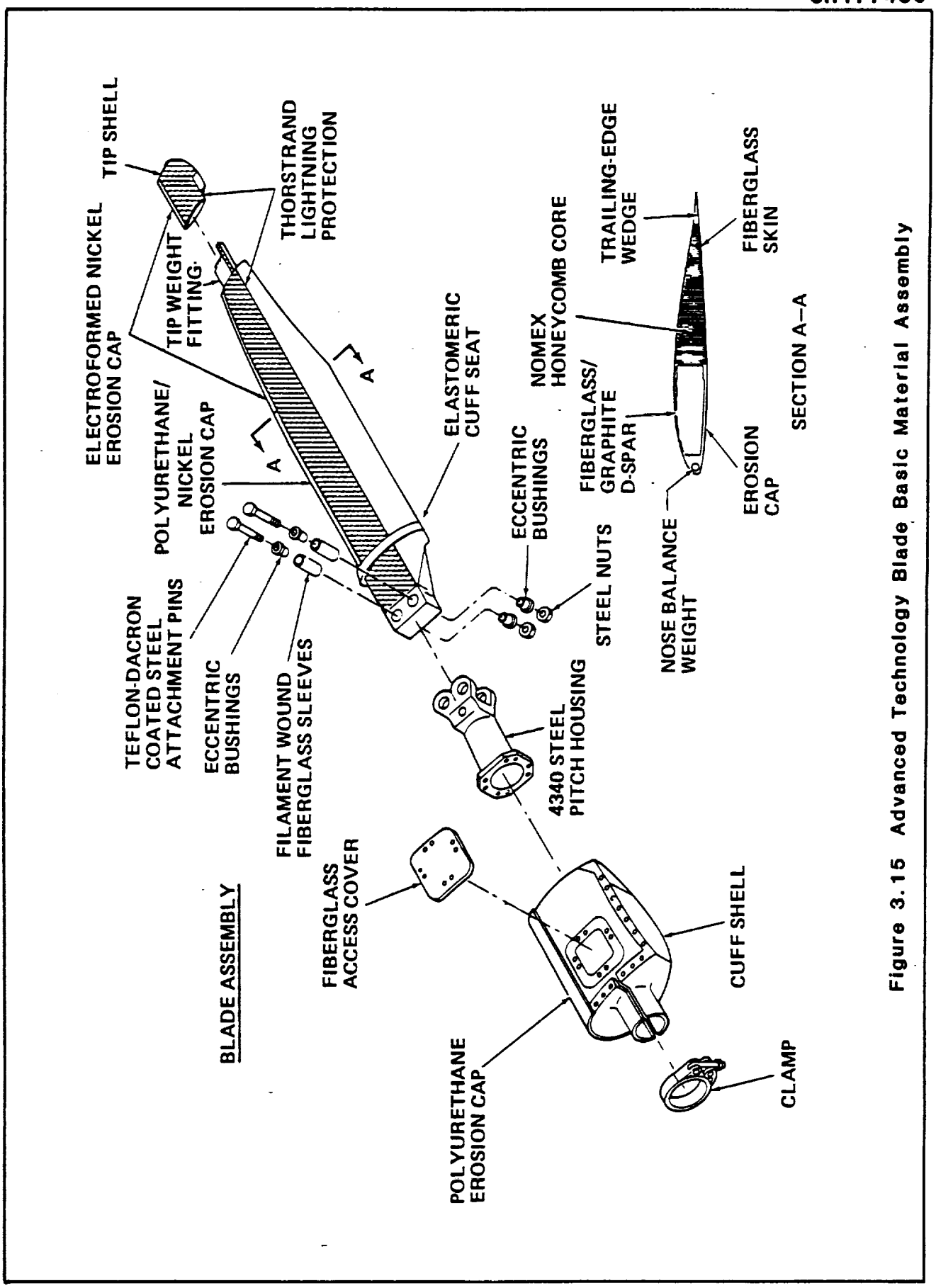

Figure 3.15 Advanced Technology Blade Basic Material Assembly

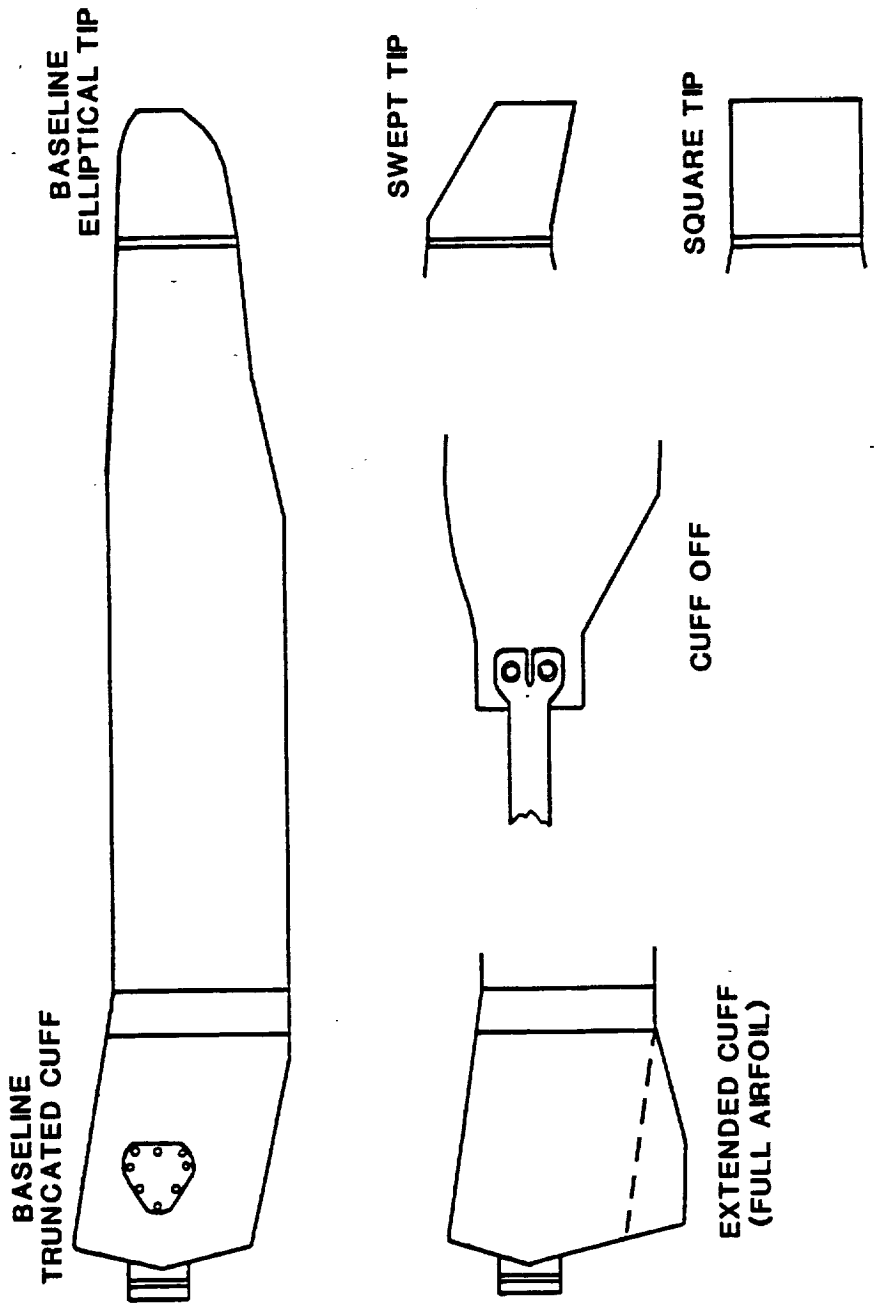

Figure 3.16 Baseline ATB with Alternate Tip and Cuff Configurations

3.6.2 XV-15 Rotor

The XV-15 blades tested in this program were the same full scale blades that had been previously tested by Bell Helicopter Textron Corporation on the Wright Patterson Air Force Base (WPAFB) whirl tower during the XV-15 development program (Reference 4). The planform, twist, airfoil and thickness/chord distributions are shown in Fig. 3.17.

4.0 INSTRUMENTATION

4.1 Instrumentation - General

The instrumentation installed for the ATB and XV-15 steel blade tests is indicated in Figure 4.1. This shows the type of data measured and which variables were monitored for safety. All data was recorded on magnetic tape. All non-steady state variables were subject to high speed sampling.

4.2 Rotor Balance Instrumentation

The rotor balance was instrumented to measure six components of rotor force and moment: thrust, sideforce, normal force, pitching moment, yawing moment, and rolling moment. Thrust and rolling moment measurements were significantly more sensitive than the others, as indicated in Table 3.1. The drive shaft flexible coupling was instrumented to measure torque and axial force. The balance rolling moment (bearing friction torque) was subtracted from the shaft torque to provide the net rotor torque. The drive shaft axial force was added to the balance thrust measurement to give the rotor thrust. Balance temperature was continuously monitored by thermocouples.

4.3 Blade and Hub Instrumentation

The instrumented blade was strain gaged to measure torsion, flap bending, and chord bending at the radial stations shown in Table 4.1. All gages were mounted on the spar beneath the airfoil contour.

Hub instrumentation was provided to measure control system position ($\theta_{.75}$, A_1, B_1), hub gimbal angles, root collective, pitch-link load, and hub yoke moments. Transducers were installed in the rotating system (hub and drive system) to measure the following:

(a) Blade pitch angle - measured by a potentiometer mounted on the blade housing. The potentiometer was a custom-fit resistance element with wiper arm.

(b) Hub gimbal angle - measured by a potentiometer attached to the gimbal inside the hub.

(c) Hub yoke bending moments - measured by strain gages mounted on the hub spindles; both flapwise and chordwise gages were provided.

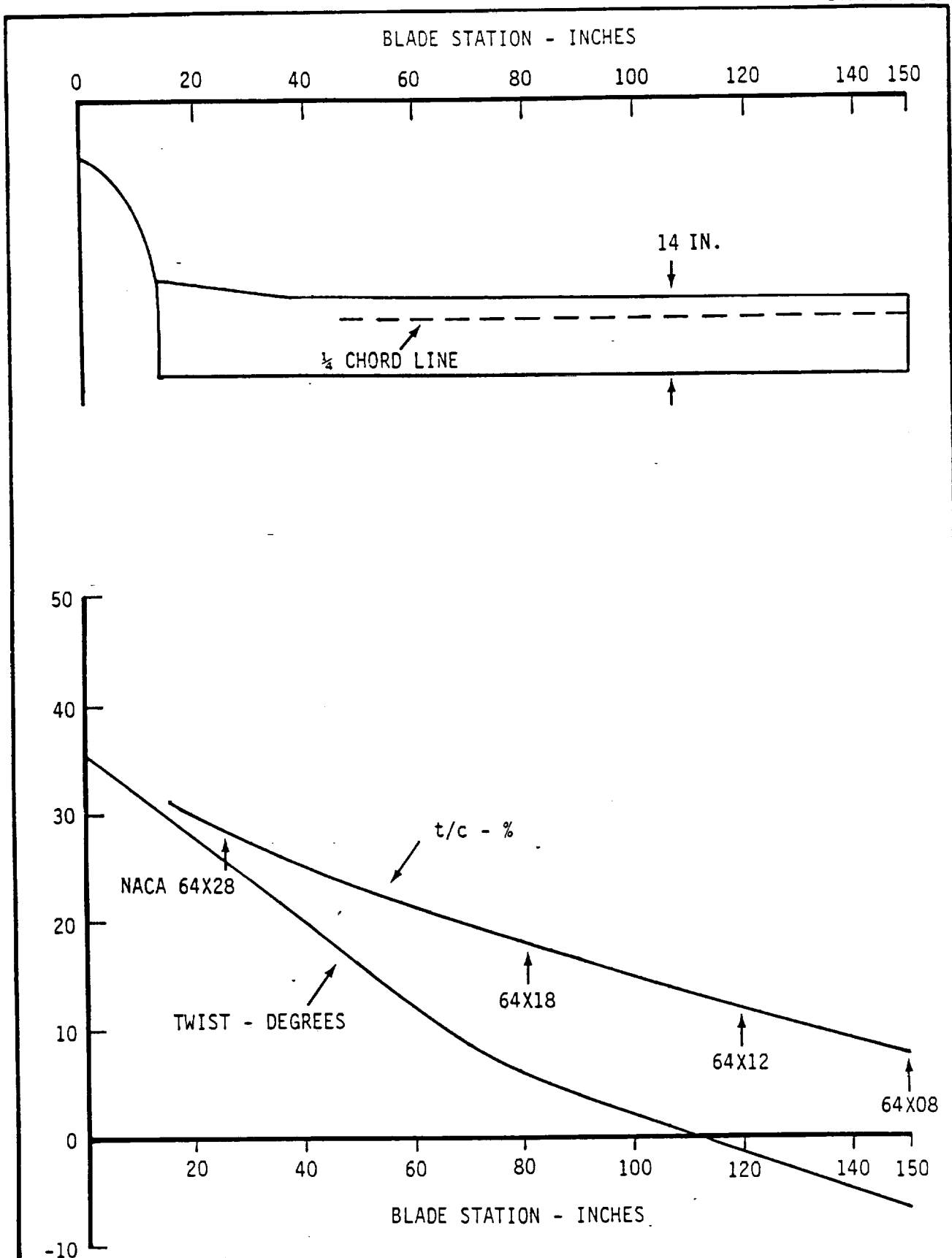

Figure 3.17 Planform, Twist, and Airfoil Distributions for XV-15 Blades

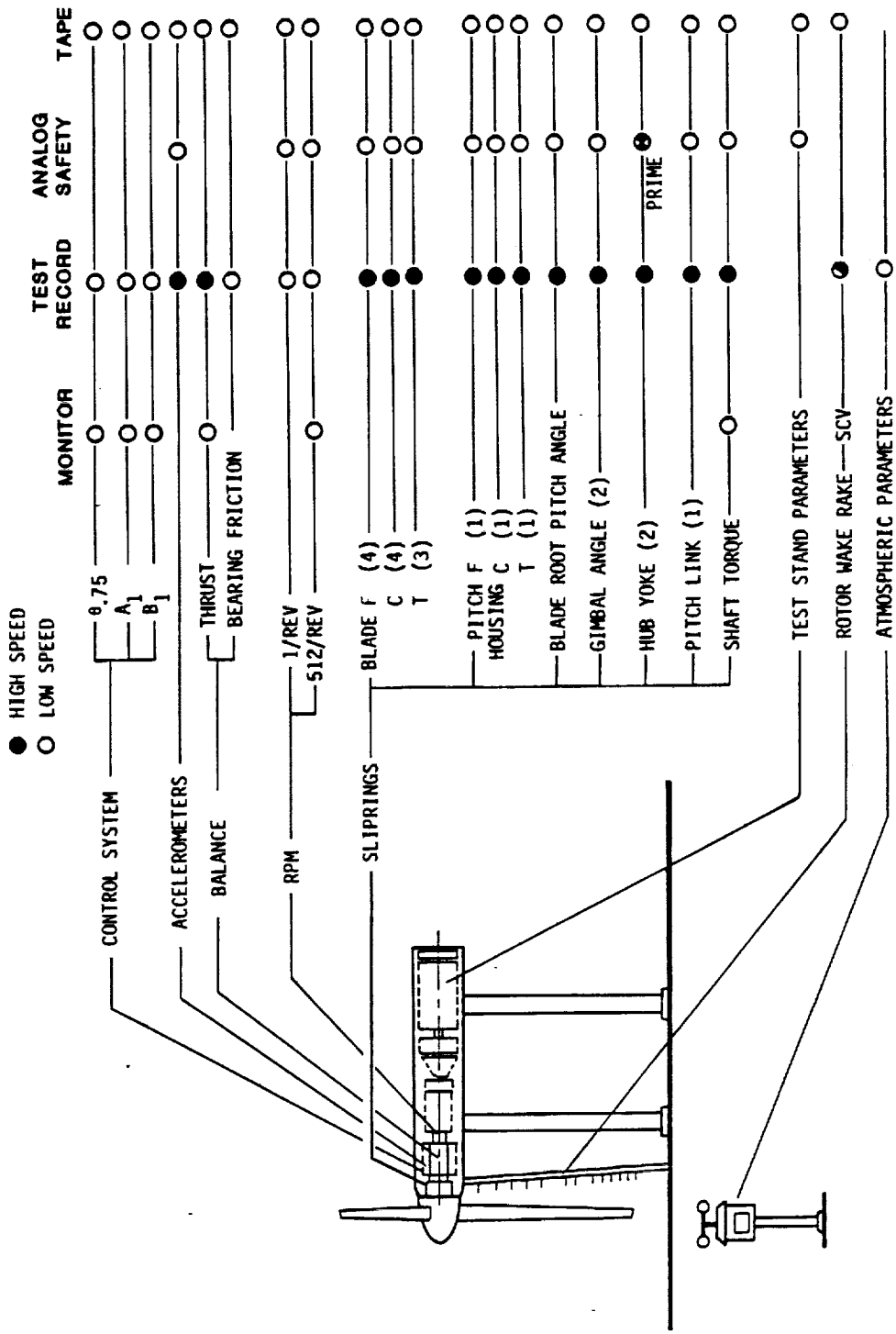

Figure 4.1 Summary of Instrumentation

Table 4.1 Placement of Blade Strain Gages

	PERCENT RADIUS					
FLAP	10.0[1]	20.6	29.0	49.0	69.0	84.0
CHORD	10.0[1]	20.6	30.0	50.0	70.0	85.0
TORSION	—	—	30.0	51.0	71.0	—

NOTE: 1) ON PITCH HOUSING

2) ON HUB SPINDLE THERE WERE IN- AND OUT-OF-PLANE BENDING GAGES AT 6% RADIUS

3) SEE RUN LOG FOR ADDITIONAL INFORMATION

(d) Pitch link load - measured by a strain gage bridge on the pitch link.

(e) Flexible coupling torque - measured by strain gage bridges (active and spare) on the forward flexible coupling of the drive shaft.

(f) Flexible coupling axial load - measured by strain gage bridges on the forward flexible coupling.

(g) Forward shaft bending - measured by (2) perpendicular bending bridges mounted on the rotor shaft.

(h) Rotor 1/rev and 512/rev - measured by a phototachometer on the drive shaft.

(i) Hub acceleration - measured by accelerometers mounted on support structure near the hub.

The signals from the rotating system were transferred to the fixed system through a 48-ring slipring assembly. As configured, the test stand was limited to 10 channels on the slipring. For the hover performance test, the recorded parameters and their corresponding slipring channels requirements were as follows:

Parameter	Channels Required
*Shaft torque	1
*Shaft axial load (AFFLEX)	1
*Pitch housing flap bending @ r/R = .10	1
*Pitch housing chord bending @ r/R = .10	1
*Pitch link load	1
Root collective	1
*Gimbal angle	1
Blade flap bending @ r/R = .31	1
*Hub yoke chord bending	1
*Hub yoke flap bending	1

*Required for safety

Although only 10 channels were available on the slipring at any one time, these channels could be reassigned to read other strain gages, if desired.

4.4 Wake Rake

A wake rake consisting of 22 pitot-static tubes was mounted behind the rotor disc plane at the station corresponding to the wing upper surface. The purpose of the rake was to measure the isolated rotor slipstream velocities and angles under different rotor operating conditions and to use this data to understand the structure of the rotor slipstream and the wing download and its distribution. The wake rake was connected to a Scanivalve to measure the pressures. The wake rake and the spacing of the pitot-static tubes is shown in Fig. 4.2.

4.5 Anemometer

A wind speed and direction transducer was installed on a narrow tower approximately 200 feet north and 200 feet east of the rotor hub centerline. The indicator was on approximately the same level as the rotor hub. The signals from the transducer were fed to the data acquisition equipment in the control room.

4.6 Acoustical Measurements

Near-field and far-field noise levels were measured. The near-field microphone represented a point on the side of the fuselage of a typical tilt rotor in hover. Far-field noise was recorded by an array of microphones at 250 ft (76m) and 650 ft (198m) radius at 0, 15, 30 and 45 degrees behind the rotor disc.

5.0 DATA ACQUISITION AND REDUCTION

5.1 Data Acquisition

The NASA-Ames OARF data system provided signal conditioning and amplification for 50 data channels. Steady-state data were recorded on digital tape. A quick-look short-form print-out was provided at the end of each run and a detailed print-out was processed overnight. A monitor program displayed up to 15 steady-state parameters on the Test Engineer's CRT. Two analog tape recorders were used for safety monitoring and acquisition of dynamic data. Complete details of the assignments of the data acquisition equipment are given in References 2 and 5.

The following quantities were measured:

Rotor balance thrust, T (lb.)
Rotor balance normal force, NF (lb.)
Rotor balance side force, SF (lb)
Rotor balance pitching moment, PMB (in.lb.)
Rotor balance yawing moment, YMB (in.lb.)
Rotor balance rolling moment, RMB (in.lb.)
Load cell axial, normal, and sideforces (lb.)
Rotor RPM
Shaft torque (in.lb.)

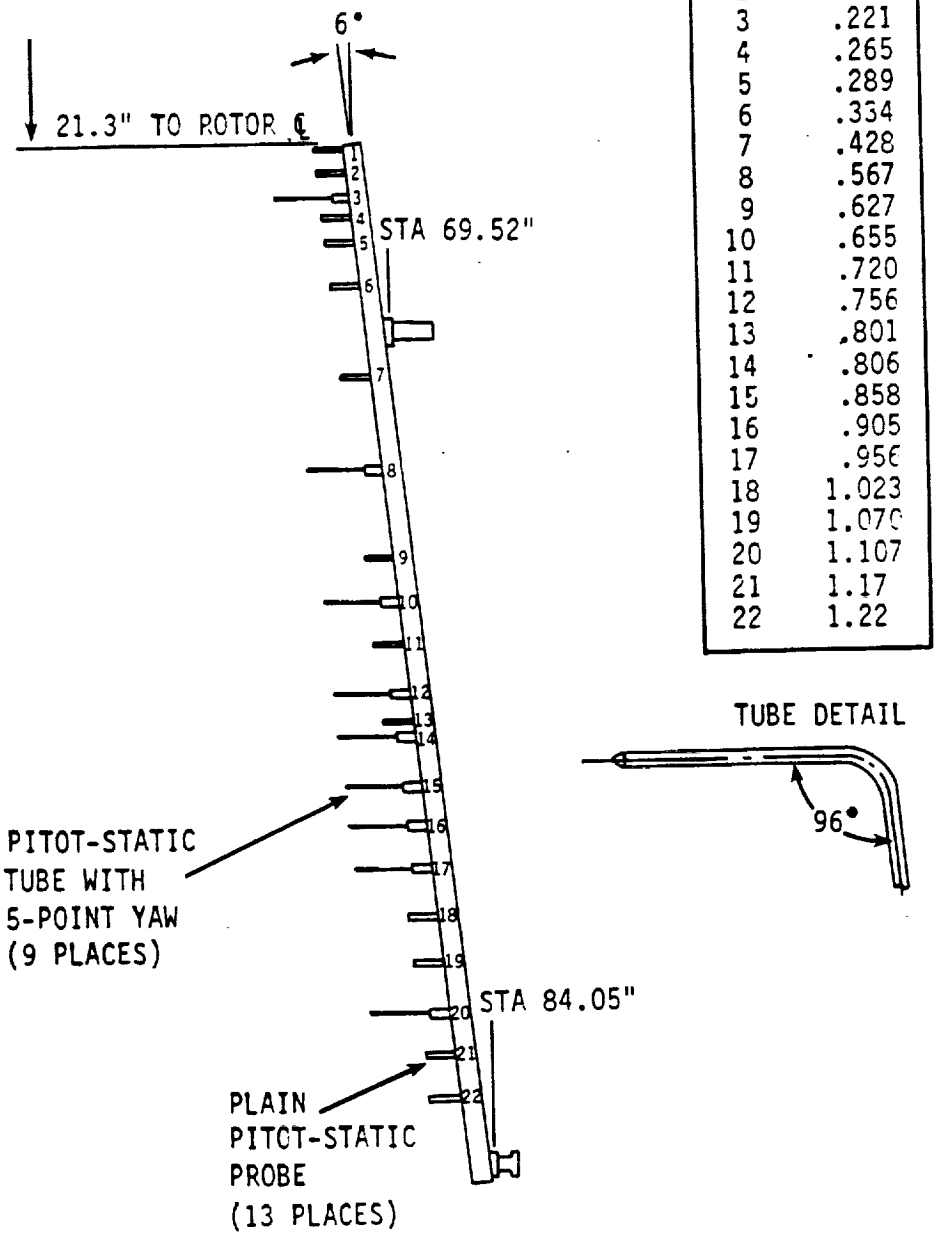

TUBE	r/R
1	.202
2	.205
3	.221
4	.265
5	.289
6	.334
7	.428
8	.567
9	.627
10	.655
11	.720
12	.756
13	.801
14	.806
15	.858
16	.905
17	.956
18	1.023
19	1.070
20	1.107
21	1.17
22	1.22

Figure 4.2 Wake Rake Details

Shaft axial load AFFLEX (lb.)
Hub gimbal angle, β (degrees)
Blade root collective, θ_0 (degrees)
Lateral cyclic (swashplate axes), A_1 (degrees)
Longitudinal cyclic (swashplate axes), B_1 (degrees)
Blade collective pitch, $\theta_{.75}$ (degrees)
Blade flap moment at 31% radius (in.lb.)
Blade chord moment at 10% radius (in.lb.)
Pitch housing flap moment at 10% radius (in.lb.)
Pitch housing chordwise moment (in.lb.)
Pitch-link load (lb.)
Ambient wind speed, V_{WIND} (knots)
Ambient wind azimuth, ψ_W (degrees)
Ambient temperature (°F)
Ambient barometric pressure (psi)
Relative humidity, (percent)
Hub horizontal acceleration (g)
Hub vertical acceleration (g)

5.2 Data Processing

The data reduction program (Reference 6) performed the following operations:

(a) Subtracted non-rotating zero values.

(b) Converted corrected voltages to engineering units.

(c) Computed rotor forces and moments from load cell readings.

(d) Computed rotor balance forces and moments from balance flexure outputs.

(e) Corrected rotor balance forces and moments for component interactions through the respective balance calibration matrices.

(f) Corrected rotor balance data for temperature effects, if significant.

(g) Corrected rotor balance thrust for flexible coupling axial load.

(h) Corrected rotor shaft torque for bearing friction (balance rolling moment).

(i) Transferred rotor balance data to the reference body axis (rotor hub centerline).

(j) Corrected rotor torque for wind effects, using the method presented in Appendix A.

(k) Computed atmospheric data from temperature, humidity, and pressure measured at the test site.

(l) From the corrected data, computed rotor parameters (V_{TIP} and M_{TIP}) and coefficients (C_T, C_P, etc.) as well as rotor horsepower and figure of merit.

Provisions were made to harmonically analyze all rotating parameters (blade, hub, shaft and control system) and vibratory balance flexure and fixed system accelerometer data at Boeing Vertol.

6.0 TEST RECORD AND DATA ACCURACY

The chronology of the testing is presented in Fig. 6.1 and the XV-15/ATB Test Run Log in Fig. 6.2. A rigorous calibration of the rotor balance had been performed at the place of manufacture before assembly of the propeller test rig at the OARF. Following installation of the rig at Ames, another calibration was made which included checks for thermal drift effects on balance readings and a determination of the interaction between the torque and axial forces at the flexible coupling. The contribution of the flexible coupling axial load (AFFLEX) was also determined. This accounts for approximately 4% of the net rotor thrust. This check calibration showed that the installed balance was behaving to specification and that the data obtained from the load cells was in close agreement with the balance data.

The XV-15 blades were installed, checked out, and testing commenced. Initial results indicated that the rotor performance was lower than expected. This was caused by an improper pretest procedure for obtaining R-cals in which the collective actuator was moved to maximum stroke and induced a false load indication in the balance. When this was understood, a new check calibration was performed using the minimum collective setting for zeroes. The results are presented in Figures 6.3 through 6.11. The check calibration was made with thrust and torque loads applied singly and in combination. The maximum applied thrust was 7000 lb. which corresponds to a C_T of .01 at hover RPM. At this condition the error in rotor thrust was only 0.03 percent, as read from the balance (Fig. 6.3). The load cell result was 0.4 percent off (Fig. 6.4). Some hysteresis is evident in both systems. Figures 6.5 and 6.6 present the variation of the difference between the actual and measured torque for a range of applied torque levels. The torque balance error is 0.3 percent (Fig. 6.5). The load cell check calibration shows considerable hysteresis compared to the balance (Fig. 6.6). Figures 6.7 and 6.8 present the variation of the difference between the applied and measured thrust at various torque levels, for a constant applied thrust of 7000 lb. Figures 6.9 and 6.10 show the variation between the applied and measured torque with a constant applied thrust of 7000 lb. The errors are essentially the same as for the case with zero torque applied. Figure 6.11 shows the effect of RPM on the correlation of balance and load cell thrust.

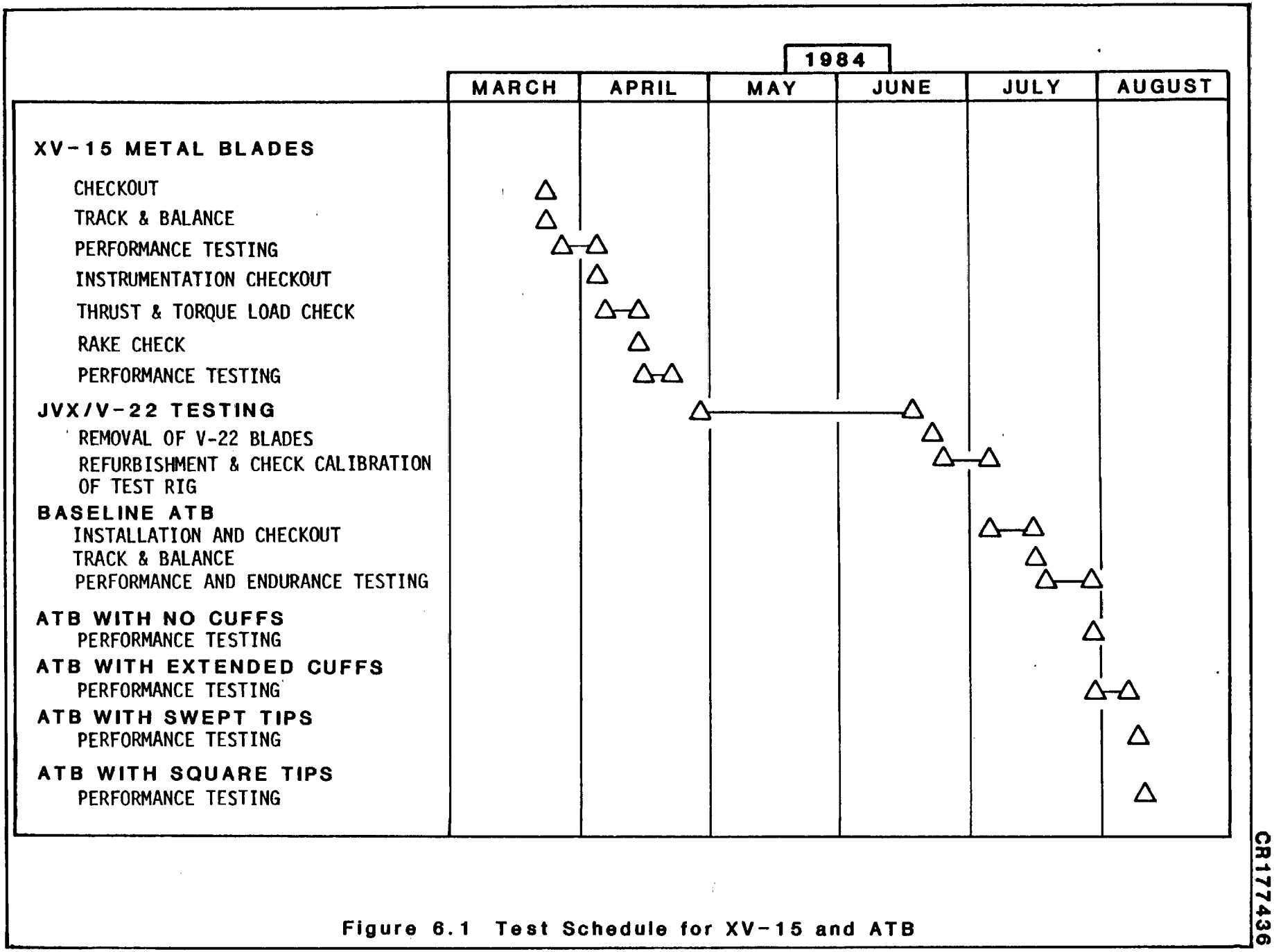

Figure 6.1 Test Schedule for XV-15 and ATB

CR177436

RUN NO.	CONFIGURATION CODE	TYPE OF RUN	WT TARE RUN	RPM	$\theta_{.75}°$	$A_{1_C}°$	$B_{1_C}°$	M_{TIP}	AVG. WIND - KTS					DATE	TIME
1	XV-15 METAL BLADE, SPINNER OFF	CHECK OUT	--	75, 178	4	0	0							3/22/84 3/23	
2	↓		--	SWEEP	VARY	TRIM 1.51	TRIM -0.37							3/27	0745 1100 1200
3	↓	TRACK	--	584	5 10	TRIM 1.51	TRIM -0.37							3/28	0615 0633
3 (CONT.)	XV-15 METAL BLADE + SPINNER	TRACK CHECK	--	600, 589	SWEEP	TRIM 1.5	TRIM -0.10							3/29	0615 0803
4	↓	PERFORM-ANCE	--	585	↓	TRIM 0.19	TRIM 0.16	0.691	1 TO 2					3/30	0609 0643
5	↓	↓	--	584	↓	TRIM 0.15	TRIM 0.62	↓	3 TO 4					4/2	0652 0737
6	↓	↓	--	585	↓	TRIM 0.15	TRIM 0.62	↓	↓					4/2	0741 0800
7	↓	↓	--	586	SWEEP -7 TO +11	TRIM 0.16	TRIM 0.63	↓	↓					4/2	0803 0828
8	↓	↓	--	587	SWEEP -7 TO +11	-0.53 -0.65 -0.61	-0.15 0.60 0.60	↓	3					4/2	0835 0857

TEST ENGINEER'S NOTES

RUN 1 SPINNER NOT ON. COULD NOT GET HARDWARE TO FIT. RUN CONTINUED ON 3/23 UP TO 400 RPM - CONTROL CONSOLE GIMBAL ANGLE NOT WORKING. DID EMERGENCY SHUTDOWN AND BROKE THE GIMBAL ANGLE POT.

RUN 2

TP	RPM	$\theta_{.75}$
11	500	5°
12	550	↓
13	584	↓
14		↓
15		6°
16		7°
17		↓
18		8°
19	590	↓
20		9°
21		↓
22		10°
23		11°
24		12°

TP 1→10 ARE ZERO POINTS AND RCAL POINTS. DID 2 START UPS AND SHUTDOWNS FOR 1 PER REV PROBLEMS.

RUN 3 UP TO 584 RPM AT $\theta_{.75}$ = 5° TRIMMED OUT ROTOR USING BLADE LOADS. GIMBAL ANGLE POT NOT WORKING. CHECKED TRACK. GREEN BLADE FWD, WHITE BLADE AFT. INCREASED $\theta_{.75}$ TO 10°. CHECKED TRACK AGAIN. LOOKS THE SAME. BALANCE RM WENT OVER 100% ALLOWABLE. ALSO SAW HIGH VIBRATION ON TEST STAND MONITORING EQUIPMENT. SHUT DOWN FOR INVESTIGATION.

RUN 3 (CONT.) UP TO 600 RPM TO CHECK TRACK AT $\theta_{.75}$ = 5° AND 10°. LOOKS OK. SHUT DOWN FOR NEW ZEROS. BACK UP TO 555 RPM AT $\theta_{.75}$ = 5° M.G. SET DROPPED OFF-LINE. SHUT DOWN AT 0652. BACK UP AT 0732. DID A $\theta_{.75}$ SWEEP FROM -2° TO +10° BY 2° INCREMENTS. NOTE $\theta_{.75_{MIN}}$ = -3.4°.

RUN 4 DID A WARM-UP RUN AT 577 RPM AND $\theta_{.75}$ = 5°. CAME DOWN FOR NEW ZERO POINT AND BACK UP TO 585 RPM. $\theta_{.75}$ = -3.5°, -2°, 0°, 2°, 4°, 6°, 8° LOST BLADE ANGLE AT TP 6. GIMBAL ANGLE OUT FOR ENTIRE RUN. SHUT DOWN DUE TO HIGH HUBYOK 1 AND 2 LOADS. TP = 3, 4, 5, 5, 7, 8, 9

RUN 6 DID A WARM-UP RUN AT 587 RPM FOR 5 MINUTES. TOOK NEW ZEROS AND BACK UP TO 584 RPM. $\theta_{.75}$ = -7.5°, -6°, -4°, -2°, 0°, 2°, 4°, 6°, 8°, 9°, 10°, 11°, 12°, 13°

RUN 6 $\theta_{.75}$ = -7.5°, -5.5°, -3.5°, -1.5°, 0.5°, 2.5°, 4.5°, 6.5°, 8.5°, 10.5°, 11.5°, 12.5°, 13.5° BLADES STALL AT $\theta_{.75}$ = 14°.

MODEL IDENTIFICATION: XV-15 METAL BLADE AT NASA AMES O.A.R.F. TEST 910

Figure 6.2 XV-15 and ATB Test Run Log

RUN NO.	CONFIGURATION CODE	TYPE OF RUN	WT TARE RUN	RPM	$\theta_{.75}^{\circ}$	$A_{1_C}^{\circ}$	$B_{1_C}^{\circ}$	M_{TIP}	AVG. WIND - KTS					DATE	TIME
9	XV-15 METAL BLADE + SPINNER	PERFORMANCE	--	582	SWEEP -7 TO+11	TRIM	TRIM	0.691	3					4/3	0607 0641
10	↓	↓	--	584	↓	↓	↓	↓	1					↓	0703 0726
11	↓	↓	--	587	↓	↓	↓	↓	1					↓	0734 0755
12	↓	↓	--	622	↓	↓	↓	0.733	2					↓	0800 0825
13	↓	↓	--	588	↓	↓	↓	0.691	2					4/4	0642 0739
14	CHECK CASES														
15	XV-15 METAL BLADE + SPINNER	PERFORMANCE	--	587	SWEEP -7 TO+11	TRIM	TRIM	0.691	2					4/5	0605 0809
16	↓	↓	--	FOR M_{TIP}	SWEEP 5,8,10,12	↓	↓	SWEEP	4					↓	0855 0943
17	INSTRUMENTATION CHECK-OUT													4/6	

TEST ENGINEER'S NOTES

RUN 13 HAD A HARD OVER ON LONG. CYCLIC JUST BEFORE SHUTDOWN. WENT FROM 0.60° TO -4° AND STAYED THERE DURING SHUTDOWN. LOST GIMBAL ANGLE AND BLADE ANGLE ON THE WAY DOWN.

RUN 16 COLLECTIVE SWEEP AT EACH M_{TIP} OF 0.6, 0.663, 0.691, 0.733

MODEL IDENTIFICATION: XV-15 METAL BLADE AT NASA AMES O.A.R.F. TEST 910

Figure 6.2 XV-15 and ATB Test Run Log (Continued)

RUN NO.	CONFIGURATION CODE	TYPE OF RUN	WT TARE RUN	RPM	$\theta_{.75}°$	$A_{1_C}°$	$B_{1_C}°$	M_{TIP}						DATE	TIME
18	THRUST CHECK LOAD													4/10	
19	↓													4/10	
20	THRUST AND TORQUE CHECK LOADS													4/11	
21	RAKE CHECK-OUT													4/12	
22	XV-15 METAL BLADE + SPINNER	PERFORMANCE	--	583	SWEEP	TRIM 0	TRIM 0.49	0.691						4/13	0605 0641
23	↓	↓	--	584	↓	TRIM 0	TRIM 0.51	0.691						↓	0646 0724
24	↓	↓	--	FOR M_{TIP}	↓	TRIM	TRIM	0.733, 0.60, 0.62, 0.65						↓	0743 0843
25	↓ + RAKE	RAKE	--	586	↓	TRIM 0.26	TRIM 0.07	0.691						4/16	0615 0746
26	↓	↓	--	586	↓	TRIM 0.26	TRIM -0.21	0.689						↓	0800 0822

TEST ENGINEER'S NOTES

RUN 25 WAKE RAKE IN POSITION

EDITOR'S NOTE: RUN NUMBERS 27, 28, AND 29 WERE NOT USED FOR TEST 910. THE XV-15 METAL BLADES WERE REMOVED AFTER RUN 26 AND TEST 910 WAS SUSPENDED FOR DURATION OF JVX PROGRAM (TEST 911). TEST 911 CONTINUED THE RUN NUMBER SEQUENCE FOR THE FIRST THREE RUNS AND THEN SWITCHED TO A NEW SEQUENCE. THUS, TEST 910 RESUMES AT RUN 30 WITH ATB TESTING.

MODEL IDENTIFICATION: XV-15 METAL BLADE AT NASA AMES O.A.R.F. TEST 910

Figure 6.2 XV-15 and ATB Test Run Log (Continued)

RUN NO.	CONFIGURATION CODE	TYPE OF RUN	WT TARE RUN	RPM	$\theta_{.75}^{\circ}$	$A_{1_C}^{\circ}$	$B_{1_C}^{\circ}$	M_{TIP}		COMPUTER DATA	RAKE DATA	DATA BEGINS AT TP NO.		DATE	TIME
30	ATB+RAKE $B^{1}001,002,003$ SPINNER OFF	CHECK OUT T AND B	--	589	10	1.0	-0.5	.677		YES	--	--		7/16/84	0638 0652
31			--	589	VARY	TRIM	TRIM	.677			--	3			1134 1215
32	SPINNER ON	PERF. DATA	--	569				.663			YES	5		7/17	0755 0823
33			--	571				.663			YES	3			0841 0912
34		CHECK LOAD	--	--	--	--	--	--		--	--	--		7/18	
35			--	--	--	--	--	--		--	--	--			
36	$B^{1.1}001,002,003$	PERF. DATA	--	569	(1)	TRIM	TRIM	.663		YES	NO	3		7/19	0749 0831
37	$B^{1}001,002,003$		--	596	(1)	TRIM	TRIM	.692		YES	YES	3			0919 0955
38		BLADE FREQ.	--	VARY	10	NOTE	NOTE	VARY		NO	NO	--			1103 1128

TEST ENGINEER'S NOTES

RUN 30 TRACK NOT CORRECTED AT THIS STAGE - TOO LIGHT FOR ADEQUATE DEFINITION. CHECK DATA POINT AT $\theta_{.75} = 10^{\circ}$

RUN 31 TRACK CHECKED AT $\theta_{.75} = 10^{\circ}$ AFTER P.L. ADJUSTMENT AND TIPS PAINTED (FLUORESCENT PAINT). TRACK AND BALANCE OK. COLLECTIVE SWEEP FOR LOADS DATA - NO WARM-UP RUN, SO PERF. DATA NOT VALID. $\theta_{.75} = -2^{\circ} \rightarrow +16^{\circ}$.

RUN 32 SPINNER FITTED. 1ST SWEEP $7^{\circ} \rightarrow 19^{\circ}$, $\Delta 2^{\circ}$, 2ND SWEEP $7.5^{\circ} \rightarrow 17.5^{\circ}$, $\Delta 2^{\circ}$; TRIP BEFORE DATA AT 19.5°. NEW WOZ, R-CAL, RESTART UNDER RUN 33.

RUN 33 1ST SWEEP $8^{\circ} \rightarrow 18^{\circ}$, $\Delta 2^{\circ}$; SECOND SWEEP $8.5^{\circ} \rightarrow 18.5^{\circ}$, $\Delta 2^{\circ}$.

RUN 36 (1) $\theta_{.75} = -4^{\circ} \rightarrow 13^{\circ}$, $\Delta 2^{\circ}$; $-3^{\circ} \rightarrow 19^{\circ}$. NO SCANIVALVE DATA, P-CAL NOT OPERATIONAL.

RUN 37 ALUM. TAPE REMOVED FROM NOTCHES. WIND APPROX. 5 KTS THIS RUN. 'ODD' ANGLE RANGE LIMITED TO $15^{\circ} \rightarrow 19^{\circ}$, $\Delta 2^{\circ}$, $+19.3^{\circ}$.

RUN 38 RPM = 300 → 625 x 25's. ROTOR ALLOWED TO BE OUT OF TRIM BY $\pm 1^{\circ}$ (FOR CYCLIC EXCITATION)

B^{1} 001,002,003: BLADES WITH BASELINE TIPS, CUFFS, FLIGHTWORTHY

$B^{1.1}$ T.E. NOTCHES AT CUFF JUNCTION SEALED WITH ALUM. TAPE

MODEL IDENTIFICATION: ATB AT NASA AMES O.A.R.F. TEST 910

Figure 6.2 XV-15 and ATB Test Run Log (Continued)

RUN NO.	CONFIGURATION CODE	TYPE OF RUN	WT TARE RUN	RPM	$\theta_{.75}^{\circ}$	$A_{1_C}^{\circ}$	$B_{1_C}^{\circ}$	M_{TIP}		COMPUTER DATA	RAKE DATA	DATA BEGINS AT TP NO.		DATE	TIME
39	ATB + RAKE B[1]001,002,003 SPINNER ON	BLADE FREQ.	--	VARY	10	NOTE	NOTE	VARY		YES	YES	--		7/20	0615
40		PERF. DATA	--	591	(1)	TRIM	TRIM	.691				4			0651 0720
41			--	592	(2)	TRIM	TRIM	.691				3			0735 0825
41 (CONT.)	(A)	BLADE FREQ.	--	VARY	10	NOTE	NOTE	VARY				29			0945
42			--									3			1035
43			--								NO	3		7/21	0623 0640
44		PERF. DATA	--	625	(3)	TRIM	TRIM	.734				3			0653
44 (CONT.)	(A)	ENDURANCE RUN	--			AS SPECIFIED				NO	NO	--			0725 0733
44 (CONT.)	(B)	PERF. DATA (CONT.)	--		(3)	TRIM	TRIM			YES	YES	15			0735

TEST ENGINEER'S NOTES

RUN 39 RPM = 323

RUN 40 $\theta_{.75}$ = -4° TO 12° ONLY. CB10 100% ALLOWABLE REACHED.

RUN 41 (2) : $\theta_{.75}$ = -4°→12°, Δ4°; 12°→18°, Δ2°; -3.5°→8.5°, Δ4°, 8.5°→18.5°, Δ2°; -3°→9°, Δ4°; 9°→17°, Δ2°, +18.5°. PERF. DATA TO TP 28.

RUN 41 (CONT.) TP 29→ RPM = 300→580, Δ20 RPM; LAT. CYCLIC INPUT = ±1° GIMBAL ANGLE FOR EXCITATION. CYCLIC INPUT CHANGED TO LONGITUDINAL AT TP 38.

RUN 42 CONTINUATION OF RPM SWEEP FOR BLADE FREQ. DATA. A_1 = 0°, B_1 = +1.0° FOR EXCITATION. 580→ 625 x 20 RPM.

RUN 44 (3) : $\theta_{.75}$ = -4.5°, -4°→16°, Δ2°, +17.5°; END PERF. DATA AT TP 14.

RUN 44 (CONT.)(A) ENDURANCE RUN BEGINNING AT 0725. INPUT CYCLIC 2.5° EVERY 4 MINS (OR LESS IF NECESSARY TO RESTRICT GIMBAL ANGLE TO ±2.5°. ALTERNATING CYCLIC INPUTS. COMPLETE AT 0733 AS WINDS FAVORABLE FOR PERF. RUN.

RUN 44 (CONT.)(B) CONTINUE PERF. RUN TP 15→40. $\theta_{.75}$ = -3.5°, -1.5°→6.5°, Δ4°; 6.5°→16.5°, Δ2°; -3°→+5°, Δ4°; +5°→17°, Δ2°; -2.5°→5.5°, Δ4°, 5.5°→15.5°, Δ2°

MODEL IDENTIFICATION: ATB AT NASA AMES O.A.R.F. TEST 910

Figure 6.2 XV-15 and ATB Test Run Log (Continued)

RUN NO.	CONFIGURATION CODE	TYPE OF RUN	WT TARE RUN	RPM	$\theta_{.75}°$	$A_{1_C}°$	$B_{1_C}°$	M_{TIP}		COMPUTER DATA	RAKE DATA	DATA BEGINS AT TP NO.		DATE	TIME
44 (CONT.)	(C) ATB+RAKE $B^1$001,002,003 SPINNER ON	PERF. DATA	--	591	4	TRIM	TRIM	.689		YES	YES	41		7/21	0833
44 (CONT.)	(D)		--	600	5			.701				48			0850 0858
45			--	601	4			.705			NO	3		7/23	0725
45 (CONT.)	(A)		--	614	6			.72				12			0742
45 (CONT.)	(B)		--	622	6			.729				30			0806
45 (CONT.)	(C)		--	626	6			.733				47			0829
46		ENDURANCE RUN	--	565	8	NOTE	NOTE	.661		NO		--			1029 1134
47	SPINNER OFF		--	625	8			.733				--		7/24	0656 0802
48			--	625	7			.733				--			0802 0903

TEST ENGINEER'S NOTES

RUN 44 (CONT.)(C) PERF. RUN AT RPM = 591 (M_T = .689). 4 : $\theta_{.75}$ = -4^0, $4^0 \rightarrow 12^0$, $\Delta 4^0$; 12^0, 14^0, 16^0, 18^0.

RUN 44 (CONT.)(D) PERF. RUN AT RPM = 600 (M_T = .701). 5 : $\theta_{.75}$ = -4^0, 0^0, 4^0, 8^0.

RUN 45(A) 6 : $\theta_{.75}$ AS 4 THEN: -3^0, $+1^0$, 5^0, $9^0 \rightarrow 15^0$, $\Delta 2^0$, 16^0, 17^0.

RUN 46 ENDURANCE RUN: RUN AT TRIMMED CYCLIC FOR 4 MINS., THEN DO CYCLIC SWEEP TO PRODUCE ± 2^0 OF GIMBAL ANGLE; REPEAT ETC, ALTERNATING LAT. AND LONG. CYCLIC INPUTS (HOLDING MAX + AND - CYCLICS FOR 10 SECS).

RUN 47 SPINNER OFF THIS RUN - REMOVED FOR REPAIR OF SURFACE CRACKS. CYCLIC INPUTS AS RUN 46.

RUN 48 ENDURANCE RUN AT $\theta_{.75}$ = 7^0. CYCLIC INPUTS AS RUN 46.

MODEL IDENTIFICATION: ATB AT NASA AMES O.A.R.F. TEST 910

Figure 6.2 XV-15 and ATB Test Run Log (Continued)

RUN NO.	CONFIGURATION CODE	TYPE OF RUN	WT TARE RUN	RPM	$\theta_{.75}$°	A_{1_C}°	B_{1_C}°	M_{TIP}		COMPUTER DATA	RAKE DATA	DATA BEGINS AT TP NO.	BLADE LAG ANGLE	DATE	TIME
49	ATB+RAKE B^{1}001,002,003 SPINNER OFF	ENDURANCE RUN	--	625	9	NOTE	NOTE	.733		NO	NO	--	-1°	7/24	1221
50	SPINNER ON	PERF. MAX C_T	--	561	7	TRIM	TRIM	.663		YES	YES	3	-1°		0639
50 (CONT.)	(A)		--	500	7			.589				13	-1°		0710
50 (CONT.)	(B)		--	500	8			.589				25	-1°		0732
50 (CONT.)	(C)		--	566	9			.663				40	-1°		0759 0814
51		ENDURANCE RUN	--	625	9	NOTE	NOTE	.733		NO	NO	--	-1°		0941 1045
52			--	625	11			.733				--	-1°		1046
53	ATB+RAKE $B^{1.2}$001,002,003	PERF. LOADS DATA	--	566	10	TRIM	TRIM	.662		YES	YES	--	-1°	7/27	0805 0852
54			--	566	10 NOTE			.665				--	0°	7/28	0639 0709

TEST ENGINEER'S NOTES

RUN 50 7 $\theta_{.75} = 0^{\circ} \rightarrow 18^{\circ}$, $\Delta 2^{\circ}$ (TORQUE LIMIT) $\rightarrow$ T.P. NO. 12.

RUN 50 (A) AS RUN 50 WITH $\theta_{.75} = 20^{\circ}$, 22° ADDED. ATTEMPTED $\theta_{.75} = 23^{\circ}$. STALL ON ROTOR. NO DATA.

RUN 50 (B) 8 $\theta_{.75} = 1^{\circ} \rightarrow 21^{\circ}$, $\Delta 2^{\circ}$, $21.5^{\circ} \rightarrow 23^{\circ}$, $\Delta 0.5^{\circ}$.

RUN 50 (C) 9 $\theta_{.75} = 0^{\circ}$, $5^{\circ} \rightarrow 19^{\circ}$, $\Delta 2^{\circ}$.

RUN 51 CYCLIC INPUTS AS RUN 46.

RUN 52 CYCLIC INPUTS AS RUN 46.

RUN 53 SK 29643-1, -2 BUSHINGS 10 : $\theta_{.75} = 0^{\circ} \rightarrow$ MAX., $\Delta 2^{\circ}$. MAX. VALUE 19° (TORQUE LIMIT). SHAFT BENDING ALLOWABLE. RAPID SHUTDOWN.

RUN 54 SK 29643-1, -2 BUSHINGS DATA ONLY AT $\theta_{.75} = 2^{\circ}$, 6°, 10°, 14°, 16° THIS RUN.

$B^{1.2}$ BLADE CUFFS OFF. GREEN TAPE ROUND BLADE ROOT END TO FAIR IRREGULARITIES AND SECURE WIRING.

MODEL IDENTIFICATION: ATB AT NASA AMES O.A.R.F. TEST 910

Figure 6.2 XV-15 and ATB Test Run Log (Continued)

RUN NO.	CONFIGURATION CODE	TYPE OF RUN	WT TARE RUN	RPM	$\theta_{.75}$°	A_{1_C}°	B_{1_C}°	M_{TIP}		COMPUTER DATA	RAKE DATA	DATA BEGINS AT TP NO.	BLADE LAG ANGLE	DATE	TIME
55	ATB+RAKE $B^{1.3}$001,002,003 SPINNER ON	PERF. DATA	--	565	11	TRIM	TRIM	.663		YES	YES		-1°	7/30	0632 0751
55 (CONT.)	(A)		--	625	NOTE			.734							0819 0838
56		NOISE (+PERF.)	--	565, 625	NOTE			.661 .729							0939 1006
57	--	BLADE CALIB., ESTESC.	--	--	--	--	--	--		--	--			8/2	--
58	SPINNER ON	LOADS DATA	--	568	NOTE	TRIM	TRIM	.663		YES	NO	3			1012 1026 1015 1036
58 (CONT.)	(A)		--	592				.690				6			
58 (CONT.)	(B)		--	626				.729				11			
59	ATB+RAKE B^{2}001,002,003	PERF. DATA	--	565	12	FOR TRIM	FOR TRIM	.663			YES	5		8/6	0706 0737
60			--	566	13			.664				3			0749 0832

TEST ENGINEER'S NOTES

RUN 55 11 $\theta_{.75} = 0^{\circ} \rightarrow 18^{\circ}$, $\Delta 2^{\circ}$; $0.5^{\circ} \rightarrow 18.5^{\circ}$, $\Delta 2^{\circ}$, $+20^{\circ}$; $1.0^{\circ} \rightarrow 19^{\circ}$, $\Delta 2^{\circ}$; $1.5^{\circ} \rightarrow 19.5^{\circ}$, $\Delta 2^{\circ}$.

RUN 55 (A) DATA AT 625 RPM. DATA BEGINS AT TP NO. 50. $\theta_{.75} = 0^{\circ} \rightarrow 14^{\circ}$, $\Delta 2^{\circ}$, ONLY.

RUN 56 $\theta_{.75} = 0^{\circ} \rightarrow 16^{\circ}$, $\Delta 4^{\circ}$, (+ AT 625, 17°)

RUN 58 NEW EXTERNAL GAUGE (FB92) ON TIP OF S/N 003. 003FB84 REPLACED 001FB84. 1 T.P. ONLY (NO. 5) AT $\theta_{.75} = -3^{\circ}$. (COLLECTIVE RANGE RESET PRIOR THIS RUN NOW $-4^{\circ} \rightarrow 20.5^{\circ}$)

RUN 58 (A) $\theta_{.75} = -1.5^{\circ}, 0^{\circ}, 4^{\circ}, 8^{\circ}, 12^{\circ}$

RUN 59 B^{2} : BLADES WITH SWEPT TIPS (ALTERNATE TIP, -1). 12 : $\theta_{.75} = 0^{\circ} \rightarrow 16^{\circ}$, $\Delta 2^{\circ}$; $1^{\circ} \rightarrow 15^{\circ}$, $\Delta 2^{\circ}$.

RUN 60 13 : $\theta_{.75} = -3^{\circ}, -1^{\circ}, 0.5^{\circ} \rightarrow 16.5^{\circ}$, $\Delta 2^{\circ}$; $-0.5^{\circ}, 1.5^{\circ} \rightarrow 15.5^{\circ}$, $\Delta 2^{\circ}$.

$B^{1.3}$ MODIFIED CUFFS (SHARP T.E.). T.E. NOTCHES FILLED. CUFF/BLADE JOINT DISCONTINUITY FAIRED WITH WAX.

MODEL IDENTIFICATION: ATB AT NASA AMES O.A.R.F. TEST 910

Figure 6.2 XV-15 and ATB Test Run Log (Continued)

RUN NO.	CONFIGURATION CODE	TYPE OF RUN	WT TARE RUN	RPM	$\theta_{.75}°$	$A_{1_C}°$	$B_{1_C}°$	M_{TIP}		COMPUTER DATA	RAKE DATA	DATA BEGINS AT TP NO.	BLADE LAG ANGLE	DATE	TIME
01	ATB+RAKE $B^2$001,002,003 SPINNER ON	PERF. DATA	--	625	14	FOR TRIM	FOR TRIM	.730		YES	YES	3	-1°	8/6	0908 0936
02	ATB+RAKE $B^3$001,002,003	↓	↓	566	15	↓	↓	.663		↓	↓	7	↓	8/7	0701 0732
03	↓	↓	↓	571		↓	↓	.663		↓	↓	7	↓	↓	0826 0911
	END OF TEST														

TEST ENGINEER'S NOTES

RUN 01 (14) : $\theta_{.75} = 0^0 \rightarrow 14^0$, $\Delta 2^0$; $1^0 \rightarrow 13^0$, $\Delta 2^0$.

RUN 02 B^3 : BLADES WITH -2 RECTANGULAR ALT. TIP. (15) : $\theta_{.75} = -1^0$, $2^0 \rightarrow 10^0$, $\Delta 2^0$; $1^0 \rightarrow 7^0$, $\Delta 2^0$.

MODEL IDENTIFICATION: ATB AT NASA AMES O.A.R.F. TEST 910

Figure 6.2 XV-15 and ATB Test Run Log (Continued)

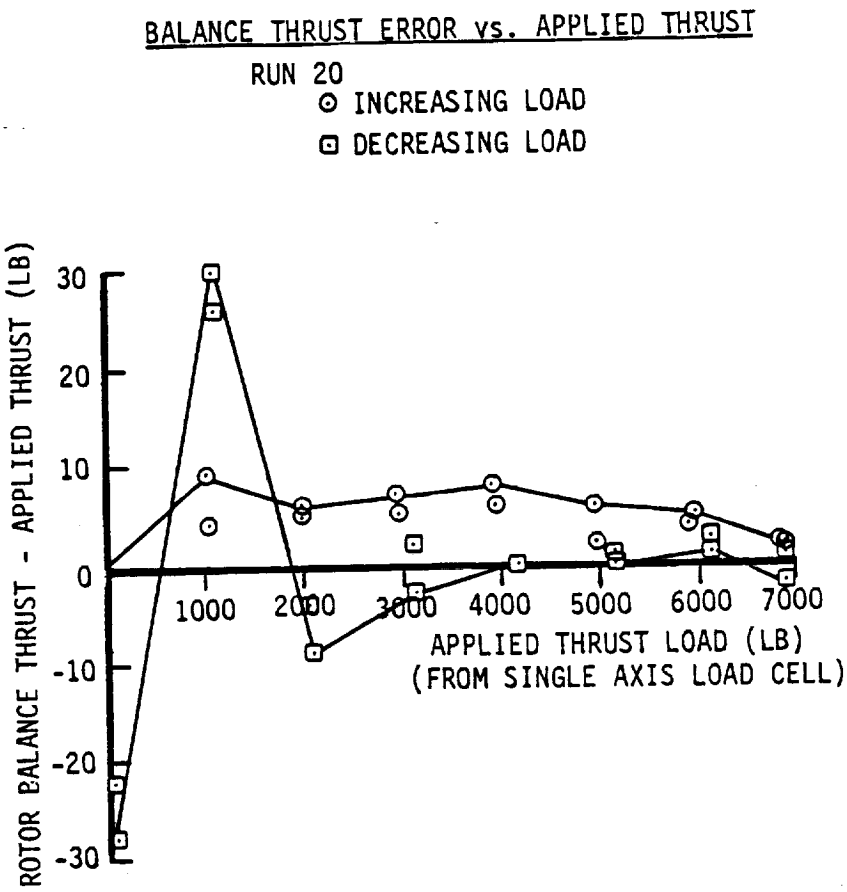

Figure 6.3 Check Calibration Results: Thrust (From Rotor Balance)

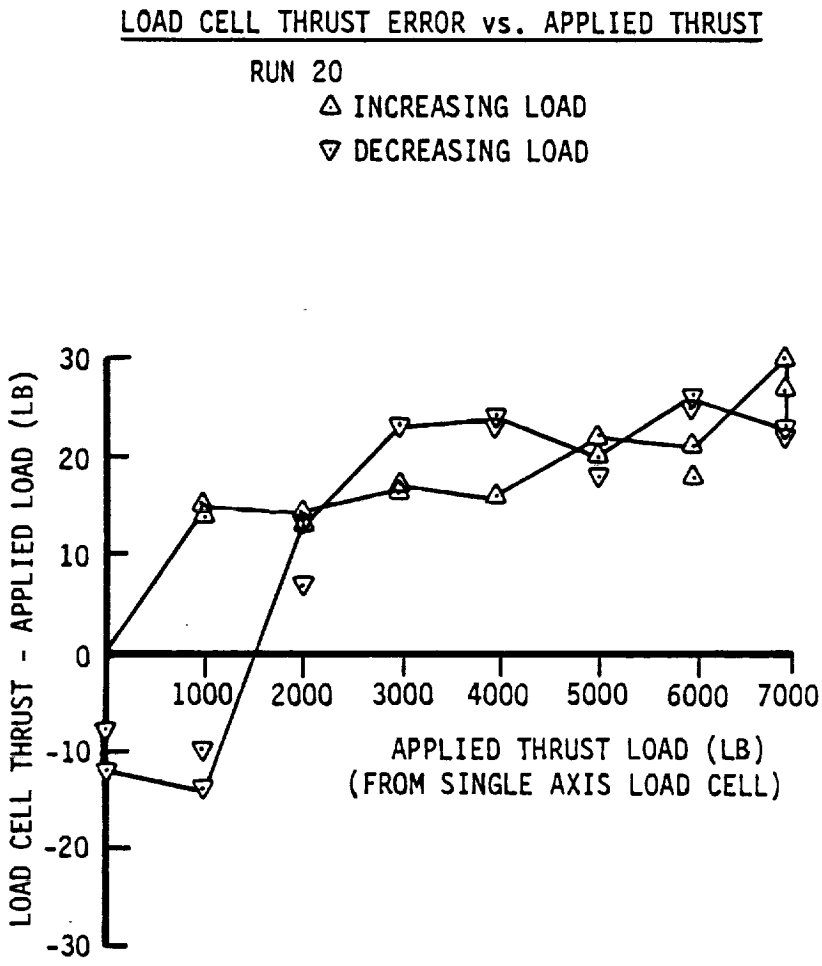

Figure 6.4 Check Calibration Results: Thrust (From NASA Load Cells)

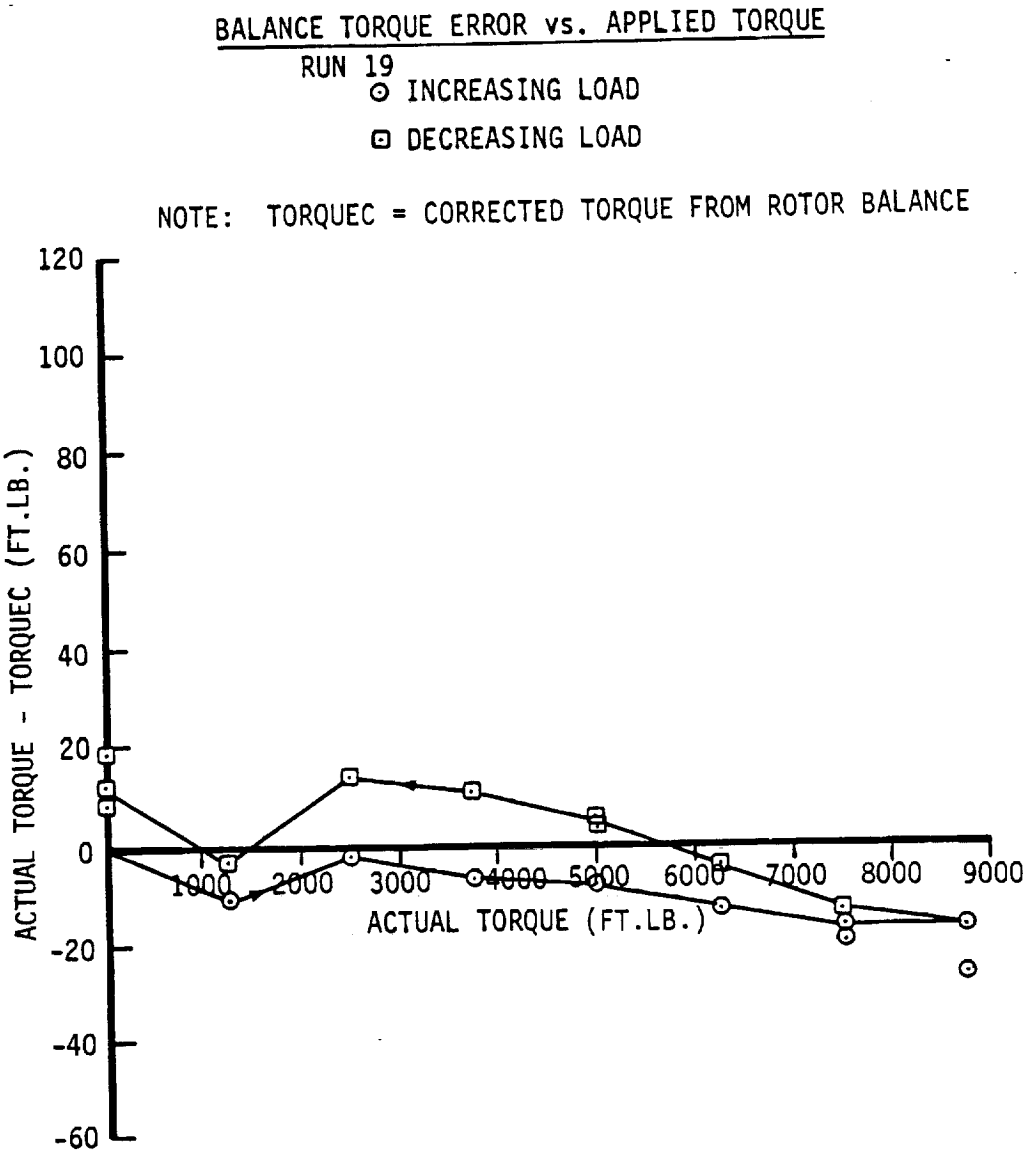

Figure 6.5 Check Calibration Results: Torque (From Rotor Balance)

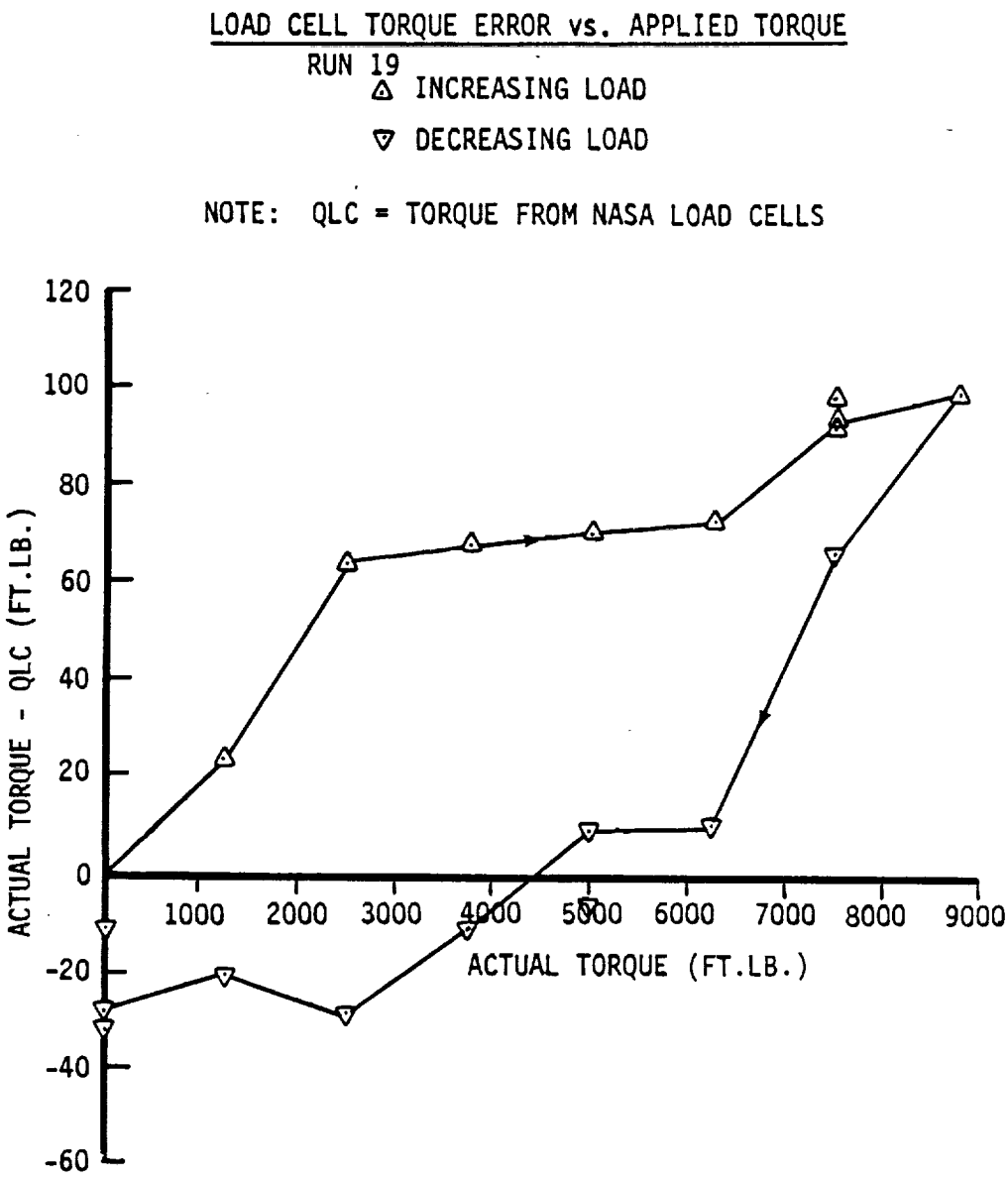

Figure 6.6 Check Calibration Results: Torque (From NASA Load Cells)

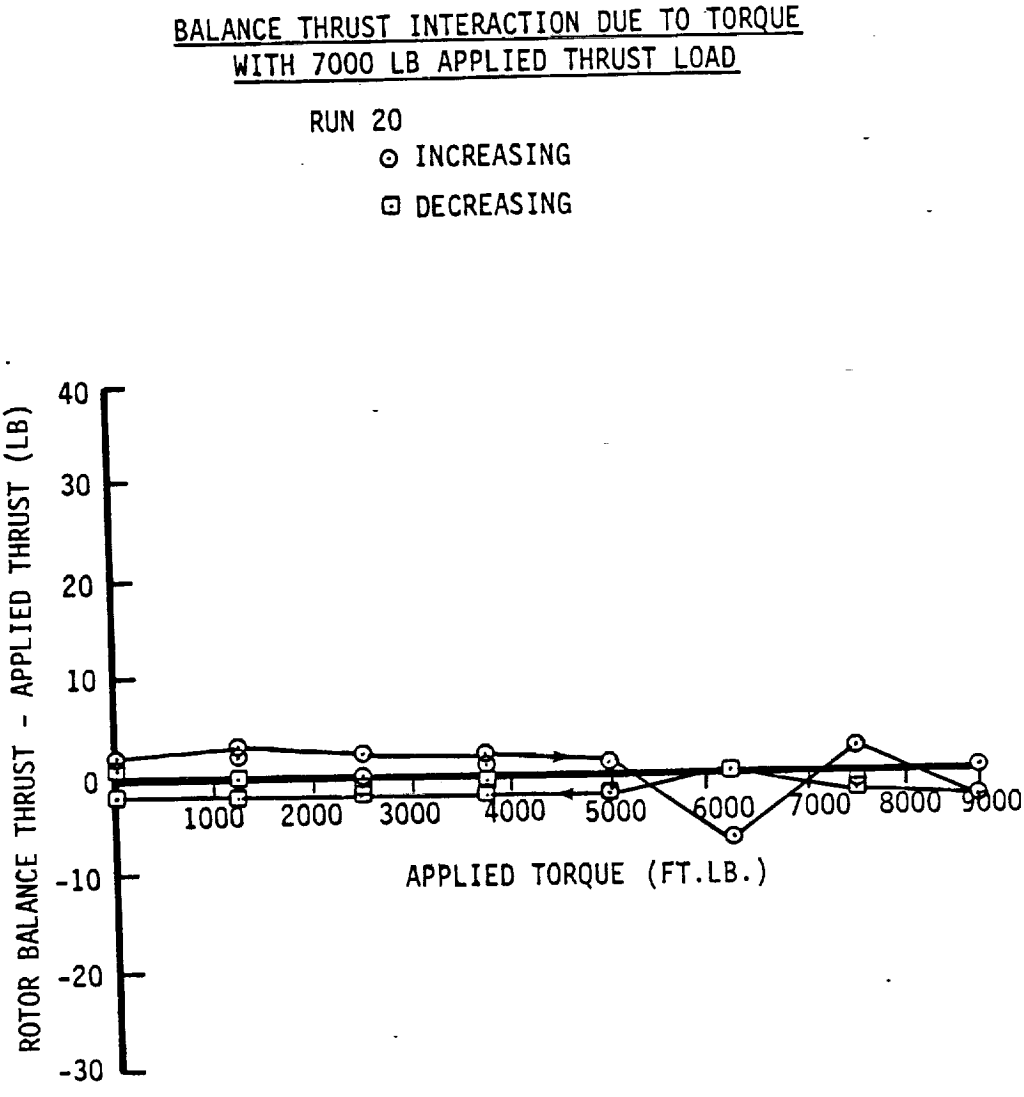

Figure 6.7 Check Calibration Results: Thrust with Torque Load Applied (From Rotor Balance)

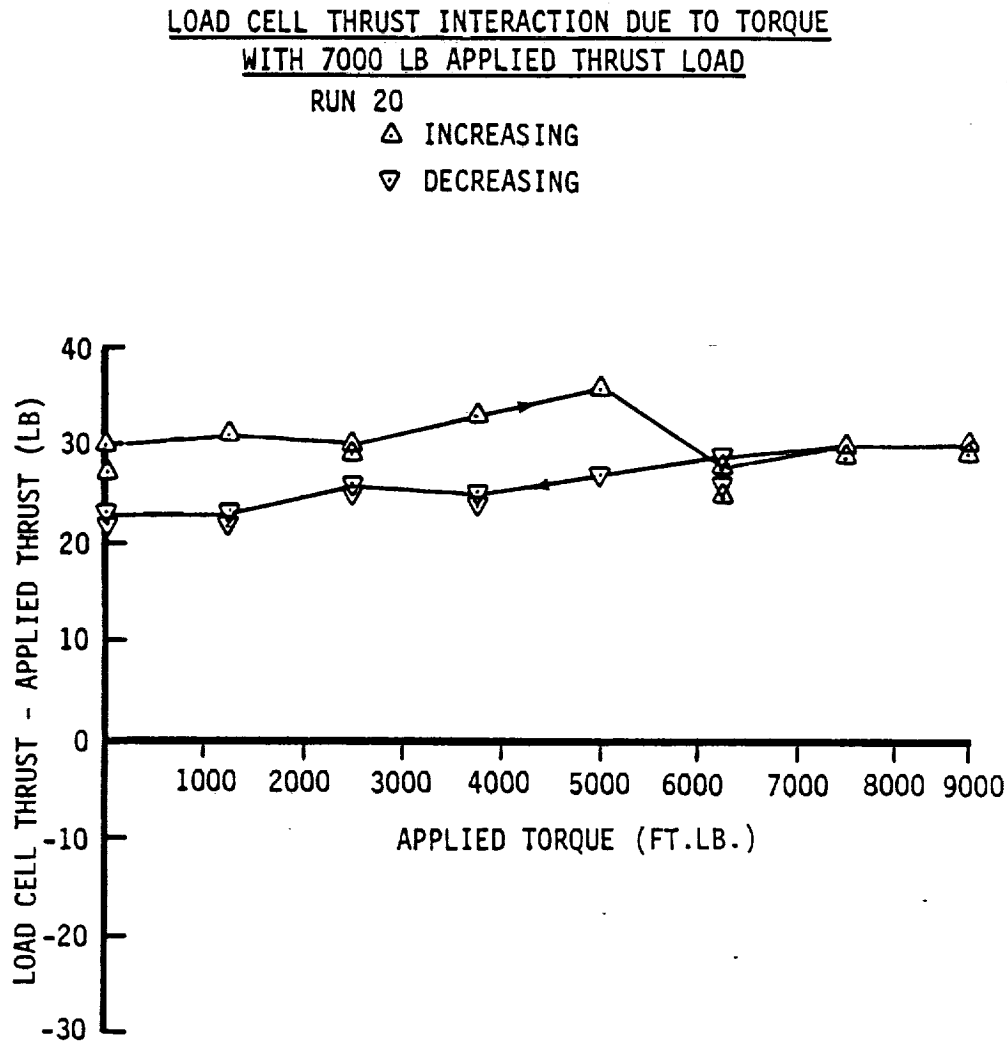

Figure 6.8 Check Calibration Results: Thrust with Torque Load Applied (From NASA Load Cells)

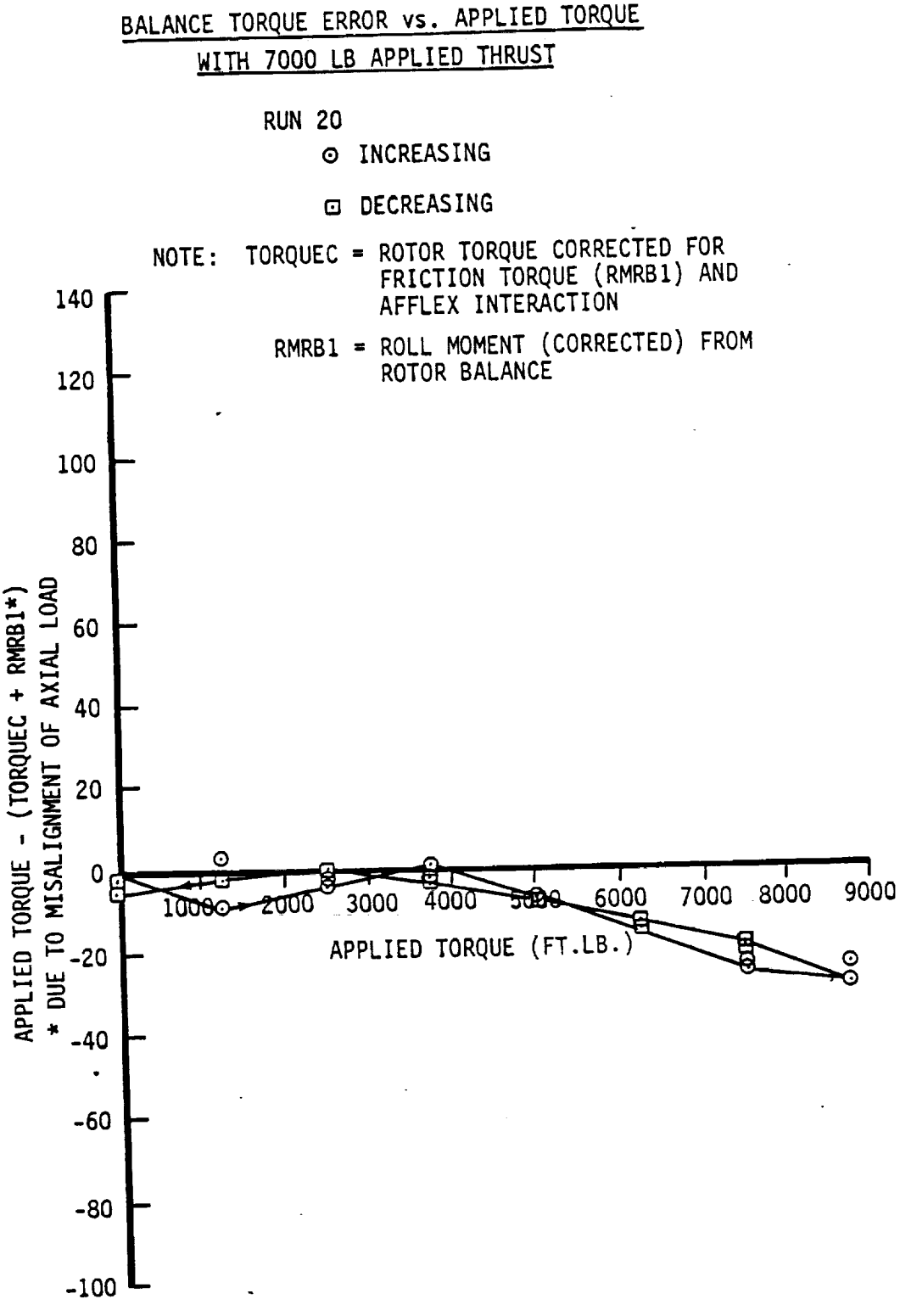

Figure 6.9 Check Calibration Results: Torque with Thrust Load Applied (Corrected for Friction Torque and AFFLEX Interaction)

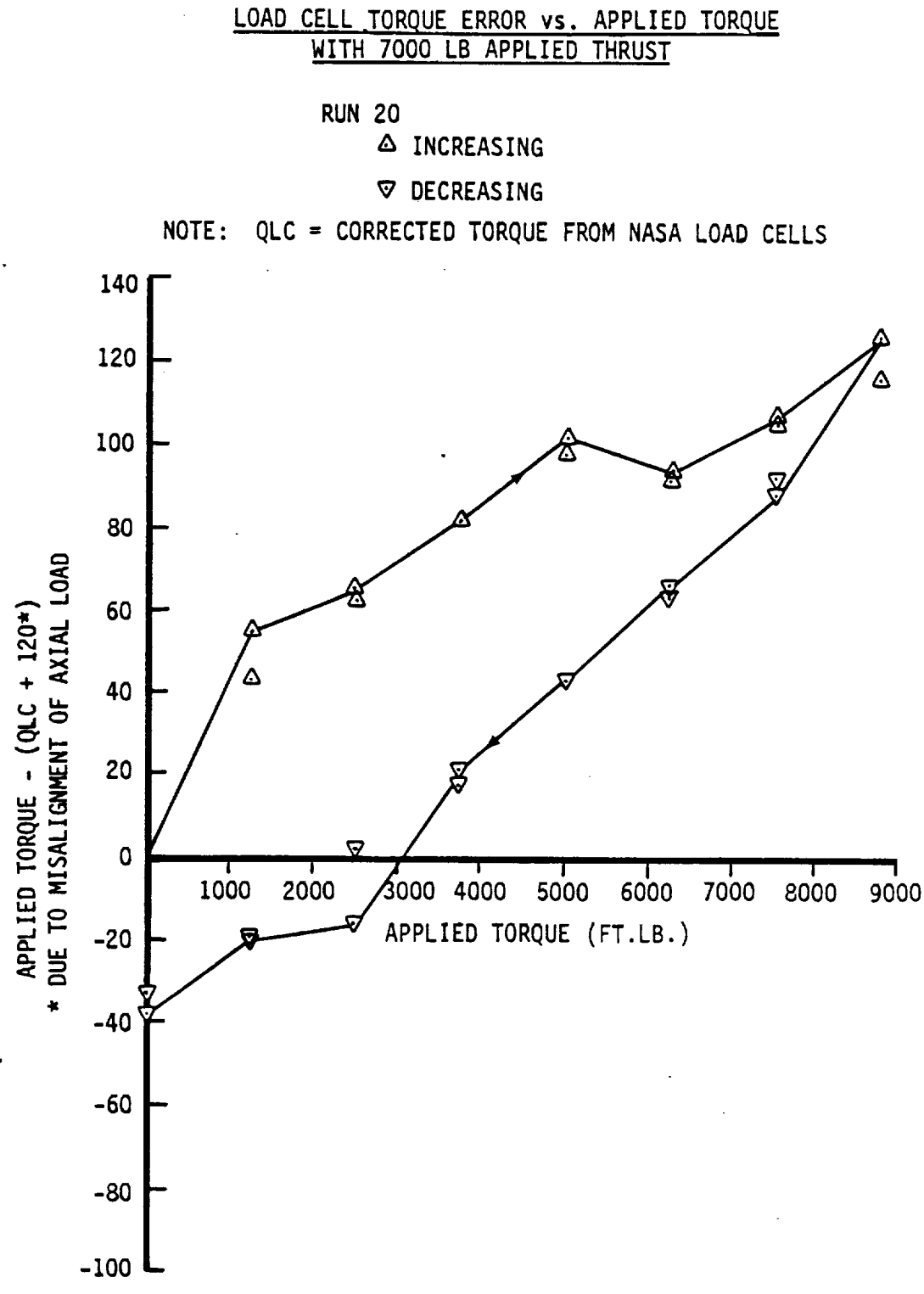

Figure 6.10 Check Calibration Results: Torque with Thrust Load Applied (From NASA Load Cells)

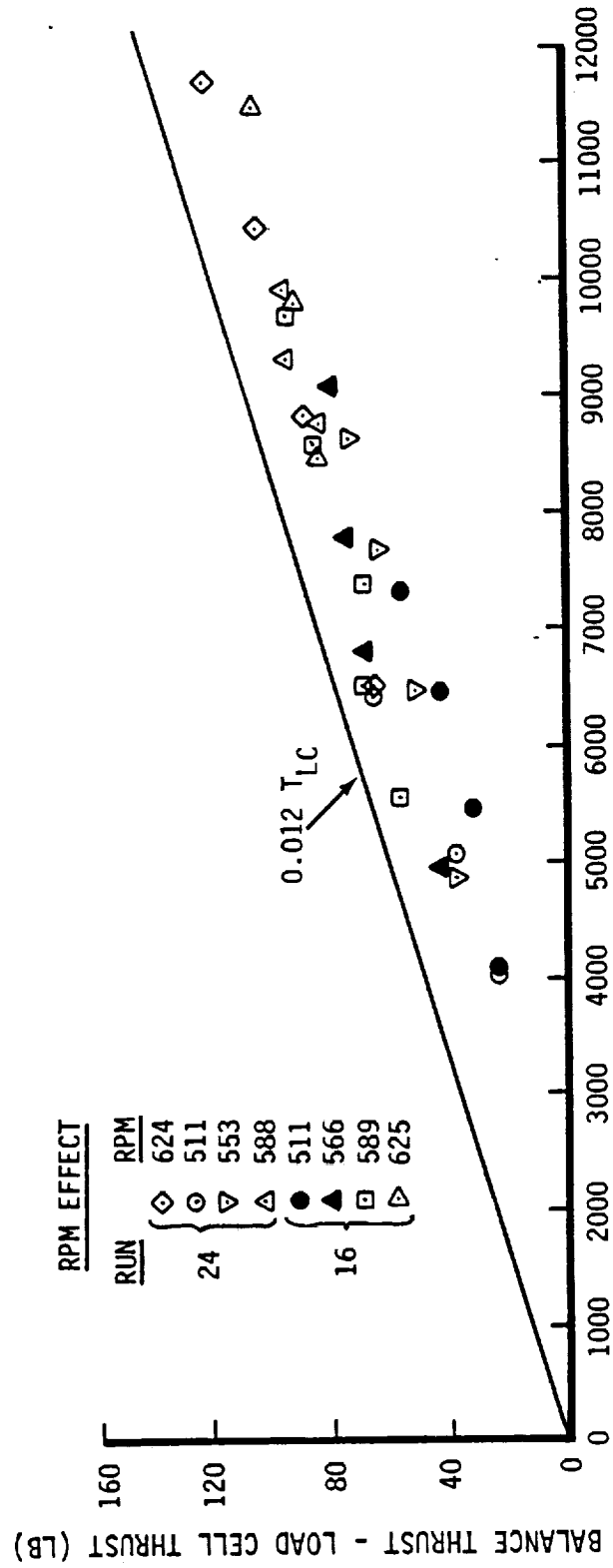

Figure 6.11 Effect of RPM on the Correlation of Balance Thrust with Load Cell Thrust

The rake to measure rotor induced velocity was installed and calibrated toward the end of the XV-15 blade testing and only a limited amount of such data is available for these blades.

At the completion of the benchmark testing on the XV-15 steel blades the rig was handed over to the V-22 program (formerly known as the JVX) for rotor performance and download testing of a scaled rotor and semispan wing installations. This V-22 test program is reported in Reference 1.

At the conclusion of the V-22 testing the rig was refurbished and an intermittent problem with the force readout from the drive system flexible coupling gages (AFFLEX) was resolved. The AFFLEX signal is a measurement of the thrust force in the drive shaft when this is stretched or compressed by flexure motions in the main balance. This component of thrust was measured by bridges located 180 degrees apart in the flexible coupling so that 1 per rev components of force would cancel. One set of gages was found to be malfunctioning and these were disconnected. The AFFLEX signal was then recalibrated with the rotor in the azimuthal location where the 1 per rev component passed through zero.

In subsequent testing the rotor was set to this position while pre- and post-test zeroes were being taken.

The Advanced Technology Blades were installed and testing commenced in the baseline configuration (i.e., elliptical tip and truncated cuff). This was followed by configuration variations which included a full airfoil cuff, swept and square tips, cuff removed, and changes in blade sweep. A check calibration of all measuring systems was performed at the conclusion of testing. This confirmed that accuracy was to the same standard of excellence as at the beginning of the test program.

7.0 ROTOR PERFORMANCE

7.1 XV-15 Metal Blade Performance

The performance of the XV-15 metal blades at the nominal operating tip Mach number of 0.69 is presented in Fig. 7.1 as a plot of rotor thrust coefficient vs. rotor power coefficient corrected to zero wind conditions. The data was gathered during six separate runs and the data scatter is small. A mean line was faired through this data and used to calculate the rotor figure of merit shown on Figure 7.2. Note that this figure of merit curve always falls below the line faired through the individual values of figure of merit, calculated from each test point. This is the correct method for defining the average rotor figure of merit; the average thrust - power relationship for the rotor is first determined, then quantities, such as figure of merit, which are functions of this relationship, may be computed. Peak figure of merit for the XV-15 rotor is 0.791 at a thrust coefficient of 0.0105. Also shown in Figure 7.2 is the performance of the XV-15 rotor as tested on the Wright Patterson AFB whirl tower in 1973 (Reference 4). The data has been adjusted for the effects of the tower. This comparison shows that the shape of the curve is the same. The peak figure of merit occurs at the same thrust coefficient but has a lower value.

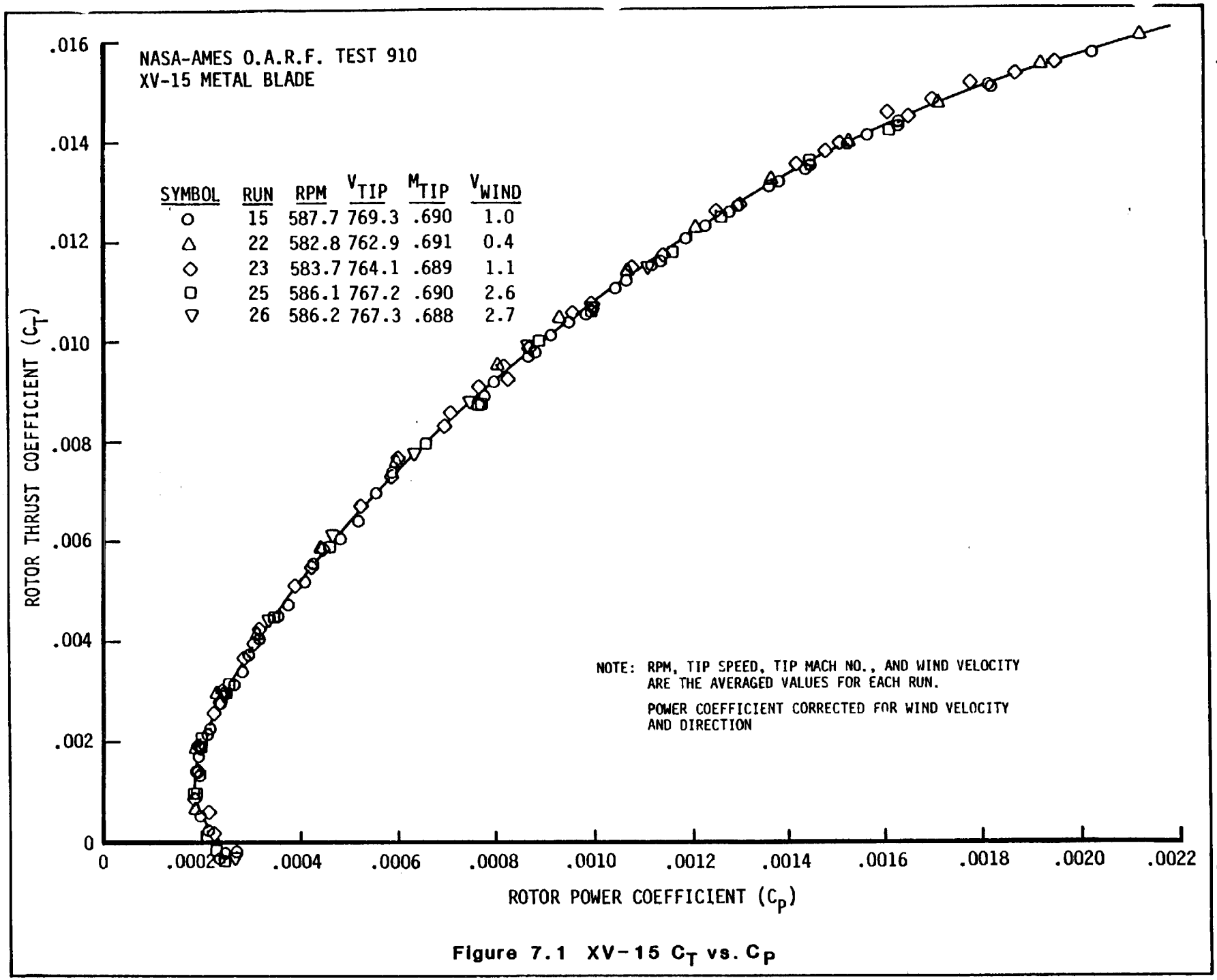

Figure 7.1 XV-15 C_T vs. C_P

CR177436

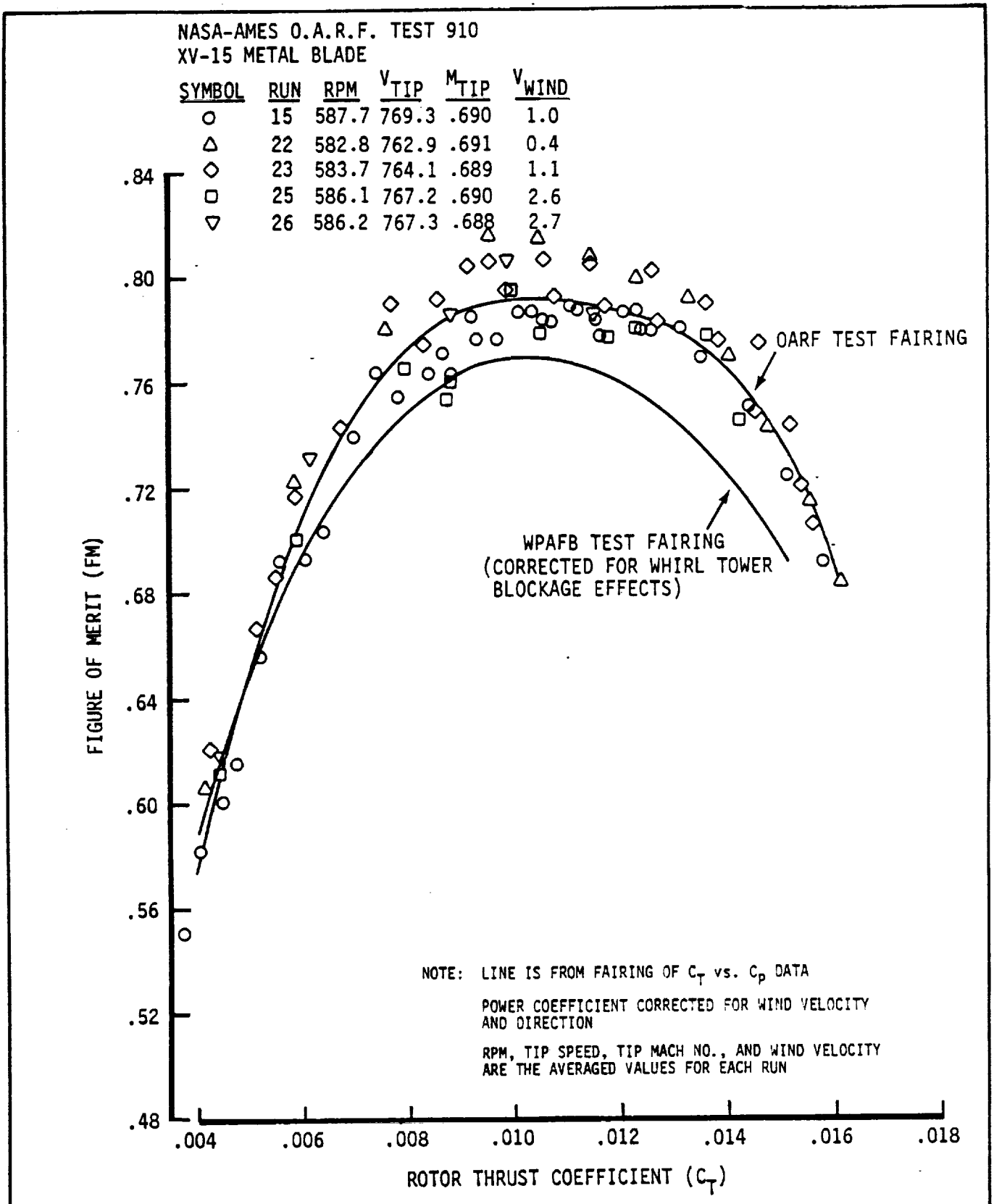

Figure 7.2 XV-15 Figure of Merit

Figure 7.3 presents the variation of thrust coefficient with collective pitch. The collective pitch values have not been corrected to zero wind conditions. It is estimated, however, that the correction would reduce the collective by 1 degree, at most. Also shown on Figure 7.3 is data (without correction to collective for tower blockage) from the whirl tower test of Reference 4. It is not known why there is a 4 degree difference between the two sets of data. The collective pitch settings recorded in the present test of the XV-15 metal blades appear to be incorrect, and are presented only as confirmation of the shape of the curve of C_T vs. $\theta_{.75}$ Calculations using performance codes support the WPAFB values of collective as does flight test experience.

Maximum thrust was not reached because alternating loads increased rapidly above a C_T value of .0161. Figure 7.3 suggests, however, that a reasonable value for maximum thrust coefficient for XV-15 would be .0165, i.e. $C_T/\sigma_{T_{MAX}} = .185$.

One measure of rotor induced efficiency is k, as defined by

$$C_P = C_{P_o} + k \frac{C_T^{3/2}}{\sqrt{2}}$$

where k = 1.0 corresponds to ideal induced efficiency. The value of C_{P_o} is defined by linear extrapolation to zero thrust of the curve of $C_T^{3/2}$ vs. C_P. This data is presented in Figure 7.4 and was used to compute the values of k presented in Figure 7.5.

The sensitivity of the XV-15 rotor performance to tip Mach number is presented in Figures 7.6 and 7.7. Tip Mach number was varied from 0.60 to 0.73. No well-defined trend is evident although there is a tendency for reduced performance to accompany increases in Mach number.

The distribution of downwash velocity in the wake of the rotor was measured by the wake rake described in Section 4.5. The rake was positioned so that the ends of the probes would coincide with the probable location of the upper surface of a wing. At 75 percent radius the distance from the rotor disc to the XV-15 wing surface is 0.40R.

In addition to measurements of the wake, a limited series of photographs were obtained of the tip vortices made visible by water vapor condensation. Figure 7.8 is a typical example and shows clearly the helical path of the vortices from each blade. By measuring from these photographs, M. Maisel of NASA Ames succeeded in constructing the shape of the outer wake. Figure 7.9 shows that, for $C_T = .0116$, the wake contracts to approximately .79R at .55R downstream of the disc. At 0.4R where the probe lies, the tip vortex is located at 0.80R. This value is confirmed by the data of Fig 7.10 which shows the radial distribution of downwash for selected values of rotor thrust coefficient. Lines have been faired through the data obtained from the pure pitot-static probes only. The data from the 5-hole angle of attack probes was considered to be less reliable. At all the values of C_T shown, the edge of the wake appears to lie at 80 percent radius.

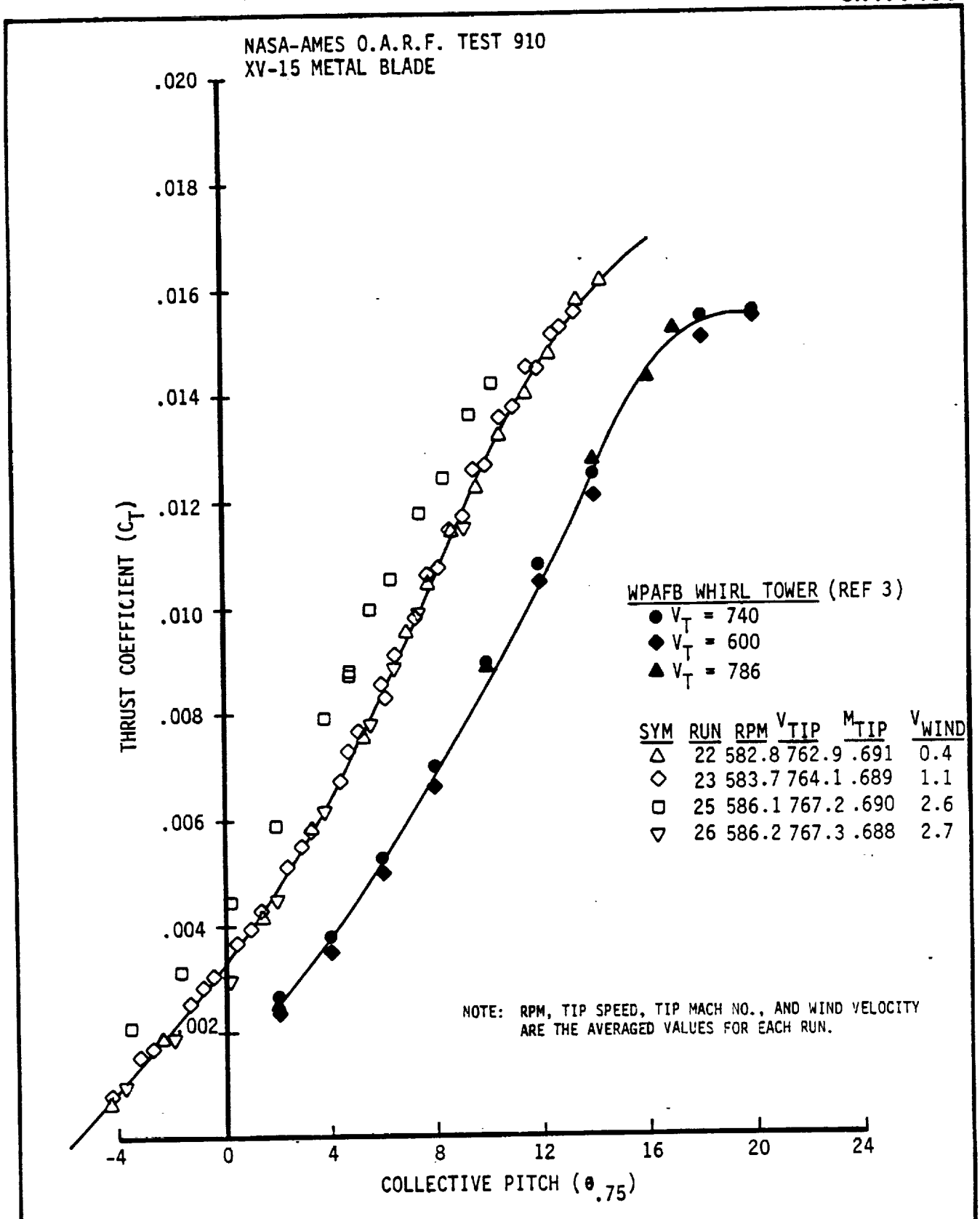

Figure 7.3 XV-15 Thrust Coefficient vs. Collective Pitch

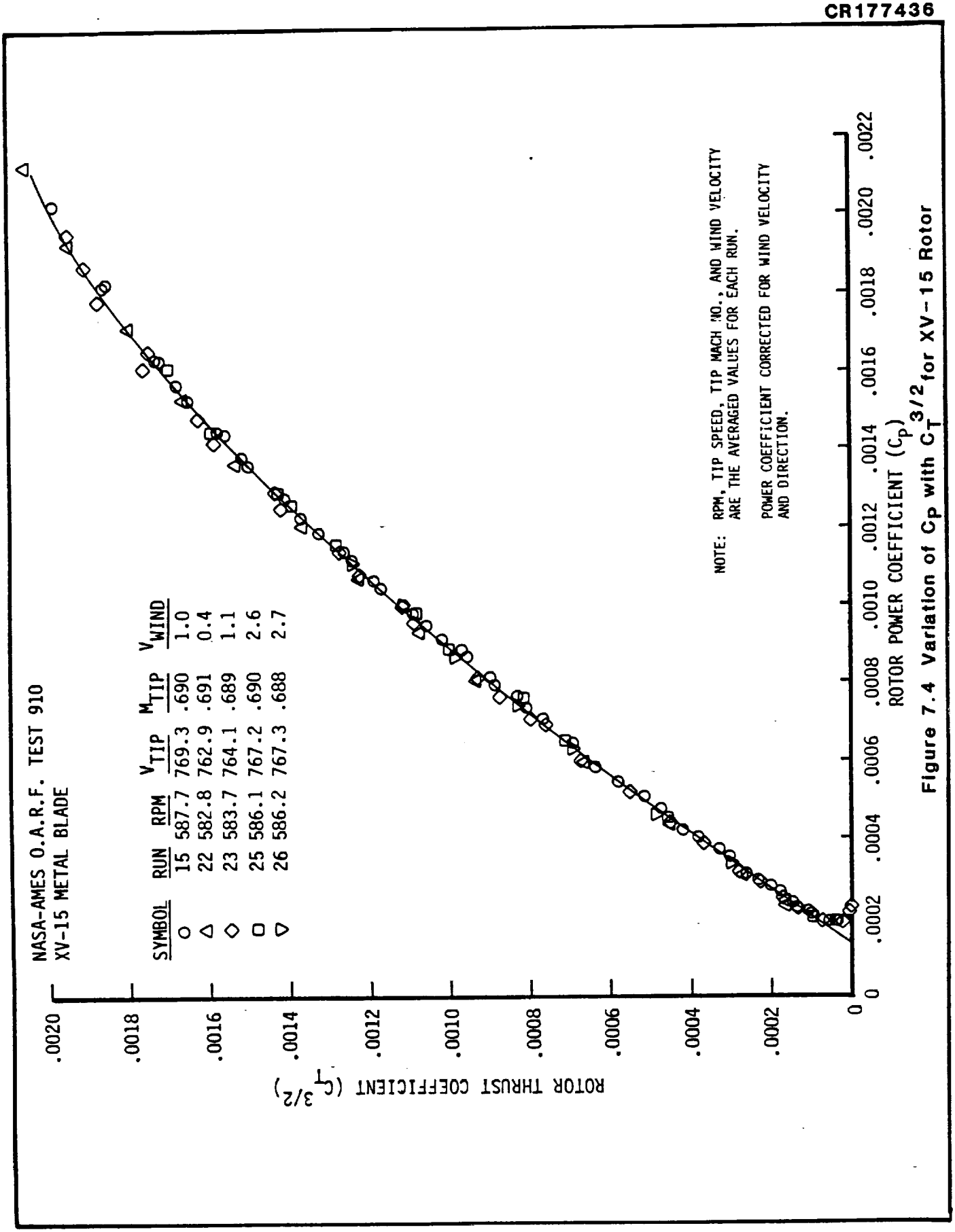

Figure 7.4 Variation of Cp with $C_T^{3/2}$ for XV-15 Rotor

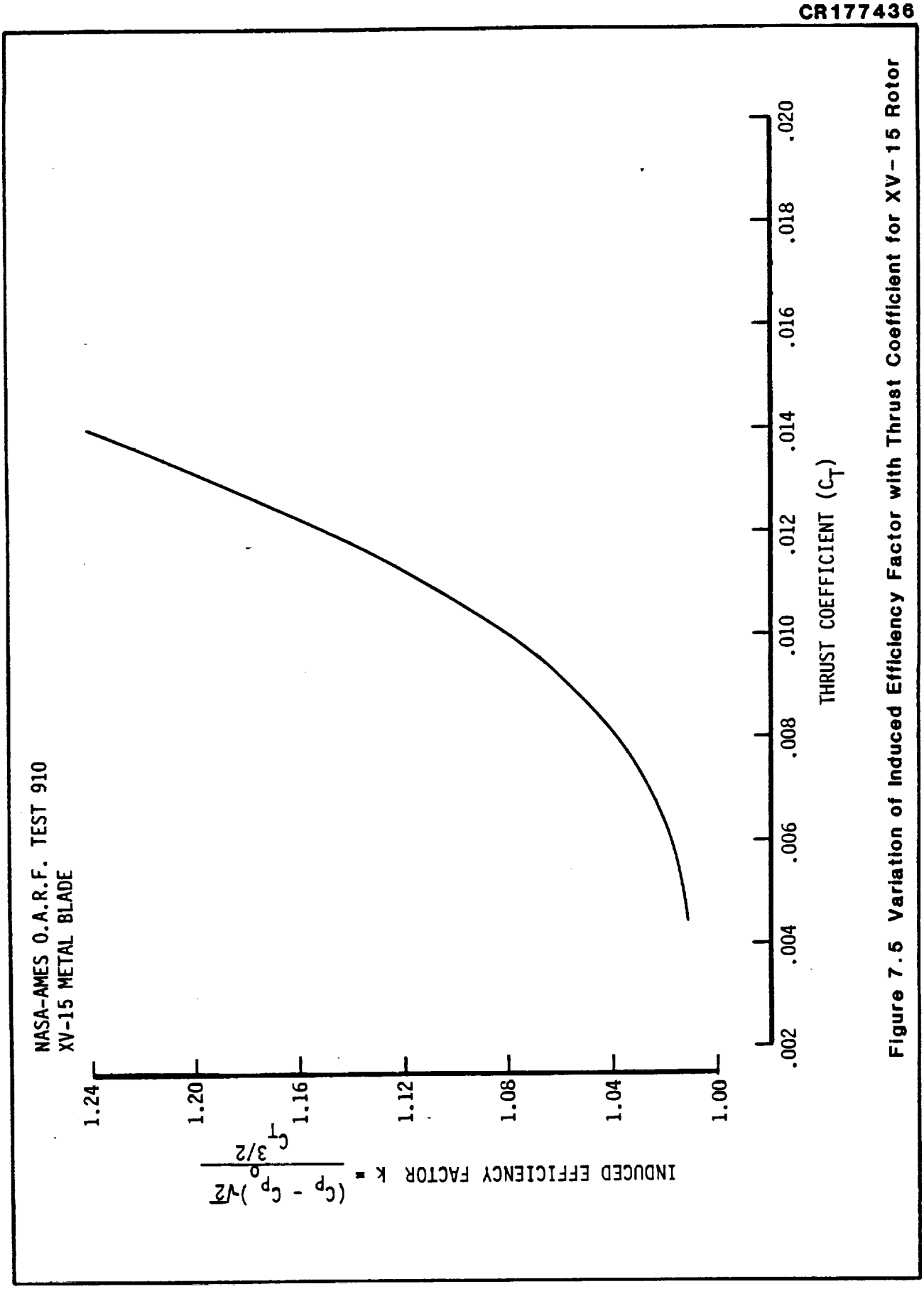

Figure 7.5 Variation of Induced Efficiency Factor with Thrust Coefficient for XV-15 Rotor

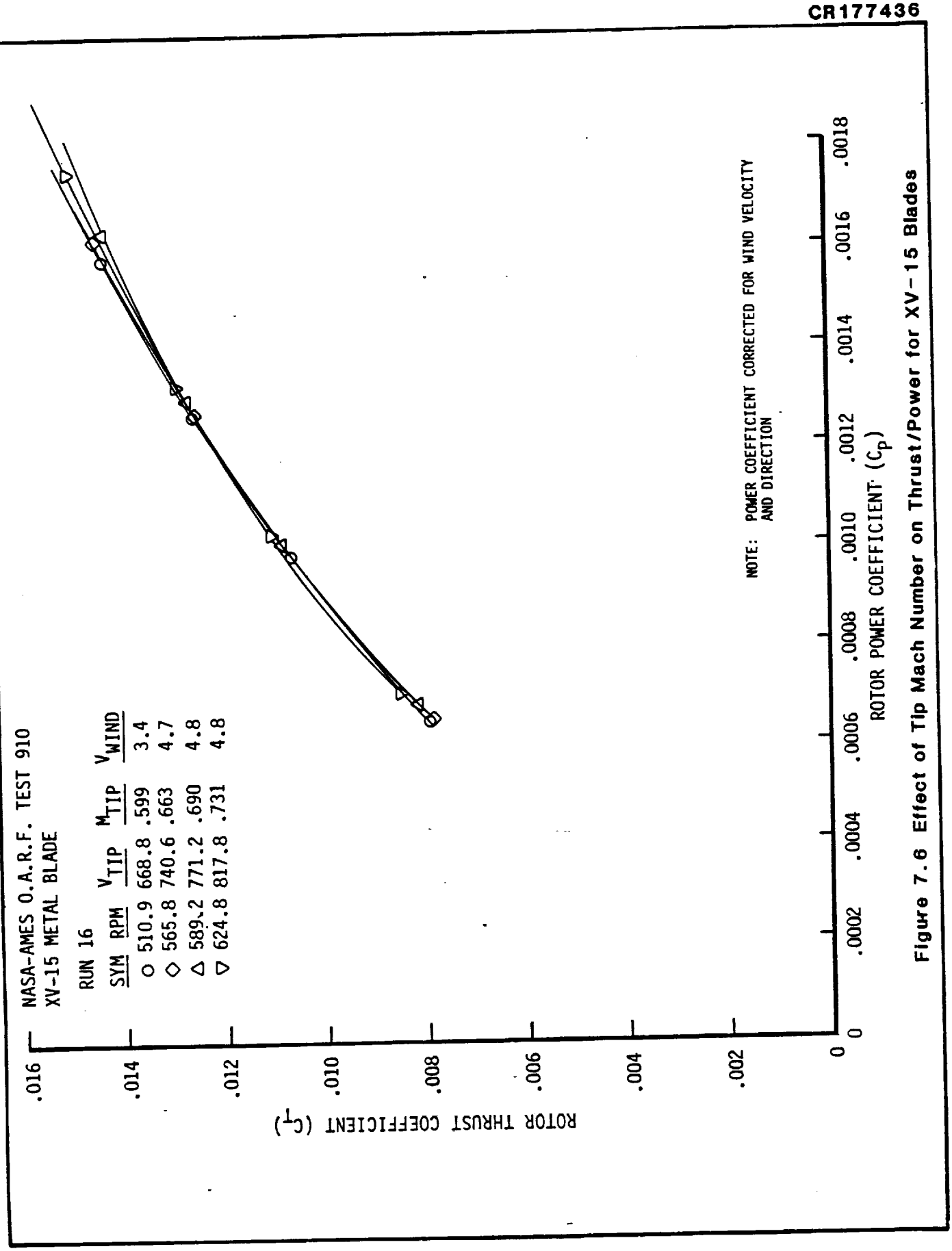

Figure 7.6 Effect of Tip Mach Number on Thrust/Power for XV-15 Blades

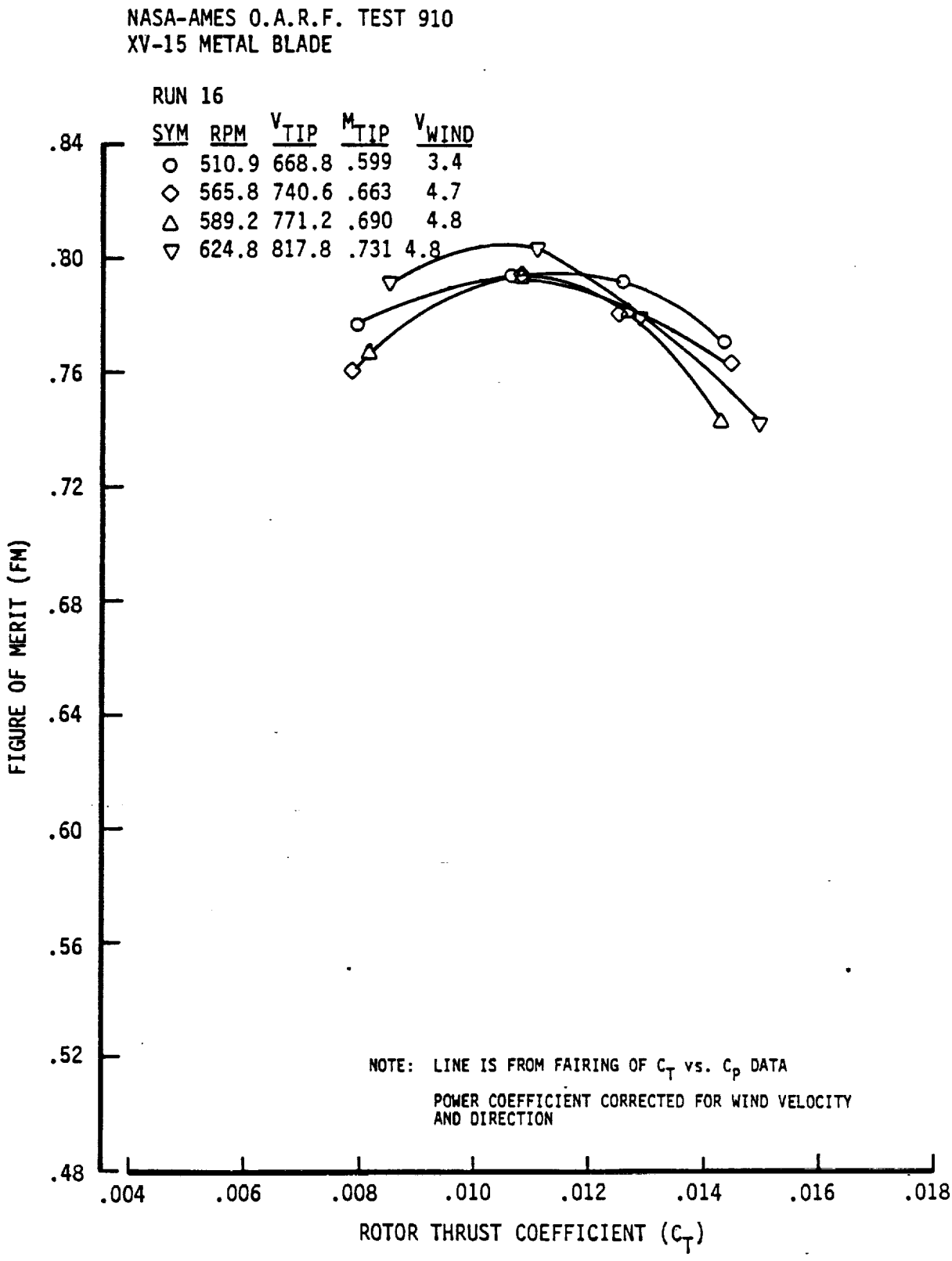

Figure 7.7 Effect of Tip Mach Number on Figure of Merit of XV-15 Blades

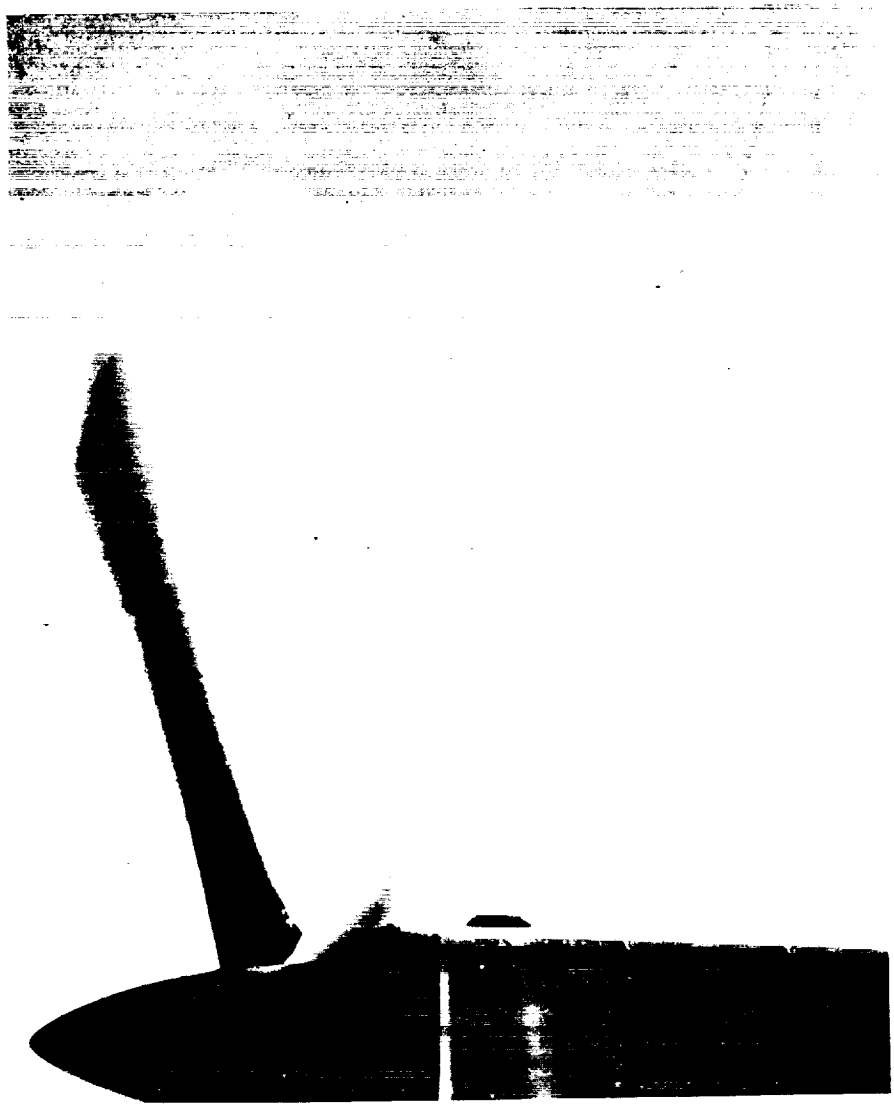

Figure 7.8 Tip Vortices of XV-15 Metal Blades

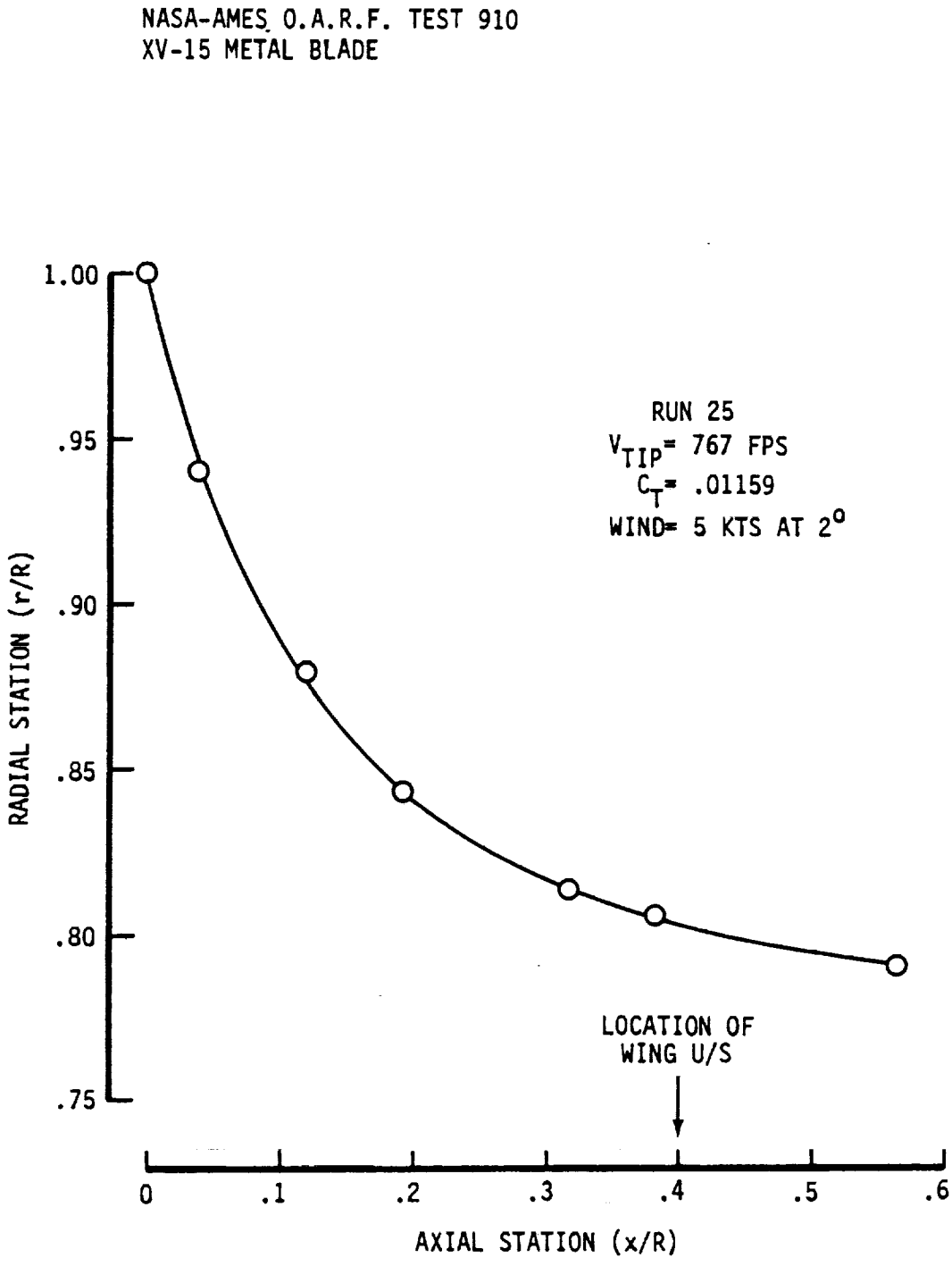

Figure 7.9 Contracted Wake Shape of XV-15 Rotor Deduced from Tip Vortex Photographs

NASA-AMES O.A.R.F. TEST 910
XV-15 METAL BLADE
Z/R= 0.4 RUN 25

SYM	TP	C_T	RPM	V_{TIP}	M_{TIP}	V_{WIND}
□	16	.00796	585.9	766.9	.690	2.9
▽	20	.01053	585.7	766.7	.690	2.4
○	22	.01246	585.5	766.4	.689	3.3
◇	24	.01422	586.9	768.3	.690	2.9

NOTE: SOLID SYMBOLS DENOTE DATA FROM ANGLE OF ATTACK PROBES

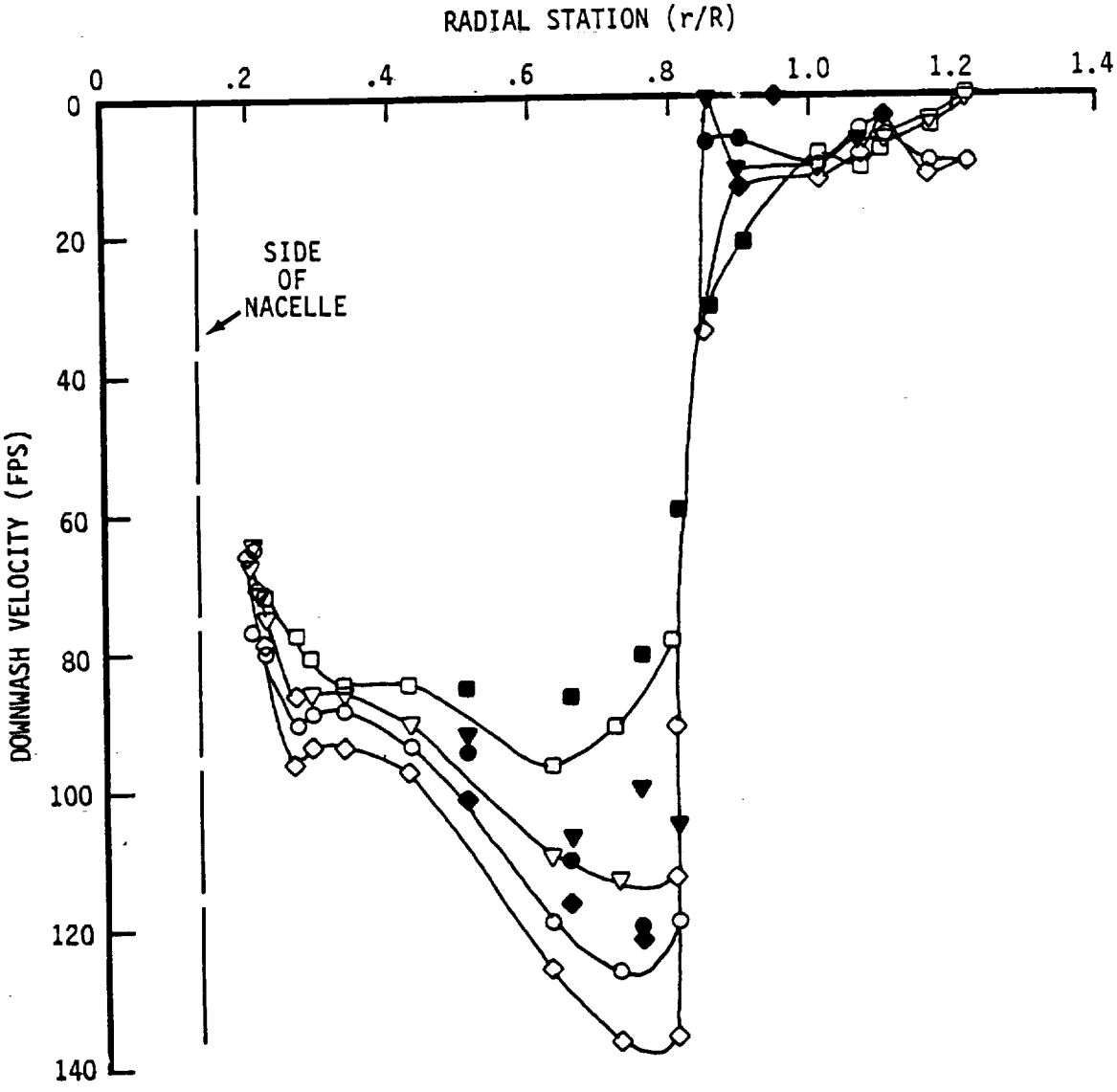

Figure 7.10 Distribution of Downwash Velocities for Various Thrust Coefficients for XV-15 Rotor

The shape of the downwash distribution changes with increasing thrust coefficient, becoming more skewed toward high downwash values just inside the tip vortex. Outside the tip vortex, the wake-induced velocity is essentially zero; the non-zero values of downwash shown are attributable to the ambient wind.

7.2 Baseline ATB Performance

The baseline ATB configuration consists of an approximately elliptical tip planform and a cuff truncated at the trailing edge to permit gimbal angles up to 12 degrees at high collective pitch settings.

Thrust versus power coefficient test data is shown in Figure 7.11. The data is shown for four different runs during which tip Mach number was held constant and for two runs at high and low Mach number. There is remarkably little scatter. The solid line in Figure 7.11 is an estimated mean faired through the data. This faired line is the basis of the figure of merit shown by the solid line in Figure 7.12. The individual test point figures of merit are also shown in Figure 7.12. As noted in the preceding paragraphs the mean figure of merit curve falls below the mean of the individually calculated test points because of the non-linearity of the figure of merit function. Peak figure of merit for the baseline blade is just under 0.80, and remains high out to the C_T obtainable at the power limit of the test rig. Note that a maximum value of $C_T = .022$ ($C_T/\sigma_T = .22$) was reached at reduced tip speed.

Figure 7.13 presents the collective pitch vs. thrust relationship and shows a change in slope between C_T values of 0.006 and 0.008. As will be shown, consistent, repeatable C_T vs. $\theta_{.75}$ relationships were obtained for all the ATB configurations and are considered to be reliable.

The plot of $C_T^{3/2}$ versus C_P is shown in Figure 7.14. The linear projection to zero thrust gives a value of ${}^{\ell}P_0$ equal to 0.000185 compared with a steel blade value of 0.00013. Figure 7.15 presents downwash distributions for the baseline ATB.

7.3 Performance of ATB with Extended Cuff

The power-thrust relationship for the ATB with the trailing edge of the cuff extended to complete the airfoil section is shown in Figure 7.16. In Figure 7.17 data is presented in figure of merit format. It is seen that the cuff extension has an effect that increases the figure of merit by approximately 0.01. Figure 7.18 shows the variation of thrust coefficient with collective pitch and Figure 7.19 presents the variation of $C_T^{3/2}$ as a function of power coefficient. The value of ${}^{\ell}P_0$ deduced from Figure 7.19 is the same as that obtained from Figure 7.14 for the blade with a truncated cuff (0.000185).

7.4 Performance of ATB with No Cuff

As expected there was a significant reduction in rotor efficiency when the cuff was removed. The results for the cuff-removed configuration are given in Figures 7.20 through 7.23. A peak figure of merit around 0.77 was found, and the ${}^{\ell}P_0$ value is 0.000197. A run was made with the blade sweep angle

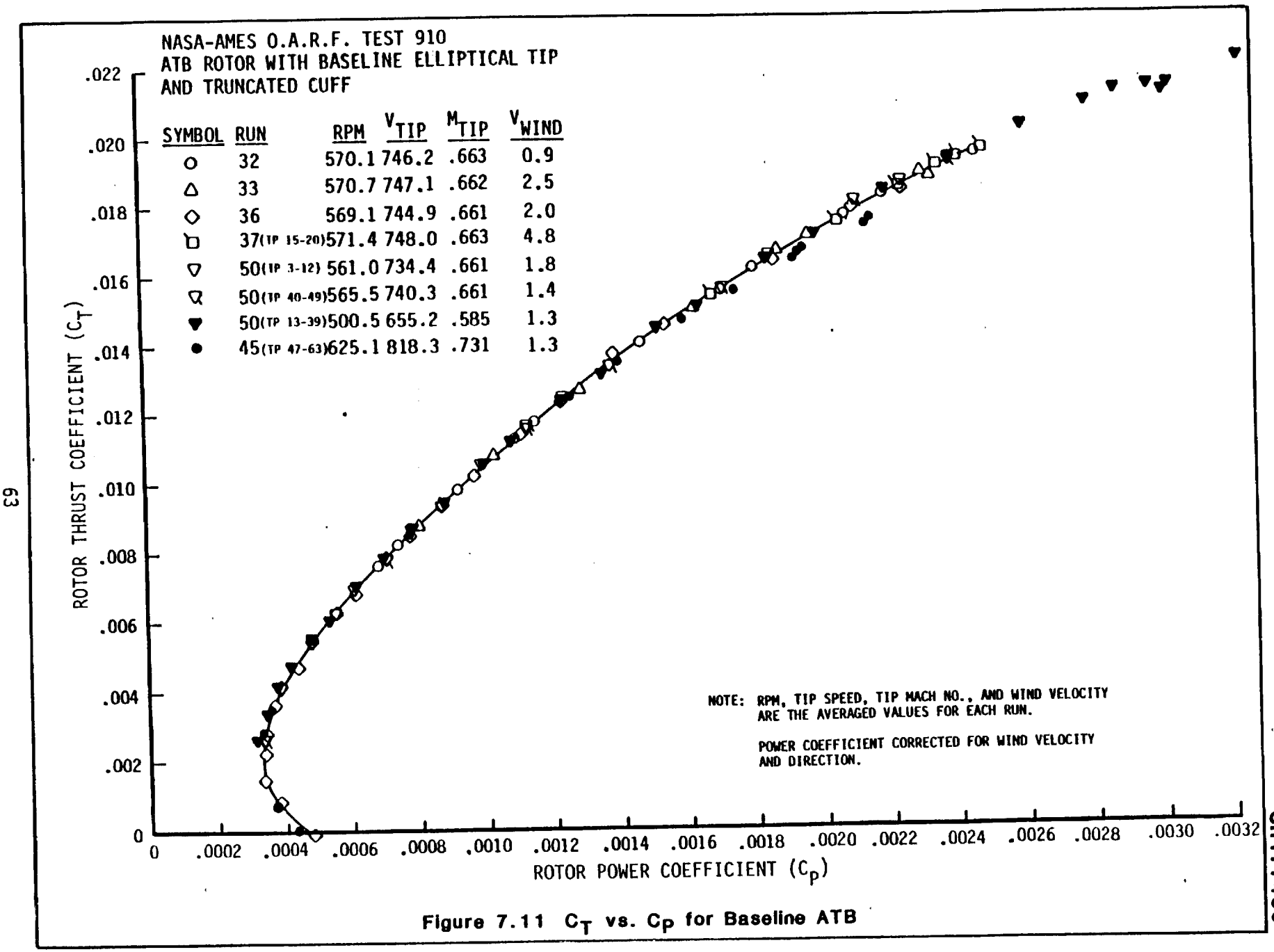

Figure 7.11 C_T vs. C_P for Baseline ATB

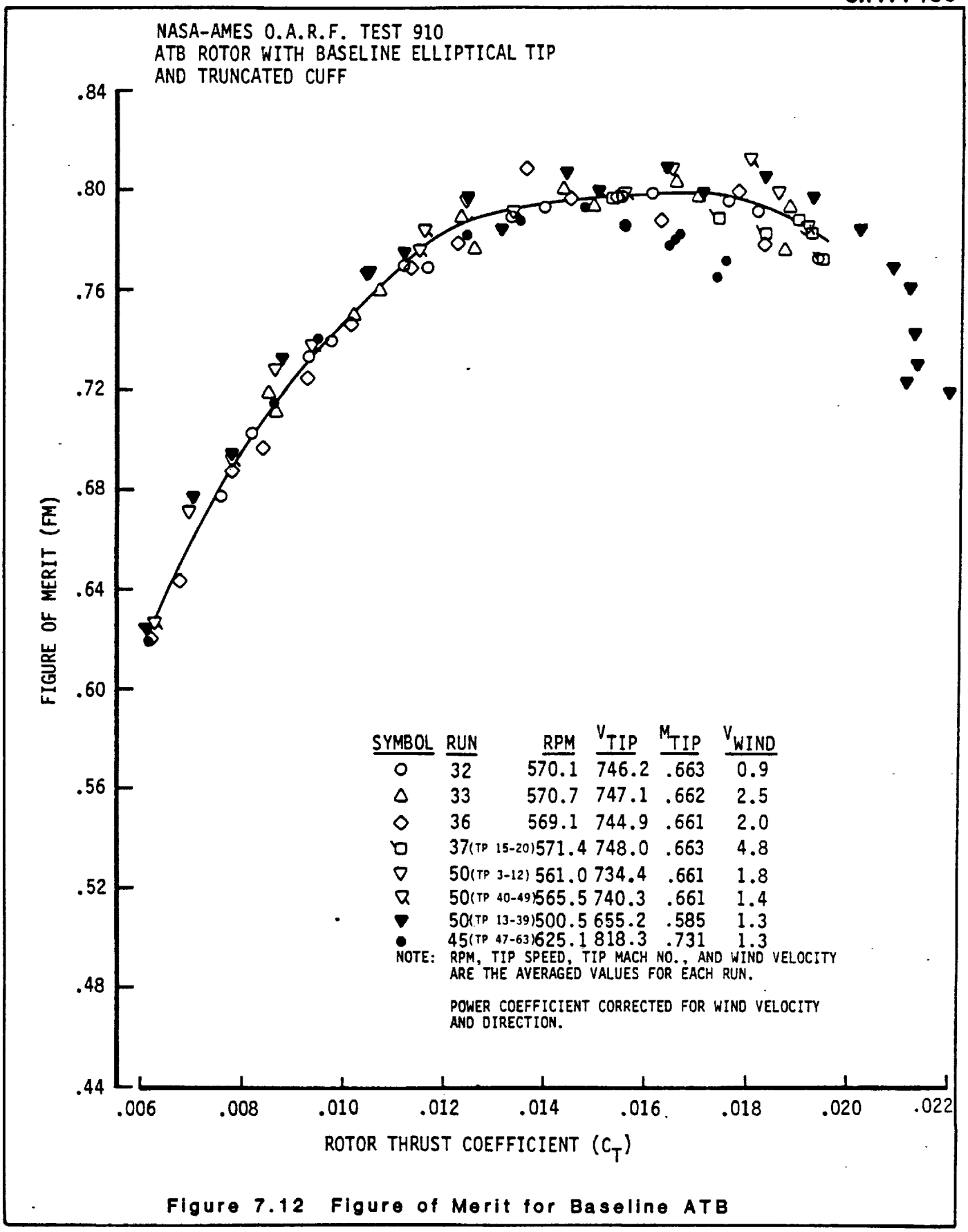

Figure 7.12 Figure of Merit for Baseline ATB

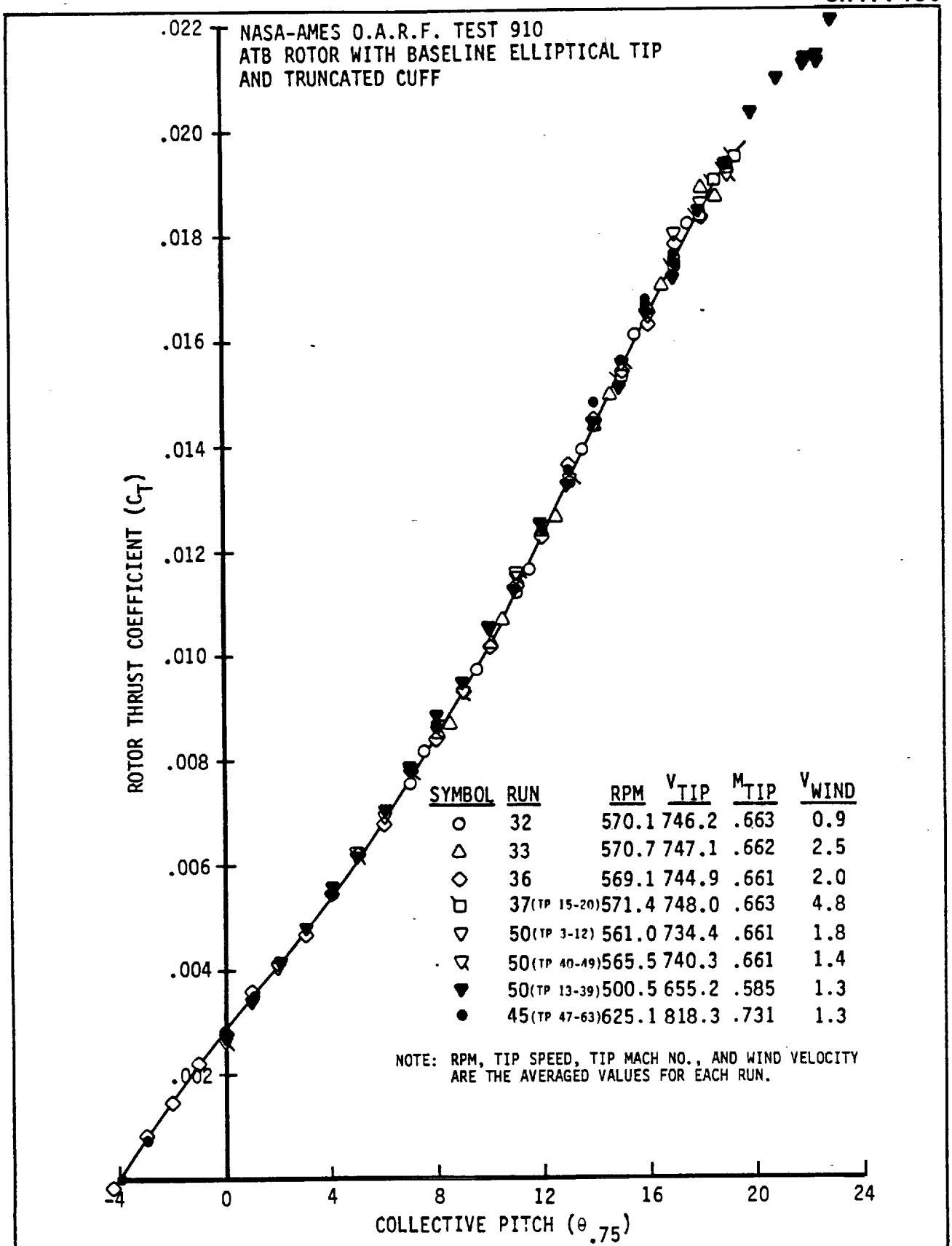

Figure 7.13 Thrust Coefficient vs. Collective Pitch for Baseline ATB

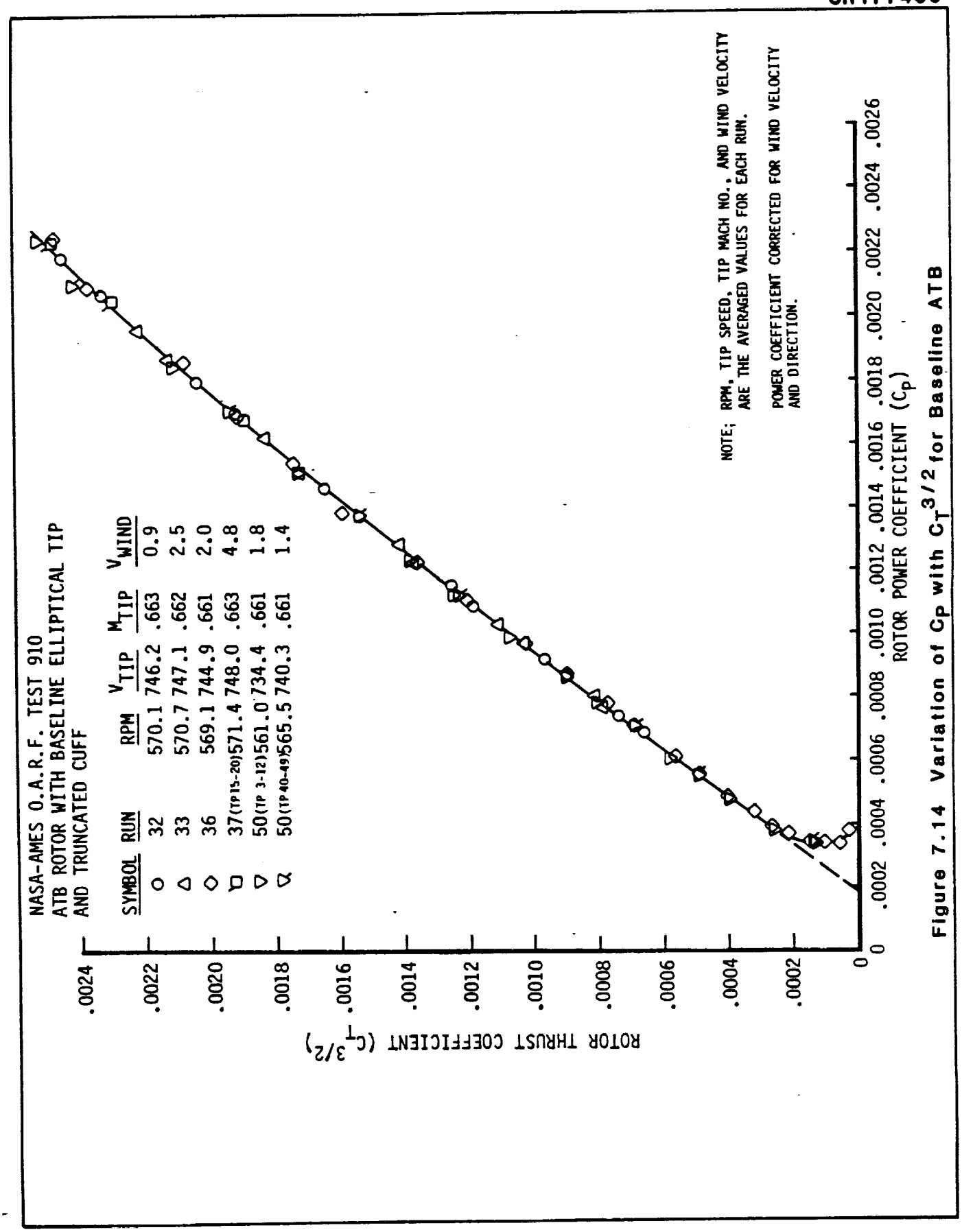

Figure 7.14 Variation of Cp with $C_T^{3/2}$ for Baseline ATB

NASA-AMES O.A.R.F. TEST 910
ATB ROTOR WITH BASELINE ELLIPTICAL TIP AND TRUNCATED CUFF

NOTE: SOLID SYMBOLS DENOTE DATA FROM ANGLE OF ATTACK PROBES

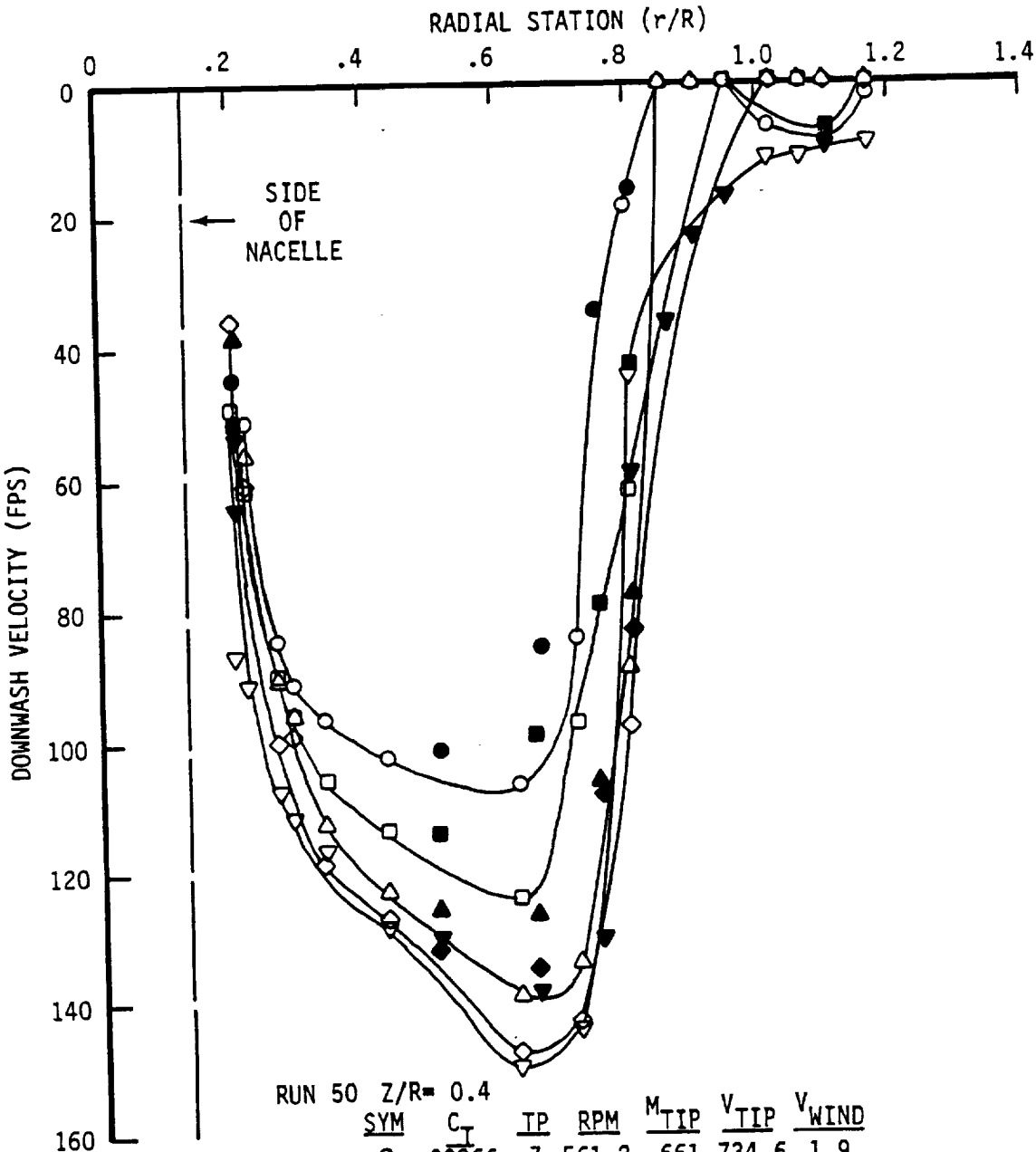

RUN 50 Z/R= 0.4

SYM	C_T	TP	RPM	M_{TIP}	V_{TIP}	V_{WIND}
○	.00866	7	561.2	.661	734.6	1.9
□	.01242	9	560.9	.660	734.2	2.2
△	.01647	11	560.5	.660	733.6	2.2
◇	.01859	12	560.1	.659	733.2	2.2
▽	.01917	49	564.5	.660	738.9	2.9

Figure 7.15 Distribution of Downwash Velocities for Various Thrust Coefficients for Baseline ATB

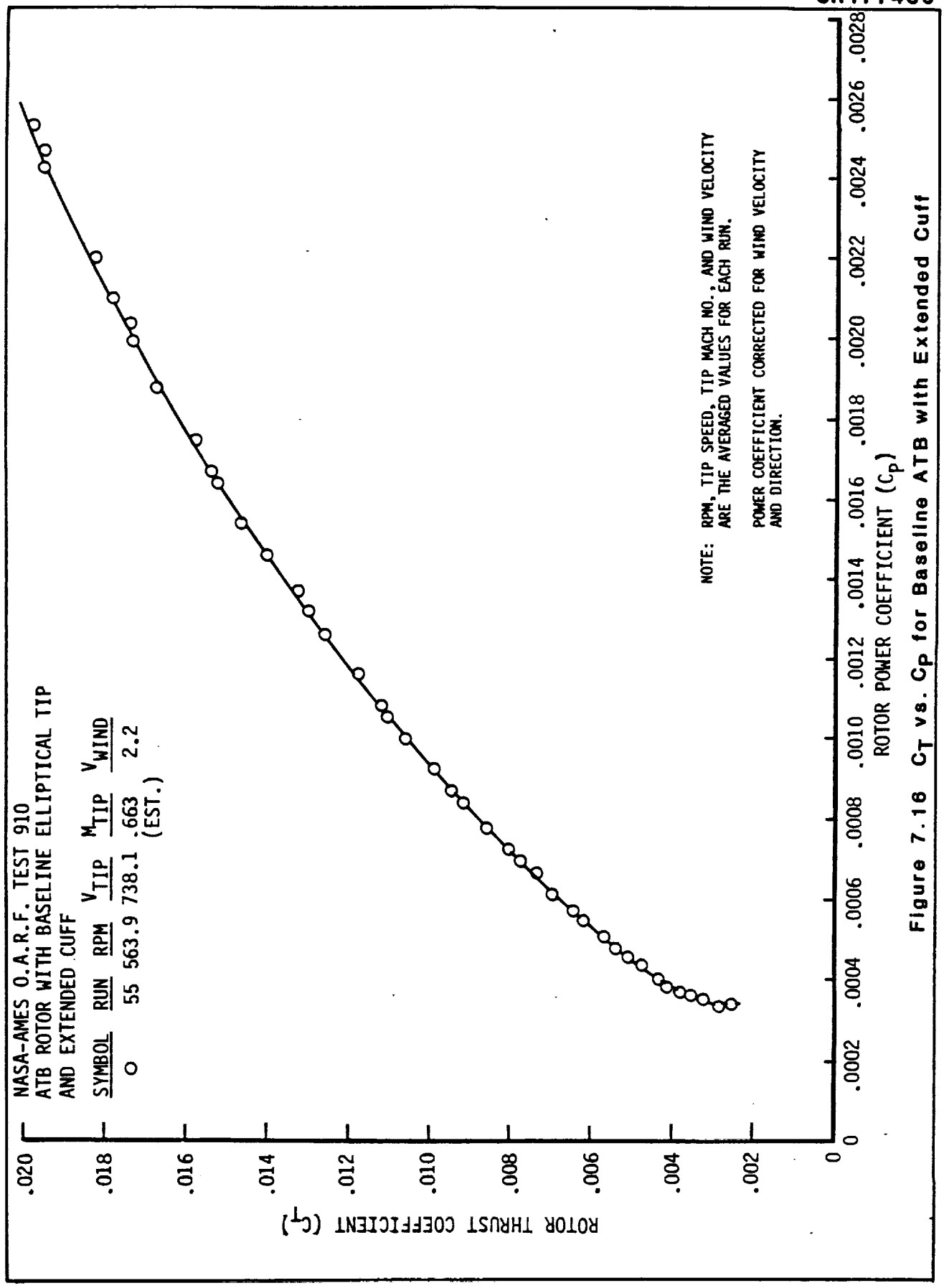

Figure 7.16 C_T vs. C_P for Baseline ATB with Extended Cuff

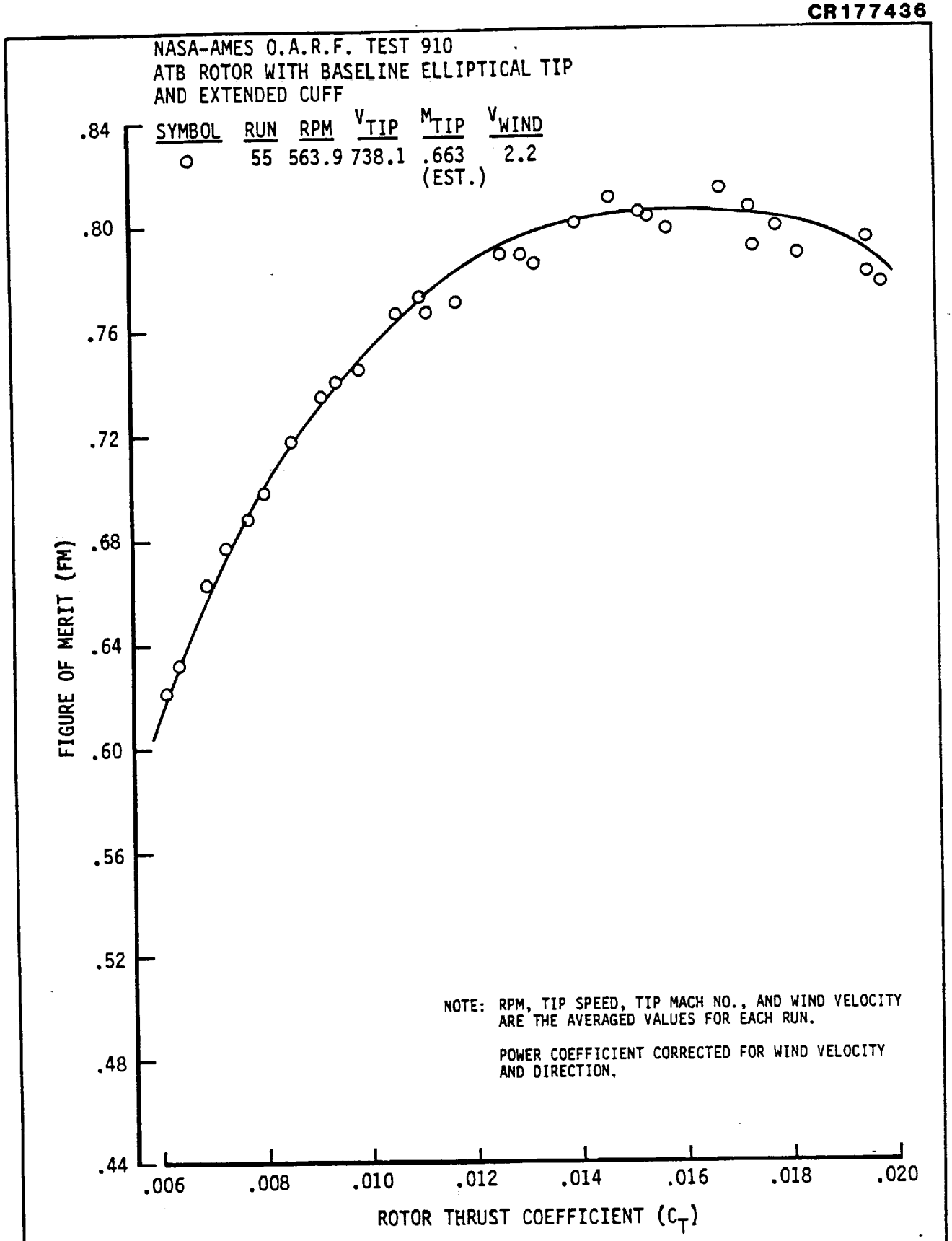

Figure 7.17 Figure of Merit for Baseline ATB with Extended Cuff

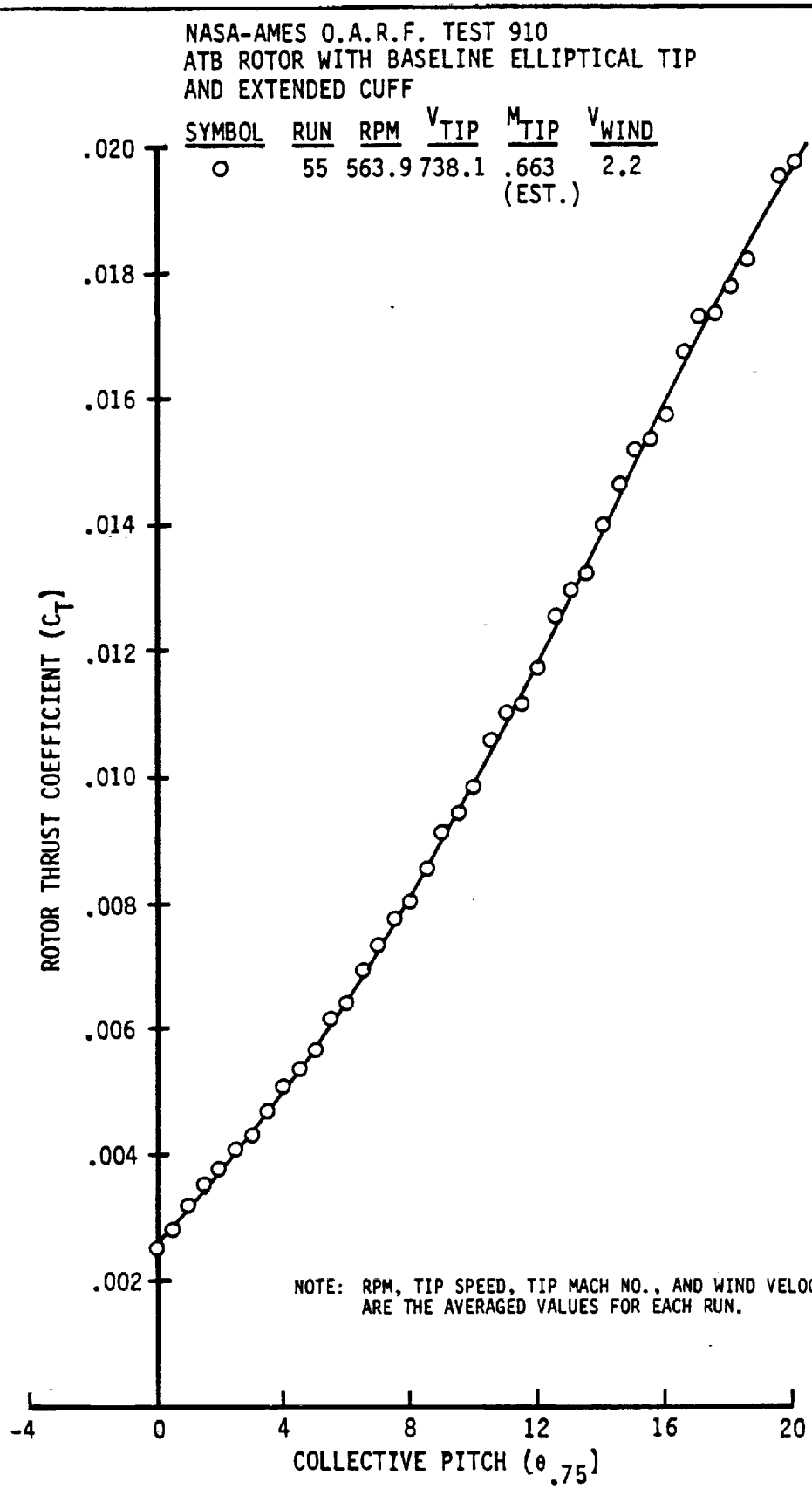

Figure 7.18 Thrust Coefficient vs. Collective Pitch for Baseline ATB with Extended Cuff

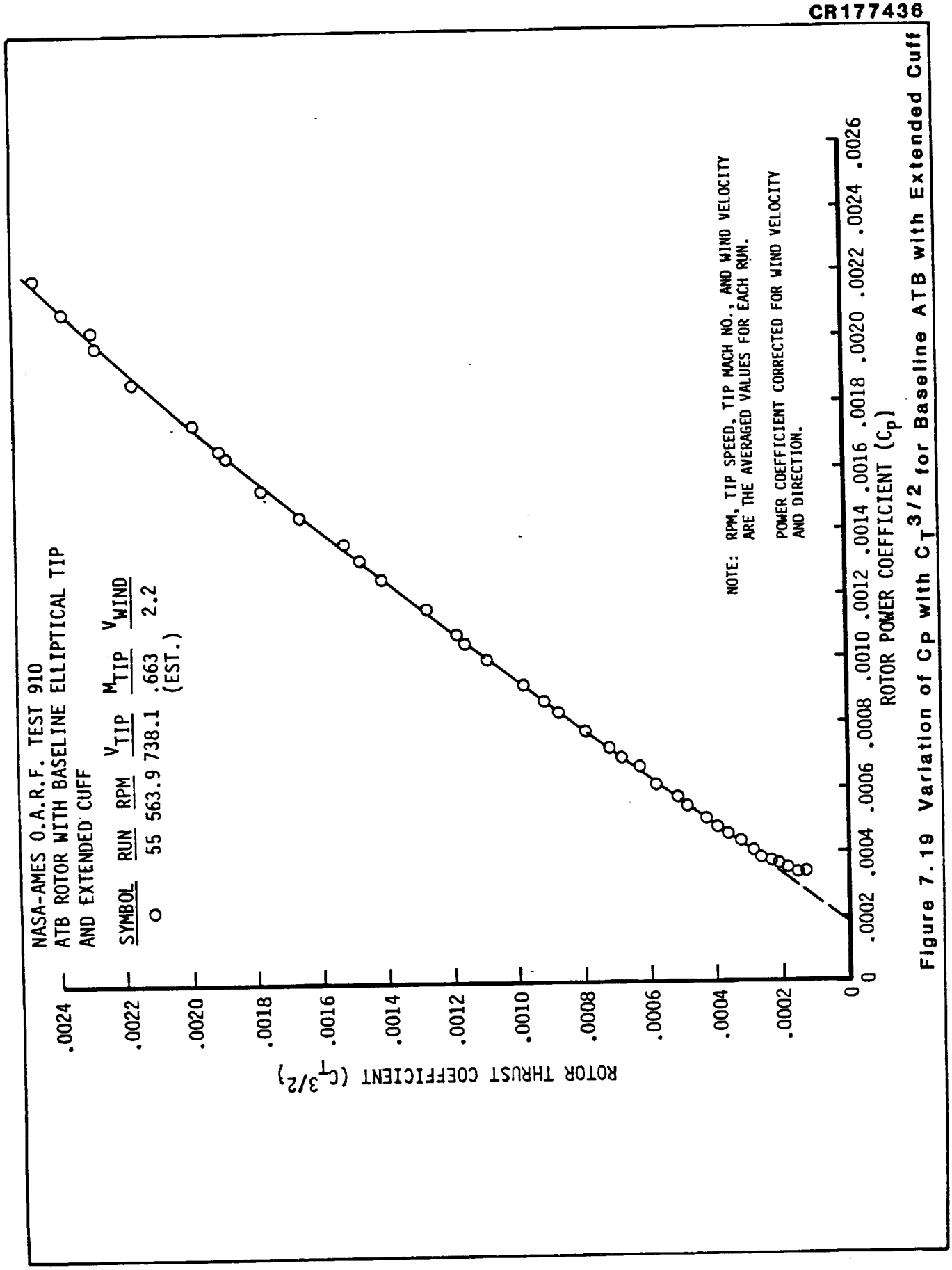

Figure 7.19 Variation of Cp with $C_T^{3/2}$ for Baseline ATB with Extended Cuff

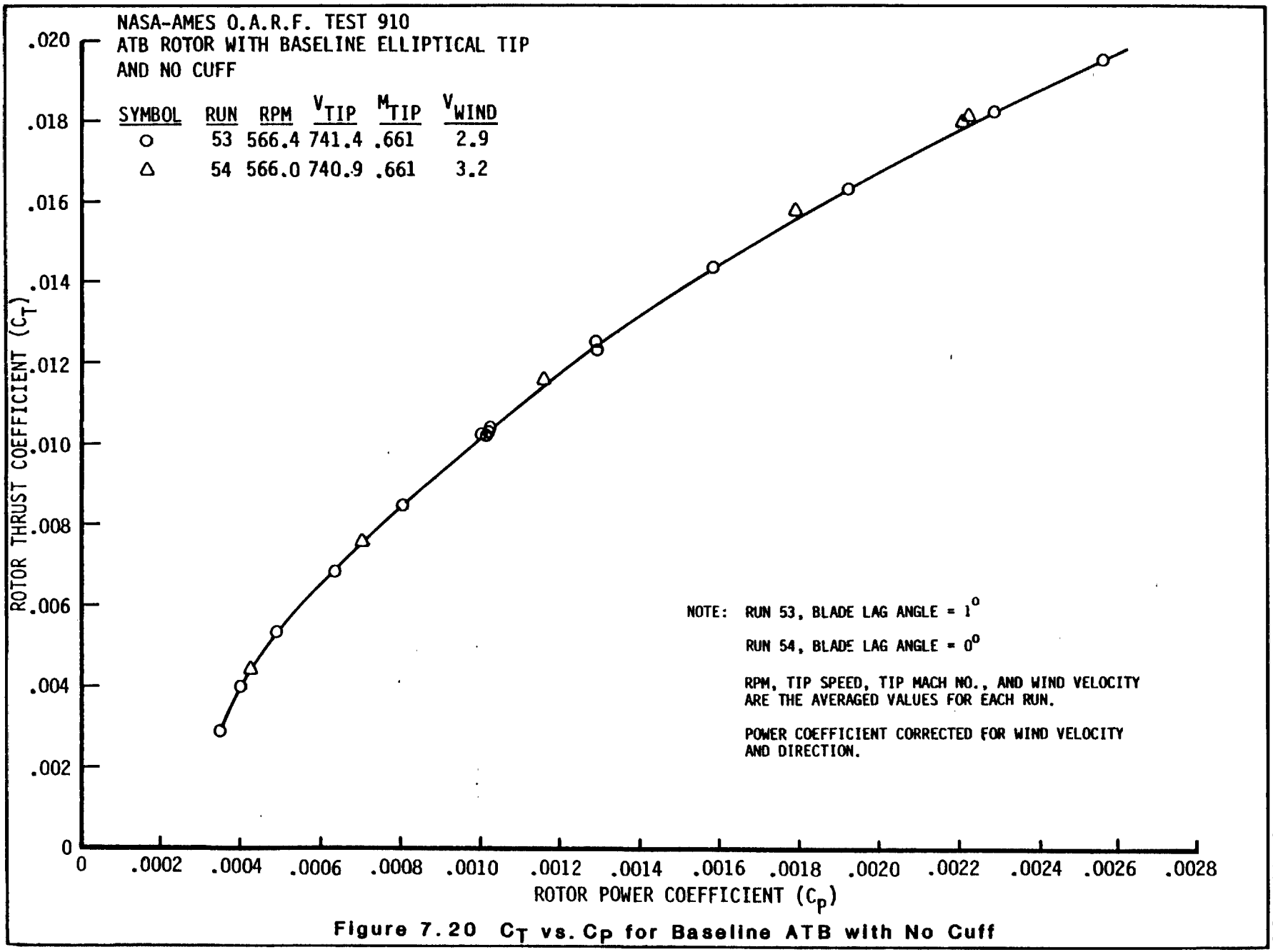

Figure 7.20 C_T vs. Cp for Baseline ATB with No Cuff

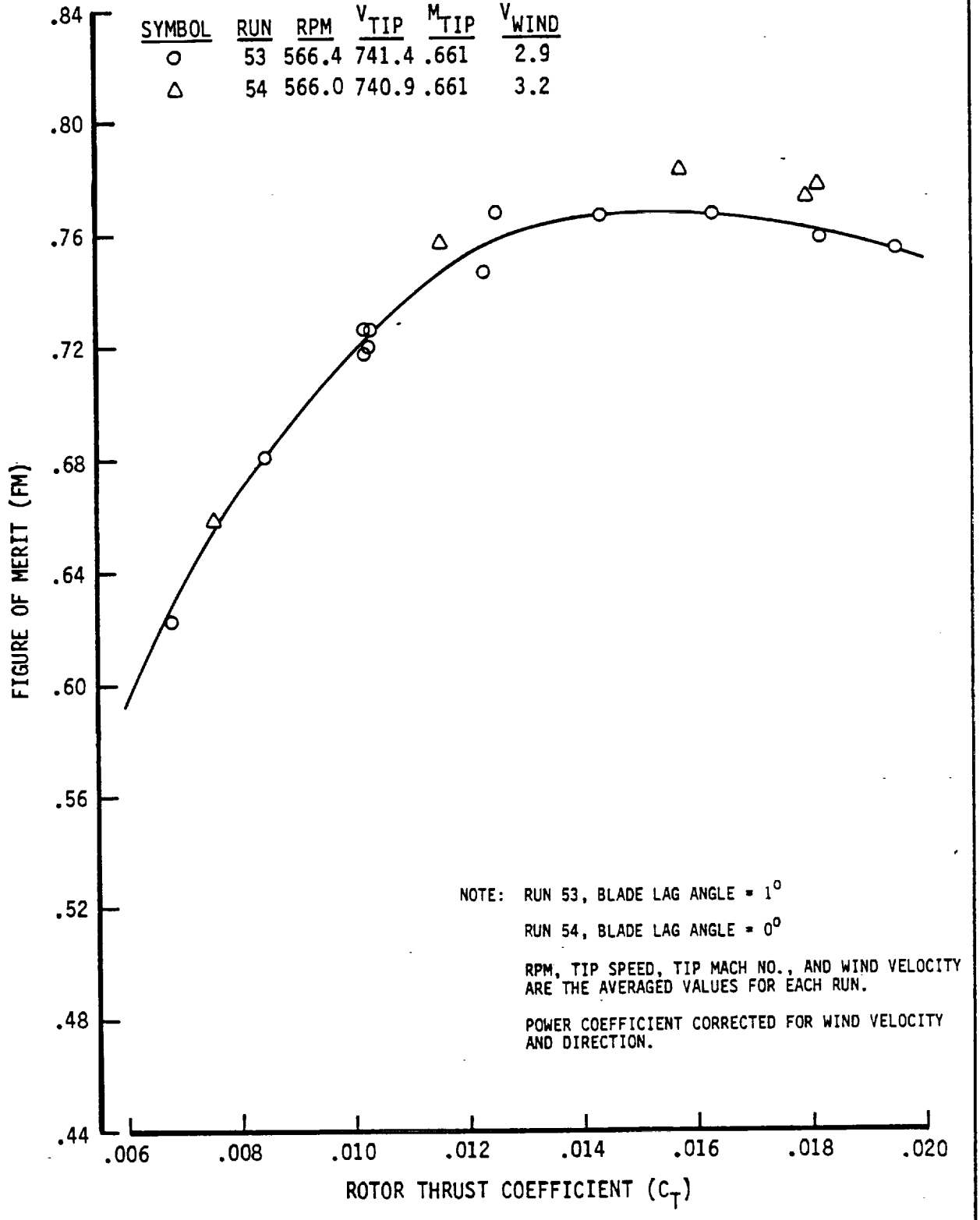

Figure 7.21 Figure of Merit for Baseline ATB with No Cuff

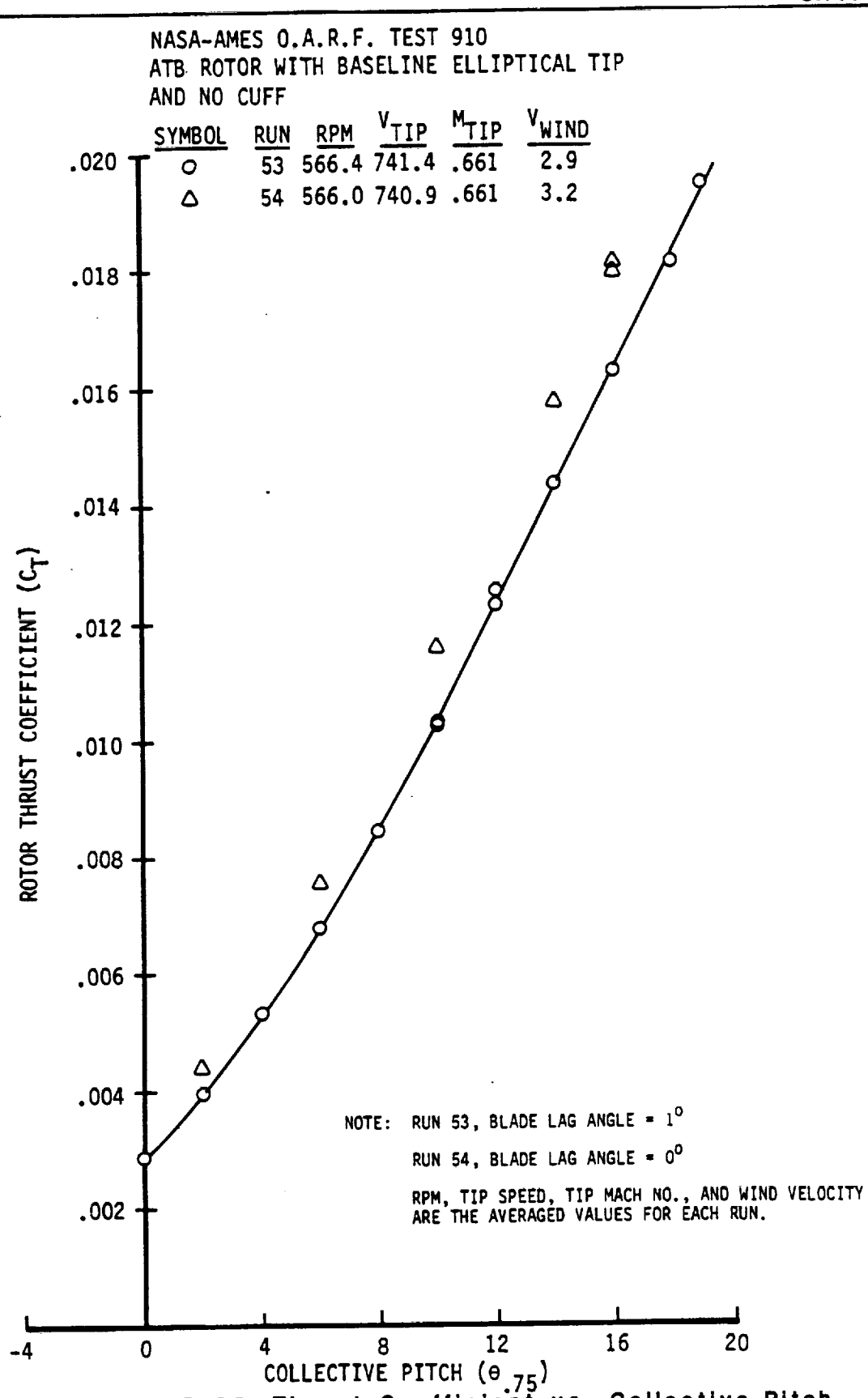

Figure 7.22 Thrust Coefficient vs. Collective Pitch for Baseline ATB with No Cuff

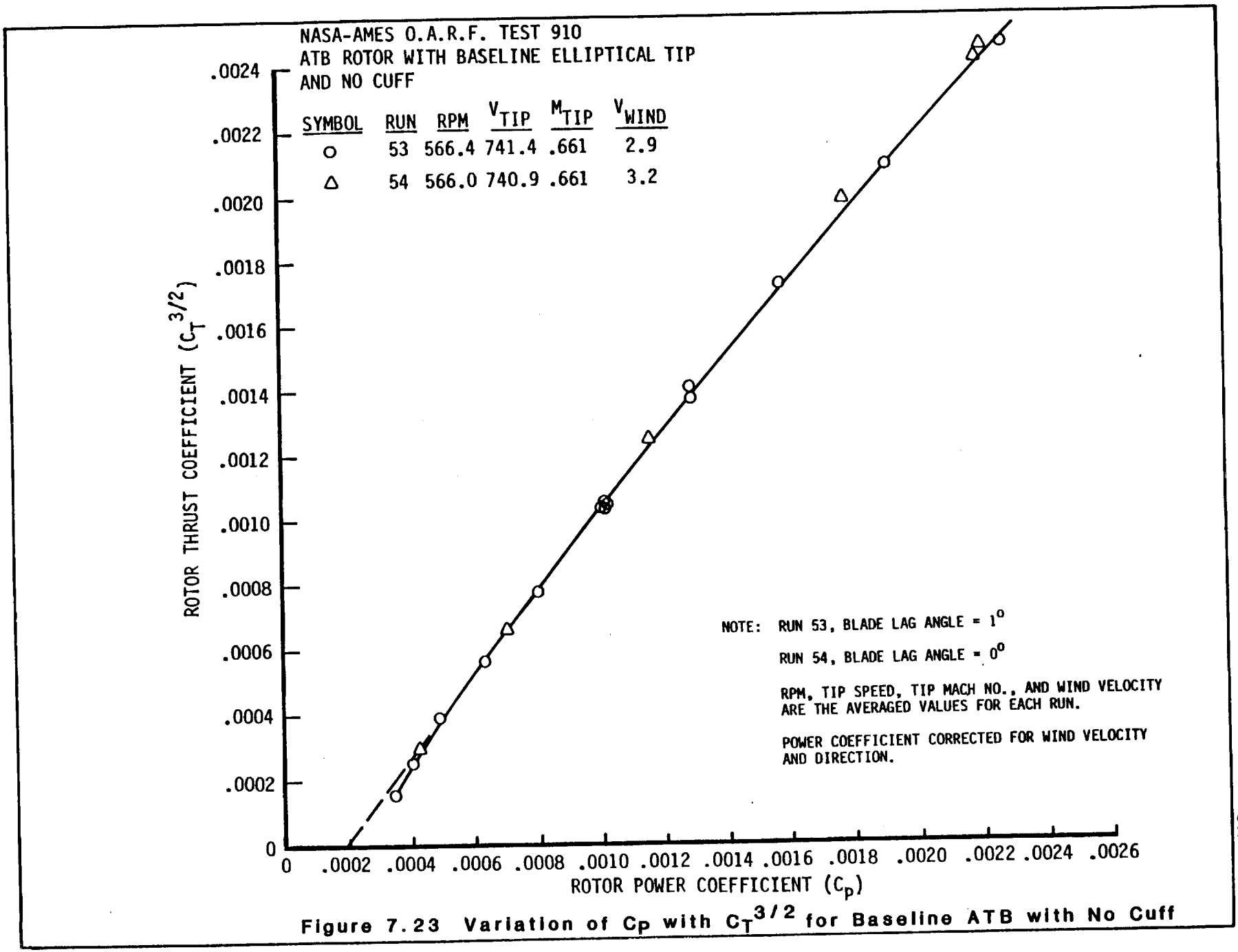

Figure 7.23 Variation of Cp with $C_T^{3/2}$ for Baseline ATB with No Cuff

set to zero degrees and there is an apparent increase of efficiency at this setting. The apparent increase in efficiency is however, within the scatter of earlier testing and is not considered to be significant.

Figure 7.22 indicates that the collective pitch required for a given C_T may be less when the blade sweep/droop is reduced to zero. The control system flexibility accounts for most of this difference. The recorded values of collective reflect the control setting at the actuator input. Because of the nose down pitching moments associated with blade sweep, the control blade setting is less in this case by the amount of control flexibility windup. At a nominal collective input of 16 degrees the difference between the swept and non-swept conditions is estimated to be 0.82 degrees. Figure 7.22 indicates a difference of almost 2 degrees suggesting that some additional mechanism may be involved.

7.5 Performance of ATB with Swept Tip and Extended Cuff

Test results for the ATB with the swept tip are shown in Figures 7.24, 25, 26 and 27.

The rate of growth of pitch link loads was almost twice that for the baseline tip and this restricted testing to a maximum C_T of .016 (compared with a C_T of 0.020 with the baseline tip at the same RPM). However at this value of C_T the figure of merit (Figure 7.25) is 0.795 and is still trending upward.

7.6 Performance of ATB with Square Tip and Extended Cuff

Test data with the square tip installed (and extended cuff) is given in Figures 7.28 through 7.31. There is a slight reduction in efficiency throughout the C_T range compared with the baseline tip configuration.

7.7 Configuration Performance Comparisons

Figures 7.32 through 7.42 summarize the comparative performance of the baseline ATB and the XV-15 blades, and of the various ATB alternate configurations.

Figure 7.32 shows that at values of C_T above .0125 the power required for the ATB becomes progressively less than that for the XV-15 blades. Figure 7.33 shows the same information in figure of merit format. Figures 7.34 and 7.35 summarize the comparative behavior of the alternate tip configuration and the XV-15 blades. Figures 7.36 and 7.37 summarize the comparative behaviors of the different cuff configurations.

It is seen that the baseline design elliptical tip outperforms the alternatives although the trend for the swept tip suggests that it might be better at C_T values beyond 0.016. The cuff comparisons clearly demonstrate that extending the trailing edge of the cuff to form a full airfoil has a significant beneficial effect on hover performance.

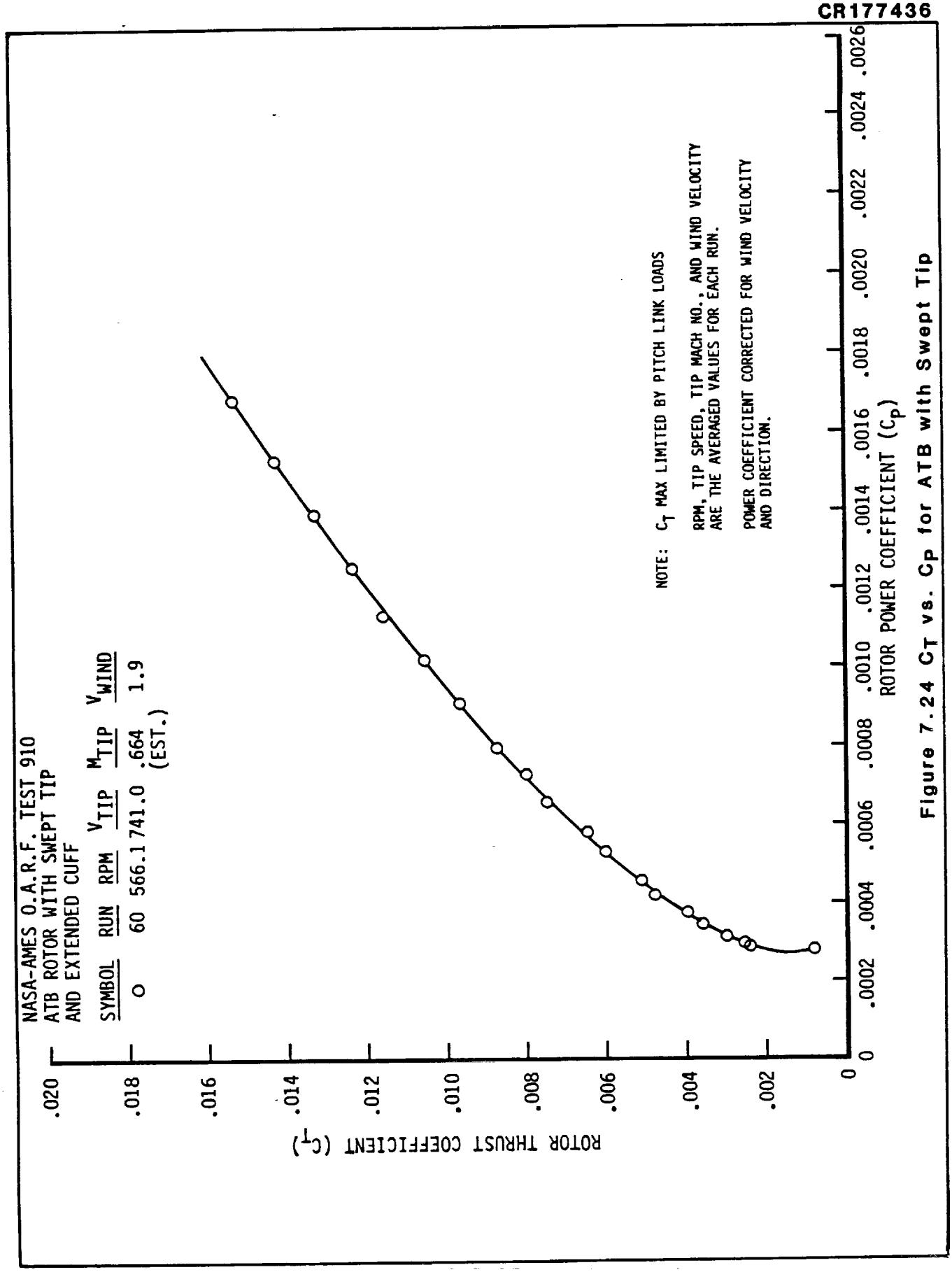

Figure 7.24 C_T vs. C_p for ATB with Swept Tip

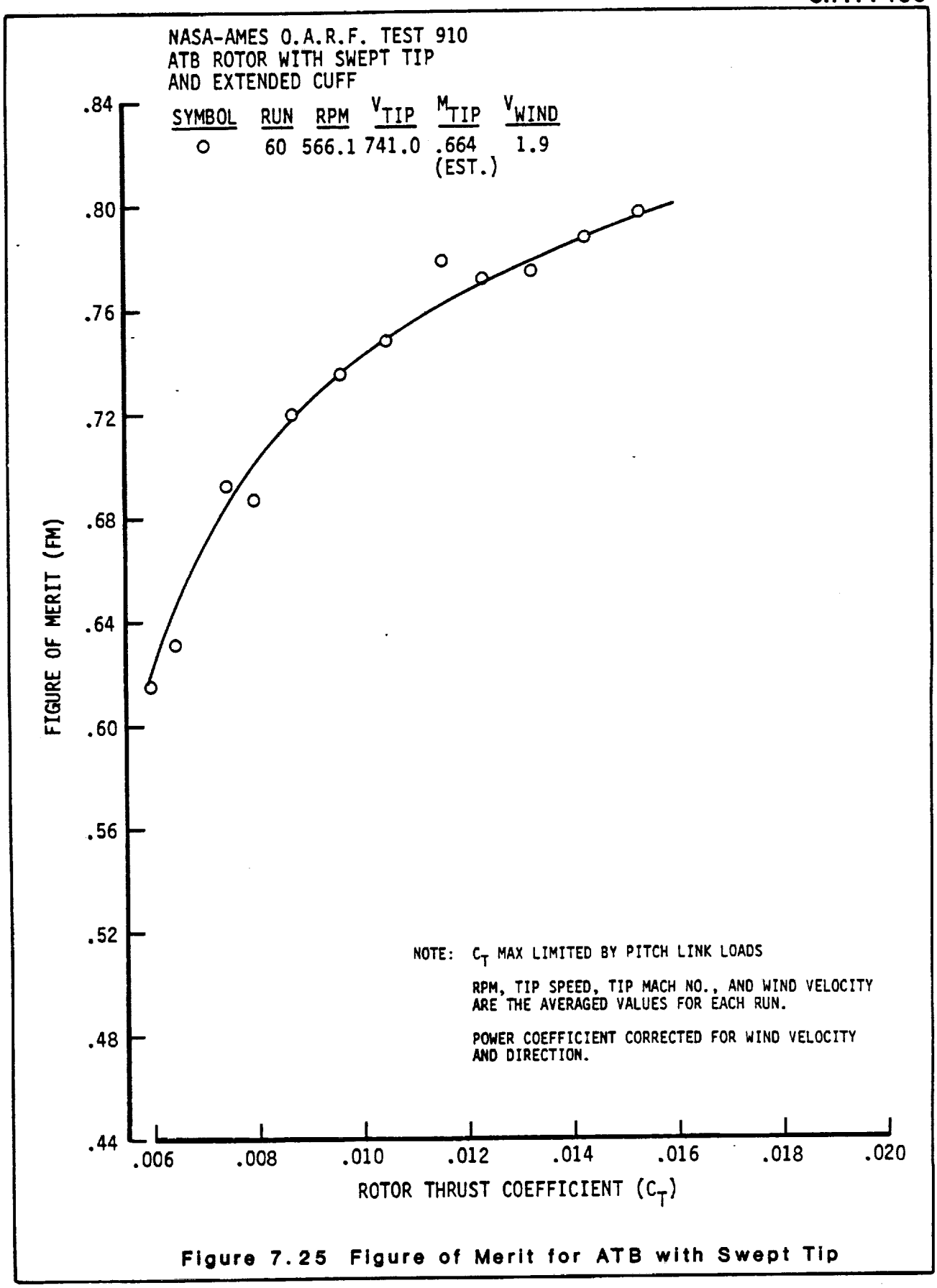

Figure 7.25 Figure of Merit for ATB with Swept Tip

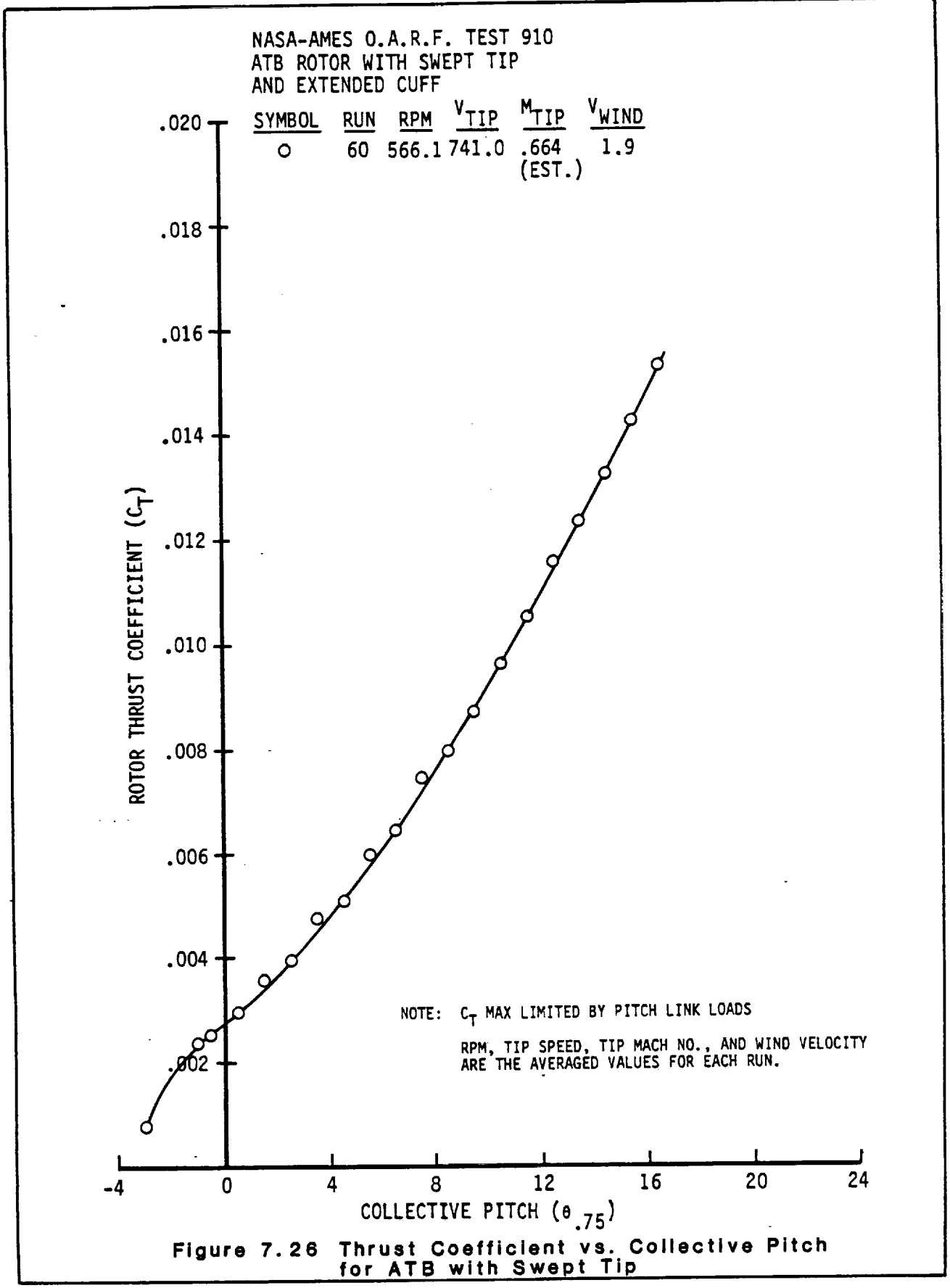

Figure 7.26 Thrust Coefficient vs. Collective Pitch for ATB with Swept Tip

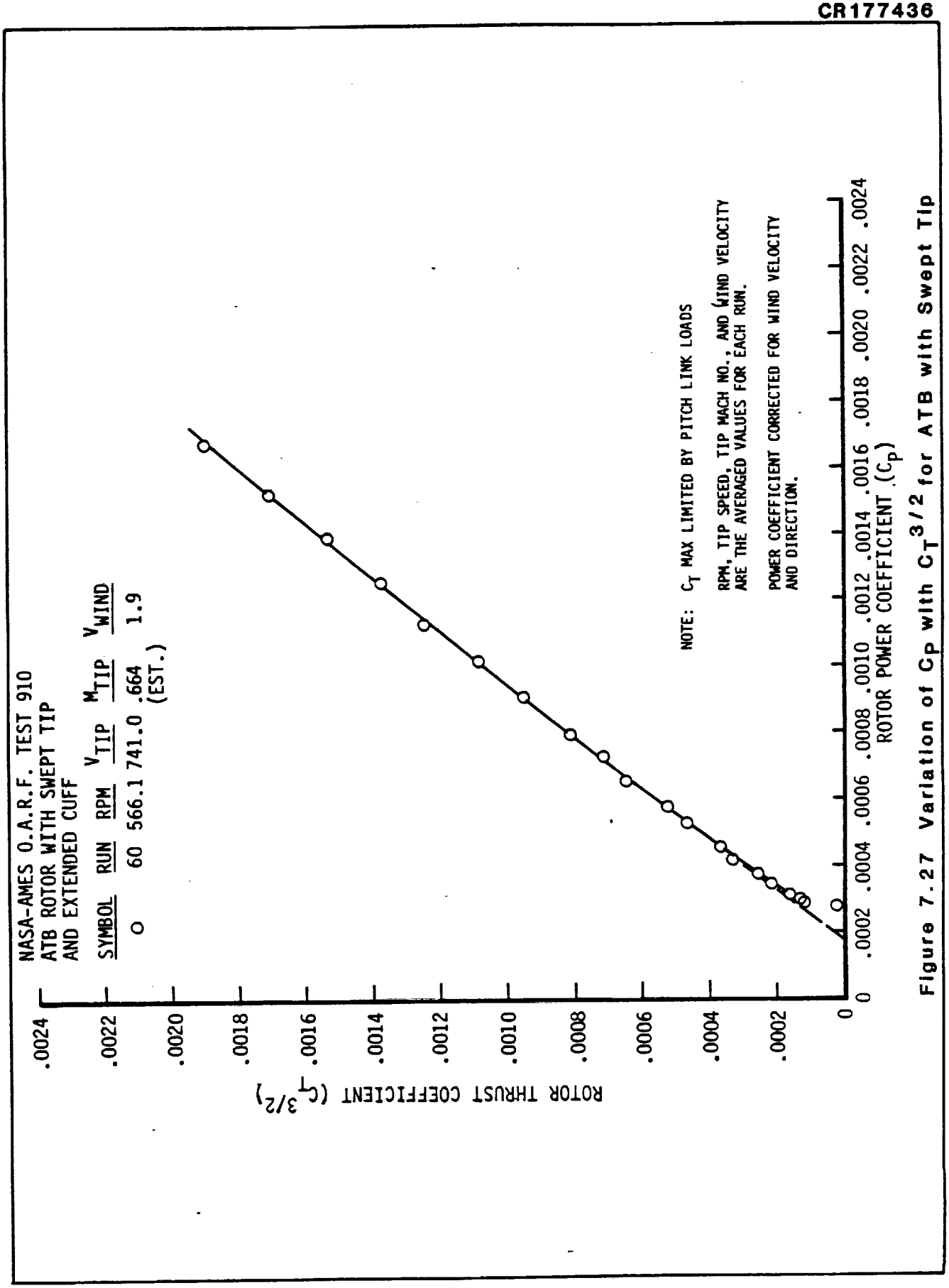

Figure 7.27 Variation of Cp with $C_T^{3/2}$ for ATB with Swept Tip

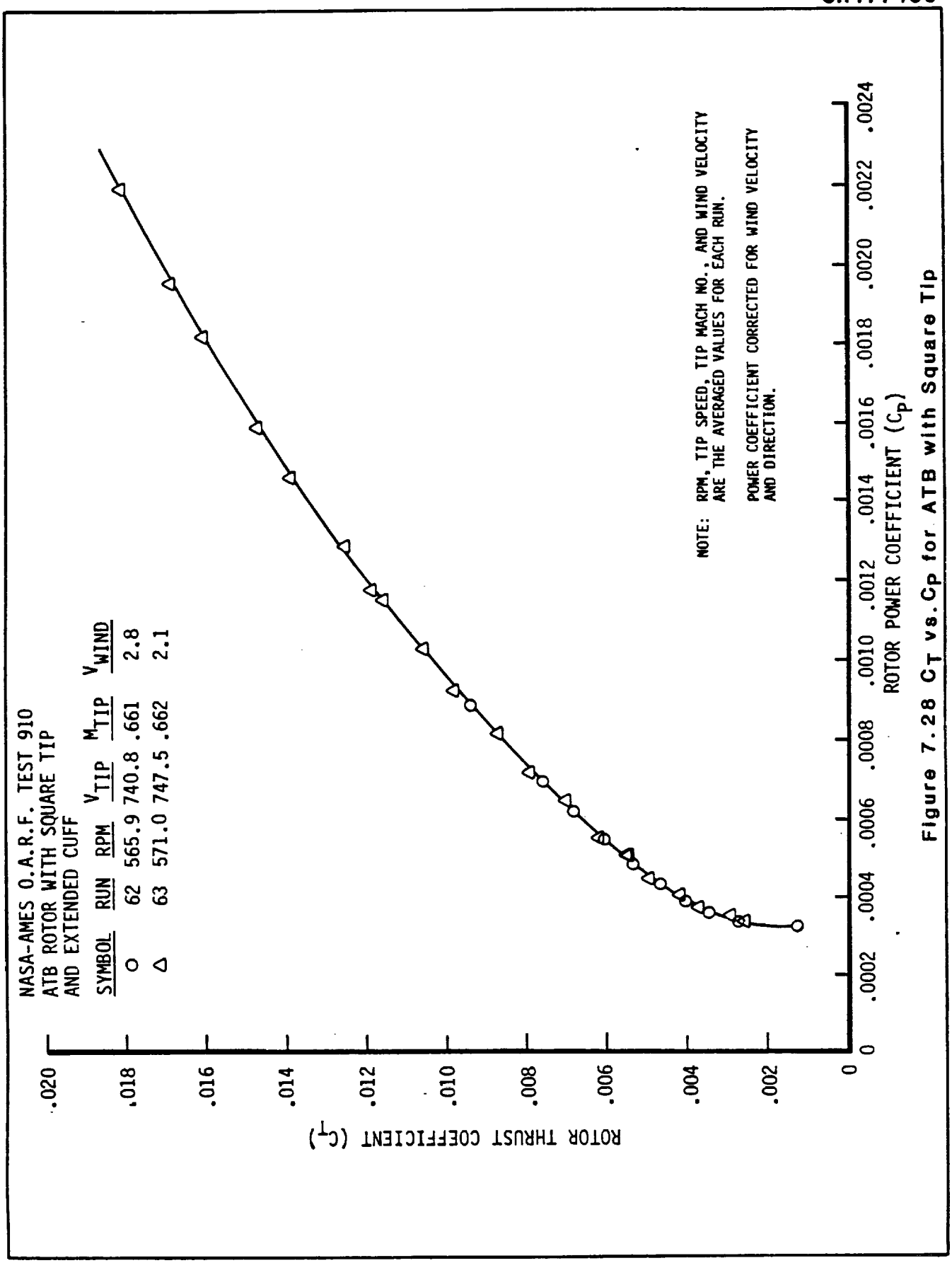

Figure 7.28 C_T vs. C_P for ATB with Square Tip

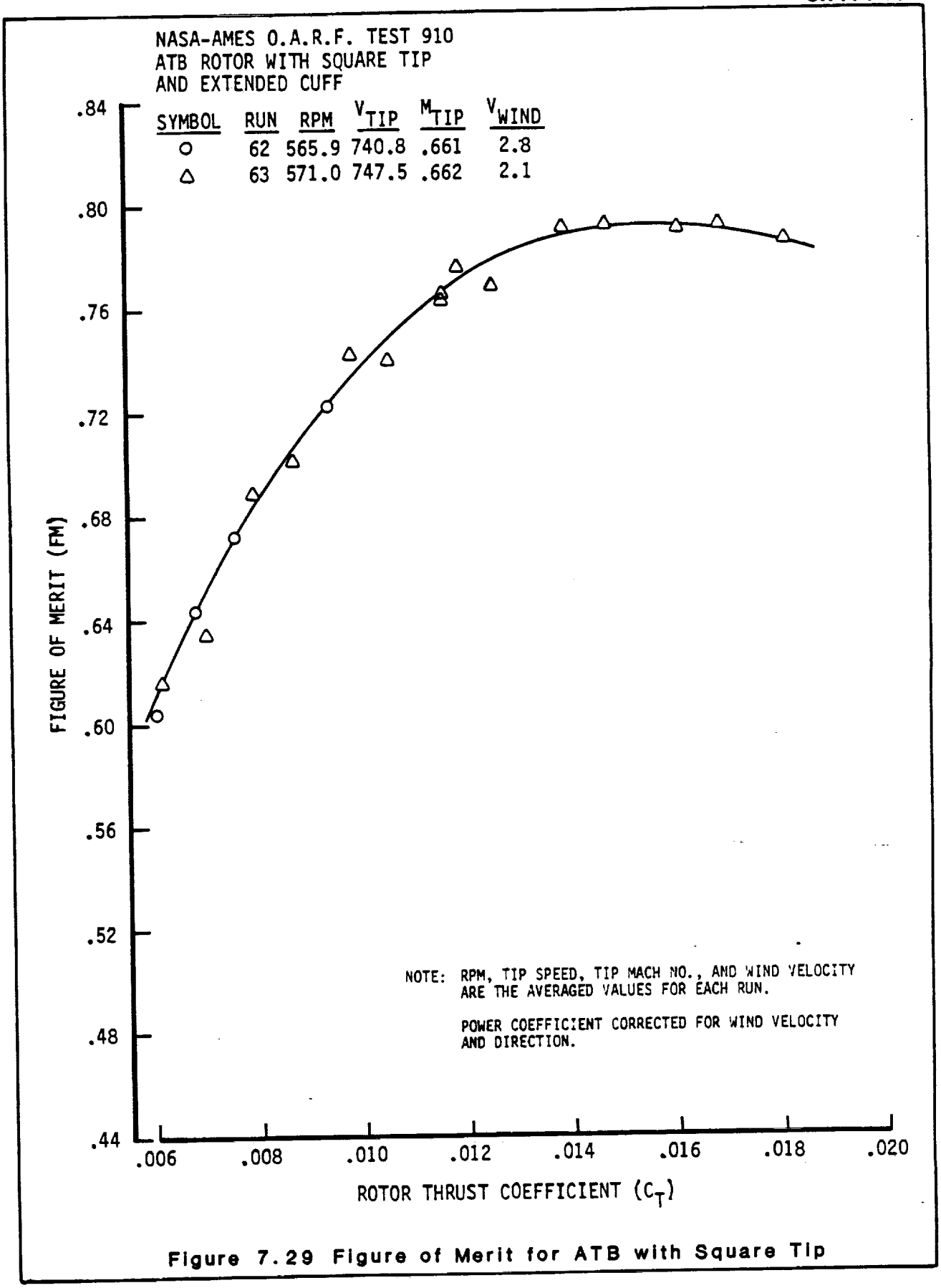

Figure 7.29 Figure of Merit for ATB with Square Tip

C-2

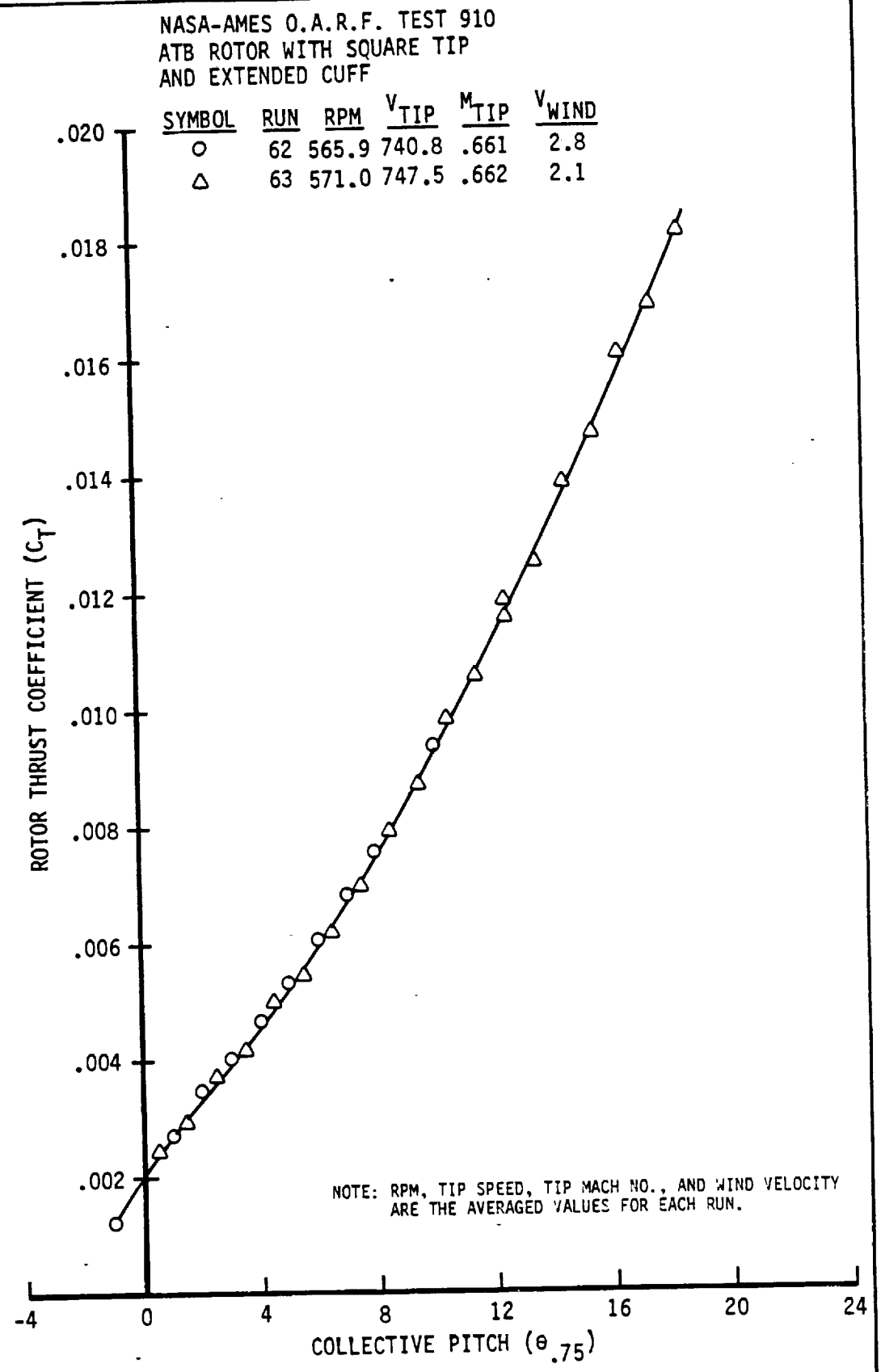

Figure 7.30 Thrust Coefficient vs. Collective Pitch for ATB with Square Tip

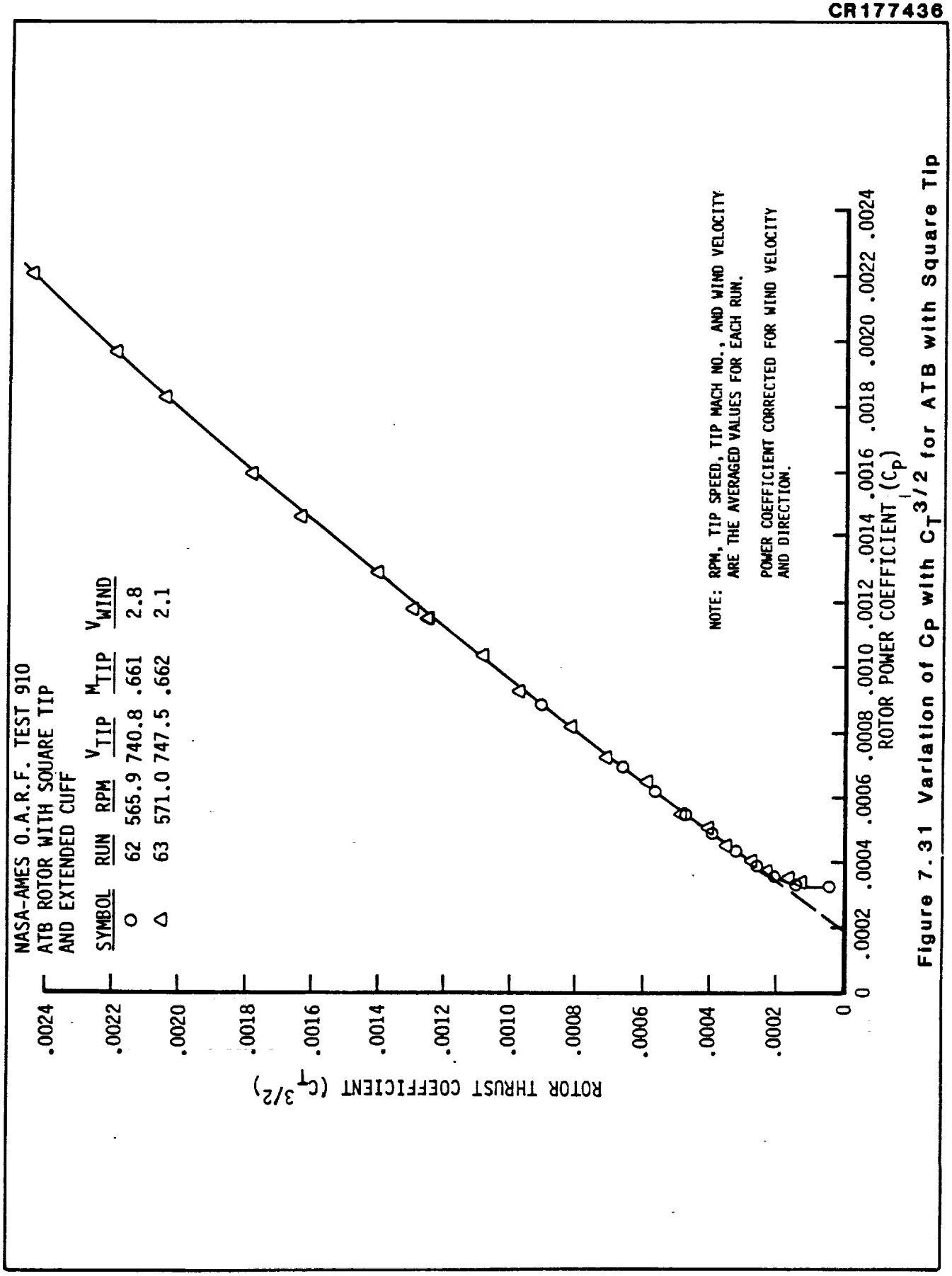

Figure 7.31 Variation of Cp with $C_T^{3/2}$ for ATB with Square Tip

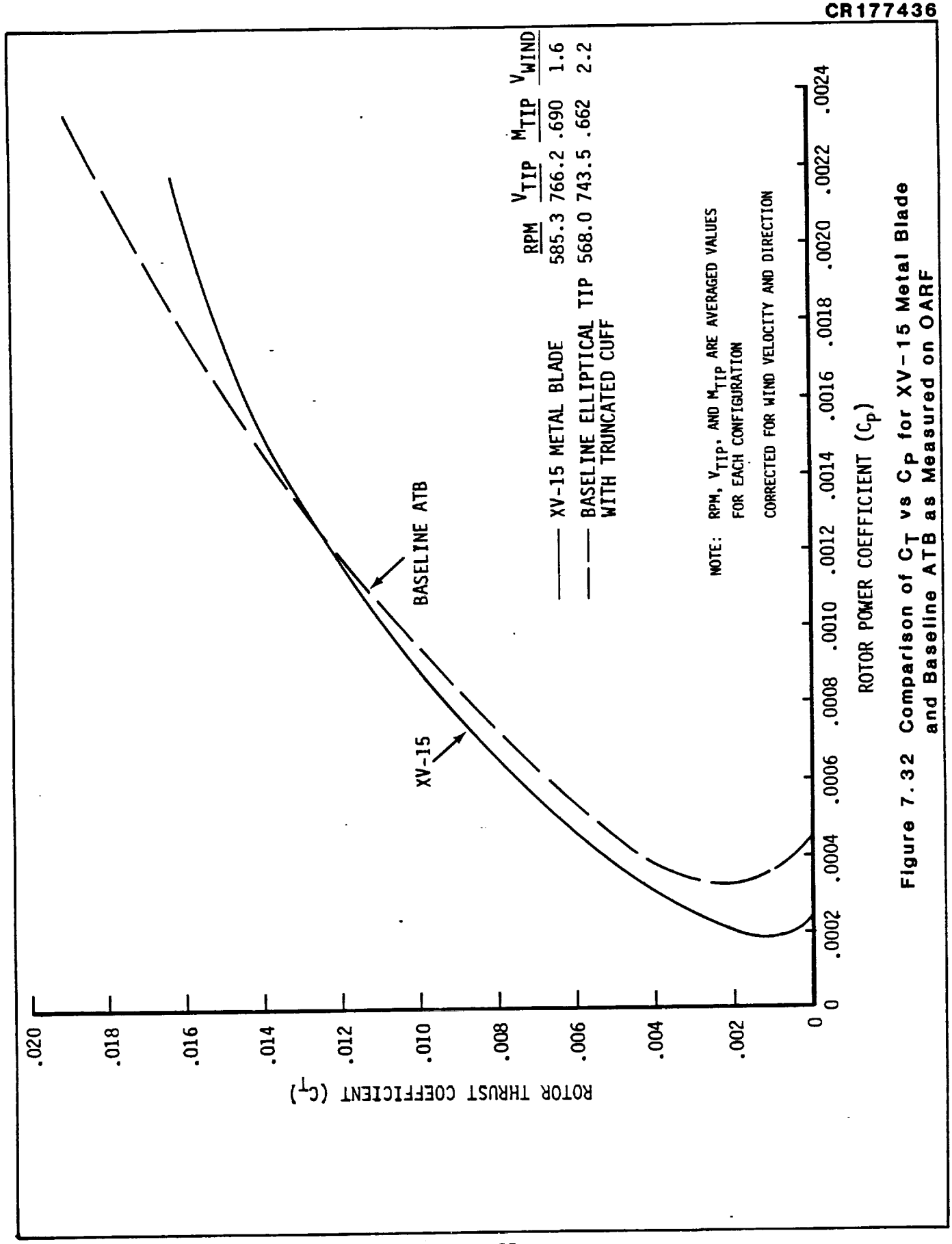

Figure 7.32 Comparison of C_T vs C_P for XV-15 Metal Blade and Baseline ATB as Measured on OARF

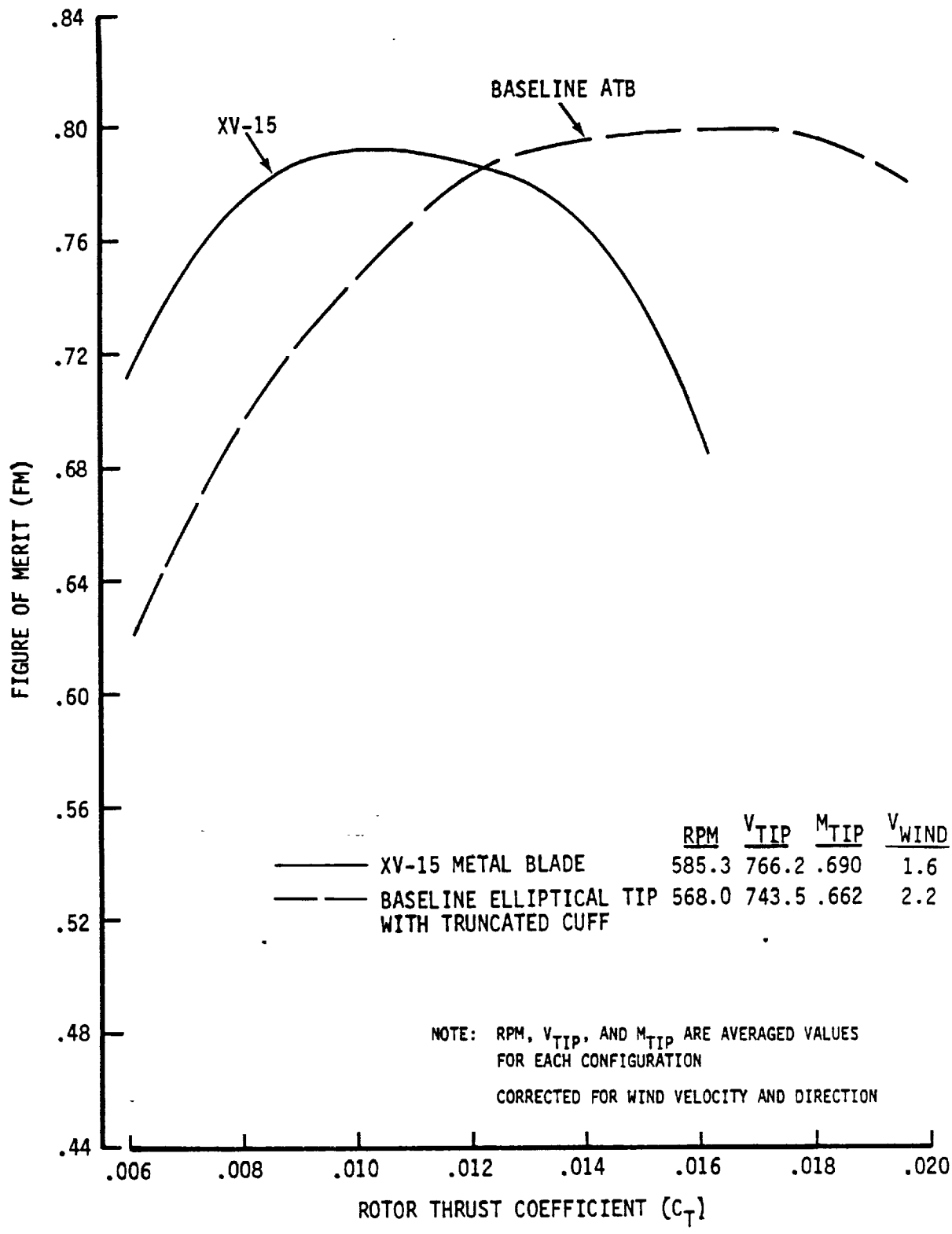

Figure 7.33 Comparison of Figure of Merit for XV-15 Metal Blade and Baseline ATB as Measured on OARF

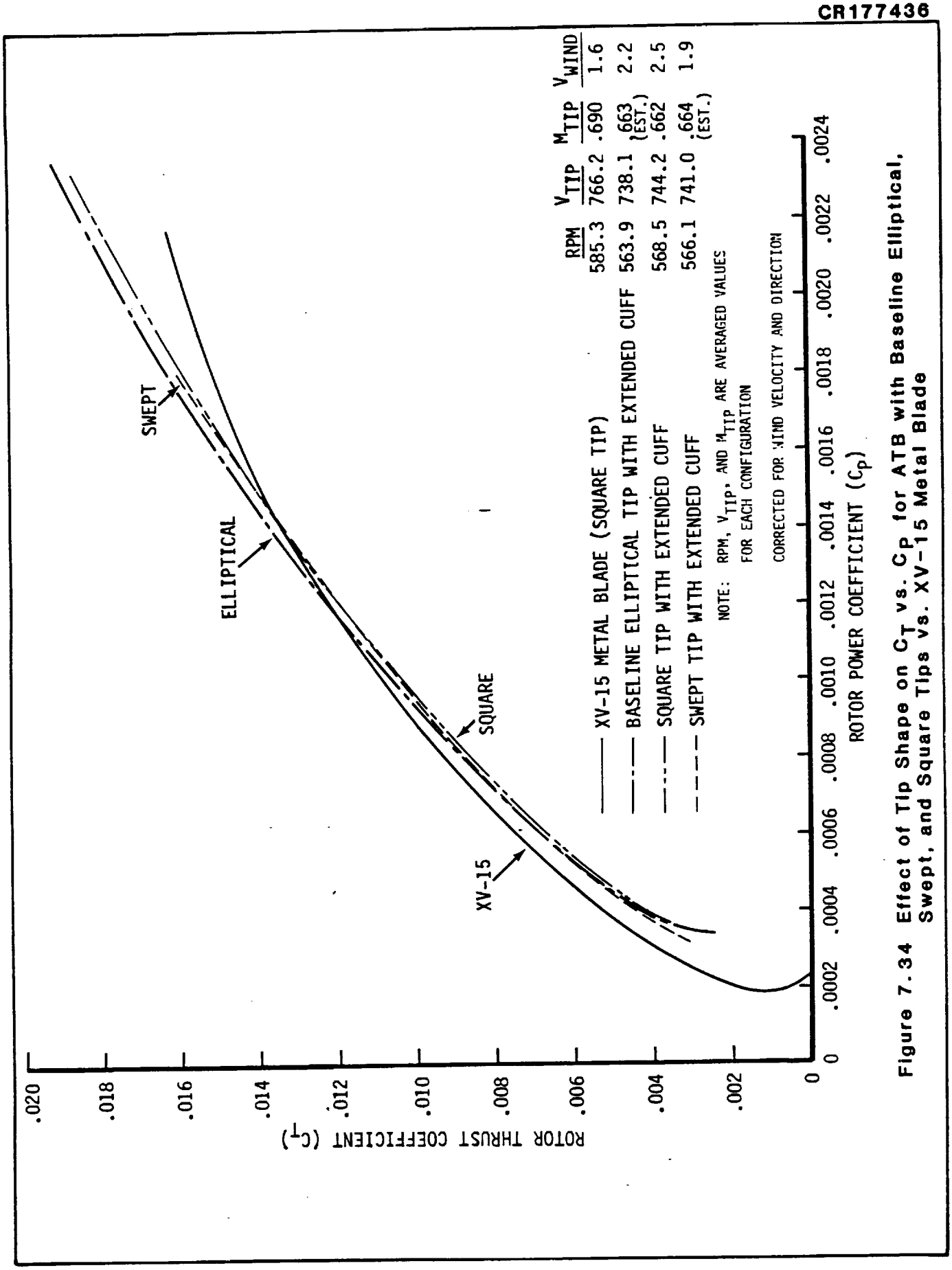

Figure 7.34 Effect of Tip Shape on C_T vs. C_P for ATB with Baseline Elliptical, Swept, and Square Tips vs. XV-15 Metal Blade

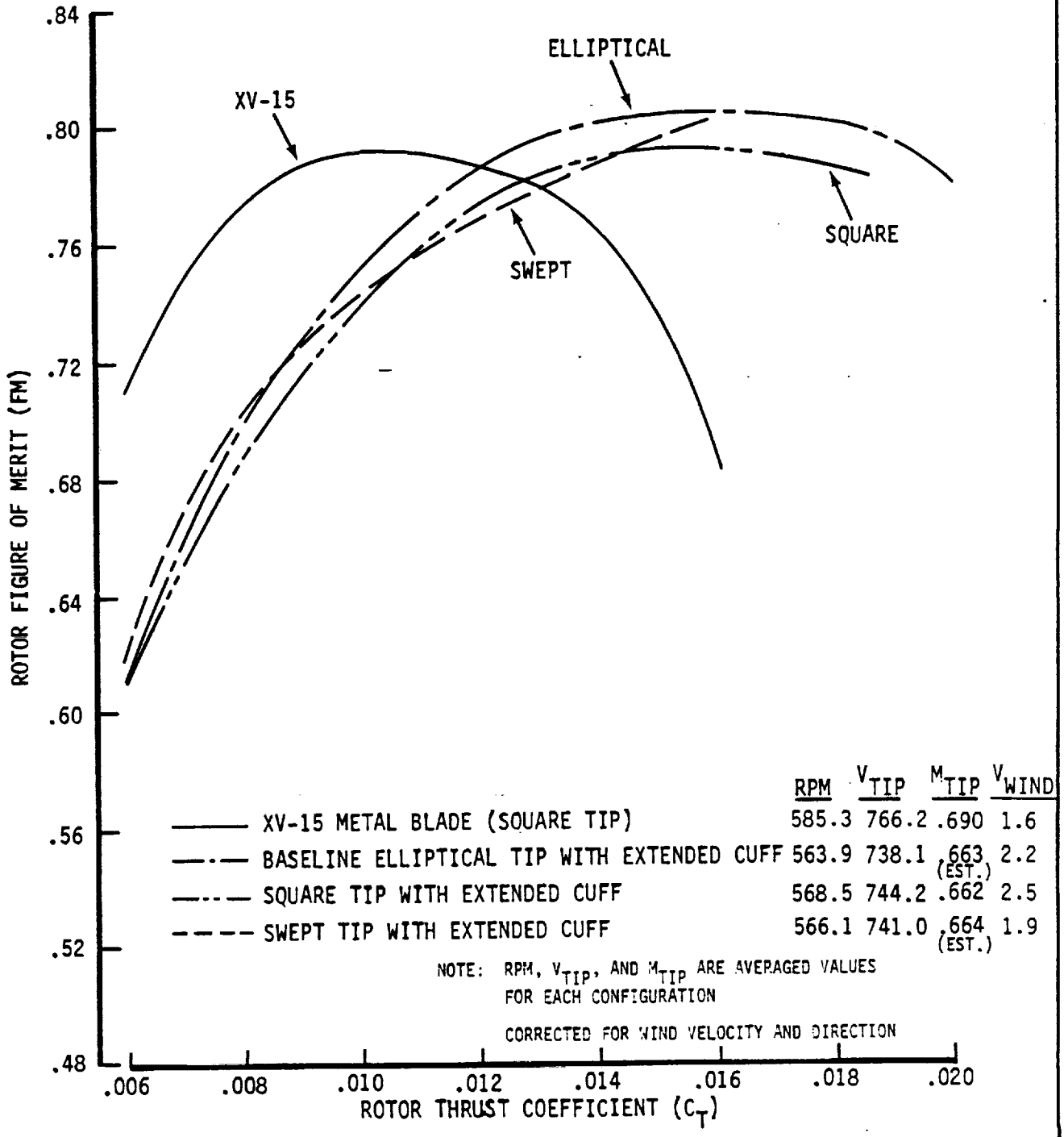

Figure 7.35 Effect of Tip Shape on Figure of Merit for ATB with Baseline Elliptical, Swept, and Square Tips vs. XV-15 Metal Blade

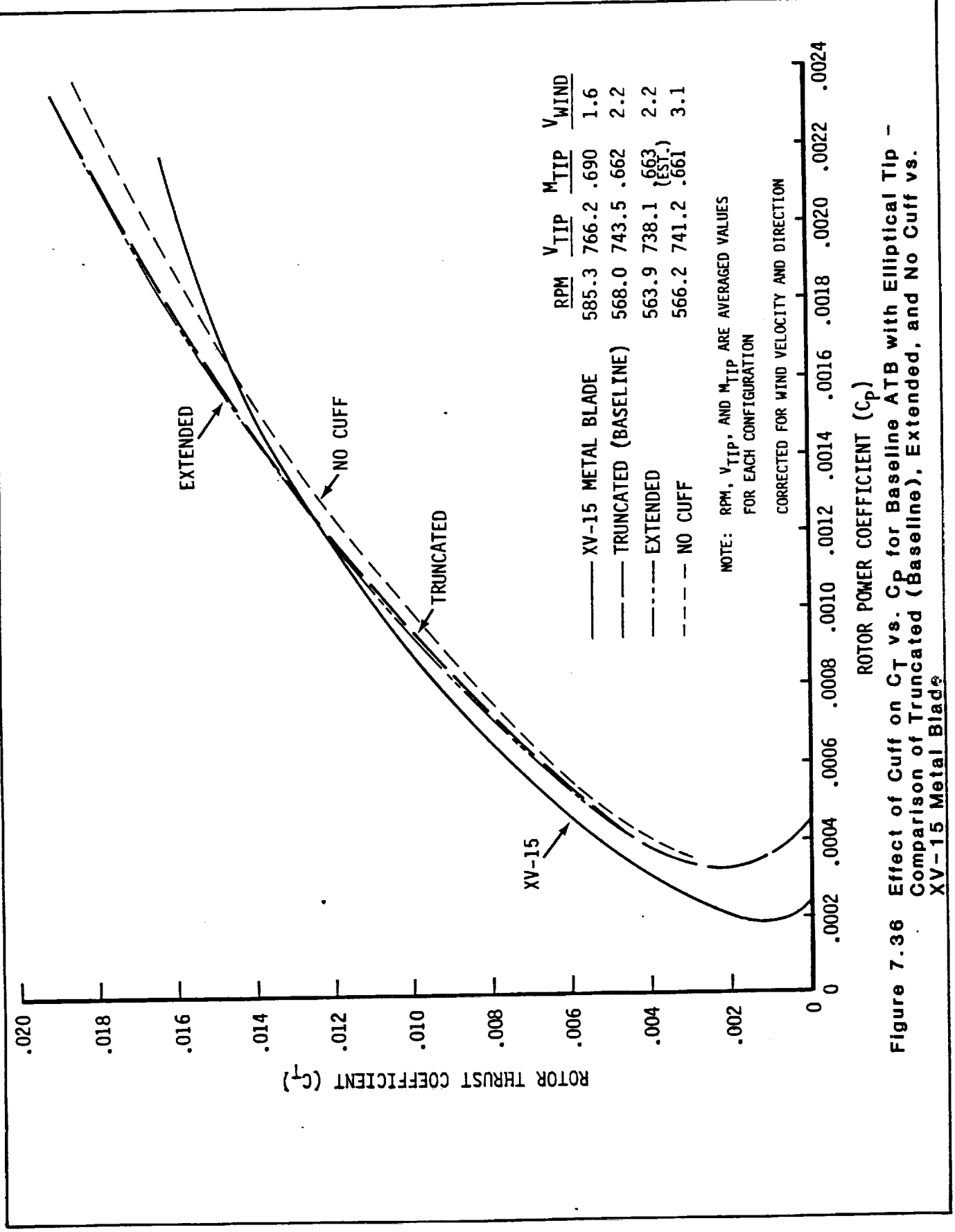

Figure 7.36 Effect of Cuff on C_T vs. C_P for Baseline ATB with Elliptical Tip - Comparison of Truncated (Baseline), Extended, and No Cuff vs. XV-15 Metal Blade

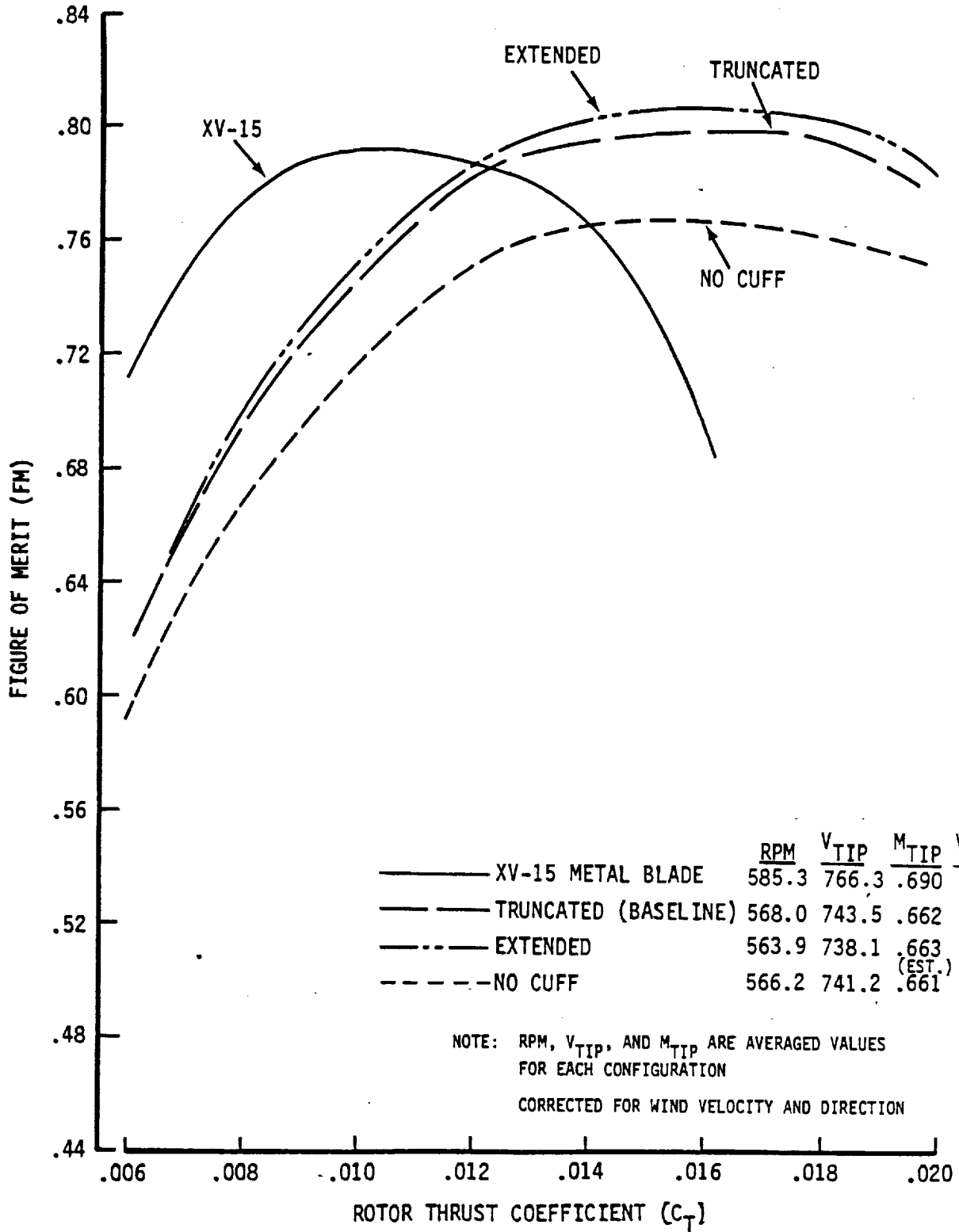

Figure 7.37 Effect of Cuff on Figure of Merit for Baseline ATB with Elliptical Tip - Comparison of Truncated (Baseline), Extended, and No Cuff vs. XV-15 Metal Blade

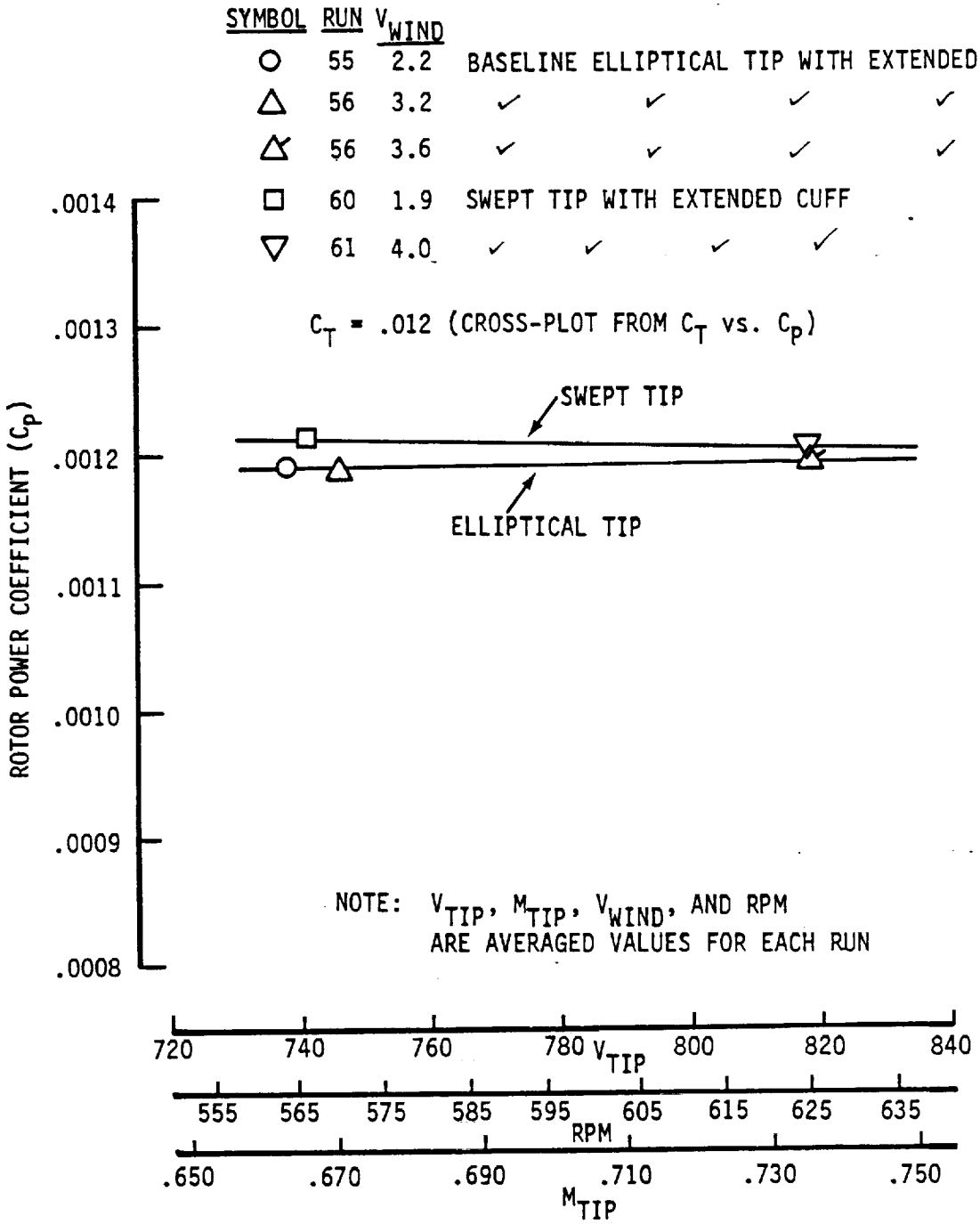

Figure 7.38 Effect of Tip Shape on C_P vs. V_{TIP}, RPM, and M_{TIP} – Comparison of Baseline Elliptical Tip and Swept Tip

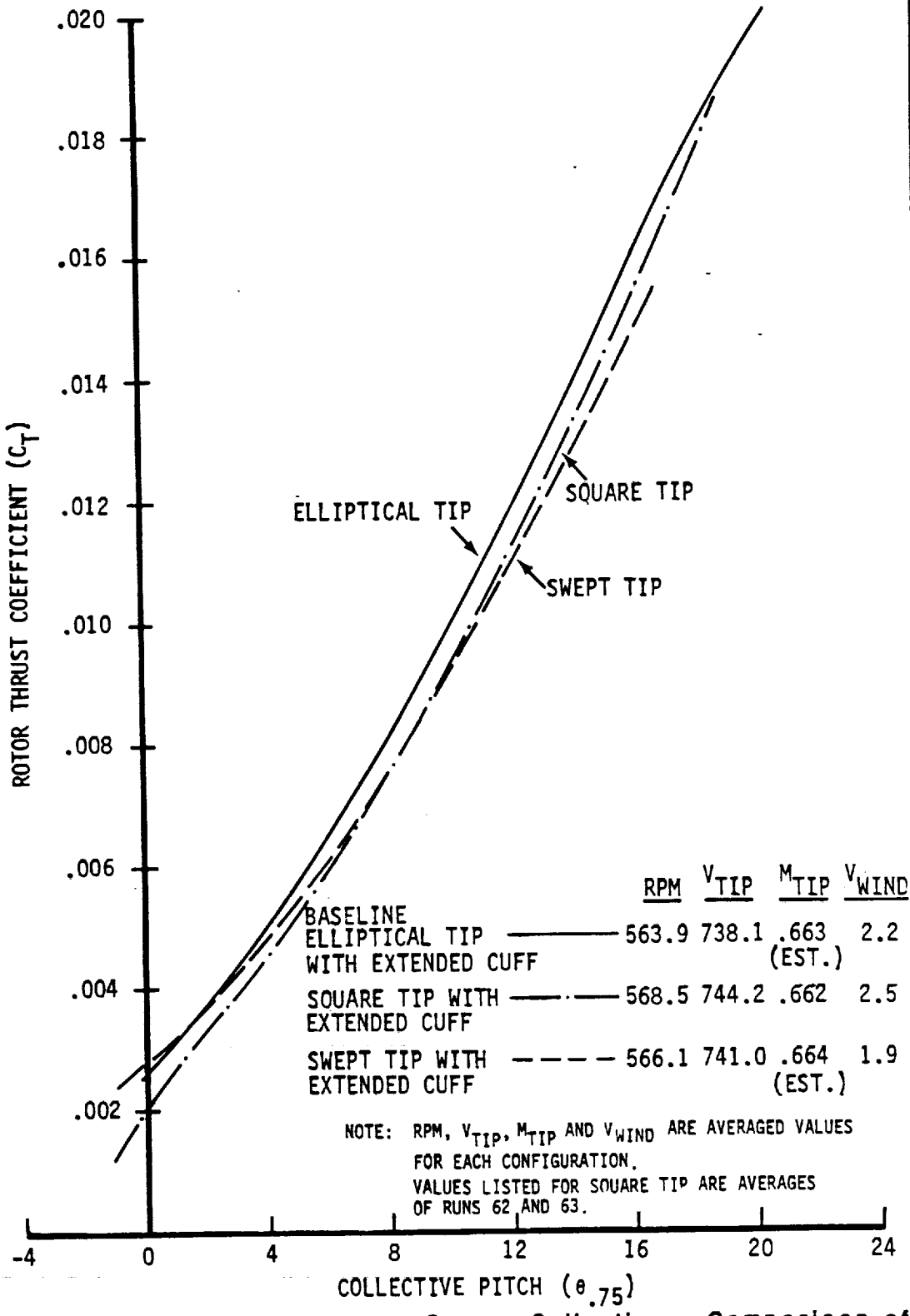

Figure 7.39 Effect of Tip Shape on C_T vs. Collective- Comparison of Baseline ATB Elliptical Tip, Swept and Square Tips

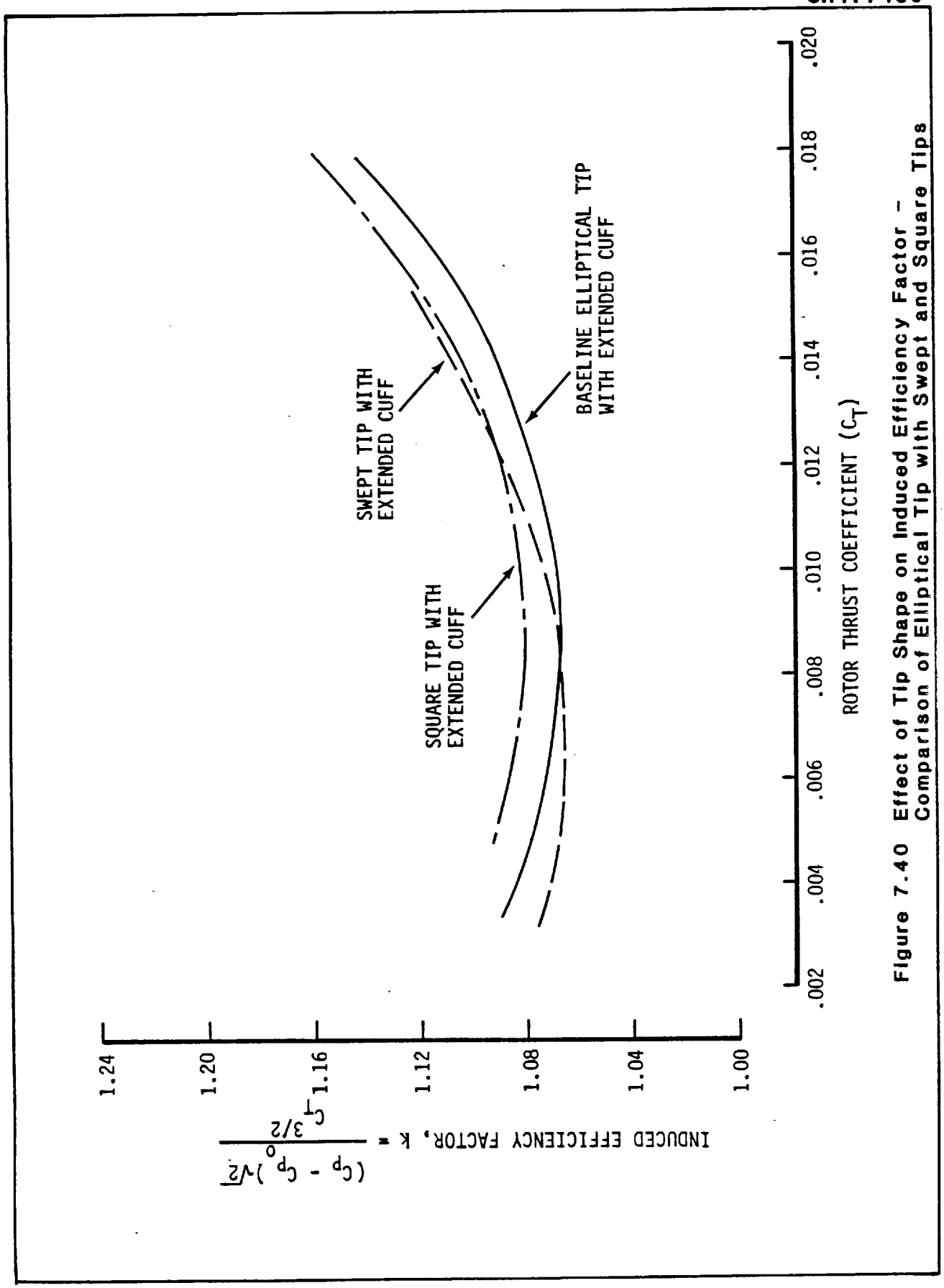

Figure 7.40 Effect of Tip Shape on Induced Efficiency Factor – Comparison of Elliptical Tip with Swept and Square Tips

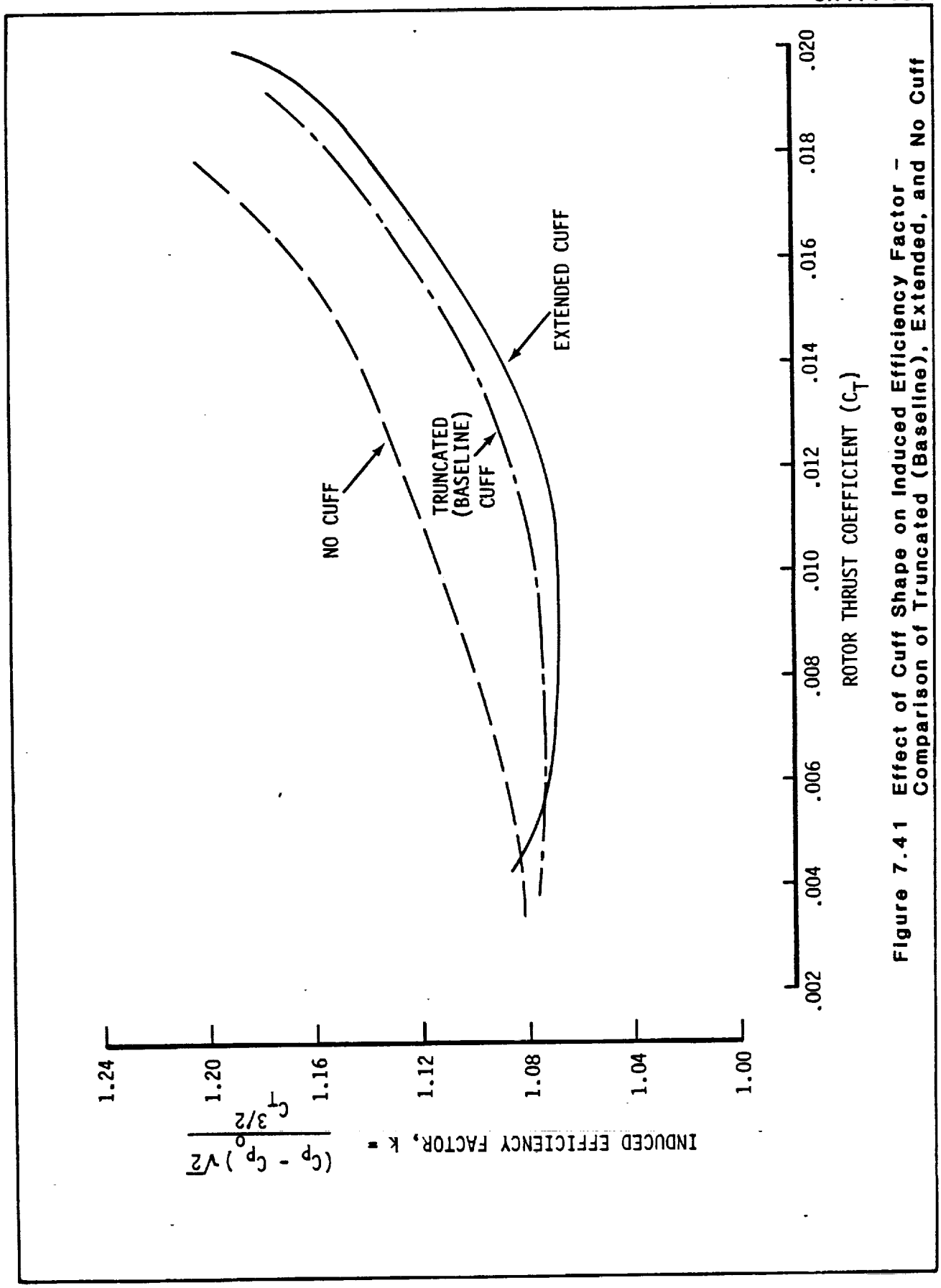

Figure 7.41 Effect of Cuff Shape on Induced Efficiency Factor – Comparison of Truncated (Baseline), Extended, and No Cuff

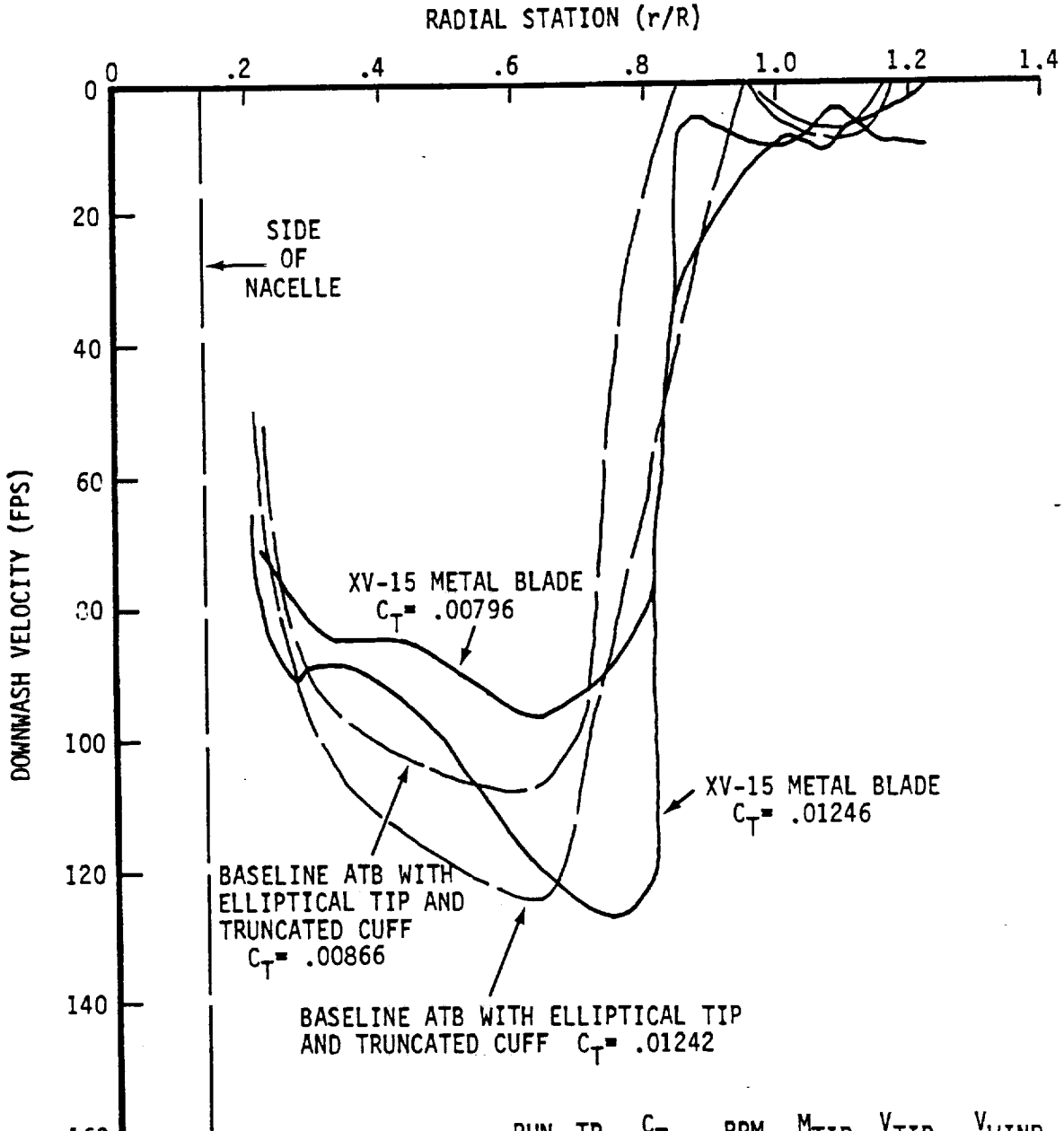

	RUN	TP	C_T	RPM	M_{TIP}	V_{TIP}	V_{WIND}
XV-15 METAL BLADE	25	16	.00796	585.9	.690	771.5	2.9
	25	22	.01246	585.5	.689	770.9	3.3
ATB ROTOR	50	7	.00866	561.2	.661	734.6	1.9
	50	9	.01242	560.9	.660	734.2	2.2

Figure 7.42 Comparison of Downwash Distributions for XV-15 Metal Blade and Baseline ATB Rotor

In Figure 7.38 the effect of tip shape on power required is shown as a function of tip speed, RPM, and tip Mach number. A comparison is made between the swept and the baseline elliptical planforms. The extended cuff configuration was used for this crossplot. At the normal operating RPM (nominally 565), and at maximum RPM (625), the elliptical tip maintains a slight advantage at C_T = .012.

Figure 7.39 compares the baseline elliptical, swept, and square tips on a C_T vs. collective basis. As in Figure 7.40, the extended cuff was used for this plot. As expected, the baseline elliptical tip has slightly better performance than the other tip configurations.

Figures 7.40 and 7.41 present the effect of tip shape and cuff configuration on induced efficiency as a function of rotor thrust coefficient.

Figure 7.42 compares downwash distributions for the metal blade and the baseline ATB at nearly similar thrust coefficients.

The photograph in Figure 7.43 show tip vortices for the elliptical tip with the extended cuff configuration. (Compare with Figure 7.8).

7.8 Theory-Test Comparison

The predictions for the XV-15 metal blades and for the Advanced Technology Blades are compared with measured performance in Figure 1.4. The figure of merit is generally underestimated at high values of C_T. The predicted performance of the XV-15 metal blades and the baseline ATB blades was calculated using a current lifting-line/blade element program. The program, which correlates well with low twist helicopter blades, appears to overestimate the induced power for highly twisted propellers/rotors. Possible reasons for the discrepancies are discussed in the following paragraphs.

7.8.1 Rotor Wake Model

Because over 70 percent of the power absorbed by a hovering rotor is wake-induced, the successful prediction of performance depends on how well the effects of the vortex wake are modelled. An accurate wake model is one in which the strength and positions of the vortices forming the wake are correctly represented. The current wake model is semi-empirical and contains many correction factors determined by correlation of the analysis with measured helicopter rotor and prop-rotor performance. While the model yields practical results in cases where the rotor geometry and operating conditions are within the range of the empirical factors, extensions to configurations outside the data base are less reliable. This semi-empirical wake representation is outdated and is currently being replaced with a modern wake representation based upon experimentally observed rotor wake structures following Landgrebe, Kocurek, and Gray.

A comparison of the effect of the different wake representations on the calculation of figure of merit for the ATB rotor is presented in Figure 7.44. With the current wake, the peak figure of merit level is underpredicted and performance at C_T values greater than 0.009 is also underpredicted. When the empirical wake is replaced by the Kocurek wake model,

Figure 7.43 Tip Vortices of Baseline ATB with Extended Cuff

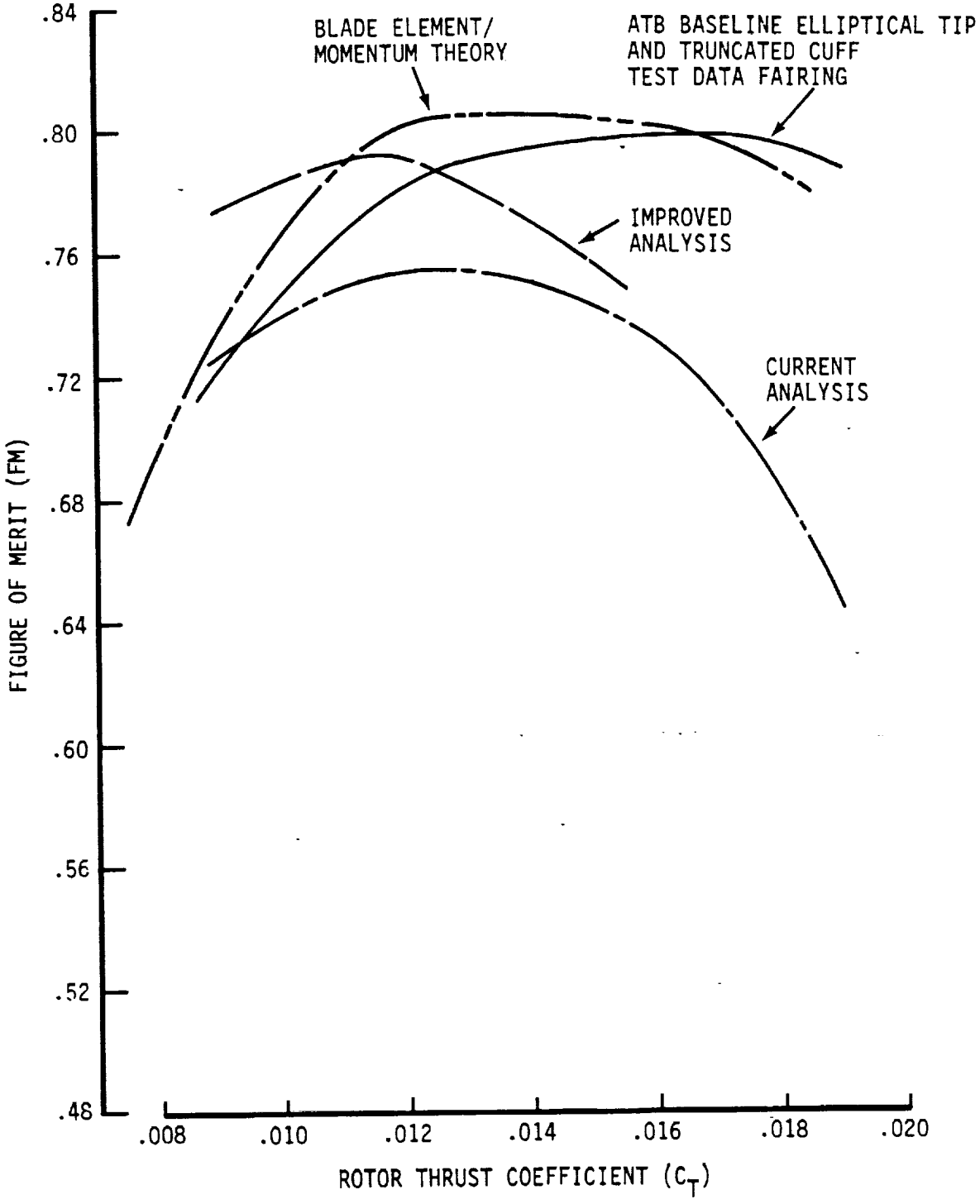

Figure 7.44 Comparison of Calculated and Measured Performance on the Advanced Technology Blade Rotor

prediction of peak figure of merit is improved. Note that neither module predicts the high figures of merit at high thrust coefficients. Also shown are the results of a blade element/momentum analysis (using the same airfoil data) which somewhat overpredicts the performance but yields a better overall shape for the curve.

Although there has been much work on experimentally observed rotor wake structures for helicopter rotors, there have been no tests conducted specifically for highly twisted rotors or propellers. Some progress in this direction was made during this test as described in sections 7.1 and 7.7. Further detailed experiments using pressure instrumented blades and lasers to measure the detailed wake structure should be conducted for representative rotors. These results can be mathematically modelled and incorporated into suitable analysis techniques.

While the introduction of more realistic wake models may improve the prediction techniques, other areas also require attention.

7.8.2 Airfoil Behavior at High Angles of Attack

Highly twisted tilt rotor blades operate in hover with the root sections at or beyond stall angles of attack. Two-dimensional airfoil data obtained from the wind tunnel usually does not define the post-stall lift, drag, and pitching moment behavior because testing is rarely conducted beyond stall. It has been shown by the OARF results and elsewhere that the root area can influence rotor performance significantly. Additional test data both at model and full scale is therefore required on representative airfoils at high angles of attack to establish the basic shape of the post-stall behavior for the root section.

7.8.3 Spanwise Flow Effects

There is evidence that two-dimensional airfoil data is not entirely applicable near the root of a rotating blade. Figure 7.45 from Reference 7 shows that propeller blade sections near the root appear to have extended lift-curves and higher lift-curve slopes than those obtained from two-dimensional wind tunnel tests. The mechanism suggested for this improved performance is boundary layer thinning arising from centrifugal spanwise pumping and the effect of Coriolis forces on the boundary layer. Development of a method to account for this effect is recommended and could be conducted as part of the previously recommended experiments on pressure instrumented blades.

8.0 ROTOR AND CONTROL SYSTEM LOADS

Rotor and control loads were continuously monitored throughout the hover testing of the XV-15 Metal Blade and Advanced Technology Blades to ensure that static and dynamic limits were not exceeded. In general, testing was limited by steady spindle flap bending at the extremes of the thrust range. While oscillatory loads did not limit performance testing, it was necessary

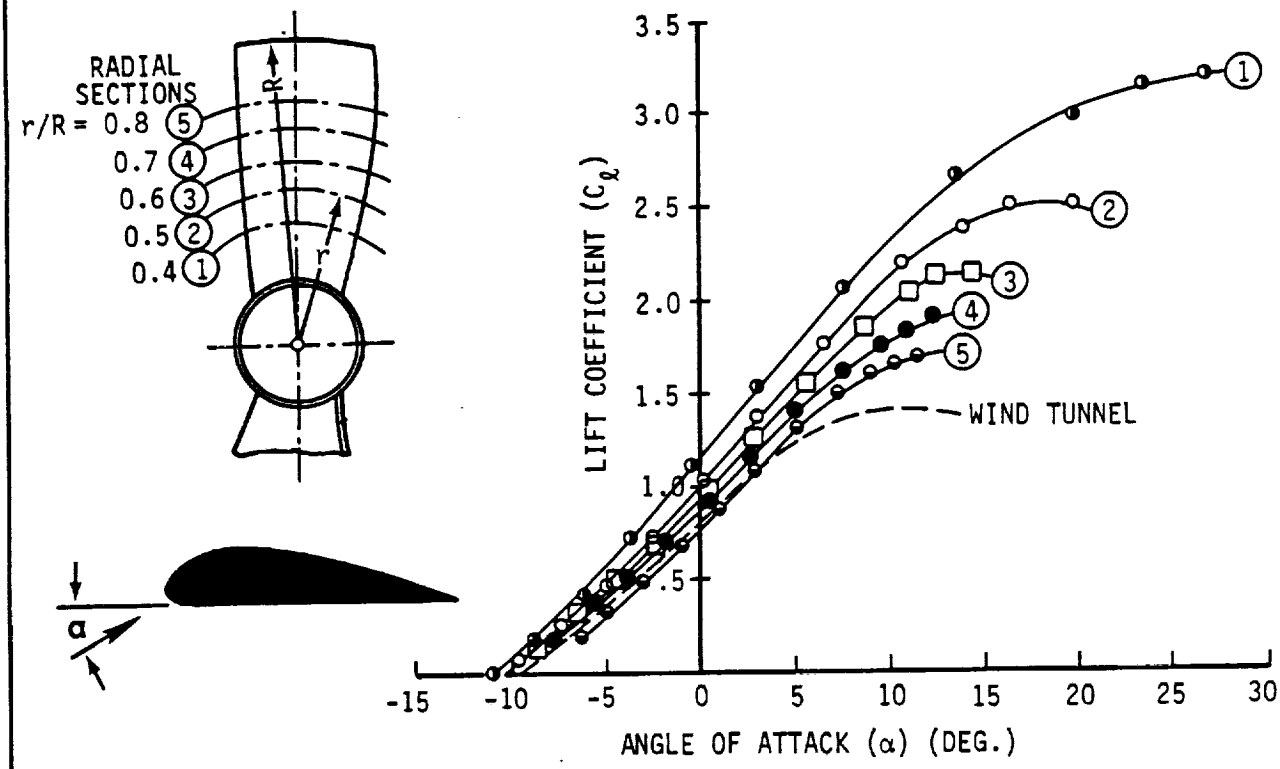

Figure 7.45 Local Lift Coefficients, C_ℓ, at Various Radial Sections on a Rotating Propeller (Reference 7)

to use cyclic to control flapping and flap-induced loads to acceptable levels. Even with cyclic control, transient bending loads frequently exceeded the endurance limit of the hub yoke spindle necessitating frequent damage counts to determine the percentage of spindle life used. (Total life used did not exceed 5 per cent.)

The sign convention used in reporting the measured loads is as follows:

+ Flap Bending -- Compression in the blade upper surface

+ Chord Bending -- Compression in trailing edge

+ Pitch Link Load -- Consistent with blade torsion leading edge up

It should be noted that, in any given run, substantial scatter is present in the loads data because of cyclic adjustments and variations in wind direction and magnitude. However, although not ideal for correlation studies, the data indicate general trends.

8.1 XV-15 Metal Blade

The rotor system, blades, hub, and controls were essentially the same as previously tested on the Aero Propulsion Laboratory Whirl Stand at Wright-Patterson Air Force Base and documented in Bell Helicopter Report No. 300-099-010 (CR 114626), Reference 4.

Figures 8.1 and 8.2 present a summary of the measured steady and oscillating yoke spindle and pitch link loads as a function of C_T. Comparing the data from the previous testing at Wright-Patterson with the current Ames testing does not indicate any significant differences in the measured loadings.

The upper end of the thrust range was generally limited by blade stall as evidenced by an increase in rotor noise, a rapid increase in oscillatory pitch link loads, and difficulty in controlling gimbal angle. In the preliminary run-ups, operation was limited by oscillatory loads in the hub yoke spindle. Bending moment allowables initially imposed on the spindle for this test, (± 20,000 in.lb. as compared to ± 58,000 in.lb. in the previous whirl test) were based on later knowledge of the endurance limits for the titanium material and were routinely exceeded during spin-up and shut-down. This limitation was overcome by utilizing an S-N curve for the spindle to allow short time exceedance of the ± 20,000 in.lb. endurance limit. A running damage count was maintained to ensure safety of operation.

8.2 Baseline Advanced Technology Blade (ATB)

Figures 8.3 through 8.22 present a summary of the measured steady and oscillating yoke spindle, pitch link, and flap bending loads as a function of C_T and RPM.

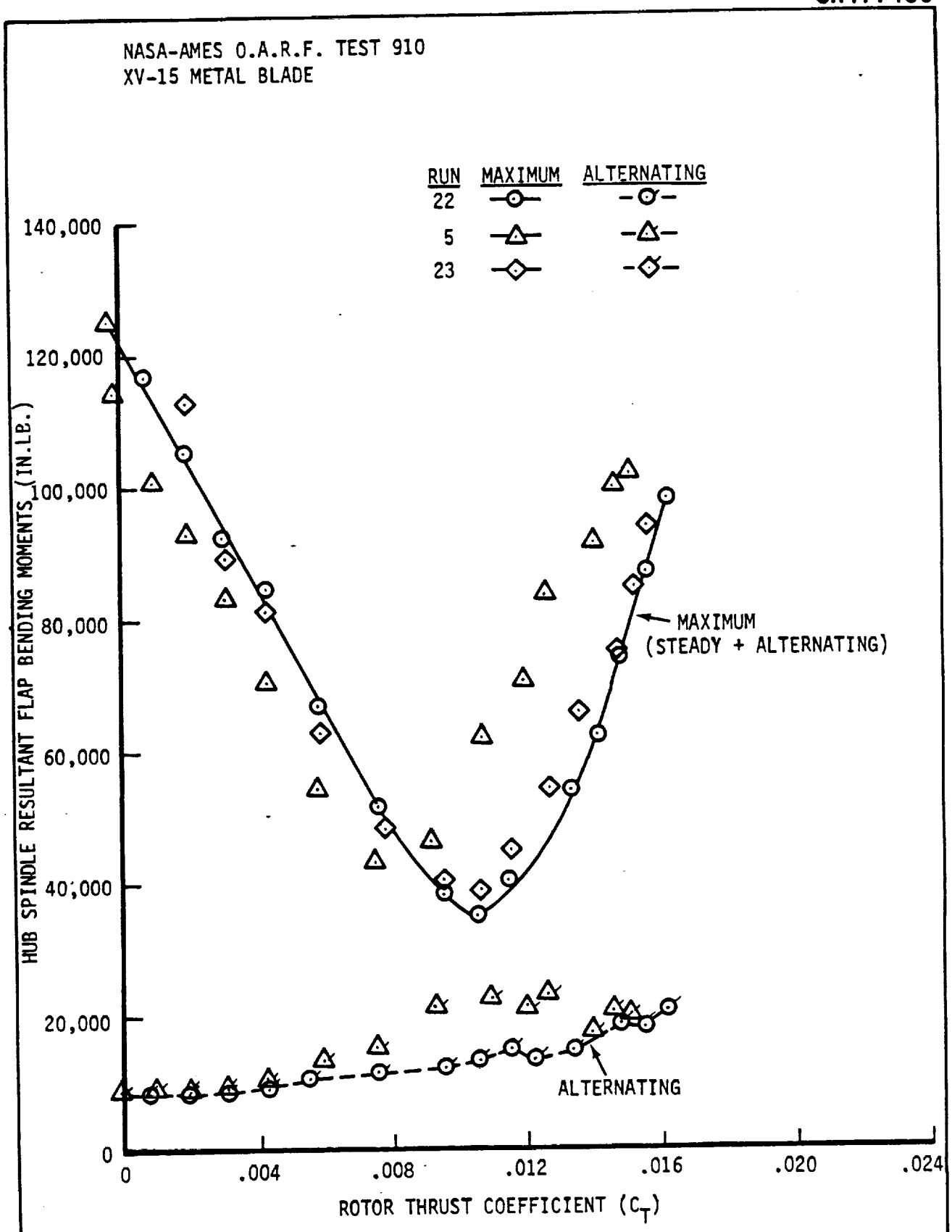

Figure 8.1 XV-15 Metal Blade: Hub Spindle Resultant Flap Bending Moments vs. C_T

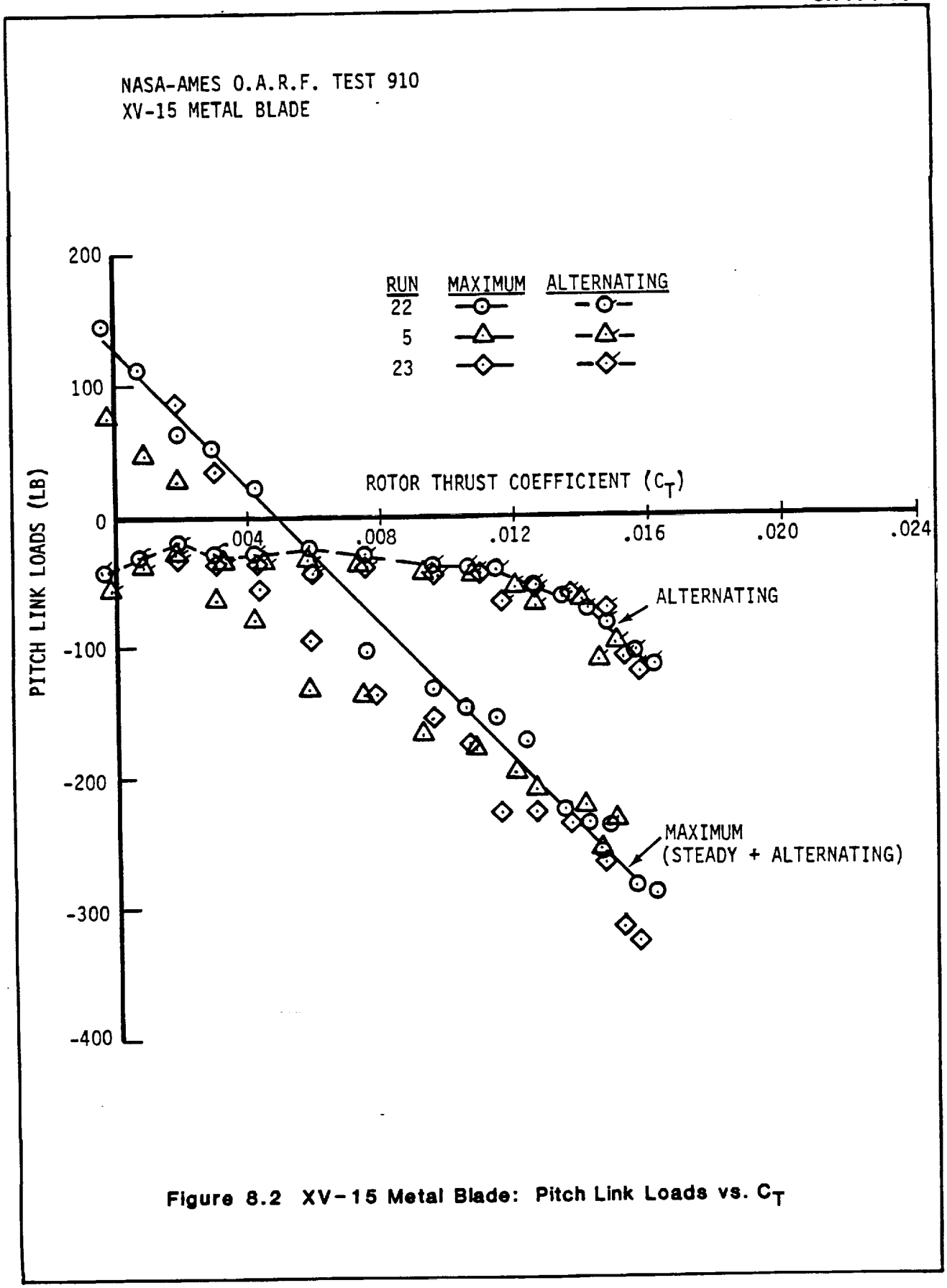

Figure 8.2 XV-15 Metal Blade: Pitch Link Loads vs. C_T

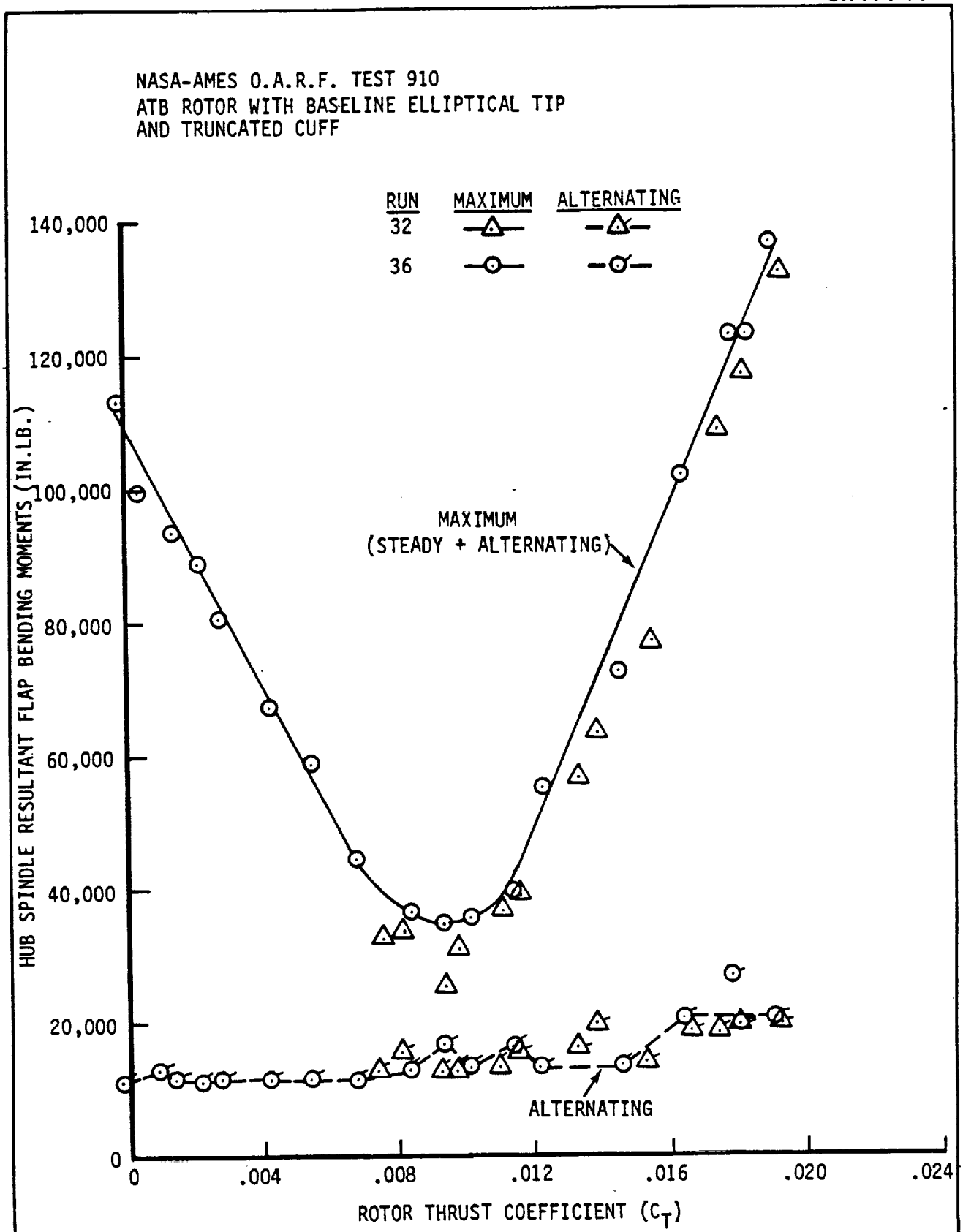

Figure 8.3 Baseline ATB: Hub Spindle Resultant Flap Bending Moments vs. C_T (Runs 32 and 36)

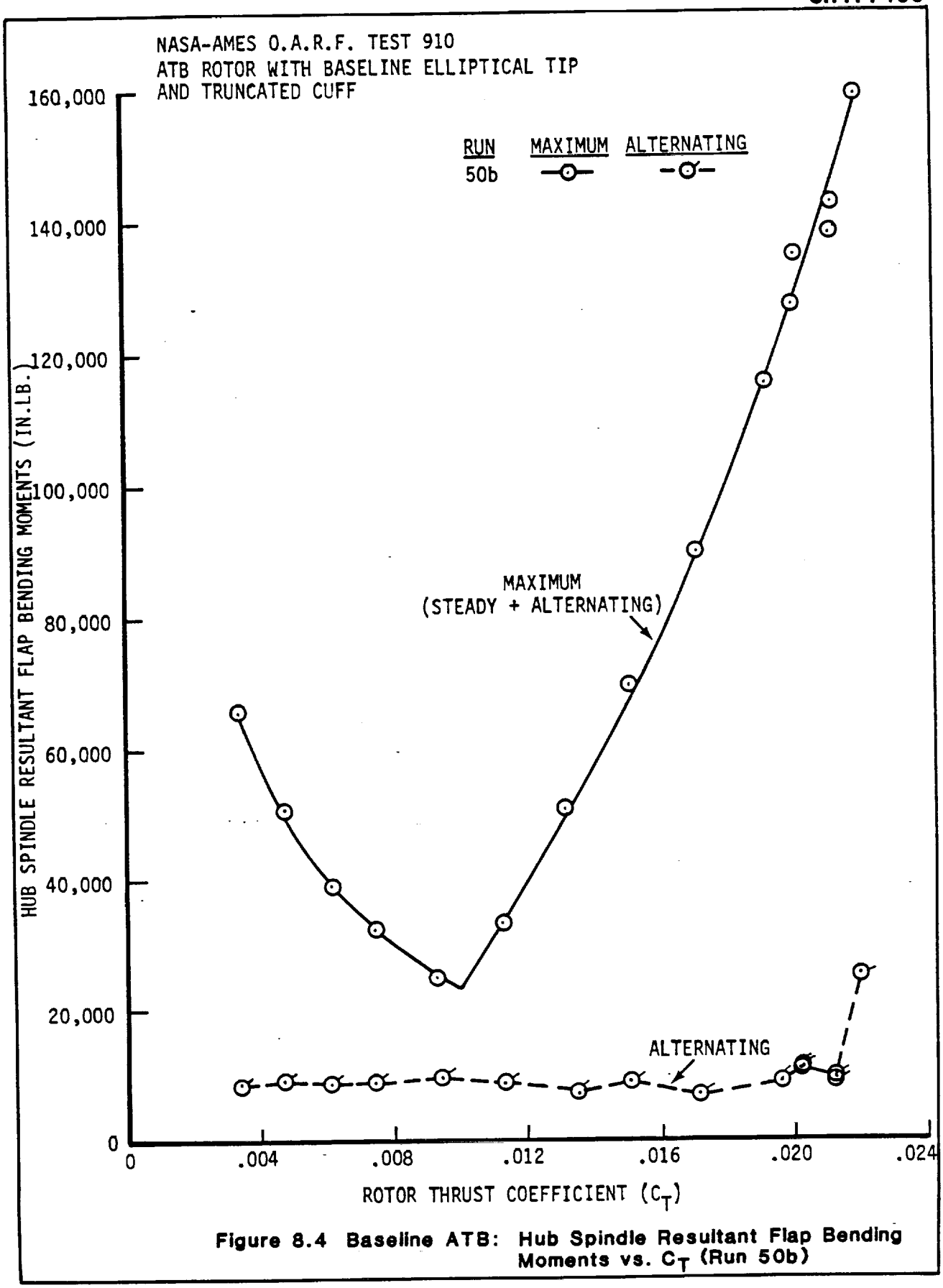

Figure 8.4 Baseline ATB: Hub Spindle Resultant Flap Bending Moments vs. C_T (Run 50b)

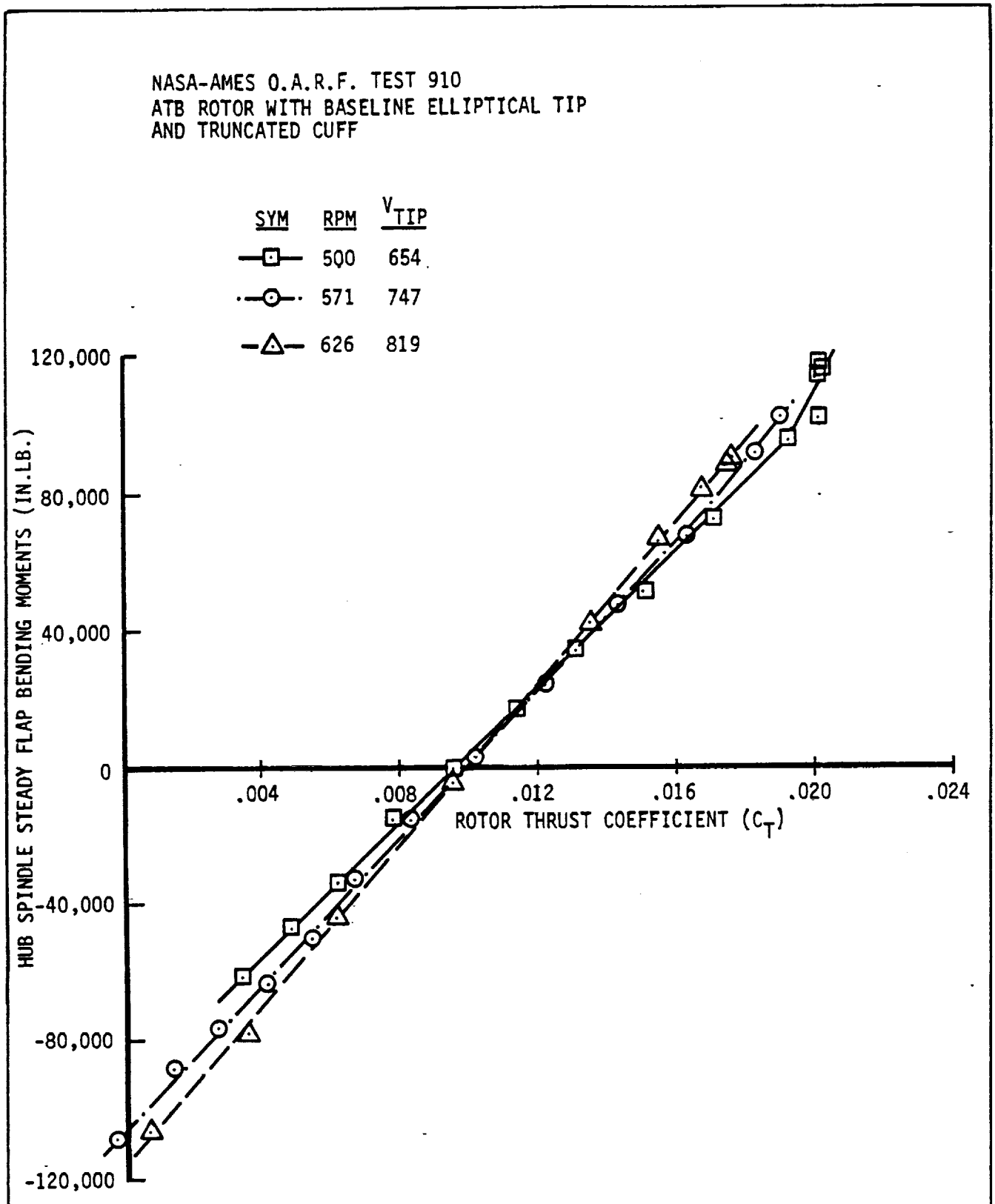

Figure 8.5 Baseline ATB: Hub Spindle Steady Flap Bending Moments vs. C_T – Effect of RPM

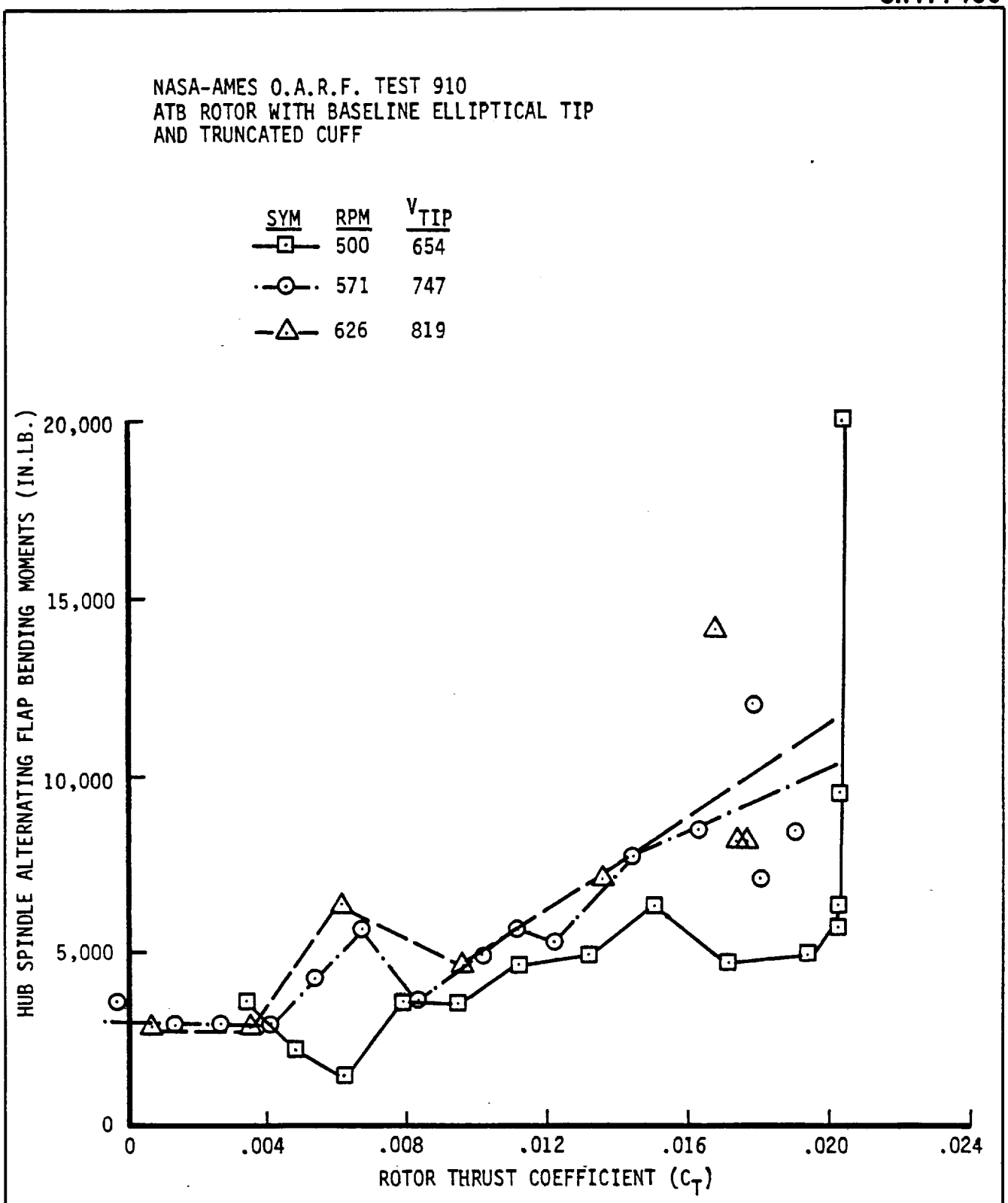

Figure 8.6 Baseline ATB: Hub Spindle Alternating Flap Bending Moments vs. C_T - Effect of RPM

NASA-AMES O.A.R.F. TEST 910
ATB ROTOR WITH BASELINE ELLIPTICAL TIP
AND TRUNCATED CUFF

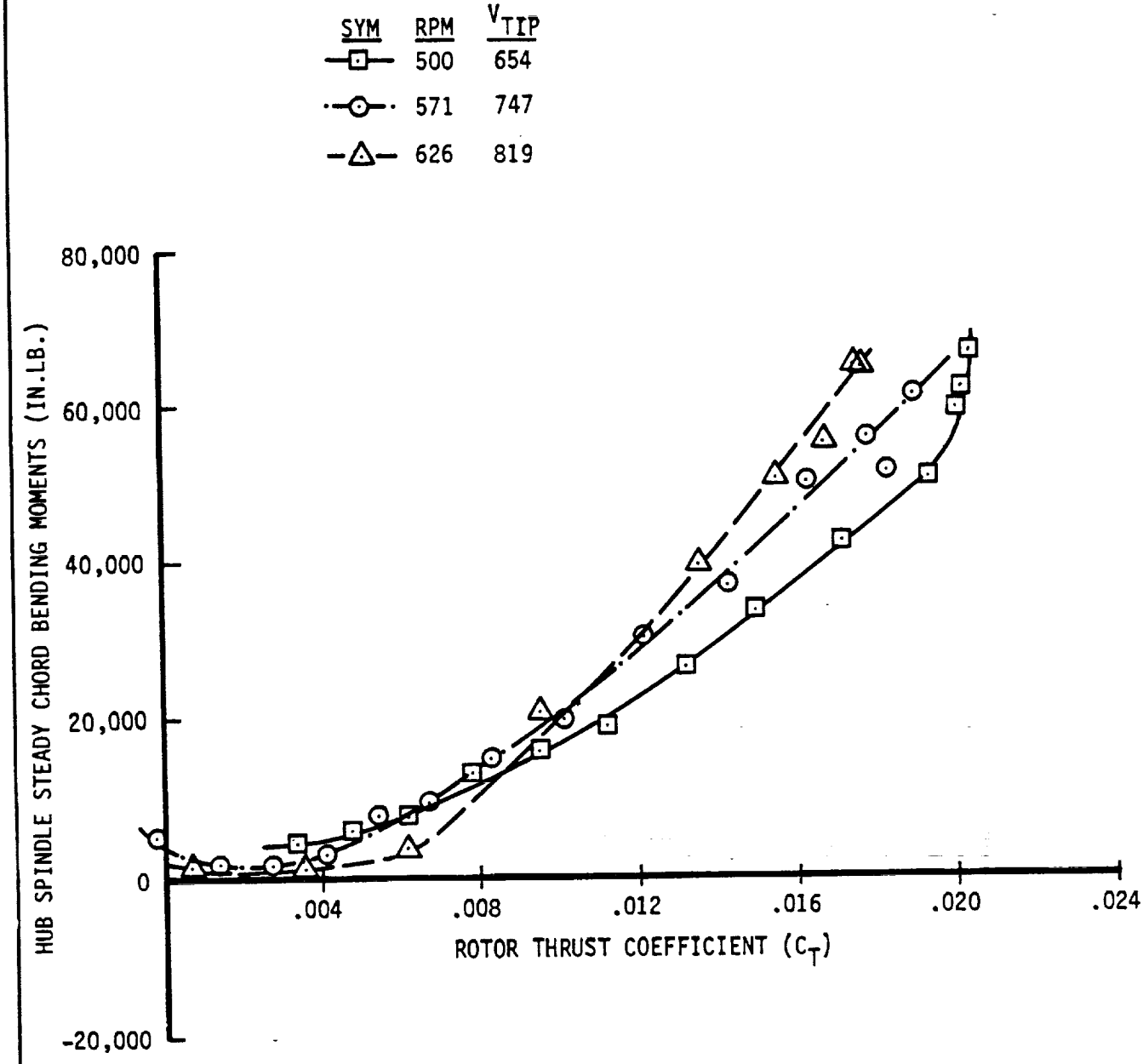

Figure 8.7 Baseline ATB: Hub Spindle Steady Chord Bending Moments vs. C_T - Effect of RPM

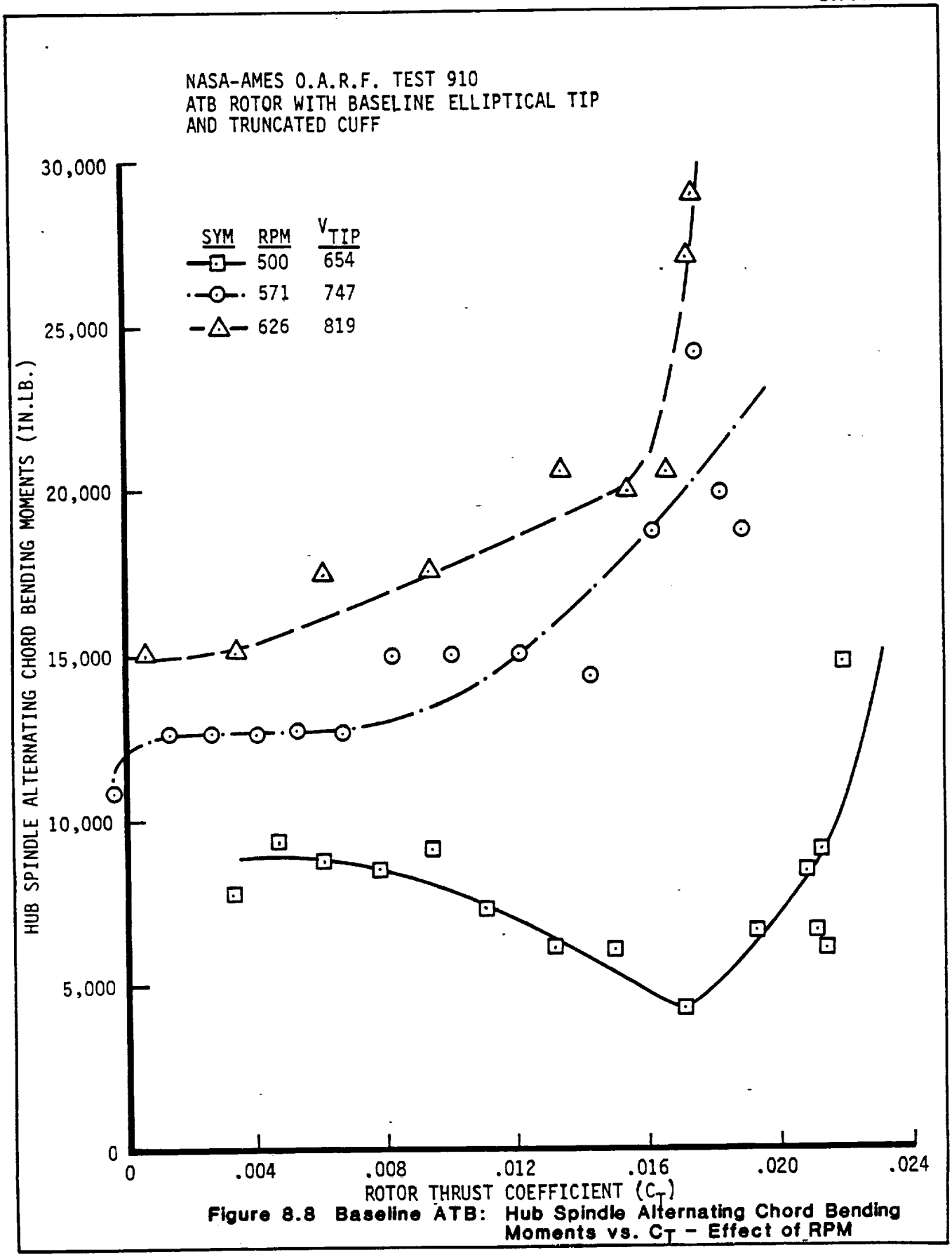

Figure 8.8 Baseline ATB: Hub Spindle Alternating Chord Bending Moments vs. C_T – Effect of RPM

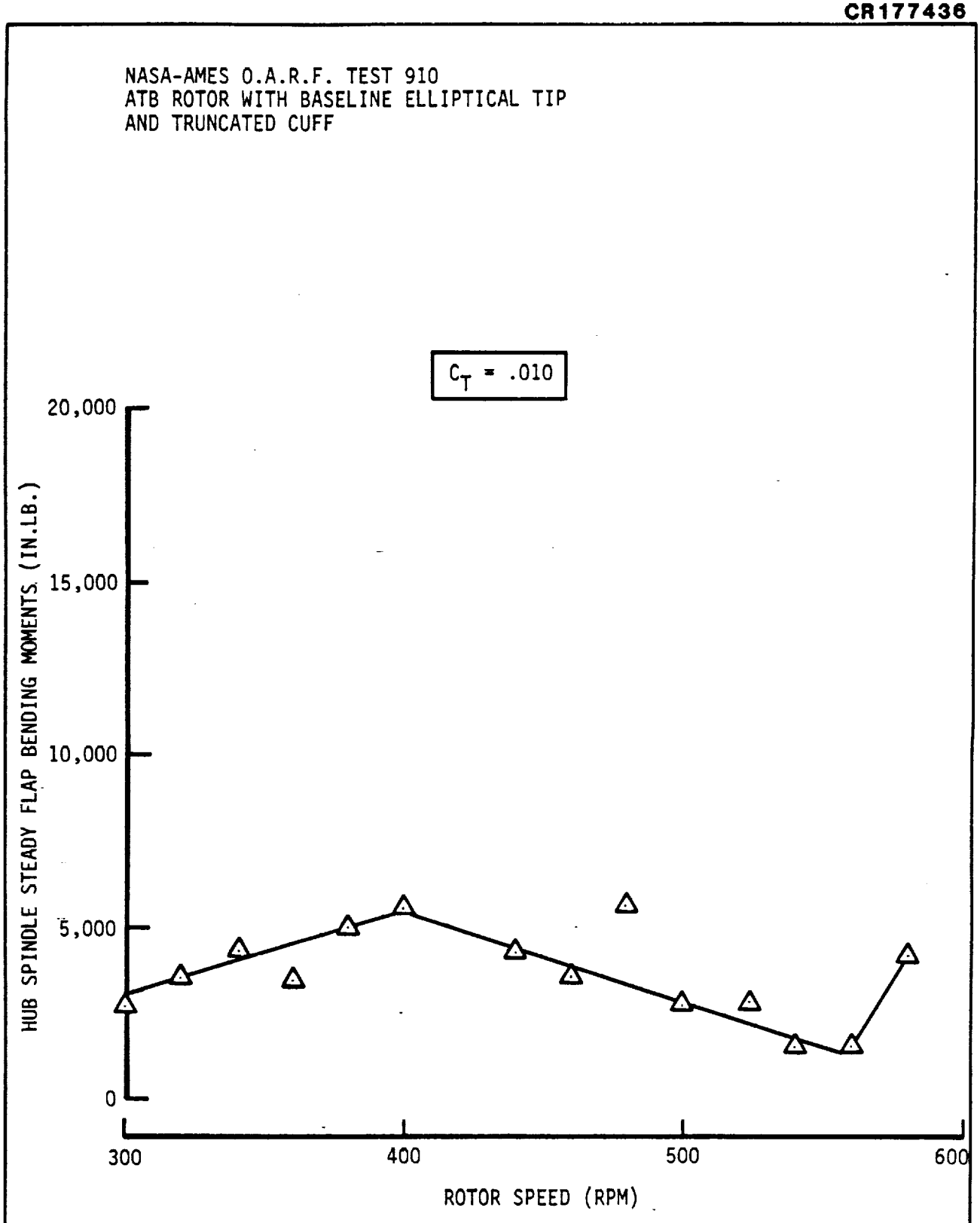

Figure 8.9 Baseline ATB: Hub Spindle Steady Flap Bending Moment vs. RPM

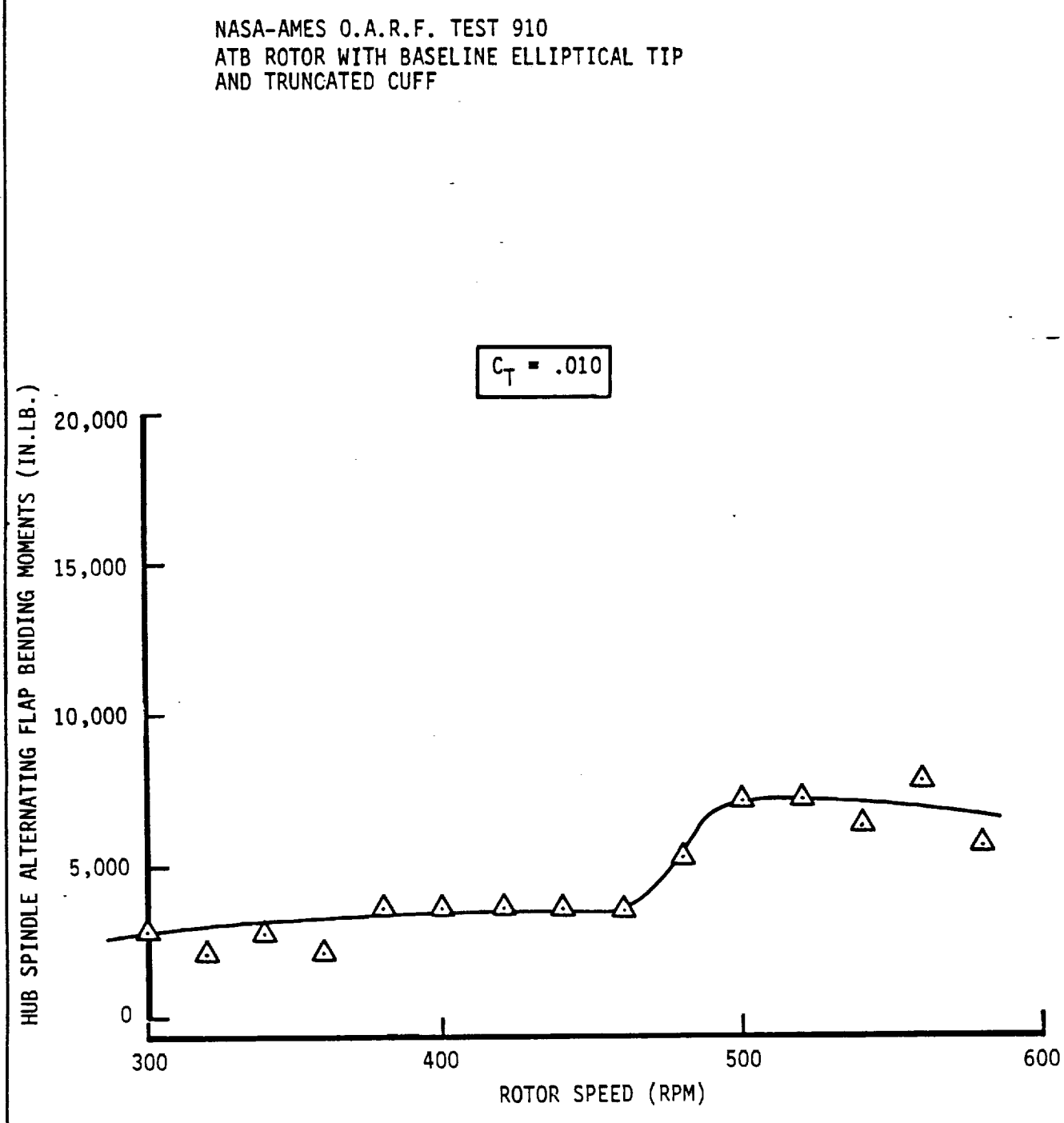

Figure 8.10 Baseline ATB: Hub Spindle Alternating Flap Bending Moments vs. RPM

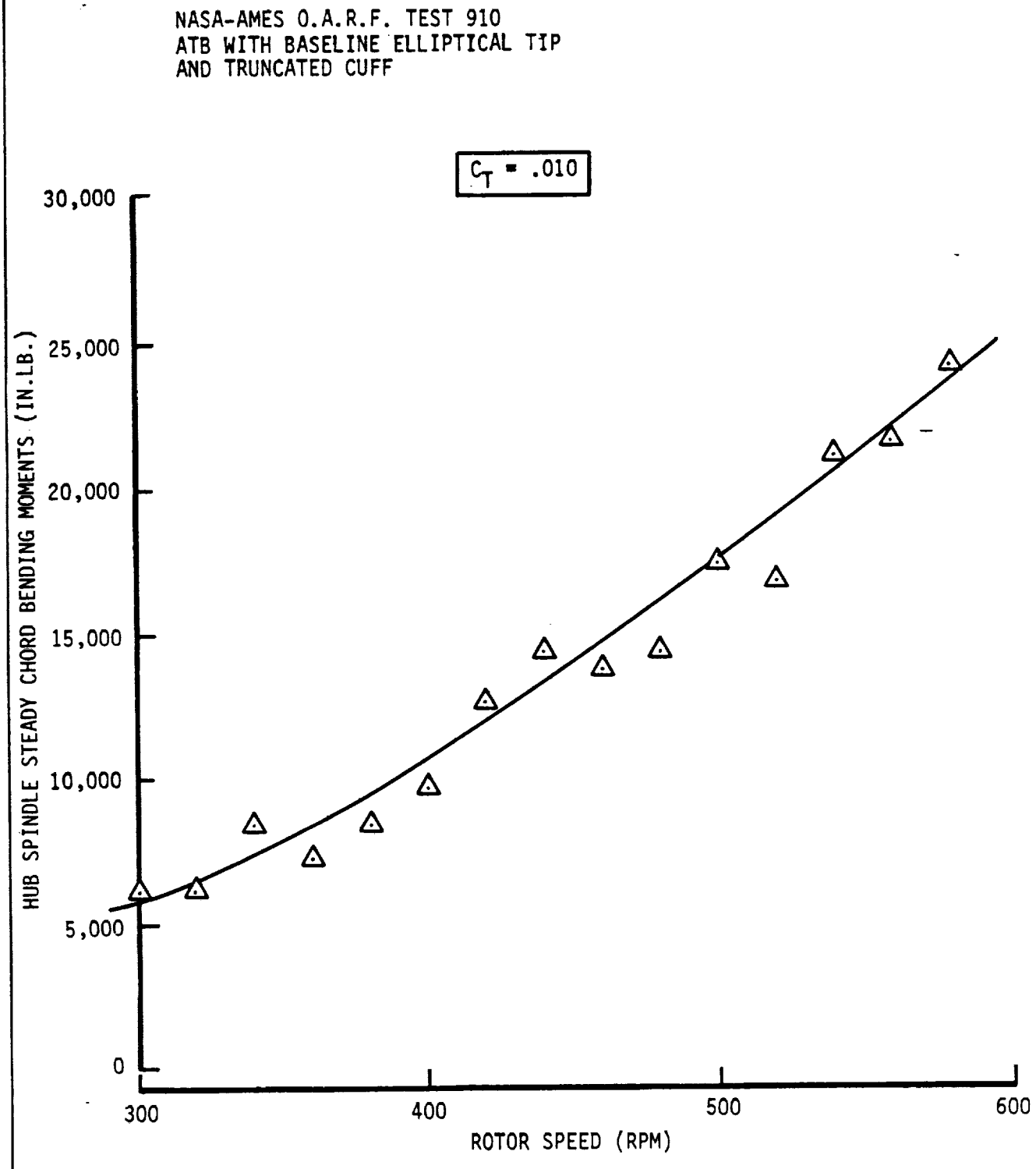

Figure 8.11 Baseline ATB: Hub Spindle Steady Chord Bending Moments vs. RPM

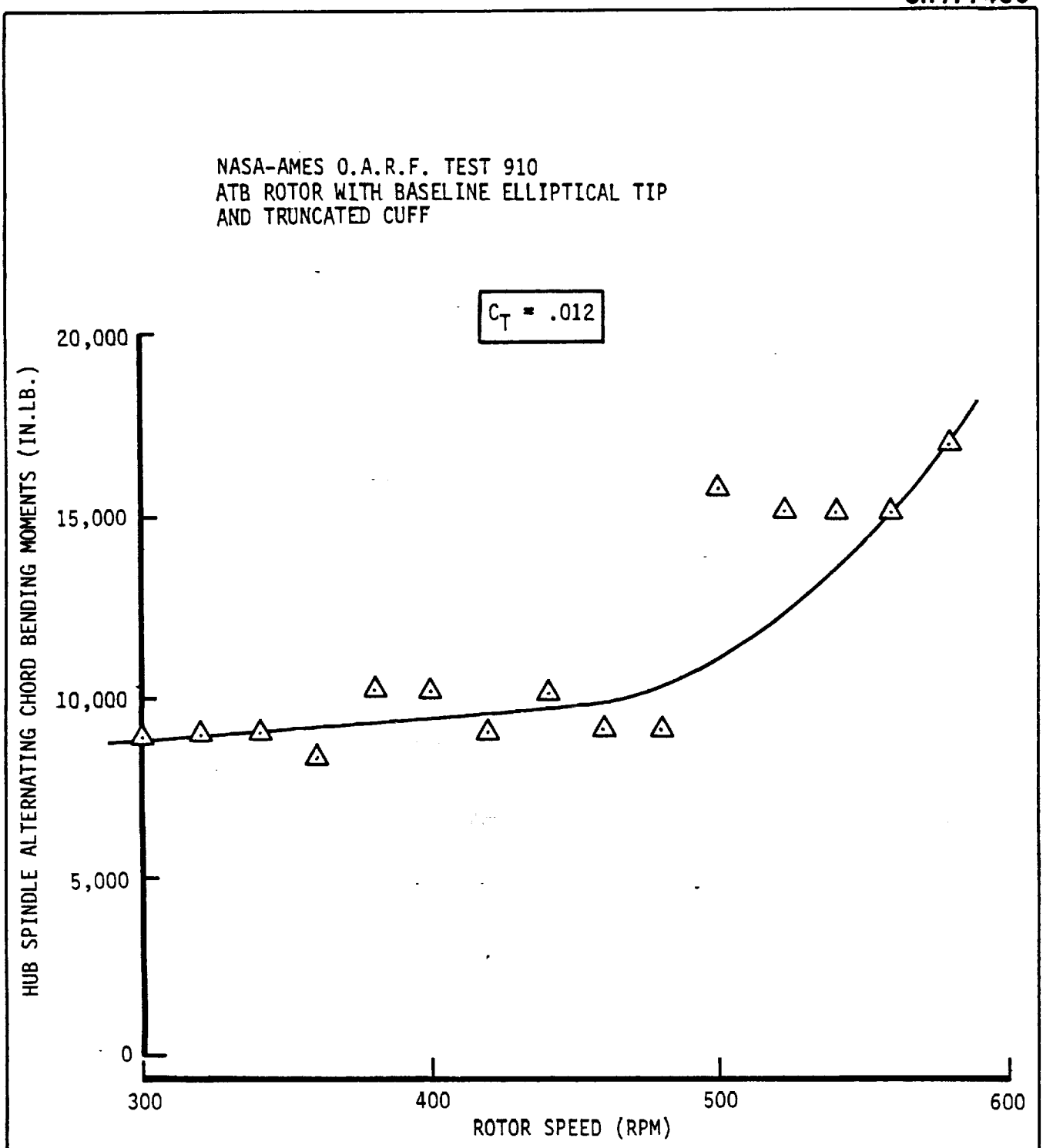

Figure 8.12 Baseline ATB: Hub Spindle Alternating Chord Bending Moments vs. RPM

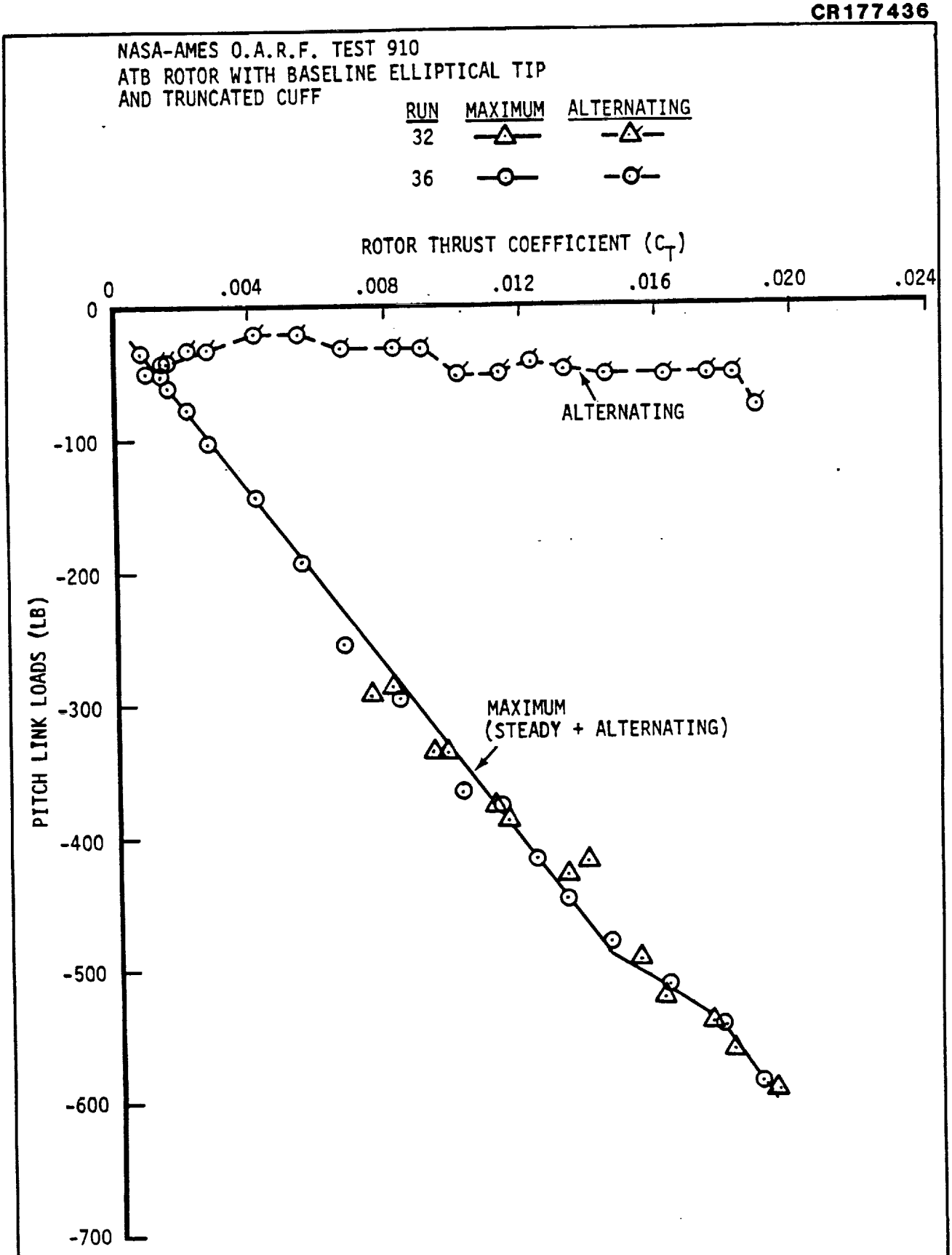

Figure 8.13 Baseline ATB: Pitch Link Loads vs. C_T (Runs 32 and 36)

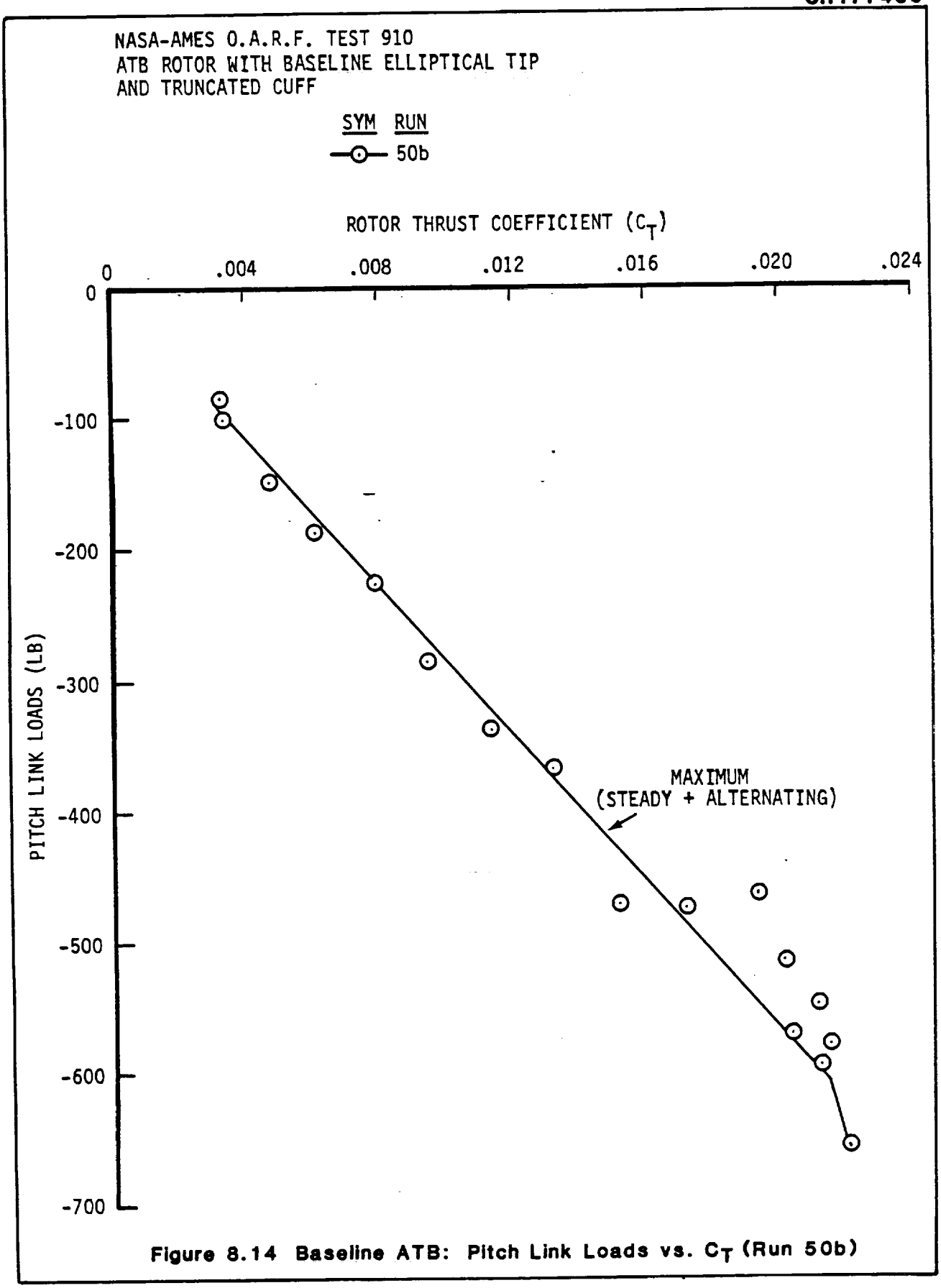

Figure 8.14 Baseline ATB: Pitch Link Loads vs. C_T (Run 50b)

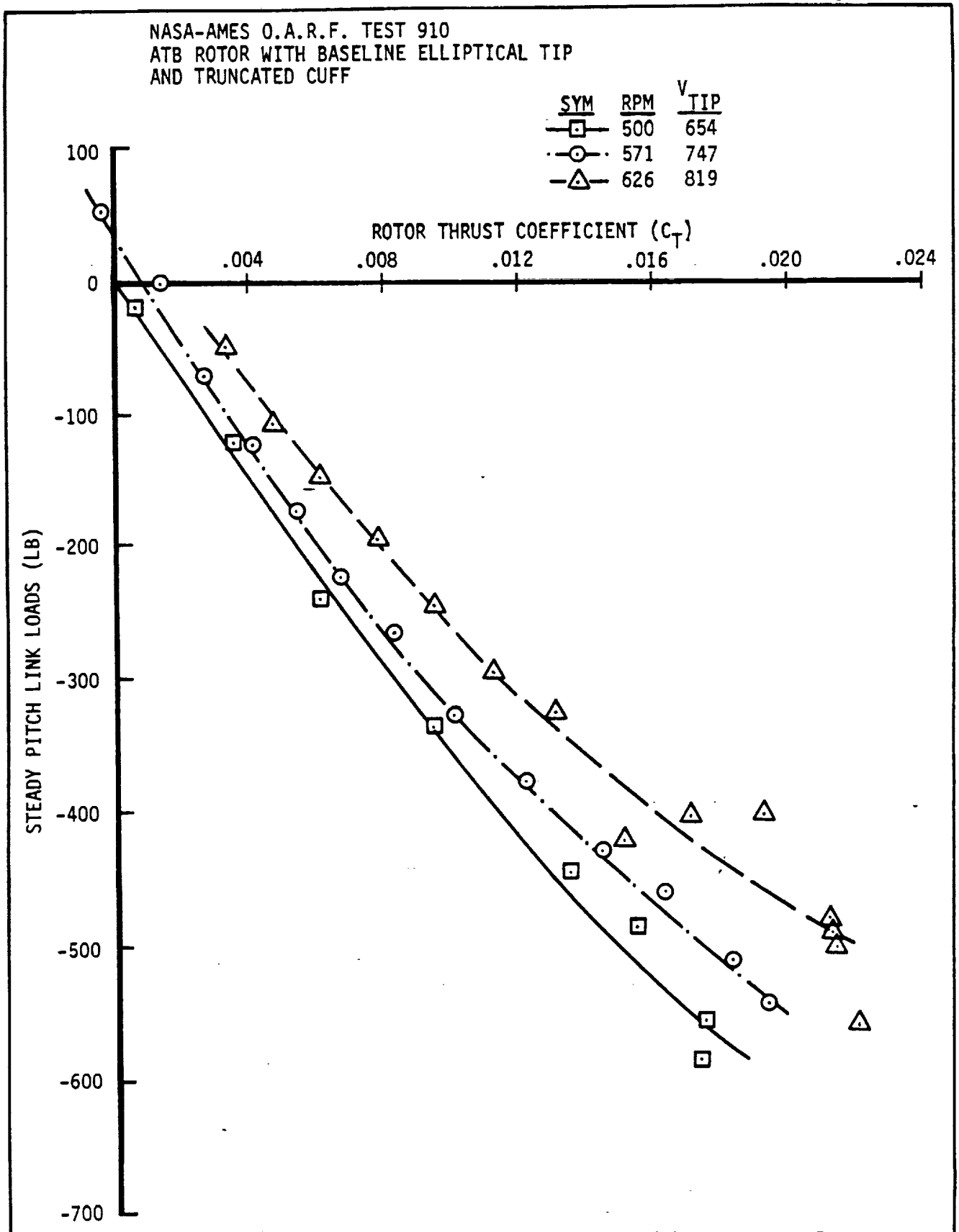

Figure 8.15 Baseline ATB: Steady Pitch Link Loads vs. C_T – Effect of RPM

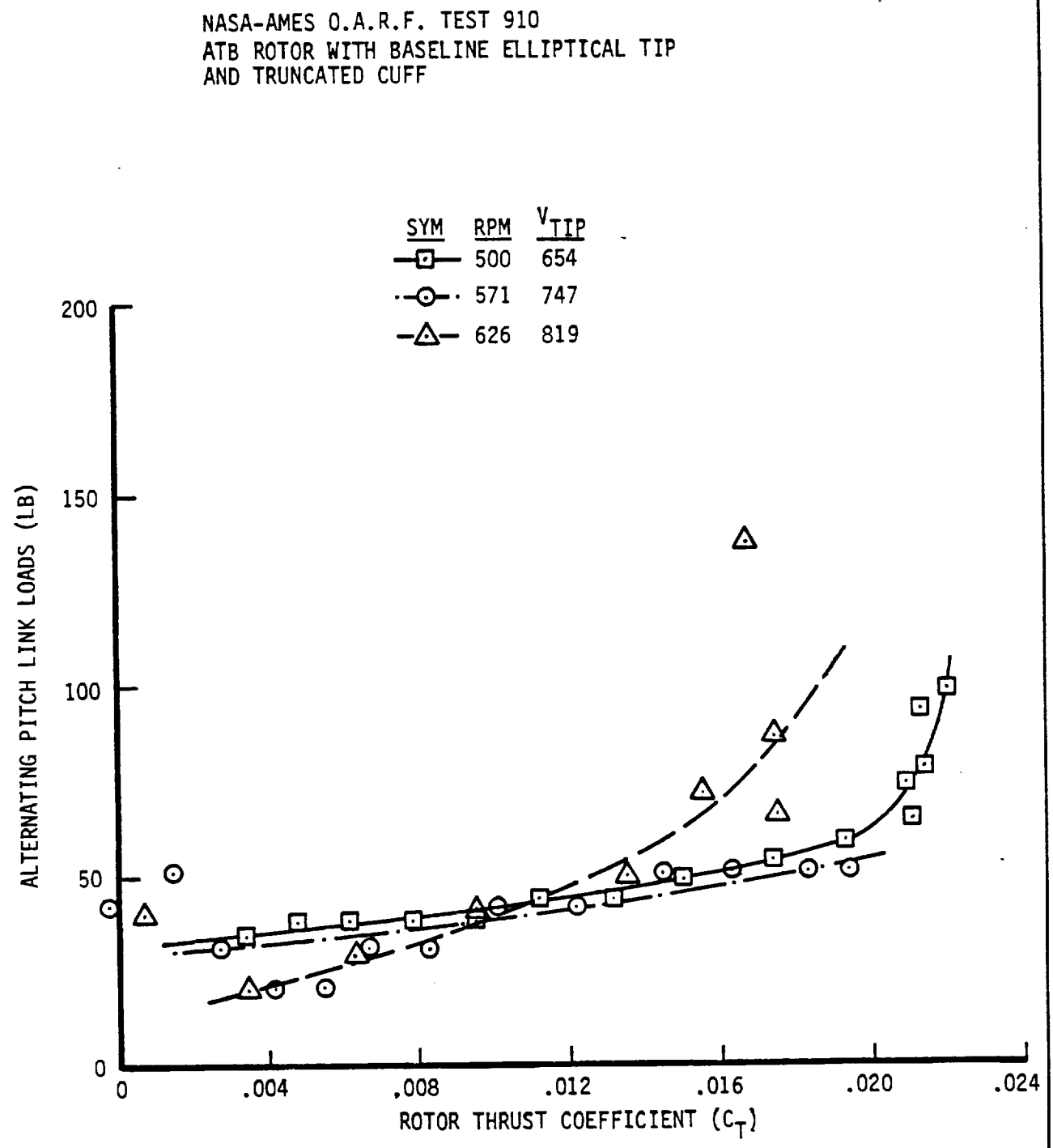

Figure 8.16 Baseline ATB: Alternating Pitch Link Loads vs. C_T - Effect of RPM

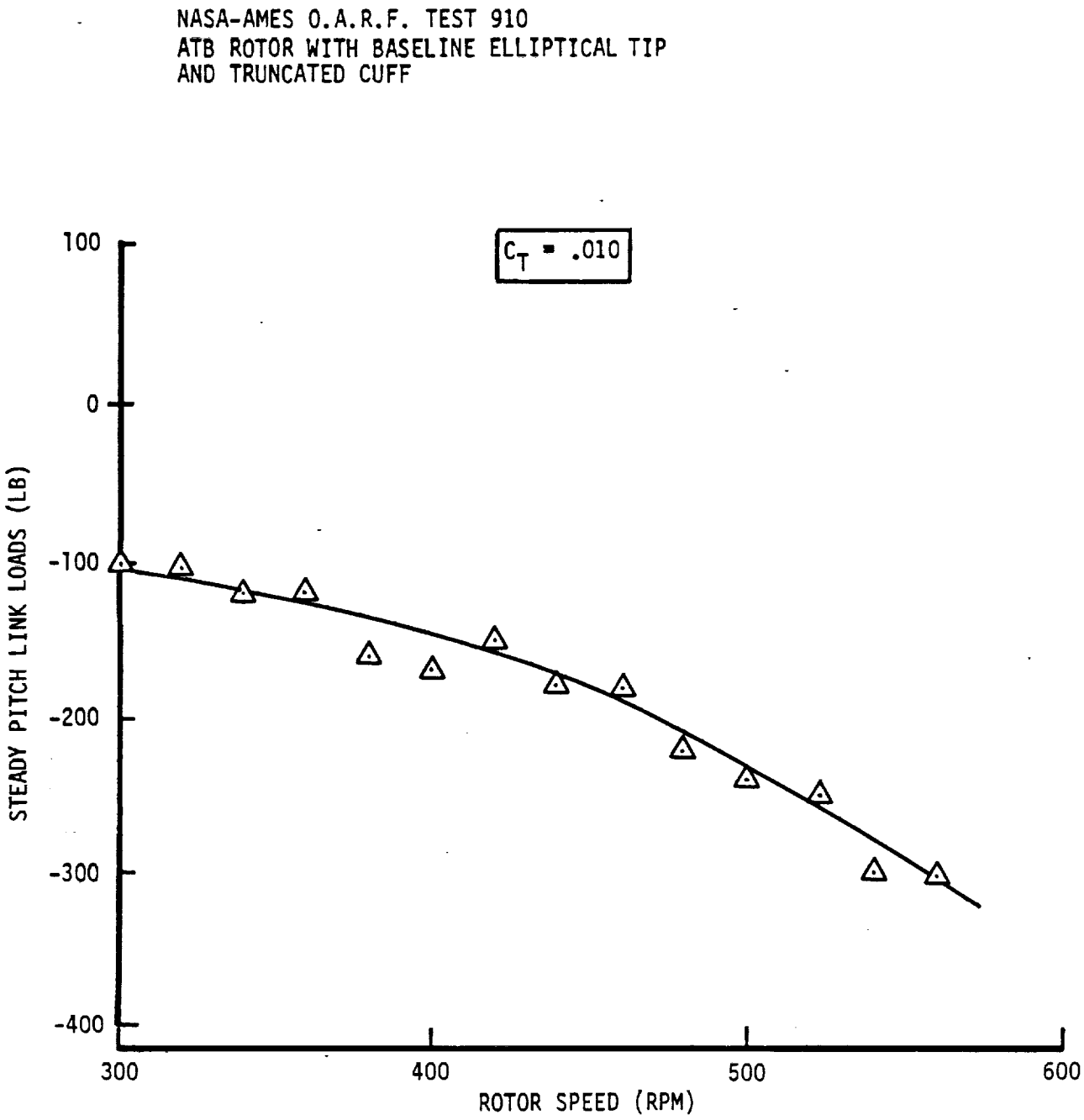

Figure 8.17 Baseline ATB: Steady Pitch Link Loads vs. RPM

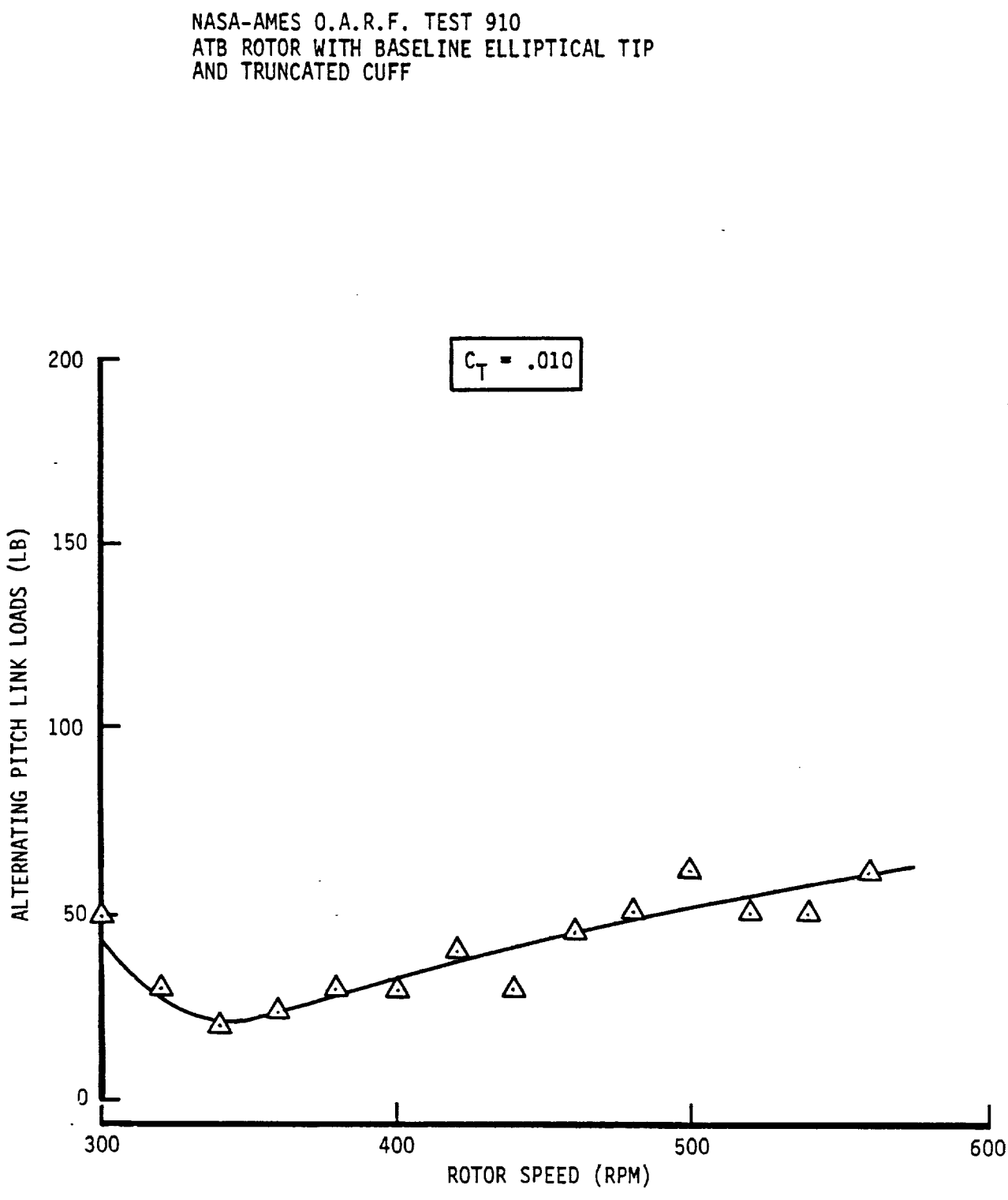

Figure 8.18 Baseline ATB: Alternating Pitch Link Loads vs. RPM

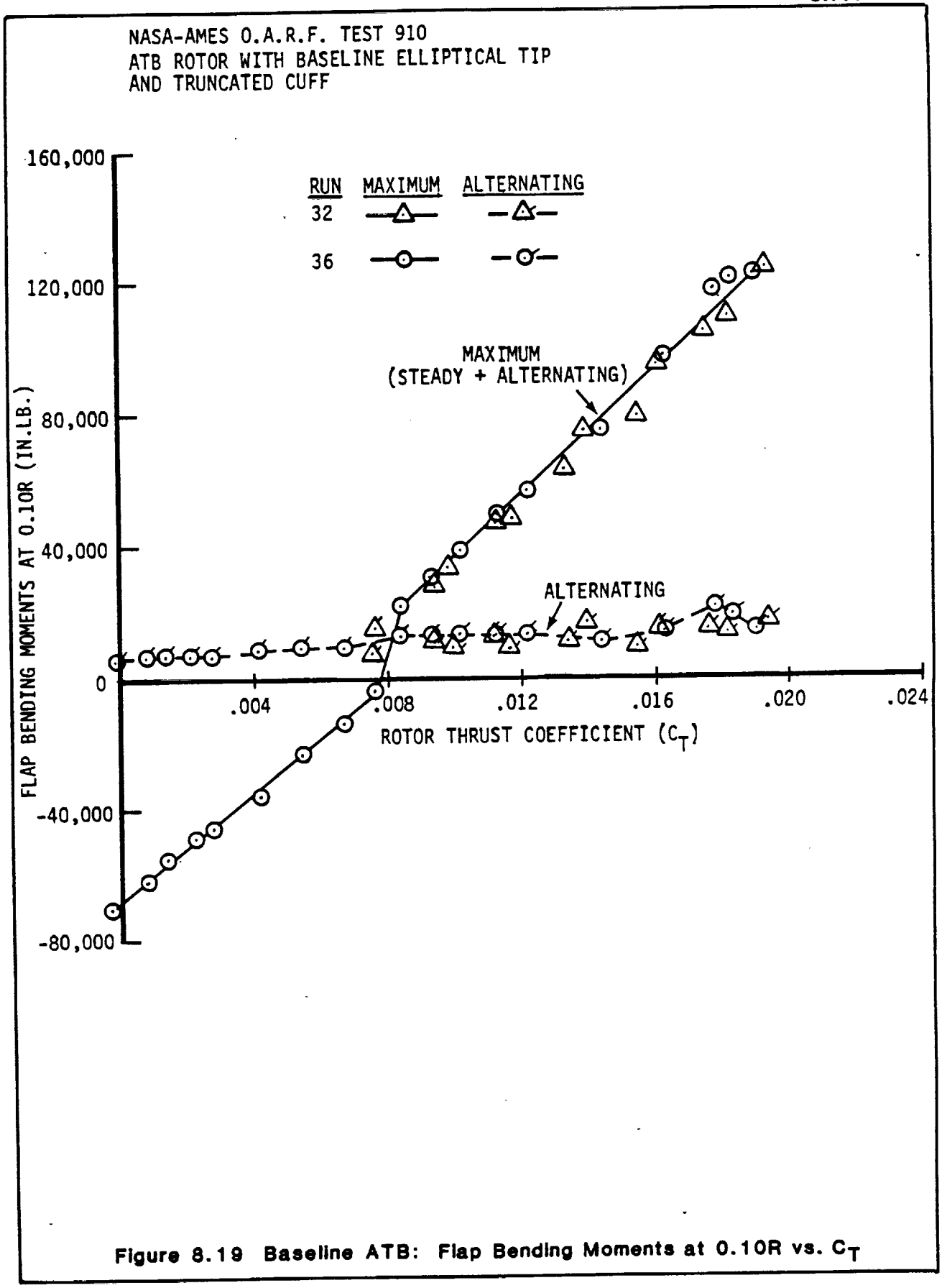

Figure 8.19 Baseline ATB: Flap Bending Moments at 0.10R vs. C_T

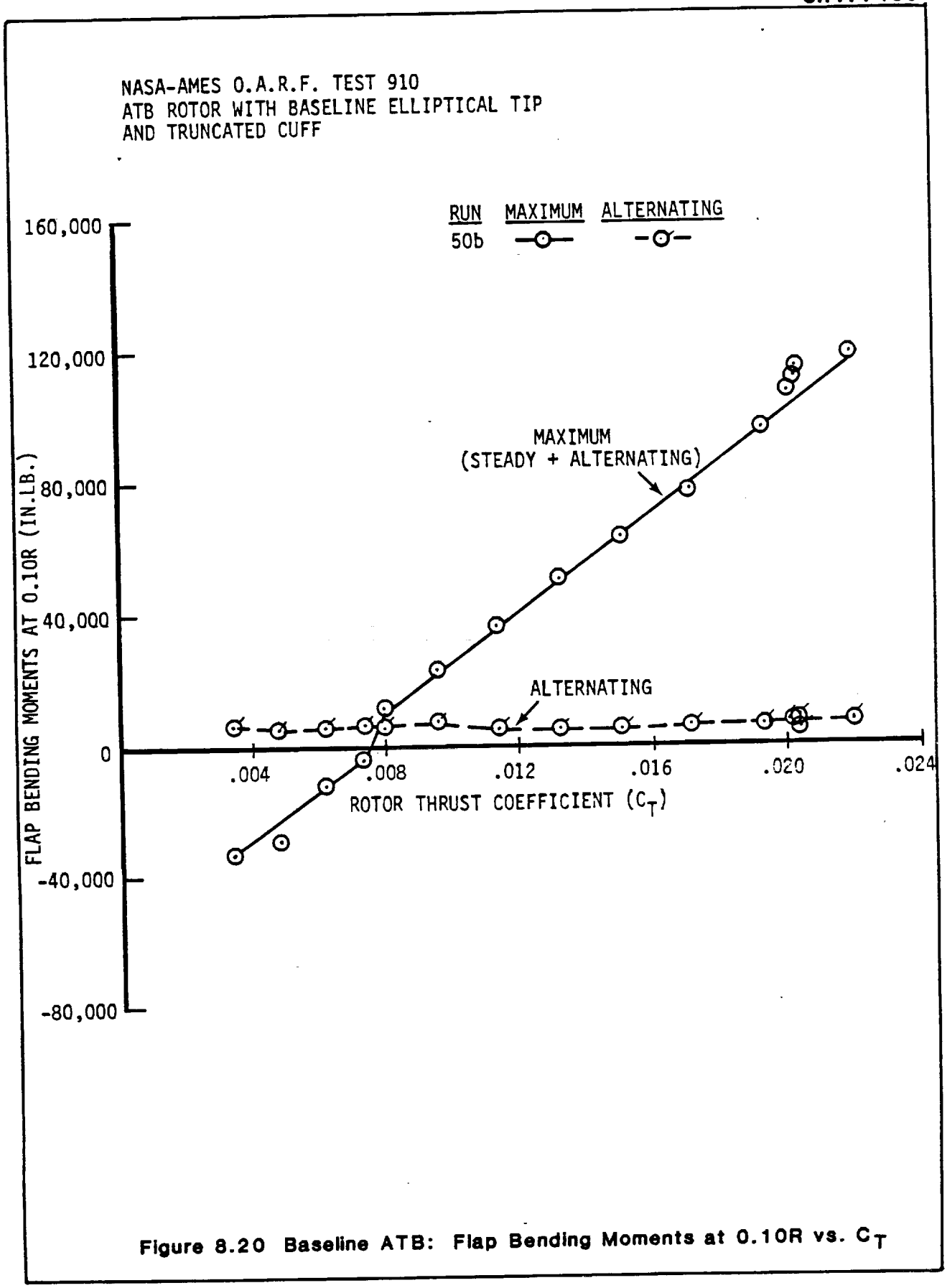

Figure 8.20 Baseline ATB: Flap Bending Moments at 0.10R vs. C_T

NASA-AMES O.A.R.F. TEST 910
ATB ROTOR WITH BASELINE ELLIPTICAL TIP
AND TRUNCATED CUFF

SYMBOL	RPM	V_{TIP}
—⊙—	564	738
·—◇—·	592	775
—△—	626	819

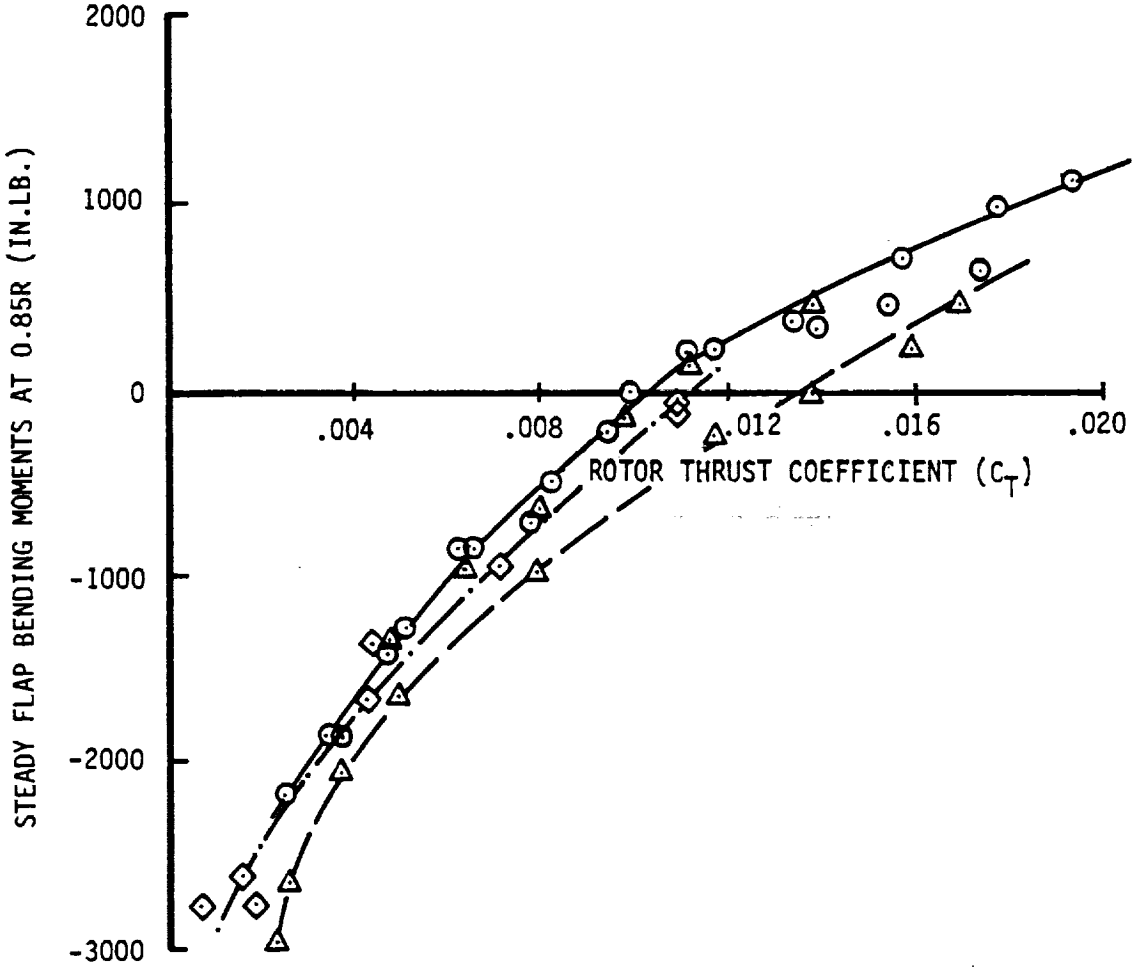

Figure 8.21 Baseline ATB: Steady Flap Bending Moments at 0.85R vs. C_T – Effect of RPM

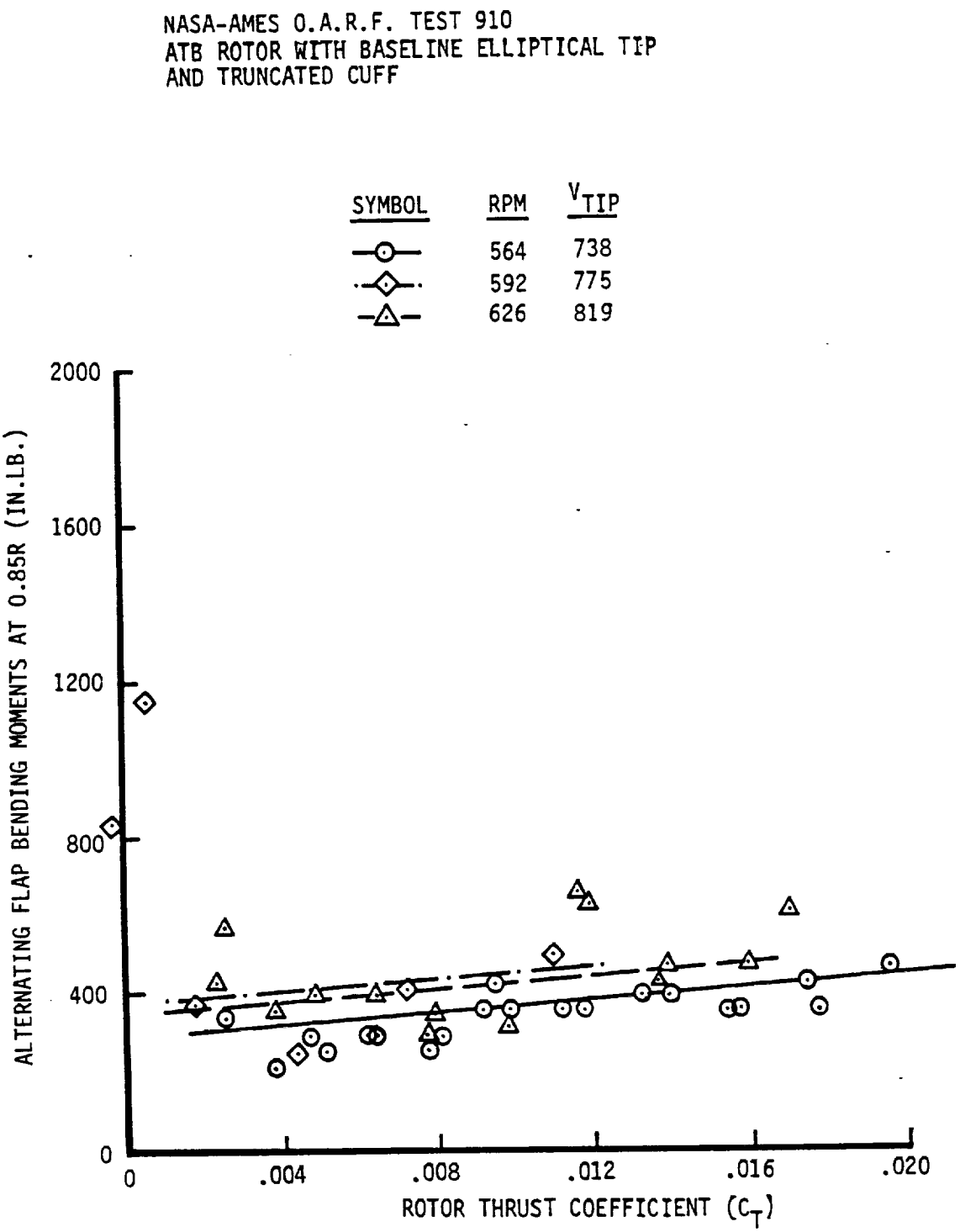

Figure 8.22 Baseline ATB: Alternating Flap Bending Moments at 0.85R vs. C_T – Effect of RPM

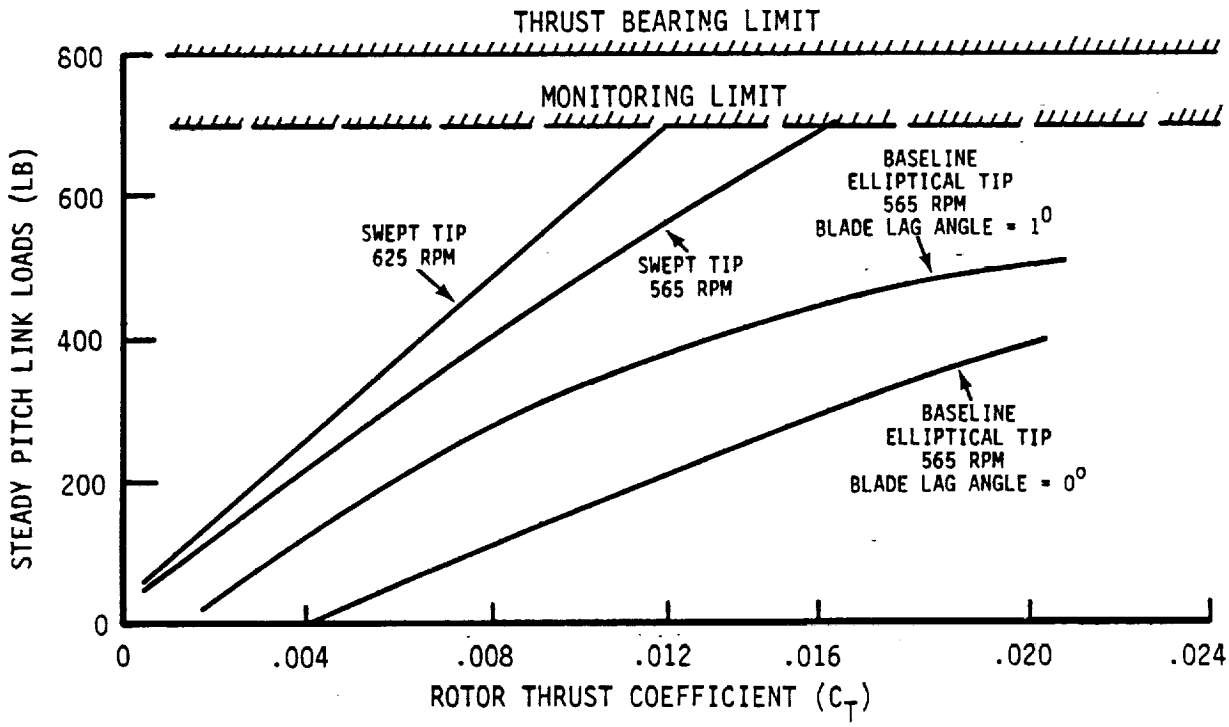

Figure 8.23 Effect of Blade Sweep (Lag Angle) and Tip Shape on Steady Pitch Link Loads

A comparison of the ATB loads with the XV-15 Metal Blade loads indicates that load trends are similar, with the greatest difference being in the oscillatory loads. This is to be expected since oscillatory loads are dependent on wind conditions and cyclic control adjustments, and it was evident that the the oscillatory loads were affected by these.

In general, the ATB blades were tested to significantly higher thrust coefficients (C_T) than the metal blade without encountering any signs of instability, flutter, or excessive loads. As expected the steady spindle beam moments and steady pitch link loads were proportionately higher than the metal blade for the same C_T due to the increased chord of the ATB.

Load trends with RPM followed expected patterns. For the same C_T, increasing the RPM increases blade thrust and blade loads.

8.3 Alternate Configurations: Advanced Technology Blade

Two alternate configurations had a notable effect on blade loads. These were the 0.0 degrees blade sweep (the baseline has 1 degree sweep) and the swept tip configurations. As expected there was an effect on steady pitch link loads as shown in Figure 8.23. As noted in sections 7.5 and 7.7, the swept tip performance data was following a trend which suggested that peak performance might be better than the baseline ATB when pitch link loads restricted the test before peak figure of merit was reached.

9.0 ACOUSTICS

Near-field and far-field noise levels were measured during the hover test program. The near-field microphone location represented a point on the fuselage side of a typical tilt rotor in hover. The microphone location simulates a point on a fuselage 8 ft aft (2.4 meters) and with 2 ft (0.6m) radial clearance from the tip path plane. Far-field noise was recorded with an array of microphones at 250 ft and 650 ft radius, at 0, 15, 30 and 45 degrees behind the rotor disc.

Figure 9.1 shows comparative XV-15 metal blade and ATB overall near-field sound pressure levels as a function of rotor thrust. The ATB noise level is approximately 2-3 dB lower than the metal blades over the normal operating range.

Far-field noise data for the 15 degrees aft location is shown in Figure 9.2. The ATB OASPL is approximately 5-6 dB lower than that from the XV-15 metal blades.

These comparative trends are expected since the tip pressure loading is less for the tapered, higher solidity ATB with its more even thrust distribution over the span.

Table 9.1 summarizes runs during which acoustics data was acquired during the OARF testing in 1984. This includes JVX isolated rotor runs as well as XV-15 metal blades and ATB test runs. The acquisition and analysis of the acoustics data from these tests was an Ames Research Center activity. Additional information may be obtained from Ames personnel (M.D. Maisel).

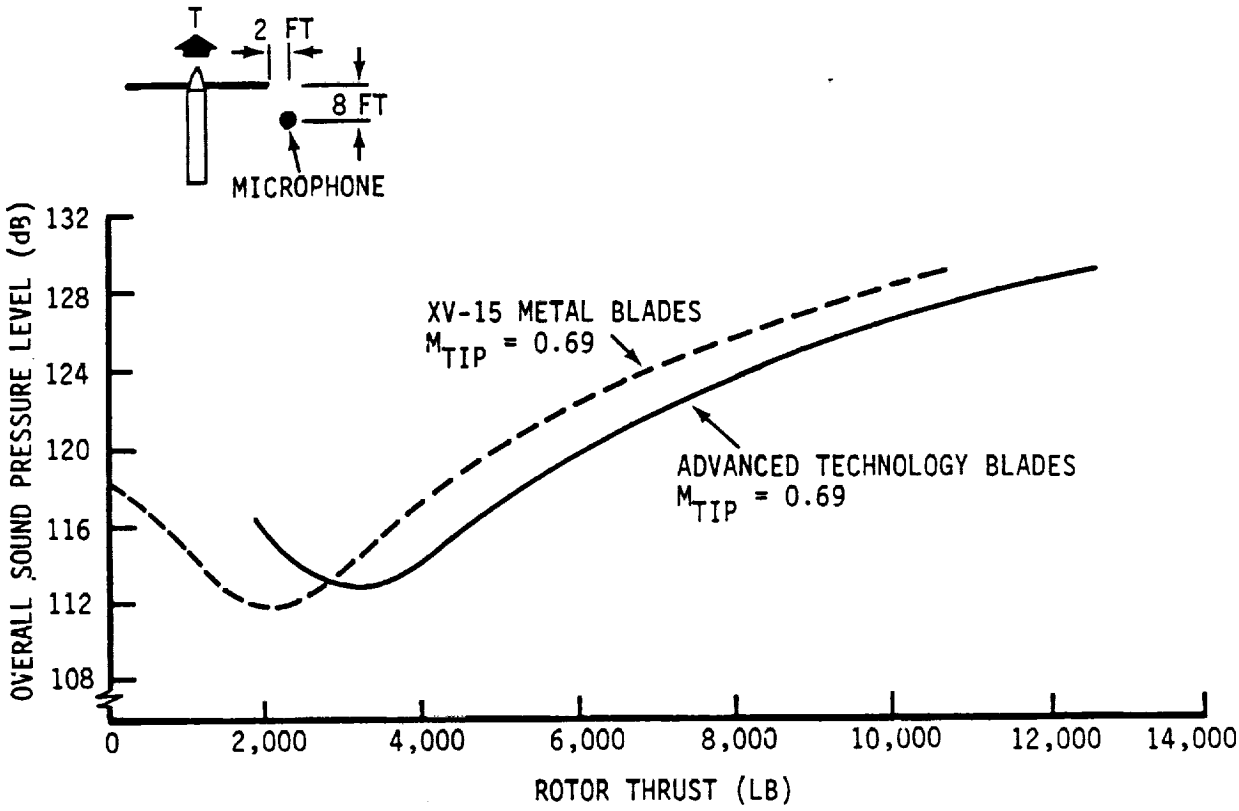

Figure 9.1 Typical Near-Field Noise Data for XV-15 Metal Blade and ATB

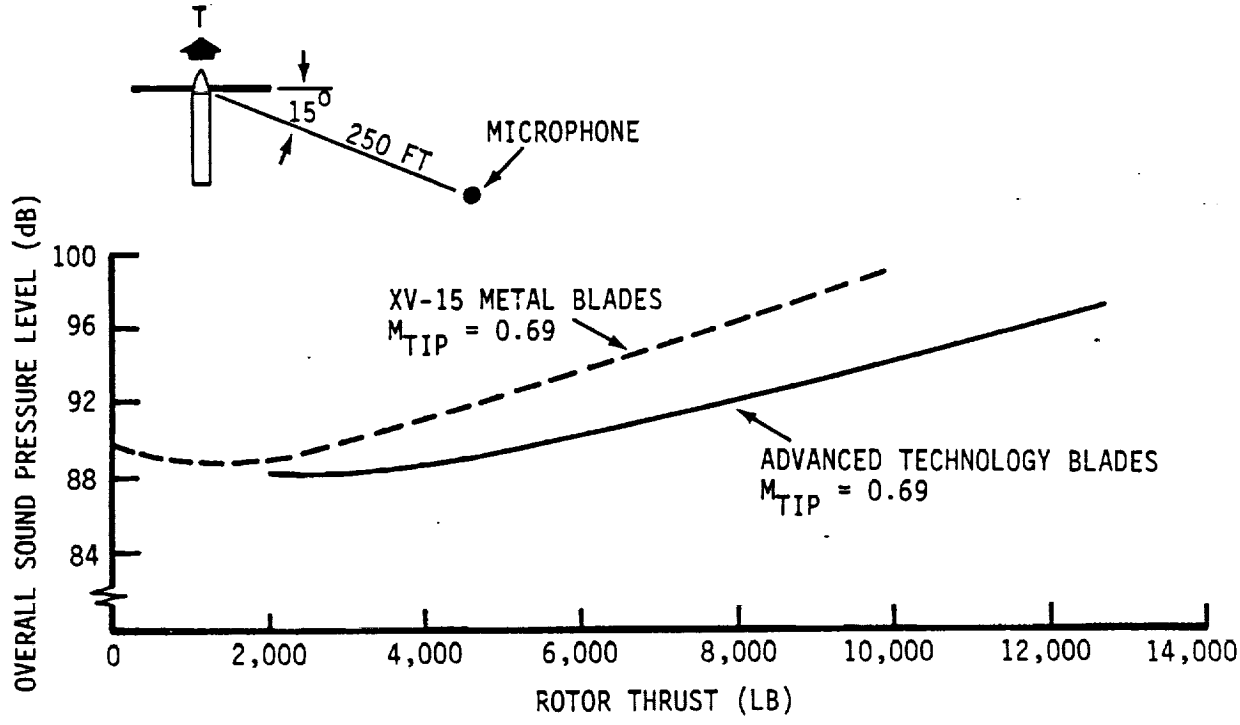

Figure 9.2 Typical Far-Field Noise Data for XV-15 Metal Blade and ATB

Table 9.1 Acoustic Data Recorded During Rotor Tests at NASA Ames O.A.R.F. (March '84 - August '84)

ROTOR	CONFIGURATION	PRIMARY TEST OBJECTIVE	RPM	V_{TIP}	RUN NUMBER	ACOUSTIC DATA REEL NO.
XV-15 METAL BLADES	FLIGHT-ISOLATED ROTOR	SHAKEDOWN & TRACK & BALANCE			1	1
					2	1
			584, 600	764, 785	3- 8	2
			585	766	9,10	3
		PERFORMANCE	587, 622	768, 814	11,12	3
			587, 625	768, 818	14-16	4
			553- 588	724- 770	22-24	5
0.6578 SCALE JVX (V-22) BLADES	DESIGN-ISOLATED ROTOR (NO WING)	SHAKEDOWN & TRACK & BALANCE	573- 580	750- 759	1,2	6
		PERFORMANCE	576, 625	754, 818	3-5	6,7
			577	755	6	7
			625	818	7	8
			515, 621	674, 813	8	8
ADVANCED TECHNOLOGY BLADES	BASELINE TIP, TRUNCATED CUFF ISOLATED ROTOR	SHAKEDOWN & TRACK & BALANCE	570, 589	746, 771	30,32,33	9
		PERFORMANCE	569- 595	745- 779	36,37	9
			590	772	40	10
		DYNAMICS	300- 600	393- 785	41	10
		PERFORMANCE/ENDURANCE	590, 625	772, 818	44	10
		PERFORMANCE	500- 566	655- 741	50	11
	BASELINE TIP, EXTENDED CUFF	PERFORMANCE	570, 625	746, 818	56,58	11
	SWEPT TIP EXTENDED CUFF	PERFORMANCE	565, 625	740, 818	59,61	12
	SQUARE TIP EXTENDED CUFF	PEFORMANCE	565, 570	740, 746	62,63	12

10.0 CONCLUSIONS AND RECOMMENDATIONS

10.1 Conclusions

Full scale rotor hover performance was obtained for the basic XV-15 rotor and the Advanced Technology Blade (ATB). The following conclusions can be drawn from the results:

1. Accuracy and reliability of the performance data is very high as shown by the low level of scatter in the data and repeatability of data taken at different times. (See for example, Figure 7.11).

2. Both the ATB and the XV-15 rotors performed at levels significantly better than anticipated from theoretical estimates. Measured peak values of figure of merit were in the range 0.79 to 0.81 whereas predicted values did not exceed 0.79. Peak performance occurred at higher values of C_T and did not drop off as quickly as predicted (Figure 1.4).

3. The performance of the baseline XV-15 rotor is higher than that measured during a previous test of the same blades on the WPAFB whirl tower when corrected for tower blockage effects (Figure 7.2).

4. Of the three tip shapes tested on the ATB blades, the elliptical tip outperformed a rectangular tip and a swept tip (Figure 7.35). The swept tip and elliptical tips had the same solidity; the solidity of the rectangular tip was slightly higher. However, testing of the swept tip was curtailed but did indicate that its performance might match or exceed that of the elliptical tip at high thrust.

5. Testing of the ATB with no cuff, truncated cuff, and full cuff showed that performance is improved as more blade area is added to the cuff region (Figure 7.37).

6. A value of C_T/σ_T = .22 was reached with the ATB before loads limited further testing (Figure 7.11). The corresponding value for the XV-15 was .18, (Figure 7.1).

7. Comparison of the ATB and XV-15 blade loads indicates that load trends are similar. The ATB blades were tested to significantly higher thrust levels than the XV-15 without encountering any instability, flutter, or excessive loads.

8. Acoustical measurements show (Figures 9.1 and 9.2) that the ATB with the elliptical tips was 2-3 dB lower than the XV-15 metal blades in the near-field and 5-6 dB lower in the far-field.

10.2 Recommendations

1. A program of research should be initiated aimed at developing better wake models for use in tilt rotor hover performance analyses. The program would consist of experimentally determining the wake vortex structure for different rotor operating conditions (tip speed, collective) for representative blade planforms, twist distributions, and number of blades. It would also be desirable to make these measurements with blades having pressure instrumentation so that the blade circulation distribution can be determined. The combination of blade circulation distribution and wake geometry can then be used to derive wake models for use in hover performance analyses.

2. There is a need to acquire a better understanding of behavior of the thick root sections used on tilt rotor blades especially near and beyond stall. A program of wind tunnel test and analysis to define the stall and post-stall behavior should be initiated. This would include two-dimensional testing as well as measurements on the root sections of rotor blades.

11.0 REFERENCES

1. McVeigh, M. A. and Bartie, K., "V-22 Large-Scale Rotor Hover Performance and Wing Download Test", Bell Boeing Document D901-99140-1, March 1985.

2. Benson, R. G., Ekquist, D., et al, "XV-15/Advanced Technology Blade Hover Test Plan for NASA-Ames OARF", Boeing Document D210-12262-1, December 1983.

3. Silcox, H. F., et al, "System Safety Analysis for Advanced Technology Blades (ATB) on NASA-Ames Test Rig", Boeing Document D210-12256, Volumes 1-5, January 1984.

4. Helf, S., et al, "Full-Scale Hover Test of a 25-Foot Tilt Rotor", BHT Report 300-099-010, NASA CR114626, May 1973.

5. Devlin, J. F., "Instrumentation Requirements for Advanced Technology Blade Rotor Test at NASA-Ames OARF", Bell Boeing Document D901-99025-2, May 1984.

6. Walton, I., "Data Reduction Requirements for JVX/XV-15 Large-Scale Rotor Test at NASA-Ames OARF", Bell Boeing Document D901-99050-3, October 1983.

7. Schlichting, H., "Boundary Layer Theory", McGraw-Hill, NY, 1968.

8. Hoerner, S. F., "Fluid Dynamic Drag", published by Hoerner Fluid Dynamics, 1965.

APPENDIX A - CORRECTIONS FOR EFFECTS OF WIND

A.1 Introduction

The XV-15 and ATB rotor diameters are 25 feet. The ATB rotor has a thrust-weighted solidity of 0.10, the XV-15 rotor has a solidity of 0.089. The rotor data was generally acquired in conditions where the ambient wind velocity was not zero. A correction for the effect of wind is therefore required to arrive at true hover performance. The method used to correct for the effect of wind on hover performance is presented below.

A.2 Correction for Wind Effects

In a wind of speed V at an angle α to the rotor shaft, the rotor develops a thrust T and a normal force NF. The rotor power is

$$C_P = C_{P_{PRO}} + \mu\, C_T \cos\alpha - \mu\, C_{NF} \sin\alpha + k\, \bar{v}_i\, C_T \qquad (1)$$

where $\mu = V/V_T$, $\bar{v}_i = v_i/V_T$, v_i is the mean induced velocity, and k is a correction factor for the ideal induced velocity.

During the test the rotor was trimmed to zero flapping. The rotor balance measured T and NF. Wind speed (V) and direction (α) were measured by an anemometer mounted at a height above the ground. Using Hoerner's recommended model for the wind boundary layer, (Reference 8), it was determined that if the anemometer were positioned at the same height as the hub, the mean wind speed would be read. The effect of the wind can be calculated as follows.

The power required to hover in zero wind conditions is:

$$C_{P_H} = C_{P_{PRO}} + k_H\, \bar{v}_{i_H}\, C_T$$

Since $C_{P_{PRO}}$ does not vary significantly with small changes in ambient wind conditions, we may substitute for $C_{P_{PRO}}$ from Equation (1).

The adjusted power for hover in zero wind may then be written:

$$C_{P_H} = C_P - \mu\,(C_T \cos\alpha - C_{NF} \sin\alpha) + k_H \bar{v}_{iH} \left\{ 1 - \frac{k\, \bar{v}_i}{k_H\, \bar{v}_{iH}} \right\} C_T \qquad (2)$$

The ratio $v_* = \bar{v}_i / \bar{v}_{iH}$ is obtained by solving

$$v_*^4 + 2 v_*^3 V_* \cos\alpha \text{ SIGN } C_T + v_*^2 V_*^2 - 1 = 0 \qquad (3)$$

where $V_* = V/v_{i_H}$

Equation (3) is solved for V_* by iteration using the Newton-Raphson method

$$v_{*n+1} = v_{*n} - (F/F')_n \ .$$

where $F = v_*^4 + 2v_*^3 V_* \cos\alpha \text{ SIGN } C_T + v_*^2 V_*^2 - 1$

$$F' = 4v_*^3 + 6v_*^2 V_* \cos\alpha \text{ SIGN } C_T + 2v_* V_*^2 \qquad (4)$$

and a starting value is given by an approximation developed by Wayne Johnson, viz

$$v_* = 1 - \mu\cos\alpha/\sqrt{2\ |C_T|} = 1 - 0.5V_* \cos\alpha$$

Figure A.1 shows the induced velocity ratio (and ideal power ratio) for different wind speeds and directions for $C_T = .015$. The effect of not applying a wind correction is shown in Figure A.2 where true hover performance is compared to that which would be calculated from measurements made in a 3 knot wind. The effect of the wind is substantial, amounting to approximately 2 points in figure of merit when the flow is axial.

On the basis of the above analysis the method for wind correction is:

1) Calculate v_* using the full iterative quartic solution.

2) Calculate the hover power using equation (2). From estimated hover performance the value of k_H is 1.16. It is assumed that $k = k_H$ since only very low advance ratios are involved.

A.3 Data Reduction and Correction Procedure

The following are the steps in the data reduction and correction procedure.

1. Record the main balance thrust (axial force), rolling moment (friction torque), normal force and shaft torque. Record mean wind speed (V) and direction (α).

2. Subtract the friction torque from the shaft torque to yield a true rotor torque.

3. Put data in coefficient form, C_T, C_P, etc.

4. Calculate the following:

   (a) $V_* = V / (V_T \sqrt{|C_T|/2})$

   (b) $v_* = 1 - .5\, V_* \cos\alpha$

   (c) F and F' from equation (4)

   (d) $v_{*n+1} = v_{*n} - F/F'$

   (e) $\Delta = - F/F'$

   If $|\Delta| \geq .00001$ set $v_{*n} = v_{*n+1}$ go to step (b) and iterate until $|\Delta| < .00001$.

   (f) set $v_* = v_{*n-1}$

5. Calculate the corrected hover power coefficient from

$$C_{P_H} = C_P - \mu (C_T \cos\alpha - C_{NF} \sin\alpha) + k_H (1-v_*) \frac{|C_T|^{3/2}}{\sqrt{2}}$$

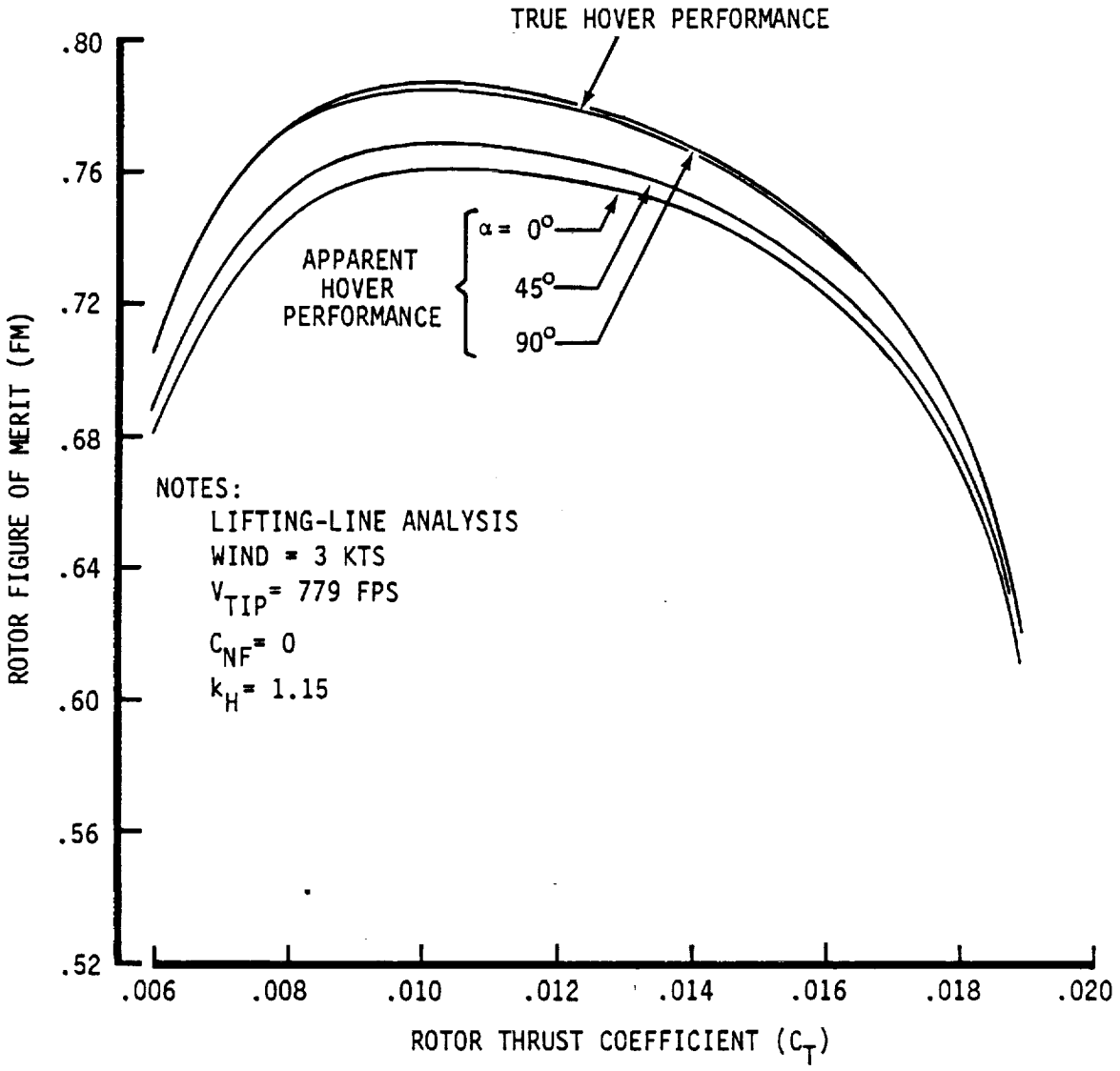

Figure A.2 Effect of Wind on Hover Performance

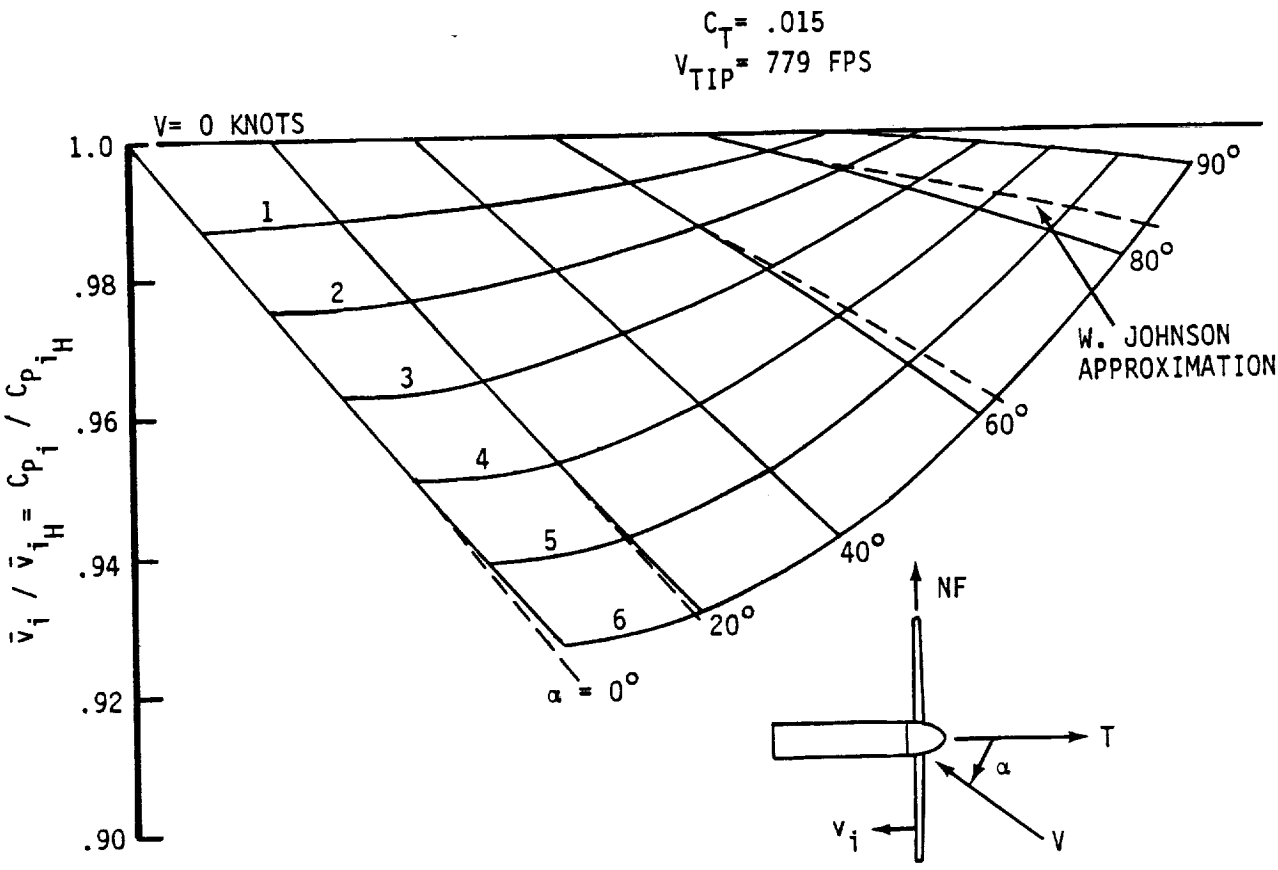

Figure A.1 Effect of Wind on Induced Power

1. Report No.	2. Government Accession No.	3. Recipient's Catalog No.
CR 177436		

4. Title and Subtitle	5. Report Date
Hover Performance Tests Of Baseline Metal and Advanced Technology Blade (ATB) Rotor Systems for the XV-15 Tilt Rotor Aircraft.	October 1986
	6. Performing Organization Code

7. Author(s)	8. Performing Organization Report No.
K. Bartie, H. Alexander, M. McVeigh, S. La Mon, and H. Bishop	D210-12380-1
	10. Work Unit No.

9. Performing Organization Name and Address	11. Contract or Grant No.
Boeing Vertol Company P.O. Box 16858 Philadelphia, Pennsylvania 19142	NAS2-11250
	13. Type of Report and Period Covered
	FINAL

12. Sponsoring Agency Name and Address	14. Sponsoring Agency Code
NASA/AMES RESEARCH CENTER MOFFETT FIELD, CALIFORNIA 94035	505-61-51

15. Supplementary Notes
POINT OF CONTACT: TECHNICAL MONITOR, MARTIN D. MAISEL
M/S 237-5, NASA AMES RESEARCH CENTER
MOFFETT FIELD CA 94035 (415) 694-6372

16. Abstract : Rotor hover performance data were obtained for two full-scale rotor systems designed for the XV-15 Tilt Rotor Research Aircraft. One rotor employed the rectangular planform metal blades (rotor solidity=0.089) which were used on the initial flight configuration of the XV-15. The second rotor configuration examined the non-linear taper, composite-construction, Advanced Technology Blade (ATB), (rotor solidity = 0.10) designed to replace the metal blades on the XV-15. Variations of the baseline ATB tip and cuff shapes were also tested.

A new six-component rotor force and moment balance designed to obtain highly accurate data over a broad range of thrust and torque conditions is described in the report. The test data are presented in non-dimensional coefficient form for the performance results, and in dimensional form for the steady and alternating loads. Some wake and acoustics data are also shown.

17. Key Words (Suggested by Author(s))		18. Distribution Statement
ROTOR	ROTOR LOADS	UNLIMITED
HOVER PERFORMANCE	STATIC PERFORMANCE	SUBJECT CATEGORY 05
TILT ROTOR	TEST	
XV-15		
ROTOR BLADE		

19. Security Classif. (of this report)	20. Security Classif. (of this page)	21. No. of Pages	22. Price*
UNCLASSIFIED	UNCLASSIFIED	151	

*For sale by the National Technical Information Service, Springfield, Virginia 22161